

Wind power in forests: Winds and effects on loads

Bergström, Hans; Alfredsson, Henrik ; Arnqvist, Johan; Carlén, Ingemar; Dellwik, Ebba; Fransson, Jens ; Ganander, Hans; Mohr, Matthias; Segalini, Antonio; Söderberg, Stefan

Publication date:
2013

Document Version
Publisher's PDF, also known as Version of record

[Link back to DTU Orbit](#)

Citation (APA):
Bergström, H., Alfredsson, H., Arnqvist, J., Carlén, I., Dellwik, E., Fransson, J., ... Söderberg, S. (2013). Wind power in forests: Winds and effects on loads. *Elforsk.* (Elforsk rapport; No. 13:09).

DTU Library

Technical Information Center of Denmark

General rights

Copyright and moral rights for the publications made accessible in the public portal are retained by the authors and/or other copyright owners and it is a condition of accessing publications that users recognise and abide by the legal requirements associated with these rights.

- Users may download and print one copy of any publication from the public portal for the purpose of private study or research.
- You may not further distribute the material or use it for any profit-making activity or commercial gain
- You may freely distribute the URL identifying the publication in the public portal

If you believe that this document breaches copyright please contact us providing details, and we will remove access to the work immediately and investigate your claim.



Wind power in forests

Winds and effects on loads

Elforsk rapport 13:09



Hans Bergström, Henrik Alfredsson, Johan Arnqvist,
Ingemar Carlén, Ebba Dellwik, Jens Fransson, Hans Ganander,
Matthias Mohr, Antonio Segalini, Stefan Söderberg March 2013

Wind power in forests

Winds an effects on loads

Elforsk rapport 13:09

Hans Bergström, Henrik Alfredsson, Johan Arnqvist,
Ingemar Carlén, Ebba Dellwik, Jens Fransson, Hans Ganander,
Matthias Mohr, Antonio Segalini, Stefan Söderberg March 2013

Preface

This report is the final report from the Vindforsk III project V-312, Wind Power in forests.

Vindforsk – III is funded by ABB, Arise windpower, AQSystem, E.ON Elnät, E.ON Vind Sverige, Energi Norge, Falkenberg Energi, Fortum, Fred. Olsen Renewables, Gothia wind, Göteborg Energi, Jämtkraft, Karlstads Energi, Luleå Energi, Mälarenergi, O2 Vindkompaniet, Rabbalshede Kraft, Skellefteå Kraft, Statkraft, Stena Renewable, Svenska Kraftnät, Tekniska Verken i Linköping, Triventus, Wallenstam, Varberg Energi, Vattenfall Vindkraft, Vestas Northern Europe, Öresundskraft and the Swedish Energy Agency.

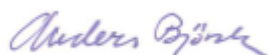
Reports from Vindforsk are available from www.vindforsk.se

The project has been led by Hans Bergström at Uppsala University. The work has been carried out by Uppsala University, WeatherTech Scandinavia, the Royal Institute of Technology (KTH), DTU Wind Energy in Denmark and Teknikgruppen AB.

Comments on the work have been given by a reference group with the following members:

Lasse Johansson, AQ System
Fredrik Osbeck, Arise Windpower
Anders Björck, Elforsk
Anton Andersson, E.ON Vind Sverige
Helena Hedblom, Fortum
Kristina Lindgren, O2
Daniel Eriksson, Skellefteå Kraft
Måns Hakansson, Statkraft Sverige
Anders Ryllin Stena Renewable
Johannes Lundvall, Stena Renewable
Irene Helmersson, Triventus
Sven-Erik Thor, Vattenfall Vindkraft
Staffan Engström, Ägir konsult, representing Wallenstam Energi

Stockholm March 2013



Anders Björck

Programme manager Vindforsk-III

Electricity- and heatproduction, Elforsk

Sammanfattning

I projektet V-312, Vindkraft i skog, har forskare och en doktorand vid Uppsala universitet, WeatherTech Scandinavia, Kungliga tekniska högskolan (KTH), DTU Wind Energy i Danmark och Teknikgruppen samarbetat. I projektet har det gjorts mätningar med hög vertikal upplösning av turbulensen i atmosfären, även ned mellan träden, syftande till att möjliggöra en bättre teoretisk beskrivning av de observerade egenskaperna. Dessutom har flera mesoskaliga modeller använts för att modellera vindarna ovanför skogen. Mätningarna i atmosfären har kompletterats med vindtunnelmätningar där bottnen i vindtunneln har bestyckats med små cylindriska träpinnar vilka skulle simulera effekterna av träd och ge upphov till en känd friktionskraft som påverkar strömningen. De kombinerade nya kunskaperna om vind och turbulens i gränsskiktet över en skog har använts för att driva en datormodell som beskriver dynamiken hos vindturbinerna. Detta har sedan använts för att simulera lasterna på turbinerna som uppstår i det turbulenta vindfältet.

Några viktiga resultat:

Mätningar – Avsnitt 3

Flera metoder användes för att beräkna skrovlighetslängd (z_0) och nollplansförskjutning (d) representativa för försöksplatsen i Ryningsnäs avseende vindkraft i skogen. Storleken på dessa visades vara mellan 2 och 3 m respektive 15 m. Mellan 25 och 140 m höjd återfinns tre strömningsregimer: i) "roughness sublayer", ii) ytskiktet och iii) Ekmanskiktet. Avseende vindenergi förefaller det som effekterna av i) kan försummas. I hur hög grad strömningen på navhöjd kontrolleras av dynamiken i ytskiktet befanns vara starkt beroende av vindhastighet och skiktning. Vid neutral skiktning var ytskiktshöjden ≈ 100 m, för stabil skiktning < 100 m.

Vindförhållandena visade sig avseende skjuvning och turbulens alltid vara i konflikt med åtminstone ett av IEC standardens kriterier för de starkaste turbinerna. (Resultaten indikerar emellertid att Ryningsnäs har ett extremare vindklimat än vad som visade sig typiskt för andra platser som analyserades). För nära neutrala förhållanden var turbulensintensiteten i medeltal över 20 %. Under stabila förhållanden blir både vindskjuvning och vindvridning med höjden mycket stora och effekterna av träden tycks begränsad till mycket lägre höjder. Vindvridningen visade en medeldifferens mellan 40 och 140 m på mer än 10° (upp till 23°) för stabila skiktningar.

Data från 42 svenska skogsplatser gav en skrovlighetslängd på i medeltal 1,3 m, lägre än värdet för Ryningsnäs (= 2,1 m med utnyttjande av samma metod). Detta resultat antyder att Ryningsnäs har ett extremare vindklimat än vad som var typiskt för övriga platser i analysen. Skjuvningsexponenten visade sig ligga mellan 0,25 och 0,40 med ett medianvärde på 0,33.

Resultaten visade att topografin har en stor betydelse för medelvind och turbulensförhållanden. För platser med stor topografisk variabilitet erhöles lägre skrovlighet och mindre skjuvningsexponent. Betydelsen av atmosfärens termiska skiktning belystes. Medianvindprofilen som årsmedel för alla 42 platserna hamnade mellan vindprofilerna i Ryningsnäs för neutral och stabil skiktning.

Turbulensintensiteten (TI) är sammansatt av olika bidragande delar för olika stabiliteter. En viktig slutsats för närvarande är att det förekommer vågor under mycket stabila förhållanden, vilka kan vara ursprunget till organiserade strukturer i turbulensen. Perioden för dessa strukturer uppskattades med hjälp av flera olika tekniker och befanns vara ≈ 30 s. Inflytandet på turbulensstatistiken varierar signifikant mellan olika situationer och en bättre förståelse av fenomenen behövs

Hastighetsspektra av alla tre komponenterna hos vindhastigheten har skalats med en metod som ger en form på spektra som är generellt användbar för de flesta atmosfäriska förhållanden. Parametriseringar av de storheter som ingår i skalningen har presenterats. En modell som beskriver hastighetsspektra utvecklades, vilken tillsammans med nya modeller som beskriver profiler av vindhastighet och vindvridning användes för den modellering av laster som presenteras i avsnitt 6.

För Skogaryd beräknades nollplansförskjutningen och parameteriseringar utvecklades för att beskriva vindprofilen inom "roughness sublayer". En ny metod att modellera vinden i "roughness sublayer" har presenterats och arbete pågår att inkludera detta i mesoskaliga modeller.

Vindtunnelstudier – Avsnitt 4

Vindtunnelstudier genomfördes med syfte att förstå typiska egenskaper hos det turbulenta gränsskiktet över skogar och kalhyggen. Skogen modellerades av cylindriska pinnar av konstant höjd (=skogshöjd h_c). En sådan modell kan realistiskt beskriva strömningen över skogen. Resultaten för de lägre höjderna överensstämmer bra med mätningarna från Ryningsnäs och Skogaryd. Mätningar av turbulensstatistik gjordes på flera avstånd i strömningsriktningen längs skogen, 15-30 gånger h_c från skogskanten uppströms.

En ökad skogstäthet medför en ökning av rörelsemängdstransporten till skogen, vilket alltså medför att vindgradienten ökar nära skogstoppen. Den vertikala hastighetsvariansen påverkas också signifikant av skogens täthet, medan övrig vindstatistik inte påverkas.

Vindtunnelmätningarna är inte i överensstämmelse med data från Ryningsnäs avseende de vertikala profilerna. Båda följer emellertid samma diagnostiska samband avseende transporten av rörelsemängd. Den observerade skillnaden vad det gäller de vertikala profilerna kan hänföras till en otillräcklig längd av skogsmodellen i vindtunneln.

En skalning av hastighetsspektra med hjälp av integralskalan för tid visar att spektra faller samman anmärkningsvärt väl till en kurva. Resultatet representerar en ny möjlig metod att parameterisera spektra för strömning i skog upp genom gränsskiktet.

Effekten av olika öppningar (kalhyggen) i skogen (med längden 2, 4 och $6h_c$) tycks begränsad till området närmast skogstopparna. Ett område med förstärkt blandning i strömningen har hittats för fallet med övergång "skog till slätt". Turbulensen över öppningen ökade inte eftersom turbulensnivån inte längre kan upprätthållas där det saknas träd. Vindhastigheten i strömningsriktningen ökar över öppningen upp till ungefär två skogshöjder. På högre höjder tycks effekterna av öppningen vara små eller till och med

negativa. När strömningen närmar sig nedströmskanten på öppningen, möter vinden skogen och avlänkas uppåt.

Mesoskalig modellering av skogen runt Ryningsnäs – Avsnitt 5.1

Resultaten från tre mesoskaliga modeller (WRF, COAMPS och MIUU) analyserades och jämfördes med mätningarna från Ryningsnäs. Vissa viktiga slutsatser kan dras, vilka också är giltiga för andra skogsplatser: Modellresultaten beror inte enbart på horisontell och vertikal upplösning utan även i hög grad på det turbulensschema eller gränsskiktsschema som valts i modellen. Modellresultaten över skogen bör valideras inte enbart i termer av medelvindhastighet utan också avseende vindskjuvning.

Vissa mesoskaliga modellers resultat avseende vindhastighet är mycket känsliga för valet av skrovlighet, medan andra modellers resultat inte är det. Vad det gäller Ryningsnäs ger modellerna en skjuvningsexponent som är lägre än vad mätningarna visar. För att få medelvind i navhöljd att överensstämma mellan mätningar och beräkningar behöver högre skrovlighetslängder än de som normalt används i WRF och MIUU-modellerna användas. Validering för fler platser behövs dock för att dra tydliga slutsatser om vilka skrovlighetslängder som bör användas.

Idealiserad mesoskalig modellering av skogskanter – Avsnitt 5.2

Idealiserade 2-dimensionella skogs-simuleringar har gjorts med MIUU-modellen (övergångar slätt-till-skog och skog-till-slätt), isolerade skogsområden och öppningar i skog. En skrovlighetslängd på 1 m valdes för skogen. Simuleringarna gjordes med hög horisontell (100 m) och vertikal upplösning

Den procentuella minskningen/ökningen av vindhastighet och turbulensintensitet (TI) över skog och öppningar studerades. De absoluta värdena som presenteras bör dock användas med försiktighet då resultaten ännu inte kunnat valideras. Trots detta ger modellresultaten intressant information om avståndsberoendet av vindhastighet och turbulens, d.v.s. hur vind och turbulens påverkas av övergångar skog/öppen mark. Avseende vindhastigheten kvarstår effekter av skogen upp till ≈ 10 km eller så nedströms över en slätt. TI å andra sidan anpassas mycket snabbare än vindhastigheten till den nya ytan. Reduktion i vindhastighet och ökning av TI över skog är mindre för högre höjder. På högre höjder behöver dock båda ett längre avstånd för att anpassa sig till en ny yta.

För övergångar slätt-till-skog tycks reduktionen av vindhastigheten med avstånd till skogskanten beskrivas av en "power law" (liknande tillväxten av ett IBL över skogen). Ökningen av TI beskrivs bäst av en "power law" tillsammans med en linjär term. För övergången skog-till-slätt ökar vindhastigheten exponentiellt med ökande avstånd nedströms från skogskanten. TI avtar på motsvarande sätt exponentiellt med avståndet.

Skogsversion av mesoskaliga modeller – Avsnitt 5.3

Mesoskaliga modeller har sin lägsta vertikala nivå på höjden $z_0 + d$ (där vindhastigheten sätts till noll), vilket ger en vertikalt förskjuten modellberäknad vindprofil. Därför måste modellresultaten efteranalyseras där värdet på d för skogen måste användas, ett värde som vanligen inte är känt. Genom att införa ett skogsskikt i den mesoskaliga modellen undviks detta

problem och vindprofilen beräknas hela vägen ned till marken. Dock måste härvid andra parametrar anges, vilka vanligen inte är kända, såsom "leaf area index" och skogens täthet. Man behöver också en mycket hög vertikal upplösning hos modellen.

En skogsversion av MIUU-modellen har utvecklats. Den nya skogsversionen har visats ge resultat som överensstämmer med standardversionen och med vindtunnelmätningar. För en 2D övergång slätt-till-skog överensstämmer resultaten från båda versionerna av modellen kvalitativt, liksom med data från vindtunnelmätningarna. Modellresultaten var i god överensstämmelse med vindhastigheten från Ryningsnäs under neutrala förhållanden. Ovanför skogen ger skogsversionen en reduktion i vindhastighet som är ungefär dubbelt så stor som den av standardversionen.

Lastberäkningar – Avsnitt 6

En vindmodell utvecklades för att användas i Teknikgruppens lastberäkningar, baserad på mätningarna vid Ryningsnäs. Vindmodellen visade sig mycket användbar i arbetet med att förstå lasterna på vindturbiner i skogslandskap. Resultaten pekar på att vindturbiner i en svensk tallskog kan utsättas för mer allvarliga utmattningslaster än vad som täcks in av rådande IEC61400-1 klasser för vindturbiner.

Inledande studier med användande av cyklisk pitch-kontroll antyder en möjlighet att minska de utmattningslaster som orsakas av stor vindskjuvning. Höga turbulensnivåer begränsar dock klart effekterna av en enkel lastkontroll. Det måste betonas att den begränsade studie som gjorts här pekar på en stark påverkan på utmattning av både blad och torn, men också på mycket stora lastvariationer som beror på de vindförhållanden som används samt på val av turbin. Platsbedömningar för att definiera vindförhållanden specifika för olika platser samt för verifiering av utformning kommer att vara en viktig del i utvecklingen av vindturbiner avsedda för skogsförhållanden.

Summary

Within the project V-312, Wind power in forests, researchers and a PhD student at Uppsala University, WeatherTech Scandinavia, the Royal Institute of Technology (KTH), DTU Wind Energy in Denmark and Teknikgruppen have been cooperating. Within the project atmospheric turbulence measurements with high vertical resolution have been done, also down between the trees, to make it possible to give better theoretical descriptions of the observed properties. Several mesoscale models have also been used to model the above forest winds. The atmospheric measurements have been complemented by wind tunnel measurements using a wind tunnel floor designed with small cylindrical wooden sticks that should simulate the effect of the trees generating a known momentum sink able to affect the flow. The combined new knowledge about the forest boundary layer wind and turbulence properties have been used as input to a dynamical wind turbine computer model, used to simulate the turbine load response to the turbulent wind field.

Some important results are:

Measurements – Section 3

For the Ryningsnäs wind-power-in-forest test site, roughness length (z_0) and zero-displacement height (d) were estimated from several methods to between 2 and 3 m and 15 m, respectively. Between 25 and 140 m height, three major flow regimes exist: i) the roughness sublayer, ii) the surface layer and iii) the Ekman layer. For wind power purposes, it seems that effects of i) can be disregarded. How much the flow at typical hub heights is controlled by surface layer dynamics was found to depend strongly on wind speed and stratification. In neutral stratification the surface layer height was found to be ≈ 100 m, in stable stratification < 100 m.

Wind conditions regarding shear and turbulence were found to always be in conflict with at least one of the IEC standardized criteria for the strongest turbines. (Results, however, indicate that Ryningsnäs has a more severe wind climate than is typical for the other sites in this analysis.) For near-neutral conditions turbulence intensity is, on average, above 20%. During stable conditions wind shear and veer (wind direction changes with height) becomes very large and the effect of the trees seems to be restricted to much lower heights. The wind veer showed a mean difference between 40 and 140 meters of more than 10° (up to 23°) for stable conditions.

Data from 42 Swedish forest sites reveal a roughness length of 1.3 m, on average, lower than that for Ryningsnäs (= 2.1 m using the same method). This result points at that the Ryningsnäs site has a more severe wind climate than was typical for the other sites included in the analysis. Shear exponents were found to be between 0.25 and 0.40 with a median value of 0.33.

Results show that topography has a large influence on average wind and turbulence conditions. Sites with large topographical variability yield smaller roughness lengths and shear exponents. The importance of thermal atmospheric stability is demonstrated. Indeed, the annual-mean median profile from all 42 sites falls somewhere between the Ryningsnäs wind profile for neutral and stable stratification.

Turbulence intensity (TI) is composed of quite different contributing parts at different stabilities. The main conclusions so far are that there is clear evidence of evanescent waves in very stable conditions, perhaps the origin of organized structures. The period of the structures was found to be ≈ 30 s using several different techniques. The relative contribution to turbulence statistics varies significantly in time and a better understanding of the phenomenon is needed.

Velocity spectra from all three velocity components have been scaled in a way that renders a shape applicable to most atmospheric conditions. Parameterisations of quantities used in the scaling are also presented. A model for the velocity spectra was developed that was used, in conjunction with new models for profiles of wind speed and veer, as input to load modelling over forests presented in Section 6.

For Skogaryd, displacement height was estimated and parameterizations of the wind profile within the roughness sublayer were developed. A new way to correct the wind in the roughness sublayer is presented and work is on-going to incorporate the results into mesoscale models.

Wind tunnel studies – Section 4

Wind tunnel studies were performed in order to understand typical features of the turbulent boundary layer above forests and clearings. The canopy was modelled with cylindrical pins of constant height (= canopy height h_c). Results are in agreement with Ryningsnäs and Skogaryd at the lowest heights. The simplified canopy model is able to realistically model the flow above a forest. Turbulence statistics were measured at several stream wise distances of 15 – 30 times h_c from the canopy leading edge.

The increase of canopy density leads to a higher momentum transfer towards the canopy, consequently increasing the velocity gradient of the wind profile near the canopy top. Vertical velocity variance is significantly affected by canopy density, while other statistics do not show this effect.

The wind tunnel measurements do not agree with data from Ryningsnäs in terms of vertical profiles. Both, however, follow the same momentum transfer processes diagnostic curves. The observed discrepancy in the vertical profiles can be attributed to an insufficient developing length of the canopy model in the wind tunnel.

Scaling of the velocity spectra with the integral time scale shows remarkable collapse of the spectra, demonstrating scale separation for two decades in frequency and suggesting a new possible way to parameterise spectra in canopy flows up to the boundary layer edge.

The effect of different forest-clearings (of length 2, 4 and $6h_c$) seems to be limited to the flow region close to the canopy top. The flow experiences a region of enhanced mixing in the rough-to-smooth transition. Turbulence over the clearing does not increase because high turbulence levels cannot be sustained anymore with trees absent. Stream wise velocities increase above the clearing up to roughly two canopy heights. Above two canopy heights, the effect of clearings seems to be small or even detrimental. When the flow is approaching the clearing downwind edge, a significant part of the flow stream enters the canopy region and is subsequently ejected upwards.

Mesoscale modelling of forests around Ryningsnäs – Section 5.1

Results from three mesoscale models (WRF, COAMPS and MIUU) were analysed and compared to measurements from Ryningsnäs. Some important conclusions can be drawn that also apply to other forested sites: Mesoscale results do not only depend on horizontal and vertical resolution, but also to a very significant degree on the turbulence or planetary boundary layer scheme chosen. Mesoscale model results over forests should be validated not only in terms of mean wind speed, but also in terms of wind shear.

Some mesoscale models are very sensitive to surface roughness with respect to wind speed, whereas other models are not. For Ryningsnäs, shear exponents of most mesoscale models used herein seem to be lower than measured. To get agreement between modelled and measured mean wind at hub height larger roughness lengths than normally used with the WRF and MIUU-models are needed. However, validations at more sites are needed to draw final conclusions about which roughness lengths that should be used.

Idealised mesoscale modelling of forest transitions – Section 5.2

Idealised 2-dimensional MIUU model simulations of forests (smooth-to-rough and rough-to-smooth transition), isolated forests and clearings have been carried out. A forest roughness of 1 m was chosen. The model was run with very high horizontal (100 m) and vertical resolution.

Percentage reduction/increase in wind speed and turbulence intensity (TI) over the forest or clearing was studied. Absolute values provided should be treated with caution as the results have not been validated yet. Nevertheless, the model gives interesting information on the horizontal fetch-dependent development of wind speed and turbulence over forests/clearings. For wind speed, forest effects seem to persist up to ≈ 10 km or so downstream over a flat surface. TI, on the other hand, adjusts much quicker to the new surface than wind speed. Wind speed reductions and TI enhancements are smaller at higher heights. At higher heights, however, wind speeds and TI need longer distances to adjust to a new surface.

For smooth-to-rough transitions, wind speed reductions seem to follow a power law with increasing distance from the forest edge (similar to growth of IBL over forests). TI enhancement is best described by a power law plus a linear term. For rough-to-smooth transitions, wind speed reductions from forest decrease exponentially with increasing distance to downstream forest edge. In the same way, TI enhancement from forest decreases exponentially.

Forest canopy versions of mesoscale models – Section 5.3

Mesoscale models have their lowest vertical level at the height of $z_0 + d$ (where wind speed is set to zero), yielding a vertically displaced model-predicted wind profile. Hence, model results have to be post-processed using a value of d for forests that is usually not known. Implementing a forest canopy in the mesoscale model avoids that by modelling the wind profile all the way down to the ground. However, other parameters that are generally not known (such as leaf area index and density) have to be specified instead of d . Also, a very high vertical resolution is needed.

A forest canopy version of the MIUU mesoscale model was developed. The new "canopy version" of the model agrees well with the "bulk version" as well

as with the wind tunnel measurements. For a 2D smooth-rough transition both versions of the model seem to agree qualitatively with each other, as well as with the wind tunnel data. Model results agree well with "neutral" wind speeds from Ryningsnäs. Over the canopy, the "canopy version" gives roughly twice the wind speed reduction compared to the "bulk version".

Load calculations – Section 6

A wind model was developed for the Teknikgruppen load calculations, based upon the atmospheric measurements made at Ryningsnäs. The wind model was proven to be very useful when trying to understand the loading conditions for turbines installed in forest terrain. Initial studies indicate that a wind turbine in the Scandinavian pine forest terrain may experience fatigue loading more severe than what is covered by the current IEC61400-1 wind turbine classes.

Some initial studies using a cyclic pitch control system indicate a potential to reduce the fatigue life consumption due to the large wind shear, but high levels of turbulence are clearly limiting the effects of simple load control. It has to be emphasized that this limited study indicate strong influence on fatigue of both blades and tower, but also very large variations of load results, depending on assumed wind forest conditions and the turbine. Site assessment to define site specific wind conditions and for verification of the design will be an important part of wind turbine development for forest conditions.

Innehåll

| | | |
|----------|--|------------|
| 1 | Introduction | 1 |
| 2 | Project and report structure | 2 |
| 3 | Atmospheric observations – presentation of measurements and results of analyses | 4 |
| 3.1 | Ryningsnäs..... | 4 |
| 3.1.1 | Data description | 4 |
| 3.1.2 | Processing of measurement data and data selection..... | 6 |
| 3.1.3 | Results from Ryningsnäs | 8 |
| 3.2 | Skogaryd | 39 |
| 3.2.1 | Data description | 39 |
| 3.2.2 | Results from Skogaryd | 40 |
| 3.3 | Comparisons with results from other sites | 48 |
| 3.3.1 | The data..... | 48 |
| 3.3.2 | Results..... | 51 |
| 3.4 | Summary | 62 |
| 4 | Wind tunnel measurements of a forest boundary layer | 65 |
| 4.1 | Introduction | 65 |
| 4.2 | Experimental setup | 65 |
| 4.2.1 | Clearing configurations..... | 67 |
| 4.2.2 | PIV Details..... | 67 |
| 4.3 | Results | 68 |
| 4.3.1 | Full forest configuration..... | 68 |
| 4.3.2 | Clearing configurations..... | 72 |
| 4.3.3 | Experiments with Particle Image Velocimetry (PIV) | 75 |
| 4.4 | Concluding remarks..... | 76 |
| 5 | Meso-scale modelling of forests | 79 |
| 5.1 | Results from several models and comparisons with observations at Ryningsnäs..... | 79 |
| 5.1.1 | Wind climatology tests using the MIUU-method | 90 |
| 5.2 | Results from modelling idealized forests..... | 96 |
| 5.2.1 | Methodology and model set-up..... | 96 |
| 5.2.2 | Influence of forest on wind and turbulence fields | 99 |
| 5.2.3 | Wind reduction downstream of forests as function of distance to forest edge | 108 |
| 5.2.4 | Influence of isolated forests on wind and turbulence fields | 117 |
| 5.2.5 | Influence of clearings on wind and turbulence field | 125 |
| 5.3 | Implementing forest canopy parameterisations in the MIUU mesoscale model..... | 133 |
| 5.3.1 | Description of forest-canopy version of MIUU model..... | 133 |
| 5.3.2 | Comparison of forest-canopy version of MIUU model with bulk-layer roughness version..... | 136 |
| 5.3.3 | Comparison of 1D MIUU model with wind tunnel measurements..... | 137 |
| 5.3.4 | Comparison of 2D MIUU model with wind tunnel measurements..... | 138 |
| 5.4 | Summary & Conclusions | 140 |
| 6 | Turbine load modelling | 145 |
| 6.1 | Background meteorological data used..... | 146 |
| 6.1.1 | IEC wind model | 146 |
| 6.1.2 | Diabatic surface layer model (Panofsky & Dutton)..... | 147 |

| | | |
|----------|---------------------------------------|------------|
| 6.1.3 | Forest wind model | 147 |
| 6.2 | Dynamic turbine model | 149 |
| 6.3 | Calculations..... | 150 |
| 6.3.1 | Wind realisations | 150 |
| 6.3.2 | Fatigue equivalent loads | 150 |
| 6.3.3 | Turbine loads | 151 |
| 6.4 | Results | 151 |
| 6.5 | Cyclic pitch analysis | 152 |
| 6.6 | Conclusions | 157 |
| 7 | Discussions and conclusions | 158 |
| 8 | References | 160 |
| 9 | Publications and presentations | 166 |

1 Introduction

The interest for establishing wind energy in forested regions has increased during recent years. Partly this is due to that Sweden has large forested areas with few inhabitants while the open flat agricultural areas which earlier have been the focus for wind energy development are more densely populated why conflicts with other interests are typically larger. Forests became interesting for wind power projects partly following the Swedish wind resource mapping pointing at that also forested regions may have high enough winds to make them economically interesting, and partly following technical developments of the wind turbines allowing hub heights reaching well over 100 m. These heights are necessary to reach for forested regions to become really interesting for wind energy.

It is known since many years that the atmospheric boundary layer above forests may not be described using the same relations which are valid over low vegetation, but the knowledge needs to be deepened as there are many uncertainties regarding details on these high vegetation turbulent boundary layers. The goal has been to create knowledge allowing better judgements of how a wind power plant in a forest environment produce and concerning turbine loads. Models better describing the properties of the wind in forested areas have been developed.

2 Project and report structure

Within the project V-312, Wind power in forests, researchers and a PhD student at Uppsala University, WeatherTech Scandinavia, the Royal Institute of Technology (KTH), DTU Wind Energy in Denmark and Teknikgruppen have cooperated. Within the project turbulence measurements with high vertical resolution have been done, also down between the trees, to make it possible to give better theoretical descriptions of the observed properties. As the real world is typically far from homogeneous it is difficult to get atmospheric data which are ideal for process studies. The atmospheric measurements have therefore been accompanied by wind tunnel measurements. A new canopy model was used in the wind tunnel designed with small cylindrical wooden sticks that should simulate the effect of the trees generating a known momentum sink able to affect the flow. The combined new knowledge about the forest boundary layer wind and turbulence properties have been used as input to a dynamical wind turbine computer model, used to simulate the turbine load response to the turbulent wind field. Access to load measurements from two wind turbines located at a forested site made it possible to compare with observed actual load response to at the same time observed winds.

Section 3

In this report results from the research project are presented. Each section ends with a summary of what has been presented there. In Section 3, Atmospheric observations – presentation of measurements and results of analyses, detailed atmospheric measurements performed within the project at two forested sites are described and the results are presented in some detail. DTU Wind Energy with Ebba Dellwik was responsible for these measurements. A number of additional measurements were also made available to the project as kind contributions. A modified Monin-Obukhov similarity model is presented which includes effects of a forest canopy. The new results are also compared to results using routine wind measurements from a large number of wind project sites. Data processing and analyses were made in co-operation between Ebba Dellwik at DTU Wind Energy, Antonio Segalini at KTH, and Johan Arnquist and Hans Bergstöm at Uppsala University.

Section 4

Wind tunnel measurements within and above a model forest are described in Section 4, Wind tunnel measurements of a forest boundary layer. Two experiments were performed and are presented. Comparisons with the atmospheric data are made. Results from ideal studies with different forest densities and clearings of different sized are presented. The influences of forest edges on the turbulent wind fields are analysed. The wind tunnel measurements and analyses were made by Antonio Segalini, Jens Fransson and Henrik Alfredsson at KTH.

Section 5

In Section 5, Meso-scale modelling of forests, results of mesoscale modelling using different grid resolutions and different models are discussed and comparisons with measurements from one of the forest sites presented. Model results on ideal forest layouts are also presented. Some results including a resolved forest canopy in a newly developed canopy version of the MIUU meso-scale model is also presented. The meso-scale model studies have been made by Matthias Mohr and Johan Arnqvist at Uppsala University, and Stefan Söderberg and Magnus Baltscheffsky at Weathertech Scandinavia, and Ebba Dellwik and Andrea Hahmann at DTU Wind Energy.

Section 6

Turbine load modelling results are presented in Section 6, Turbine load modelling. This work was made by Ingemar Carlén and Hans Ganander at Teknikgruppen. Different wind models, developed together with Johan Arnqvist at Uppsala University, have been used to generate the 3D turbulent wind field for the dynamic turbine model. One of the models represents a new set of statistical models based on the measurements as presented in Section 3. For comparisons others based on IEC wind models and reference site conditions, valid for low vegetation types, are used. Conclusions based on equivalent fatigue loads are drawn about influence of forest conditions on life time in relation to IEC wind model conditions. Some analyses are also carried out to investigate how cyclic pitch control can reduce asymmetric load variations, due to vertical shear and veer.

3 Atmospheric observations – presentation of measurements and results of analyses

Within the project, DTU Wind Energy was responsible for the instrumentation of two sites. When choosing the sites, the criteria were: location in forested areas as well as access to 220 V networks. We chose the 138 m tall mast in Ryningsnäs, run and operated by Vattenfall AB, and the Skogaryd site operated by Gothenburg University.

In this section, the experimental setups at the two sites are described in 3.1.1 and 3.2.1, respectively. Section 3.1.2 describes the data processing and quality assessment. Section 3.1.3 describes some of the experimental results from Ryningsnäs including effects of the atmospheric temperature gradient (stratification). Also results concerning structures in the turbulence are presented together with spectra. In Section 3.2.2 results from the Skogaryd site are presented. In Section 3.3 comparisons are made with measured data from a large number of other sites.

3.1 Ryningsnäs

3.1.1 Data description

The Ryningsnäs mast is located in South-Eastern Sweden approximately 30-40 km inland of the Baltic coast (Figure 3-1a). The landscape in this part of Sweden is forested, but due to both intensive forestry as well as natural variations, the land cover is generally not homogeneous (Figure 3-1b). The mast is located in the Northwestern corner of a 200 m by 250 m large clearing, shown in Figure 3-1c, surrounded by a forested area consisting of predominantly Scots Pine trees. In a related research project, a so called "point cloud" of lidar reflections were acquired from a national terrain elevation survey. This dataset was used to determine the maximum height of the trees near the mast, and the analysis showed a variation between 20 and 25 m near the mast. Since the tall trees are mixed with shorter ones, we have estimated a mean canopy height of $h_c=20$ m, which will be used as a reference length scale throughout the report. Near the mast, the terrain is generally flat, as can be seen in the topographic map (Figure 3-1d). The images to the right in Figure 3-1 cover approximately the same area and the scale is given in the lower graph, where a grid is spaced at 2km intervals. To the west and south of the mast, the lighter coloured areas in the upper right graph coincide with the low elevation area of the valley (blue and purple colours in the lower right graph). Since the valley is located only a few kilometres from the mast, it is expected to influence the wind statistics.

Two turbines, labelled T1 and T2 in Figure 3-1c are located approximately 200m from the mast, which corresponds to 2.2 rotor diameters, in the Southern and North eastern directions. The hub heights of T1 and T2 are 100 and 80 m, respectively. Approximately 750 m to the east of the mast used in the present experiment, a second 18 m tall mast denoted by a white dot in Figure 3-1c, reaching about 3 m below the canopy top, was operated within the forest for sound propagation research (Conny Larsson, personal communication).

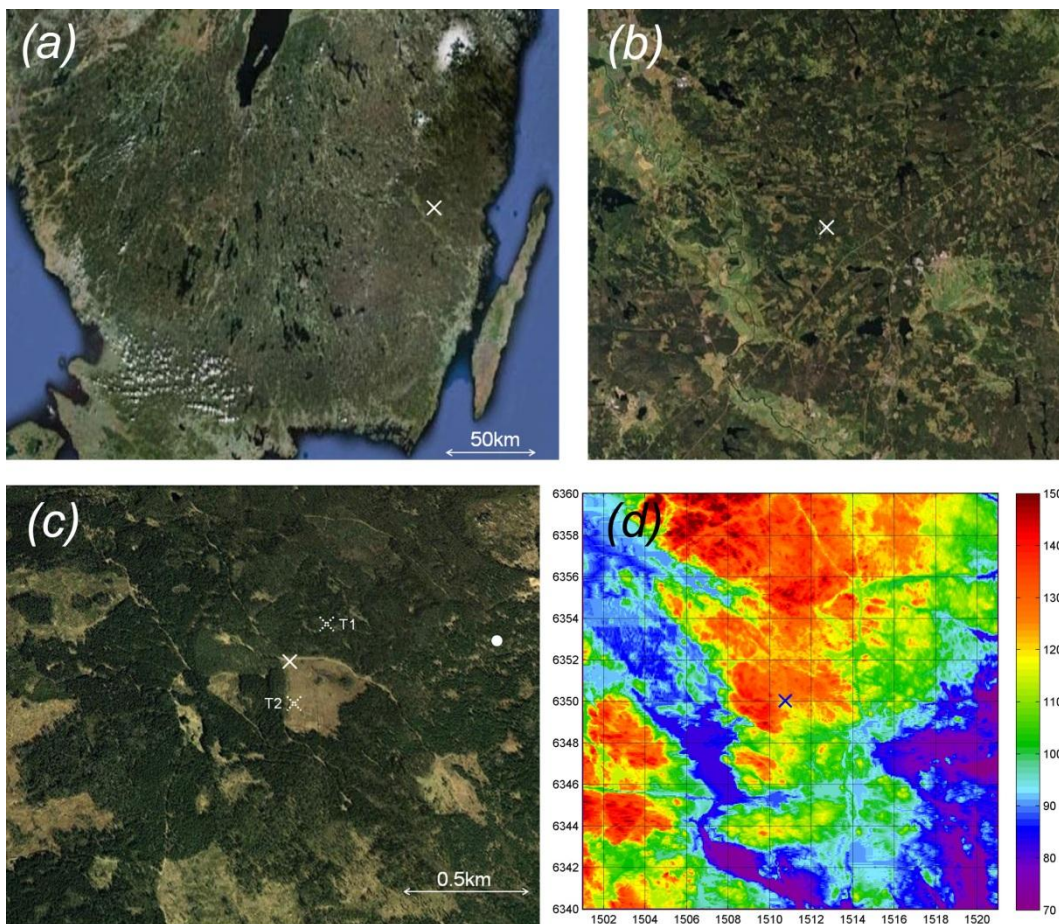


Figure 3-1: The Ryningsnäs site.

The experiment ran between November 2010 and February 2012, yielding a total of 10560 hours of available measurements. A list of the used instrumentation is provided in Table 3-1. The core instrumentation was six sonic anemometers which were mounted at several levels above ground (z), ranging from $z/h_c \approx 2$ to $z/h_c \approx 7$. In tandem with this instrumentation, six cup anemometers (Thies first class, Adolf Thies GmbH & Co., Germany) were already placed at approximately the same heights by Vattenfall Vindkraft AB. A technical drawing of the Ryningsnäs tower is provided in Dellwik et al., 2013.

Table 3-1: Instrumentation at the Ryningsnäs site.

| Instrument | Height (z/h_c) | Parameter |
|-------------------------|------------------------------------|---|
| USA-1 (Metek GmbH) | 2, 2.95, 4, 4.9, 6, 6.9 | Wind field and temperature flux |
| Risø PT-100 | -0.005, 2, 4, 4.9, 6.9 | Soil/air temperature |
| CM11 (Kipp & Zonen) | 6.9 | Incoming solar radiation |
| NR-Lite (Kipp & Zonen) | 2 | Net radiation |
| LiCor 7500 (LiCor Inc.) | 2.95, 4.9 | H ₂ O and CO ₂ concentrations |
| Pressure sensor | 0.007 | Pressure |
| Tipping Bucket | 0.25 | Rain |

The mast is a triangular lattice construction, where the length of each side is 1.2 m. The DTU booms were 5 m long, extending 3.8 m from the mast in the azimuthal direction of $\alpha \approx 318^\circ$. The cylindrical booms had supporting wires in three directions, thereby preventing vibrational movements, which could potentially reduce the quality of the wind measurements. Even so, a close examination showed small effects of boom vibrations for some directions and some wind speeds. These effects were however at a frequency where very little contribution was made to the average statistics of turbulent quantities such that the average effect was below 0.2-0.7 % depending on the atmospheric stratification. Based on the comparison between the cup and sonic anemometers, flow distortion from the mast on the mean wind speed was estimated to be small.

The sonic anemometers and the scalar concentration instruments were sampled at 20 Hz, and the other instruments were sampled at 1 Hz. In order to perform a statistical analysis, block averages of the time series have been computed over 30 minutes. More details about the measurements and the database are given in Dellwik et al. (2013).

In addition to the measurements in the tall mast, short campaigns with radio soundings, lidar and sodar measurements were performed at the site in the spring of 2011. Results from the sodar measurements will not be presented here. The soundings were used to determine boundary layer height and when determining a coefficient entering into a model to estimate boundary layer height. The soundings could be very interesting and relevant for a detailed model study, not included in the present report. Results comparing profiles from the lidar with other instruments is presented below.

3.1.2 Processing of measurement data and data selection

The sonic anemometers used in both the Ryningsnäs and the Skogaryd setups were not heated. With a relation to cold and wet periods, the measured data showed a varying frequency of random spikes in the velocity measurements. In order to remove these spikes, new algorithms were developed, tested and implemented. The sonic anemometers were also corrected for flow distortion caused by the instrument itself (e.g. Dellwik et al., 2010ⁱ) and the sonic

temperature signals were corrected for influence by the mean wind speed (Liu et al., 2001).

A number of data selection criteria were applied with the focus of minimizing the influence of instrumental errors and to characterize the measurements according to the temperature stratification of the atmosphere. The wind speed measurements were compared to Vattenfall's wind measurements (Figure 3-2), where the grey and black dots show the whole dataset and the selected high-quality measurements used for further analysis. A perfect match cannot be expected, because the Vattenfall instrumentation is based on cup anemometers that measure the length of the wind vector S , whereas the sonic anemometers were processed to give the mean wind speed in the mean wind direction U . The cup anemometers over-speed at low mean wind speeds (Figure 3-2a). The variance of the wind measurements is given in Figure 3-2b, where the cup anemometers measure lower variation in the wind than the sonic anemometers. This can be explained by the lower sampling rate of the cup anemometers.

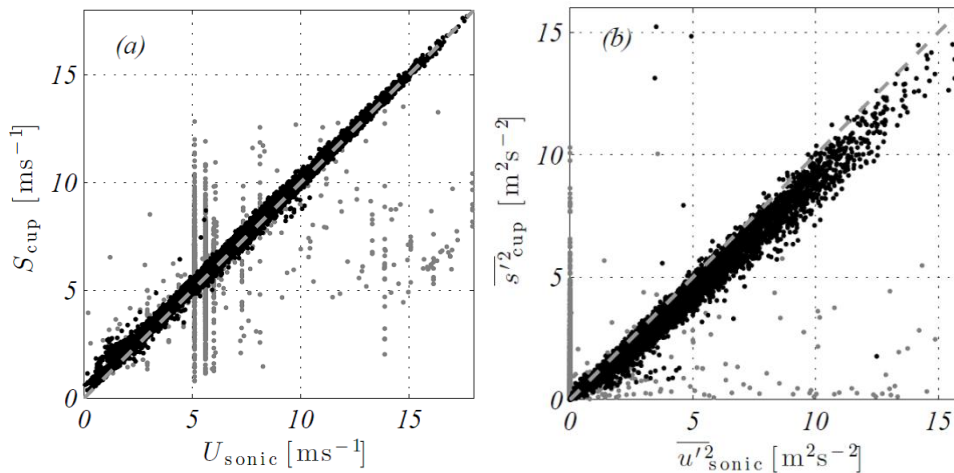


Figure 3-2: Comparison between the DTU and Vattenfall wind measurements.

The degree of how much temperature influences the profiles of wind, temperature and humidity is commonly quantified via the Obukhov length which is defined by

$$L = - \frac{u_*^3 T}{\kappa g \overline{w' T'}}, \quad (3-1)$$

where u_* is the friction velocity, T is temperature, $\kappa=0.4$ is the von Kármán constant, g is the constant of gravity, $\overline{w' T'}$ is the temperature flux. The friction velocity is in turn defined by $u_* = \left(\overline{u' w'^2} + \overline{v' w'^2} \right)^{1/4}$, where $\overline{u' w'}$ and $\overline{v' w'}$ are the vertical and transversal kinematic turbulent momentum flux. Temperature, temperature flux, and u_* can be evaluated using sonic anemometers.

For the results presented below, a distinction is made between near-neutral data, corresponding to situations where temperature effects are negligible, and data where the turbulent is either enhanced by buoyancy (unstable conditions for which $L/h_c < 0$) or dampened by temperature inversions (stable data for which $L/h_c > 0$). In Table 3-2 the different stability classes are defined and the percentage of measurement data from the tower within each stability class is given. The quality control described in the beginning of 3.1.2 reduced the dataset to 85% of its original size. The further requirement of stationarity used for part of the presented analysis below, reduced the dataset to 41% of its original size. For a more detailed analysis of temperature effects, data from a westerly sector was selected. High-quality, stationary data from this sector represented only 9% of the total dataset.

Table 3-2: Percentage of data satisfying the data quality criteria (total 85 %), stationary data (41 %) as well as the westerly sector (9 %) as a function of atmospheric stability

| Atmospheric stratification | High-quality data (%) | Stationary data (%) | Westerly sector (%) |
|----------------------------|-----------------------|---------------------|---------------------|
| $5 < L/h_c < 20$, (■) | 17.8 | 8.5 | 1.7 |
| $20 < L/h_c < 50$, (▼) | 13.1 | 6.3 | 1.4 |
| $ L/h_c > 50$, (×) | 22.1 | 10.8 | 3.2 |
| $-50 < L/h_c < -20$, (▽) | 6.1 | 2.9 | 0.7 |
| $-20 < L/h_c < -5$, (□) | 9.7 | 4.8 | 0.7 |

3.1.3 Results from Ryningsnäs

A multitude of analyses have been performed on the measured data and it is not possible to include all results in this report. For a complementary overview, please see Segalini et al. (2012) and Arnqvist et al. (2013).

Mainly, we have used the framework given by the Monin-Obukhov theory for interpreting the measured data. In this framework, one expects the wind profile in the homogeneously forested landscape to vary with height as

$$U = \frac{u_*}{\kappa} \ln\left(\frac{z-d}{z_0}\right) \quad (3-2)$$

where U is the mean wind speed, z is the height above local ground level, d the displacement height and z_0 the aerodynamic roughness.

Deviations from the logarithmic profile can be caused by land surface heterogeneities (roughness changes and orography) as well as temperature effects. The near-surface temperature effects can be modelled by established correction functions using the Monin-Obukhov theory (e.g. Kaimal and Finnigan, 1994), whereas micro-scale flow models are needed to predict local terrain and roughness-change effects. The measurements from the tall mast at Ryningsnäs are also expected to be significantly influenced from the top of the boundary layer. The location of boundary layer top can in turn be seen as an indirect temperature effect and shows a strong daily variation, typically with shallow boundary layers during night-time and thicker boundary layers during daytime. To understand wind and temperature profiles in the whole atmospheric boundary layer, the surface layer Monin-Obukhov framework

should be combined with that of the Ekman layer. The influence from the top of the boundary layer has been described by Gryning et al., 2008, Pena et al 2010, Verkaik and Holstslag (2007).

Analyses of measurements from tall masts that include all components of the wind field are however still rare in the scientific literature, and the dataset and analysis from Ryningsnäs is expected to be a valuable addition to the scientific literature.

Mölder et al. (1999) focussed instead on the flux-profile relationships in the roughness sub-layer. This layer can be loosely defined as the region closest to the forest, where the trees alter the wind characteristics from classical low-roughness surface layer theory. At Ryningsnäs, roughness sublayer characteristics are not dominant, which is why it is not described in this report.

This section contains results concerning

- General site characterization, which shows results on how the wind field varies with wind direction and is influenced by very local features.
- A more detailed analysis of the western wind direction sector.
- A description of the wind climate at Ryningsnäs
- A short discussion on structures in the forest boundary layer

Characterization of the site – neutral data

Clearing

The Ryningsnäs mast is located in a clearing with changing distance to the forest edge depending on wind direction. A variable which is sensitive to local change of topography is the flow tilt angle (Dellwik et al, 2010), defined as $\beta = \text{atan}(W/U)$. Figure 3-3 shows how β varies with wind direction for the three levels of $z/h_c = 2$ (a), $z/h_c \approx 5$ (b) and $z/h_c \approx 7$ (c). At $z/h_c = 2$ level, the edge itself is the dominant factor and the flow tilt angles are negative for the wind directions, where there is a shift from forest to clearing, and vice versa. For $z/h_c \approx 5$ (b), the flow tilt angles show less influence from the forest edge effects and the turbine wakes are more dominant with peaks in the wind directions of 50° and 180° respectively, which correspond to the direction to the turbines. Finally at $z/h_c \approx 7$ (c), the tilt angles are closer to zero for all wind directions and only small effects from the turbines and clearing persist.

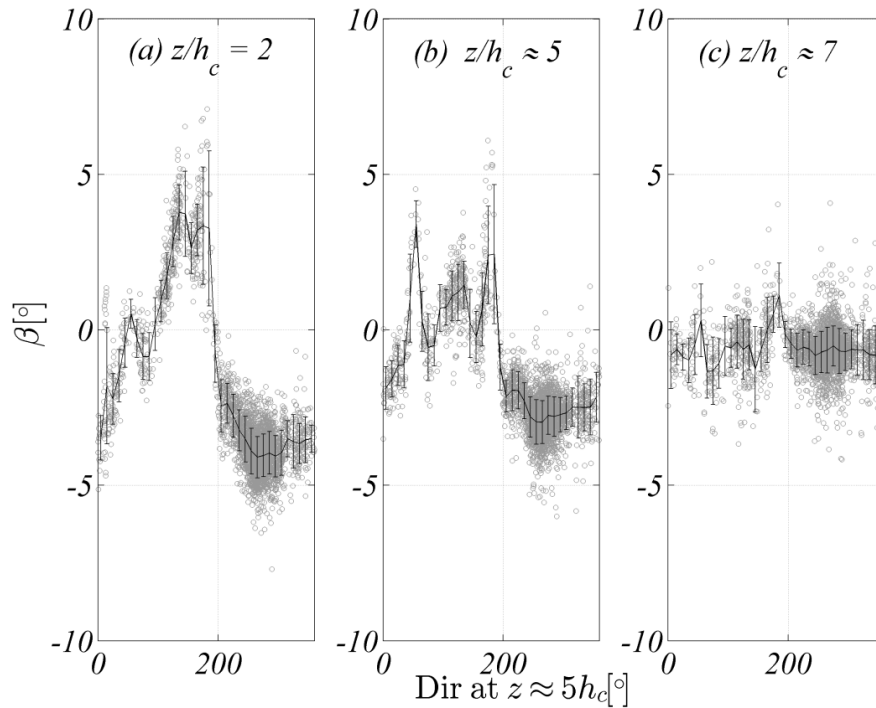


Figure 3-3: Flow tilt angles as a function of wind direction at three measurement heights.

In all directions from the mast, the flow tilt angles are generally less than 6° causing the length of the wind vector to deviate less than 0.5% from the horizontal wind. For the mean wind field analysis, we therefore assume that the influence from the clearing is negligible.

Turbines

Figure 3-4 shows how the wind field variances and the $\overline{u'w'}$ covariance vary as a function of wind direction and height. The most remarkable features correspond to wake effects from the wind turbines, where the levels can be as high as triple of the background values. The wake effects on momentum fluxes (d) show a marked increase below hub height and a strong reduction above.

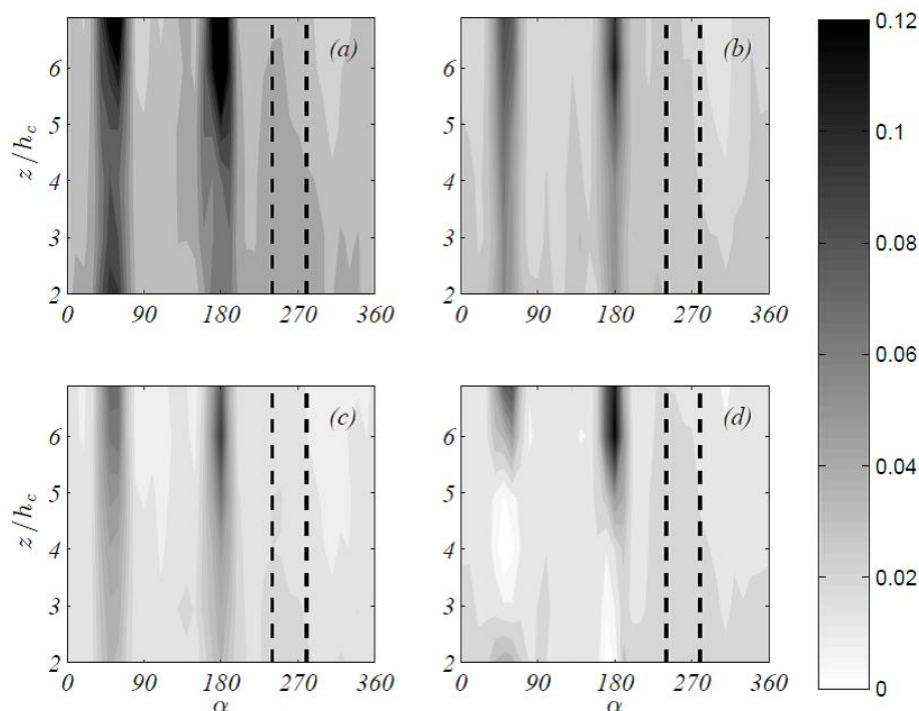


Figure 3-4: Second order moments as a function of wind direction;

(a) $\overline{u'^2}/U^2$, (b) $\overline{v'^2}/U^2$, (c) $\overline{w'^2}/U^2$ and (d) $\overline{u'w'}/U^2$, where U is evaluated at $z \approx 5h_c$.

The westerly sector used for the analysis on temperature effects below is indicated with dashed vertical lines. This sector corresponds to the most common wind direction as well as the wind directions with the strongest winds. Further, it is in this sector we can expect a fully developed forest-type boundary layer as forest is the most common land surface type for several hundred kilometres upwind of the mast.

The wind directions corresponding to the Ryningsnäs clearing show lower levels of turbulence. This result can however not directly be interpreted as an effect of the clearing, since wind speeds from southerly and easterly directions are generally lower and correspond to a different weather type.

Also a sector around 300° shows a consistent reduction in turbulence levels compared to the westerly sector. This feature is possibly caused by lower roughness areas in the valley upwind of the mast (Figure 3-1, c and d). To the north of the mast, turbulence intensities increase to values close to the westerly sector.

Roughness length and displacement height

Using the near-neutral data set with an added requirement for a minimum wind speed of 5m/s at $z/h_c \approx 2$, the roughness and the displacement height of the surface have been estimated by a least square fit to above. Wind speed measurements from the $2h_c$ and $3h_c$ levels have been used in combination with the mean of the measured u_* from these levels. The resulting parameter

values are shown in Figure 3-5 below. The yellow area correspond roughly to the directions where the clearing is upwind of the mast. In this direction interval, the displacement height is near-zero, but the roughness remains high. For the westerly wind directions (to the right of the yellow rectangle), the estimated roughness is about 2.5 m and the displacement height is close to 15 m, corresponding to $z_0/h_c \approx 12.5 \%$ and $d/h_c \approx 0.75$, which are both in line with other studies (see for example Crockford and Hui, 2007).

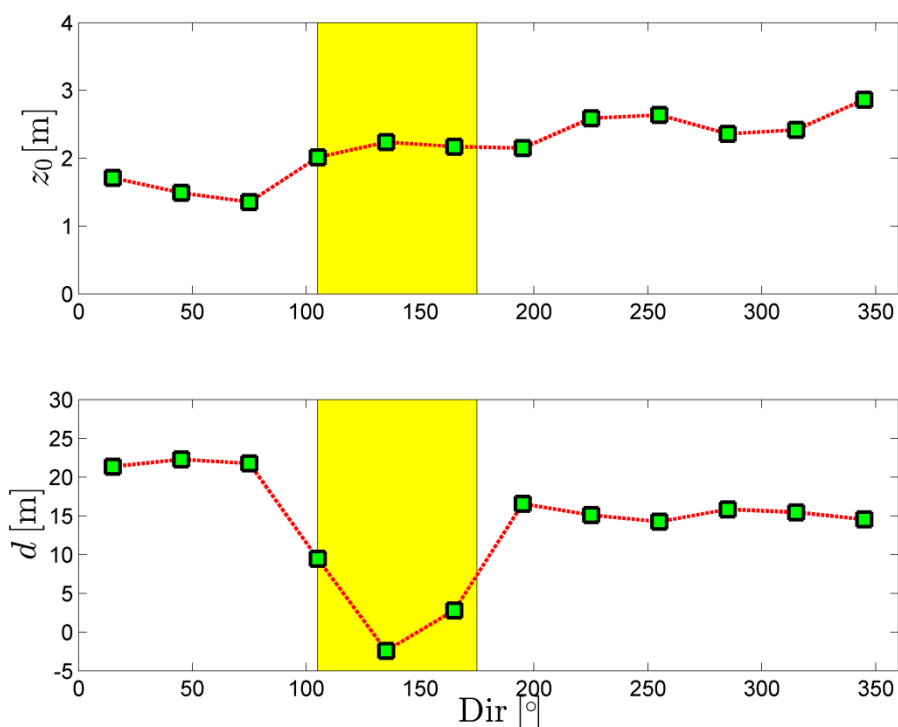


Figure 3-5: Aerodynamic roughness and displacement height as a function of wind direction in Ryningsnäs.

For the northerly directions, the roughness is slightly lower and below 2 m, but the displacement height is increased and closer to 20 m. As the forest to the north and the west of the mast is similar in age and structure, it is likely that the presented estimates are somewhat biased by the slightly sloping terrain; to the north of the mast, elevation increases, whereas it decreases slightly to the west and south.

To determine the roughness and displacement height from measured data is a difficult problem and the level of scatter in the data is high. For the results in the figures below, we have fit the data to the logarithmic profile, regardless of whether the wind profile really shows a logarithmic height dependence or not. Based on a more detailed analysis of the flux profile-relationship from the westerly directions (Arnqvist et al., 2013), the values for the westerly sector should reflect those of a measured near-logarithmic profile more closely than can be expected for the directions from the clearing sector.

Several combinations of alternative methods and slightly different data selection criteria have been used to determine d and z_0 . By use of only the

$z/h_c \approx 2$ level for the calculation of u_* and by keeping the wind measurements from $z/h_c \approx 2$ and 3, the roughness length values were close to 3 m in the western sector and the displacement height was reduced to below 15 m. This illustrates the necessity of choosing values for d and z_0 that together give a correct wind speed estimate in forested areas and that d and z_0 are not truly independent (see also Dellwik et al., 2006).

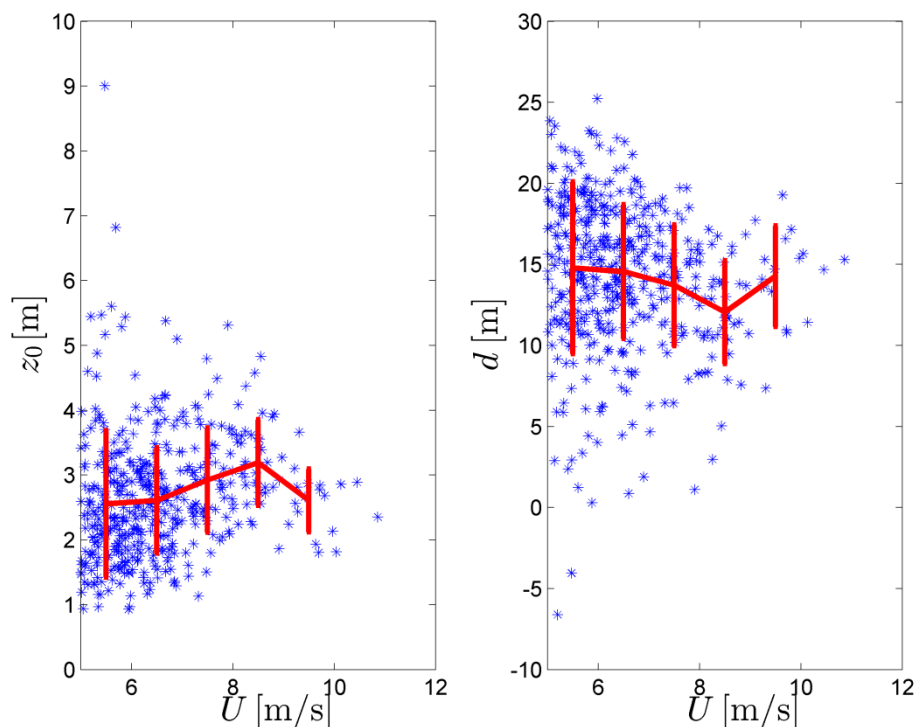


Figure 3-6: Roughness length (left) and displacement height (right) estimates as a function of measured wind speed. Blue stars correspond to the single profile estimates and the full red lines show the piecewise mean values over 1m/s intervals.

The drag forces on the trees are expected to change slightly with wind speed, either because the canopy structure is streamlined by the wind or because the wake behind the trees changes character with increasing wind speed (see for example Dellwik and Jensen, 2005, and Brunet et al., 1994). In Figure 3-6, the roughness and displacement height estimates are plotted against the $2h_c$ level mean wind speed at Ryningsnäs for the westerly wind directions. There are some weak trends in the data, but due to the large scatter in the estimates, no clear wind speed dependency could be concluded.

Westerly sector – including temperature effects

For the most common westerly wind directions, the local influence from the turbines is negligible and the effect of the clearing is small. However, there are other heterogeneities in the terrain close to the mast, in form of additional clearings as well as change of surface elevation, which can influence the measurements. From detailed analyses of flux-profile relationships, we expect

this influence to be relatively small, but further modelling studies are needed to quantify the influence of heterogeneities on the measurements.

Figure 3-7 shows how the mean wind speed at $z/h_c \approx 5$ vary with atmospheric stratification for the wind direction sector $[235^\circ, 275^\circ]$. The dashed vertical lines correspond to the limitations of the stability intervals in Table 3-1. The highest wind speed occurs during near-neutral conditions ($|h_c/L| < 0.02$), where the near-surface turbulence levels of u_* are high.

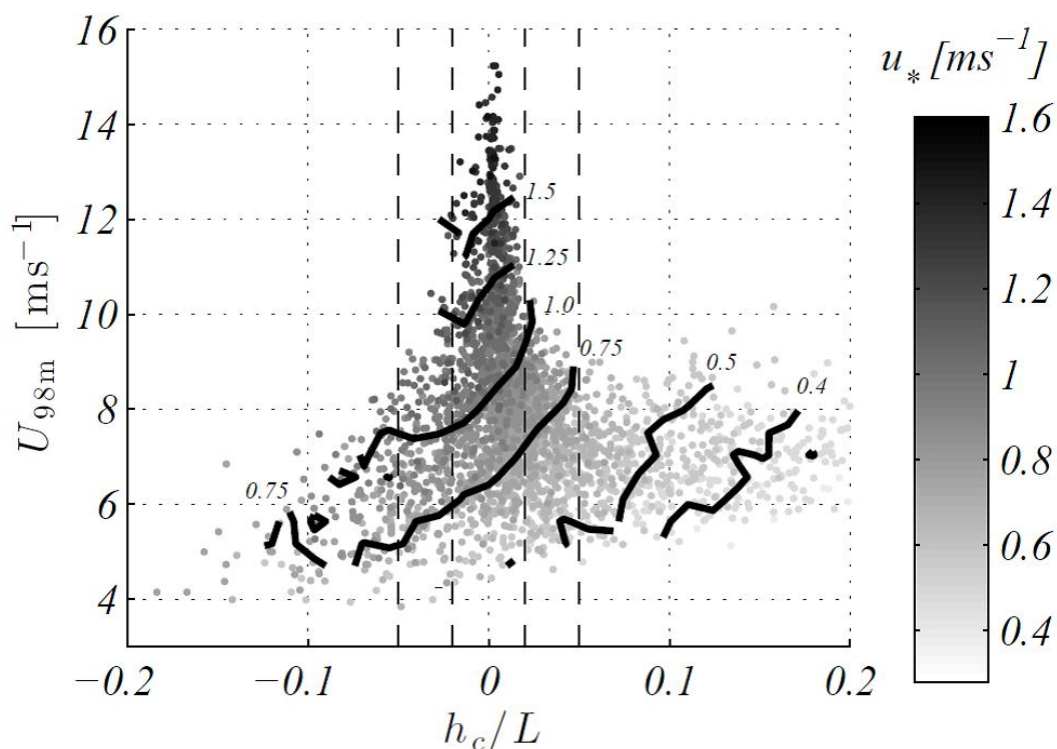


Figure 3-7: Mean wind speeds at $z/h_c \approx 5$ as a function of atmospheric stratification. Low-wind speed situations and non-stationary data are excluded.

The lowest mean wind speed situations occur during unstable conditions ($|h_c/L| < 0.05$), typical for sunny and warm days. During stable stratifications ($|h_c/L| > 0.05$), the 98 m mean wind speed is approximately 7 m/s with strong variation in surface values of u_* .

Figure 3-8 shows profiles of mean wind properties with height; (a) mean wind speed, (b) shear coefficient, (c) wind direction change with height and (d) turbulence intensity. The symbols are explained in Table 3-1. As was shown above for the 98 m measurements, the highest wind speeds occur during near-neutral conditions (crosses) and the lowest during unstable conditions (open symbols). The shear of the wind profile is generally high (b), with the highest values occurring during stable conditions when mixing is limited by the temperature inversion and the lowest during unstable conditions when mixing is enhanced. The dashed line shows $a = 0.2$ which is the shear design criterion by IEC for the A1 class turbines (IEC 61400-1 Edition 3; *Wind turbines - Part 1: Design requirements*, August 2005). The wind direction

showed marked changes with height (c)¹ and the wind direction turned more for the stable conditions. The turning is an effect caused by the Coriolis force, and is more pronounced for low boundary layers, which in turn are connected with stable situation. This effect effectively increases the shear of the wind profile, but it is usually not accounted for. The turbulence levels are generally high (d) which is expected given the high roughness of the forest. The dotted line in (d) denotes $\sigma_u / U = 0.16$, which is another of the IEC design criterion for class A1 turbines.

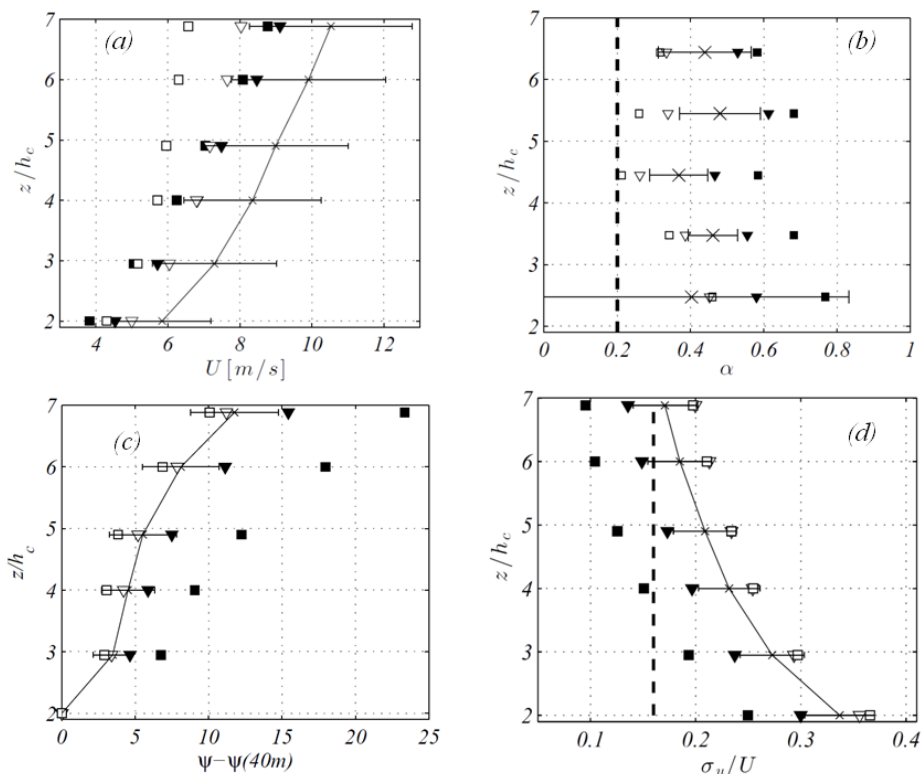


Figure 3-8: Profiles of mean wind speed (a), total turbulence intensity (b), (c) wind turning and (d) turbulence intensity. Symbols are given in Table 3-1.

In summary, the wind conditions at the Ryningsnäs site show high value of the shear coefficient and turbulence intensity, when the wind speed is high. During stable conditions, the wind speed and turbulence intensity are lower, but the shear coefficient is higher. The shear coefficient is however lower during unstable conditions, but then the wind speed is low and the turbulence intensity high. Using the IEC A1 design criteria as guidelines, favourable wind conditions for turbines never occur at Ryningsnäs.

¹ The Ryningsnäs mast itself is slightly twisted such that a small part of the wind direction change is an artifact. The twist of the mast was estimated to approximately 5°.

Wind climate at Ryningsnäs:

The previous section showed how certain wind characteristics changed with the atmospheric stratification. However, low-wind speed data as well as a multitude of low wind speed non-stationary situations were excluded from the analysis, such that the results presented in Figure 3-7 and Figure 3-8 are biased towards high wind speed situations.

For the whole measurement period of the experiment, the wind roses shown in Figure 3-9 below, give a more correct impression of the wind resource at the Ryningsnäs site. As expected, the strongest winds occur in the westerly directions. For the $z/h_c \approx 5$ level (a), shading effects of the turbines can be seen as enhanced low wind speed areas in the southern and northeasterly directions. Besides the data that were heavily afflicted with spikes, all measurements are used. For the whole experiment period, the mean wind speeds at $z/h_c \approx 5$ and $z/h_c \approx 7$ were 5.9 m/s and 7.0 m/s, respectively, but as these estimates are based on only 85 % of the dataset, they are not precise.

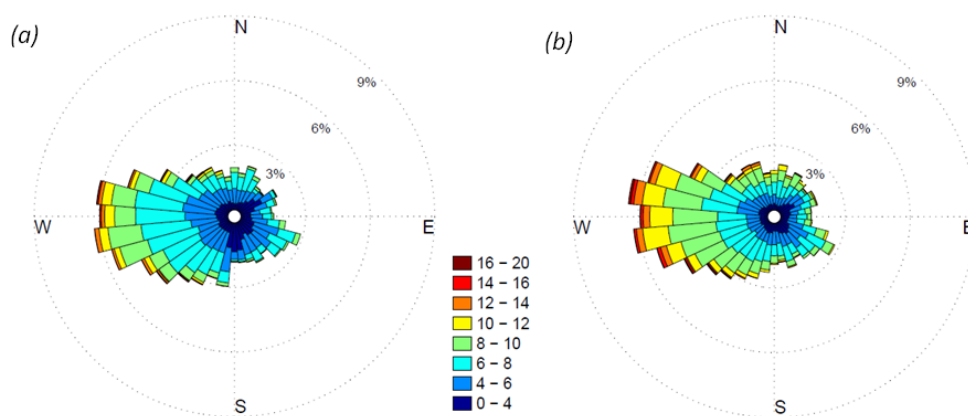


Figure 3-9: Wind roses at $z/h_c \approx 5$ (a) and $z/h_c \approx 7$ (b).

Structures in turbulent flow:

In the research field of turbulence over vegetation canopies of which forest is a special case, there has over the past ten years been a strong focus on turbulent structures. The research covers both the description of the structures (Finnigan et al 2009), the detection of the structures and a statistical description of their occurrence (Collineau and Brunet 1993ⁱⁱ, Thomas and Foken 2005) and methods for dividing the turbulence into structures and background turbulence (Thomas and Foken 2007).

Also in this project, turbulent structures have been in focus, although the work using the more classical description of the flow using Reynolds' decomposition into mean wind and statistics describing how the turbulence fluctuates around the mean has dominated. For estimation of wind turbine loads, large coherent structures in the flow can be damaging.

It has been suggested (Raupach et al 1996) that the organized structures over forests arise from a dynamical instability that comes from the inflection point in the wind profile. This instability leads to wave disturbances, which are rapidly distorted by the turbulence as well as of higher order instabilities (Finnigan et al 2009). Because of the intermittent nature of the structures, they are not generally visible as a peak in the Fourier spectrum. Even so, the period of the frequencies may be very well defined and is in the case of Ryningsnäs about 30 seconds. The frequency is however very ill-defined because of the intermittency. This results in a poor representation of the structures by Fourier spectrum which is based on waves with a fixed frequency. Another way to study the structures is by the wavelet technique (Torrence and Compo 1998) which is based on determining the correlation of a time series at a certain time with a perturbation (wavelet) that is finite in space. The wavelet is then moved to the next time step and at the final time step the process start all over but with the wavelet elongated slightly in space. In this way the time series can be mapped as correlation with a certain wavelet at a time t and of certain width k .

The inflection point in the wind profile is a necessary condition for a Kelvin-Helmholtz type of disturbance that grows exponentially with time, but it is not a sufficient one. It may therefore be possible to study the physics of the disturbance in more linear conditions when the diabatic stability is strong and thus limiting the vertical motions. 30 minute periods from Ryningsnäs was scanned for spectral peaks that would indicate waves with a period of about 30 seconds. Several time series with distinct gravity waves were found. Figure shows an example of a time series from the sonic at 80 meters, where the time series has been smoothed by a 1 s running mean. A clear wave disturbance is appearing at 1200 s but only persists through a couple of minutes before it breaks down to turbulence. In the lower part of the figure a wave energy plot is shown, with scale of the disturbance on the y-axis and time for the disturbance at the x-axis. From the wavelet energy plot the period of the wave is approximately 30 s. It also shows that initially the energy is focused at a narrow period band, but as the wave break the energy is distributed to wide band of periods.

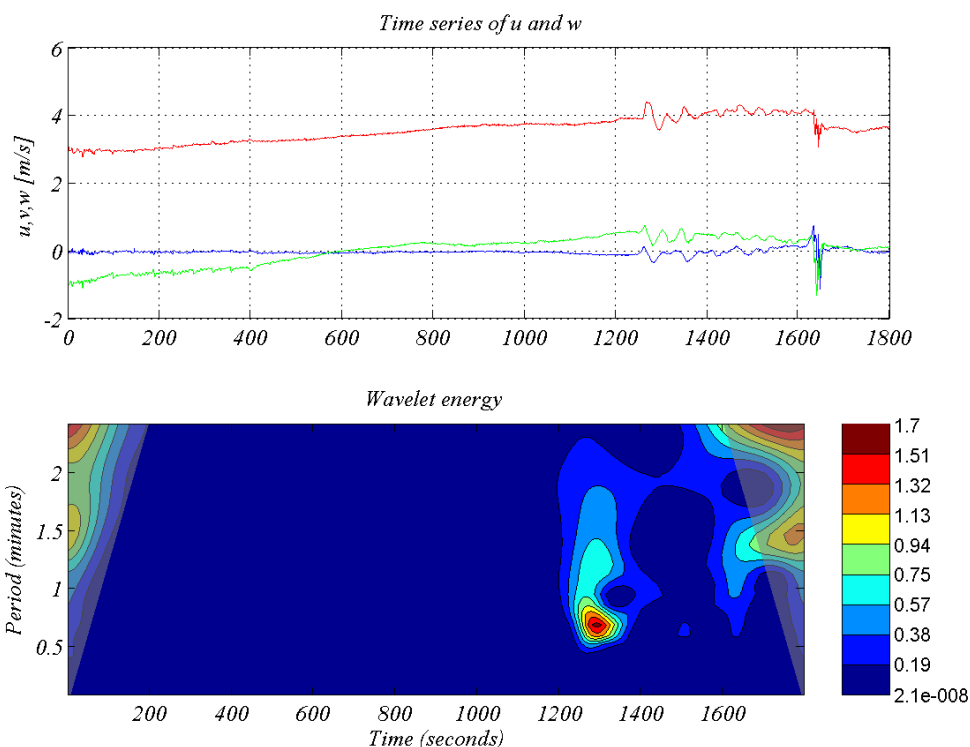


Figure 3-10: Upper: Time series of u (red), v (green) and w (blue) at 80 meters. Lower: wavelet energy for u at 80 meters. The shaded area is subject to edge effects and should not be trusted.

By using a wavelet that is very limited in space it is possible to detect sudden changes in a signal. To illustrate this, the wavelet energy for the Mexican hat wavelet of a fixed period is plotted together with a fictive time series with a clear disturbance in Figure 3-11. The sudden changes in the time series are located at the same time as the zero crossings of the wavelet signal and are noted by red dots.

This approach was used together with another wavelet, the Morlet wavelet, which has more wave crests and thus are better defined in frequency space. The Morlet wavelet was used to determine the most probable period of the coherent structures at a particular 30 minute period. The Mexican hat wavelet was then used to determine the start and end of the coherent structure. In this way the part of the structure that resembles a Mexican hat wavelet can be extracted from the time series.

The analysis was performed for over a year of data and showed that for the lowest height, 26 meters, the coherent structures where responsible for about 50 % of the variance in u . At higher heights, 80 and 120 meter, between 30-40 % of the variance in u could be attributed to the coherent structures. The wavelet approach also show that the coherent structures are more effective in transporting momentum than transporting heat. Somewhere around 50 % of the momentum transport comes from the coherent motions, but not more than 20 % of the mean heat transport. The scatter in the data is however large, and contribution to the variance by coherent structure span from 0 to almost 100 %.

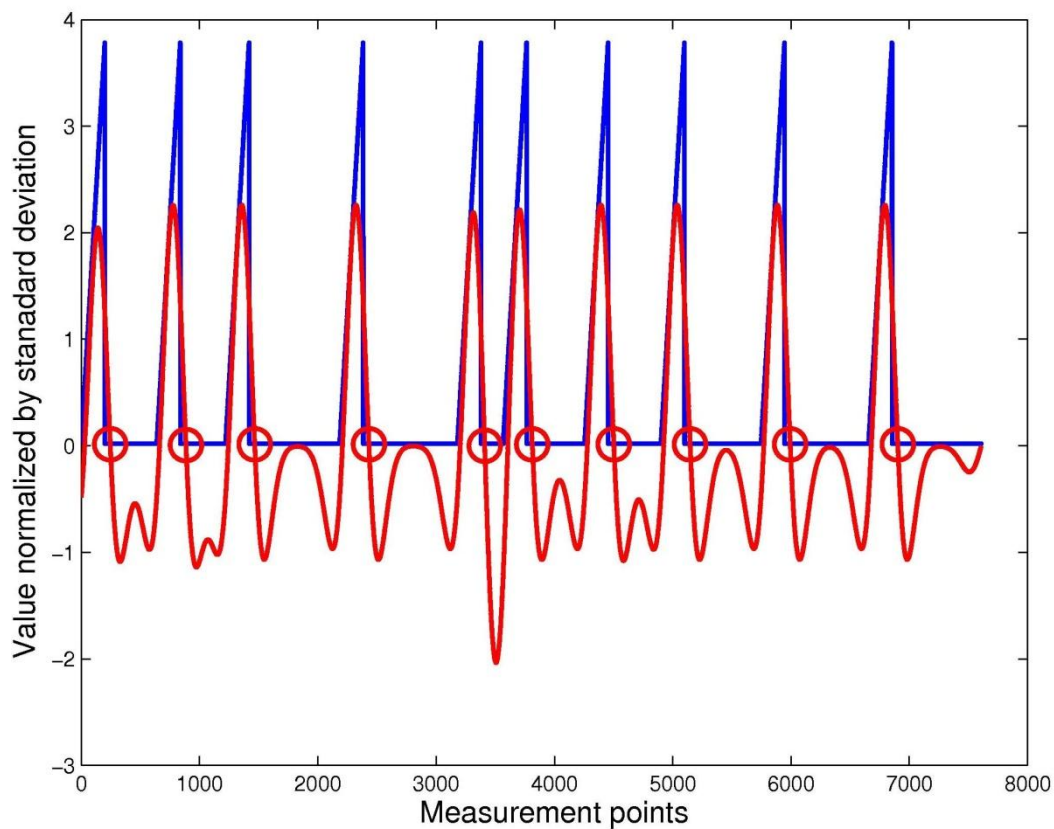


Figure 3-11: A constructed time series is used together with the wavelet energy of the Mexican hat wavelet to illustrate that zero crossings of the Mexican hat wavelet signal is located at sudden shifts in the time series.

The wavelet technique is however very tricky, as is perfectly well illustrated by Figure 3-12 and Figure 3-13. The two figures both show the same period but the former from 40 meters and the latter from 98 meter. In the 40 meters wavelet energy plot, the wave disturbance has a wide distribution in period. This is connected to the much more "dirty" time series (Figure 3-12, upper panel) that also has a lot of variance from turbulent motions. The same time period but at 98 meters has a time series much more dominated by the wave, pointing out that the turbulence is suppressed by stable stratification, while gravity waves need stable stratification to persist.

The wavelet energy plot from 98 meters show a much narrower distribution, in period space, of the wave disturbance so extraction of the wave pattern by the method described above would be more successful there. The typical time series is more like the one in Figure 3-12, even at 100 meters height. This makes the wavelet approach described above subject to large uncertainties and it is still an on-going work to evaluate it against other techniques.

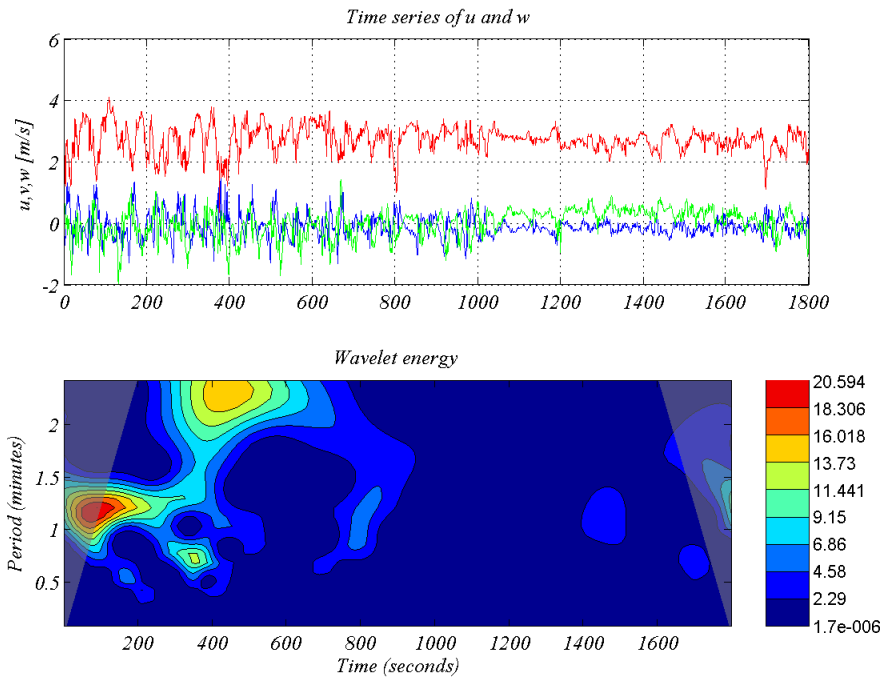


Figure 3-12: Time series of wind velocity and wavelet energy from 40 meters. The time period is the same as in Figure 3-13.

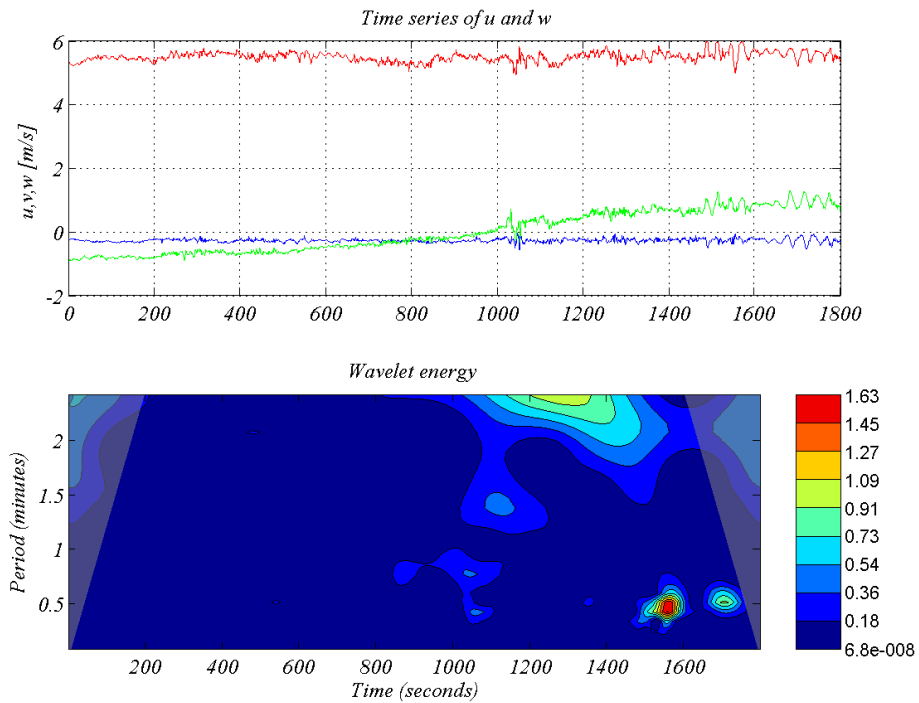


Figure 3-13: Time series of wind velocity and wavelet energy from 98 meters. The time period is the same as in Figure 3-12.

Results from lidar measurements

Between April and December 2011 a Zephir wind lidar was operating at the site. The Zephir lidar is a continuous beam lidar that focuses the beam on a specific height and measures the Doppler shift on the backscatter. The lidar was set to measure at 10, 25, 40, 70, 98, 140, 170, 200 and 250 meters height. The laser is tilted 30.4 degrees from the vertical and rotates, making a cone with about 59 m radius at 100m height. With the current height set up, the lidar made approximately 50 3-second scans at each height during a half hour. The software within the lidar then determines the wind vector based on the 147 data points collected during that 3-second scan (49 points on the circumference of the cone and three laps). This means that the constructed 30 minute mean consists of part time average and part spatial average. The zephir lidar cannot make a difference between the sign of the wind velocity, and because of that the wind direction is determined ± 180 degrees.

To overcome this problem the lidar takes a small reference measurement of wind direction at approximately 2.5 meters height. In Ryningsnäs, because of the forest and the clearing, the flow often had a reversed direction at this height. This caused the wind direction to vary significantly and the correlation with the two tower instrumentations to be very bad. In order to correct the wind direction measurements from the lidar, all individual 3-second scans were checked against the sonic-wind direction at 98 meters. If the wind direction from the reference system of the lidar was more than $\pm 90^\circ$ off the wind direction from the 98m-sonic, then the lidar wind direction was changed 180°. A scatterplot with the wind direction from the sonic-anemometer at 98 meters and the wind direction from the lidar at 98 meters after this correction is shown in Figure 3-14.

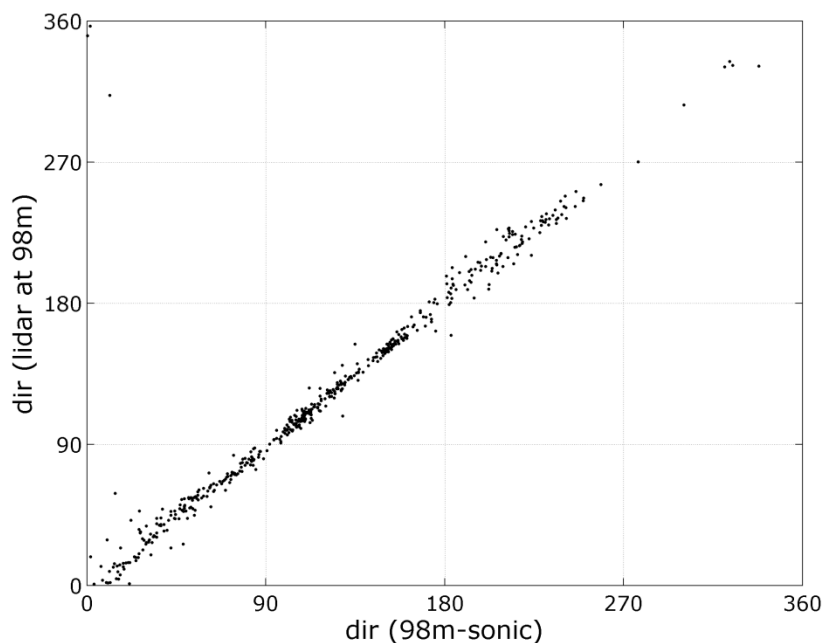


Figure 3-14: Wind direction from the 98m-sonic and the Zephir lidar at 98 meter height.

An analytical model for the wind veer described in Grisogono (2011) has been evaluated against the measurements. The analytical theory is a more advanced solution to the classical Ekman layer problem, where the wind direction α is determined by $\alpha = \text{atan}(v/u)$. The classical solution to this is found by assuming that u and v can be described by

$$\begin{aligned} u(z) &= u_g (1 - e^{-I(z)} \cos(I(z))) \\ v(z) &= u_g e^{-I(z)} \sin(I(z)) \end{aligned} \quad (3-3)$$

Where u_g is the geostrophic wind and I is:

$$I(z) = \sqrt{\frac{f}{2K}} z \quad (3-4)$$

Where f is the coriolis force and K is an eddy diffusivity.

By assuming that K can be weakly dependent on z a new formulation for K was found. In the first order approximation of this theory I is expressed as:

$$I(z) = \sqrt{\frac{2af}{K_0}} z \quad (3-5)$$

where a is a constant and K_0 is the amplitude of $K(z)$. In Figure 3-15, Figure 3-16, Figure 3-17, and Figure 3-18 this theory is shown together with measurements from the sonic anemometers, the wind vanes and the lidar.

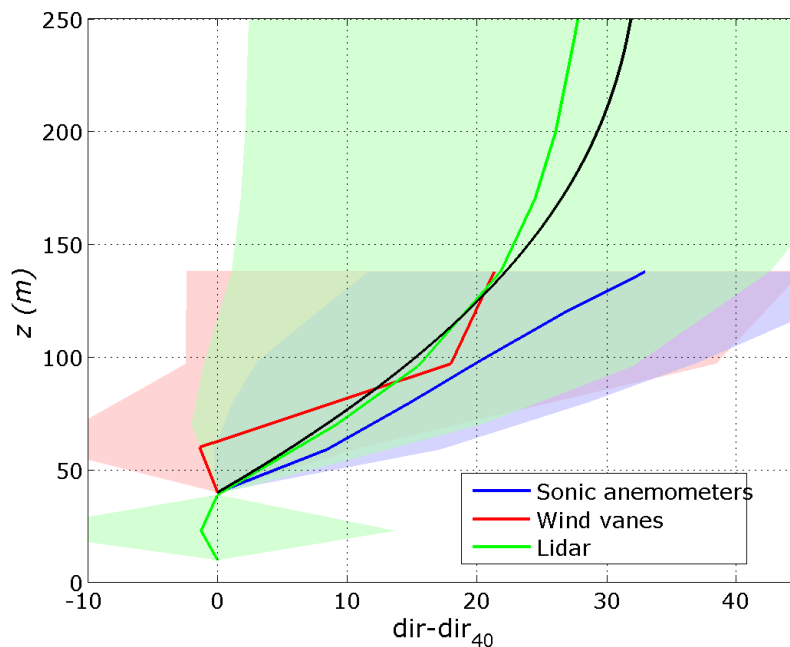


Figure 3-15: The change in wind direction from 40m in very stable conditions. Colored lines are from measurements, with shaded areas that indicate the standard deviation. Black line is calculated from theory.

The constant a is set to be equal to 5 in the figures, based on recommendations by Grisogono 2011 and K_0 is was determined, after comparison with measurements of $K(z)$ to roughly follow the equation:

$$K_0 = l \frac{\kappa}{\phi(l, L)} e^{1/2} \quad (3-6)$$

where l is in turn given by

$$l = \frac{1}{\frac{1}{115} + \frac{1}{\delta}} \quad (3-7)$$

and δ is the boundary layer height. The boundary layer height was not measured, so it was determined by the Rossby-Montgomery formula

$$\delta = C \frac{u_*}{f} \quad (3-8)$$

where C was set to 0.1 after best fit with the boundary layer height determined from a week of soundings, performed at the site in spring 2011. This value of C is rather low compared to what is found in the literature and surprisingly low considering that the rough surface would produce a lot of mechanical turbulence that could increase the boundary layer height.

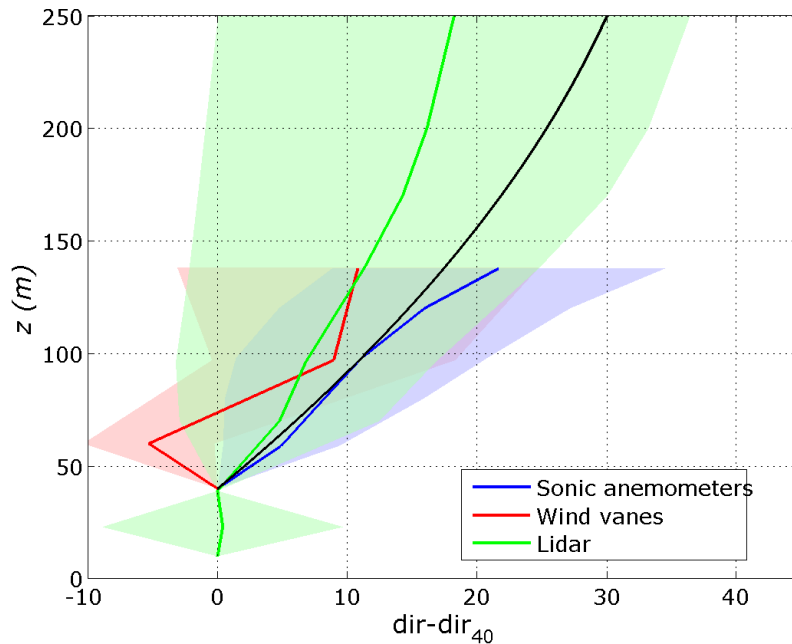


Figure 3-16: The change in wind direction from 40m in stable conditions. Colored lines are from measurements, with shaded areas that indicate the standard deviation. Black line is calculated from theory.

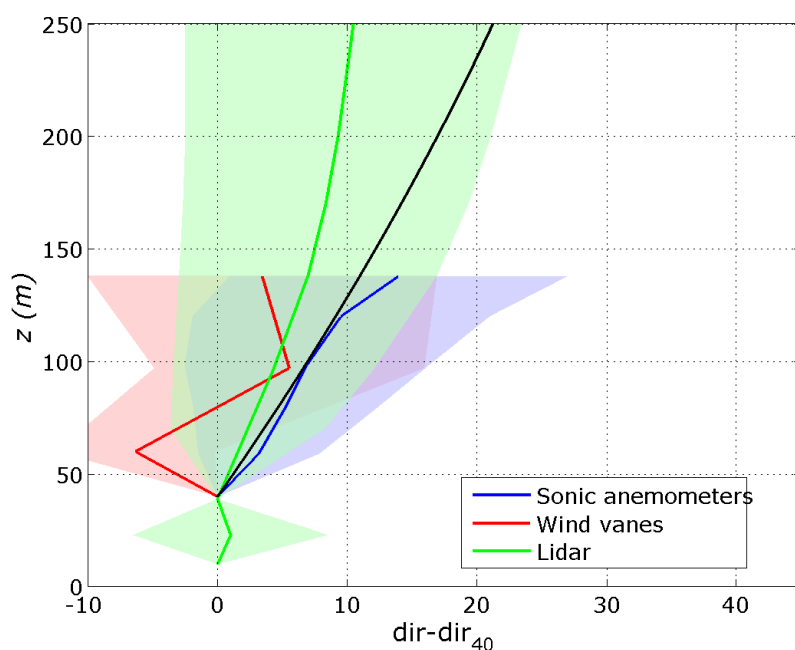


Figure 3-17: The change in wind direction from 40m in neutral conditions. Colored lines are from measurements, with shaded areas that indicate the standard deviation. Black line is calculated from theory.

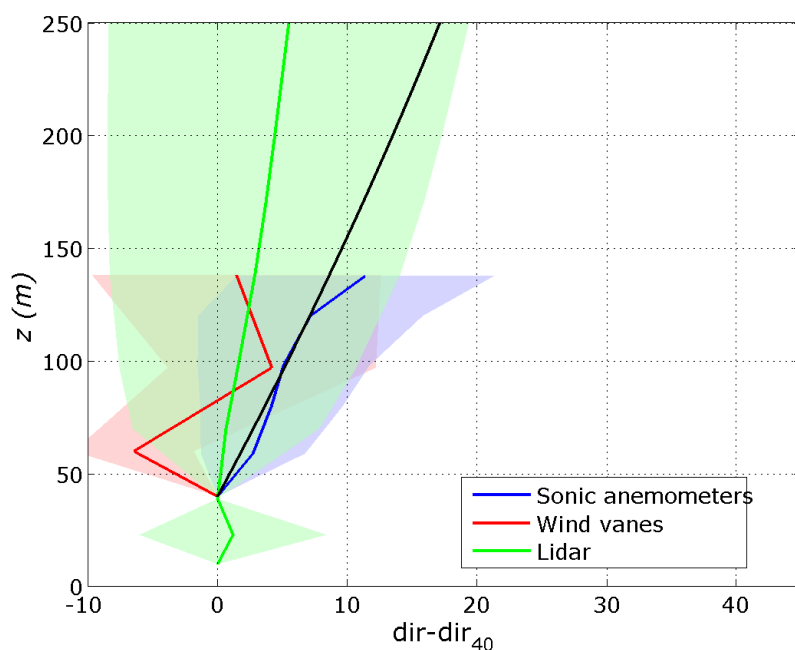


Figure 3-18: The change in wind direction from 40m in unstable conditions. Colored lines are from measurements, with shaded areas that indicate the standard deviation. Black line is calculated from theory.

The wind vanes (red line) were not calibrated to each other and therefore the wind veer is poorly determined. The increased veer with more stably stratified flow is however present with all three measurement techniques. The analytical theory is in good agreement with the measurements for very stable flow. It is noticeable that the wind veer is in average about 20° over a typical rotor diameter for very stable flows despite the very rough surface conditions. The large standard deviation in all three measurement techniques reflect the variability in boundary layer height, which is a difficult parameter to model, partly because lack of quality measurements and partly because of the large scales of the motions dominating at vertical scales approaching the boundary layer height, which makes it a more non-linear problem than surface layer turbulence.

In more neutral flow, the veer is reduced more than predicted by the analytical theory. It is not clear whether this is due to variation in the constant a , flaws in the equation for K_0 or something else. The boundary layer height should be better represented by the Rossby-Montgomery formulation in near neutral conditions but large uncertainties in determination of the boundary layer height could also add to the disagreement between measurement and theory, especially for unstable conditions.

The wind profile is shown in Figure 3-19 to Figure 3-24. Data was chosen so that all three instrumentations were working simultaneously, and none of them were flagged for bad quality. The sectors where turbine wakes and tower shadows disturbed either of the three instruments were omitted. The wind profiles from sonic anemometers and cup anemometers are in very good agreement. It is only for the unstable case (Figure 3-24) where the turbulence intensity is the biggest that there is a noticeable disagreement. The biggest part of this disagreement comes from the fact that from the sonics the raw data has been evaluated as the mean wind in the mean wind direction. The cups on the other side measure the wind speed, the length of the wind vector at every instant. If the wind direction varies a lot during the averaging period, that will result in a difference between the wind velocity and the wind speed. For very stable conditions all three measurement techniques agree very well. The span of the data is also very similar, reflecting a high correlation of the individual data points. For very stable conditions the turbulence intensity is the lowest, and the cups and sonics are expected to agree to a high extent. The lidar measurement also benefit from low turbulence intensities as the determination of the wind vector from the Doppler shift data require the fit of an absolute sine-wave to the 147 individual data points that each scan consist of. If the wind field is spatially homogenous the data points will be close to the theoretical sine wave and the fit will be determined with good precision. If there are large variations in the wind field at the scanning height this will result in a wider distribution of the data points making the fit less well determined.

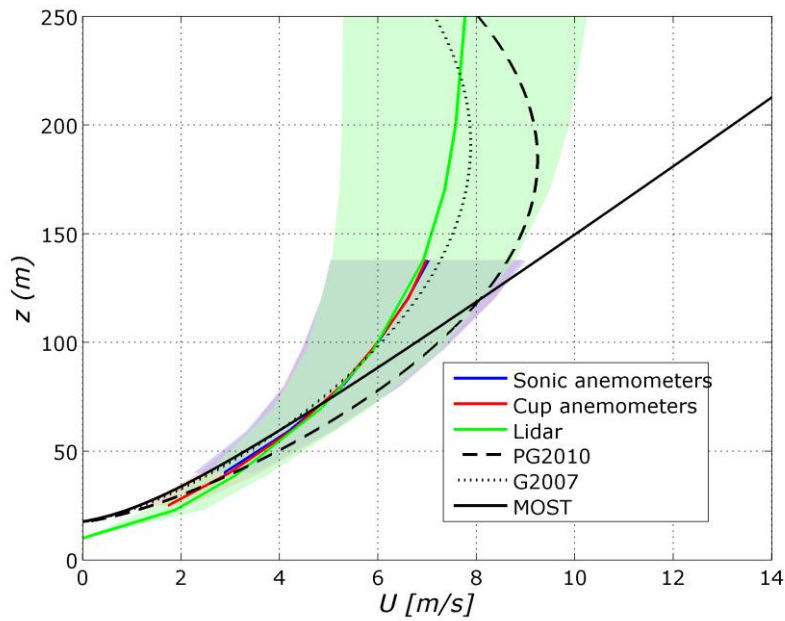


Figure 3-19: The wind profile in very stable conditions. Colored lines are from measurements, with shaded areas that indicate the standard deviation. Black solid line from MOST, dashed line from Pena et al and dotted line from Gryning et al.

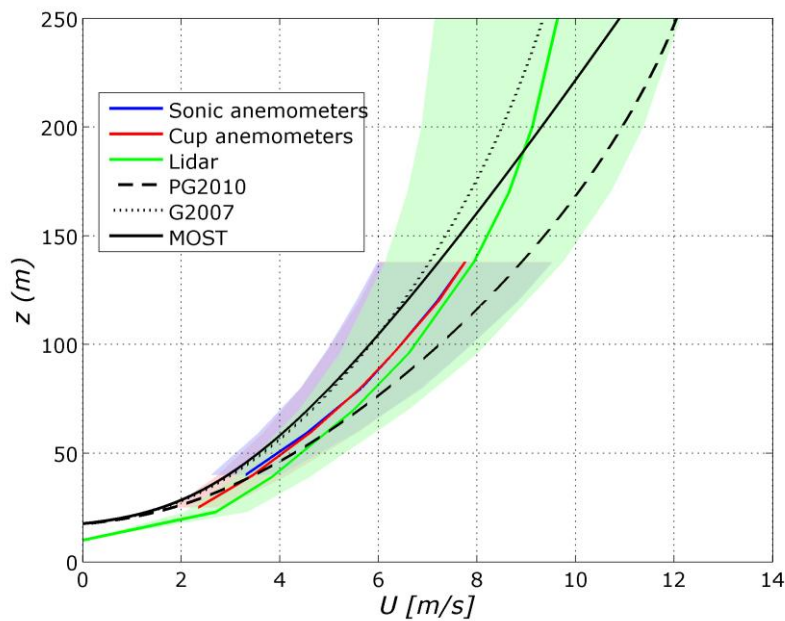


Figure 3-20: The wind profile in stable conditions. Colored lines are from measurements, with shaded areas that indicate the standard deviation. Black solid line from MOST, dashed line from Pena et al and dotted line from Gryning et al.

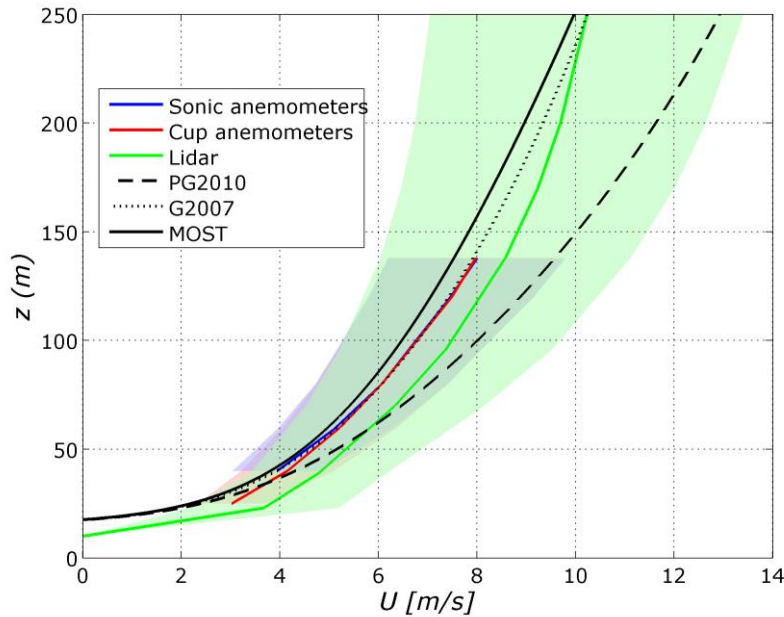


Figure 3-21: The wind profile in stable, near neutral conditions. Colored lines are from measurements, with shaded areas that indicate the standard deviation. Black line is the Monin-Obukhov similarity theory.

It is most probably a systematic error in the sine wave fit that causes the big overestimation seen in Figure 3-24. It is unfortunate that in turbulent conditions the lidar systematically overestimates the wind, but if the problem is related to the inhomogeneous wind field it should theoretically be possible to improve the results by using another type of fitting function. The lidar used did not however permit sampling of individual data points in the scan, and thus this option was not possible. The total overestimation is a little more than 0.7 m/s at 100 meters for unstable conditions, but the lidar data has also been evaluated as the wind speed, so a small part of that overestimation, about 0.1 m/s can be contributed to the difference between the wind speed and the mean wind in the mean wind direction.

Along with the measurements, modelling of the wind by the Monin-Obukhov Similarity Theory (MOST) is shown with a black line.

The wind profile from MOST is given by the expression

$$\frac{U(z)}{u_*} = \frac{1}{\kappa} (\ln((z-d)/z_0) - \Psi_m((z-d)/L) + \Psi_m(z_0/L)) \quad (3-9)$$

where $\kappa=0.4$ is the von Kármán constant and Ψ_m is the integrated stability function. The displacement height was set to 15 meters and the roughness length to 2.6 meters after the best fit for neutral data with the sonic set-up in the forest direction.

Other attempts found in the literature to Model the winds at heights where the MOST is no longer strictly applicable include Gryning et al. 2007 and Peña et al. 2010. In both the above, the wind profile is found after constructing a master length scale, the mixing length. The wind profile expression from

Gryning et al. is shown in the figures by a dotted line and the profile from Peña et al. is shown by a dashed curve. The mixing length is in both cases found by merging the height over the displacement height, a height that controls where the mixing length peaks and a length scale depending on the boundary layer height that controls and limits the growth of the mixing length for the upper part of the boundary layer. The length scale of the wind profile l_m from Gryning et al. 2007 is:

$$\frac{1}{l_m} = \frac{1}{\kappa z} + \frac{1}{\kappa l_{MBL}} + \frac{1}{\kappa(\delta - z)} \quad (3-10)$$

where l_{MBL} is a length scale controlling the maximum of the mixing length (MBL stands for Middle of the Boundary Layer, see the Gryning et. al 2007 for the rather complicated full expression). After some algebra and justified approximations the wind profile reduces to, for unstable conditions:

$$\frac{U(z)}{u_*} = \frac{1}{\kappa} \left[\ln \left(\frac{z-d}{z_0} \right) - \Psi_m \left(\frac{z-d}{L} \right) + \frac{z-d}{l_{MBL}} - \frac{z-d}{\delta} \left(\frac{z-d}{2l_{MBL}} \right) \right] \quad (3-11)$$

and for stable conditions

$$\frac{U(z)}{u_*} = \frac{1}{\kappa} \left[\ln \left(\frac{z-d}{z_0} \right) + 5 \frac{z-d}{L} \left(1 - \frac{z-d}{2\delta} \right) + \frac{z-d}{l_{MBL}} - \frac{z-d}{\delta} \left(\frac{z-d}{2l_{MBL}} \right) \right] \quad (3-12)$$

The boundary layer height δ can then be determined in the same way as above, with the Rossby-Montgomery formulation.

The mixing length formulation from Peña et al 2010 is:.

$$\frac{1}{l_m} = \frac{1}{\kappa z} + \frac{(\kappa(z-d))^{d_p-1}}{\eta^{d_p}} \quad (3-13)$$

where d_p is a constant, usually $d_p=1$, but d_p has also been suggested to be $5/4$ (Lettau 1962)ⁱⁱⁱ. The value of d_p controls how fast l_m approaches its limiting value. The length scale η is closely related to l_{MBL} and controls the maximum value that the mixing length approaches. In the determination of η and l_{MBL} two constants, A and B has to be determined. The variation with stability of the constants A and B are still an open question and adds greatly to the uncertainty determining the wind profile in this way. Stability variation of A and B was in this work taken from Garratt 1992.

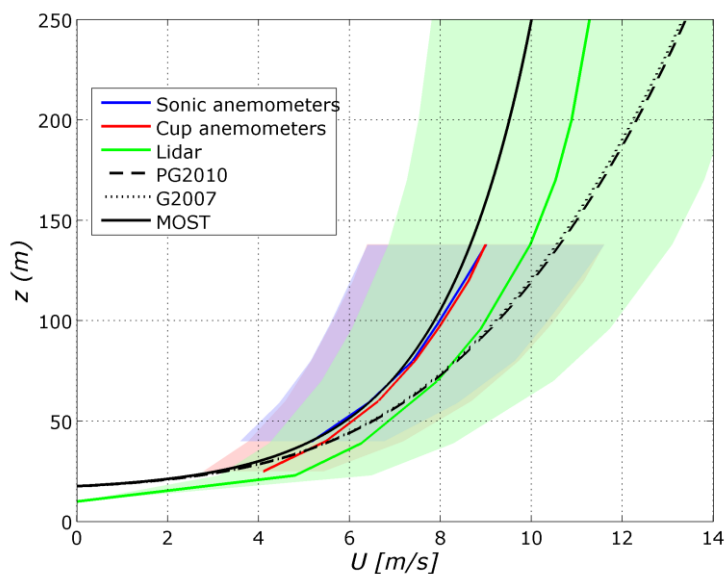


Figure 3-22: The wind profile in neutral conditions. Colored lines are from measurements, with shaded areas that indicate the standard deviation. Black solid line from MOST, dashed line from Pena et al and dotted line from Gryning et al.

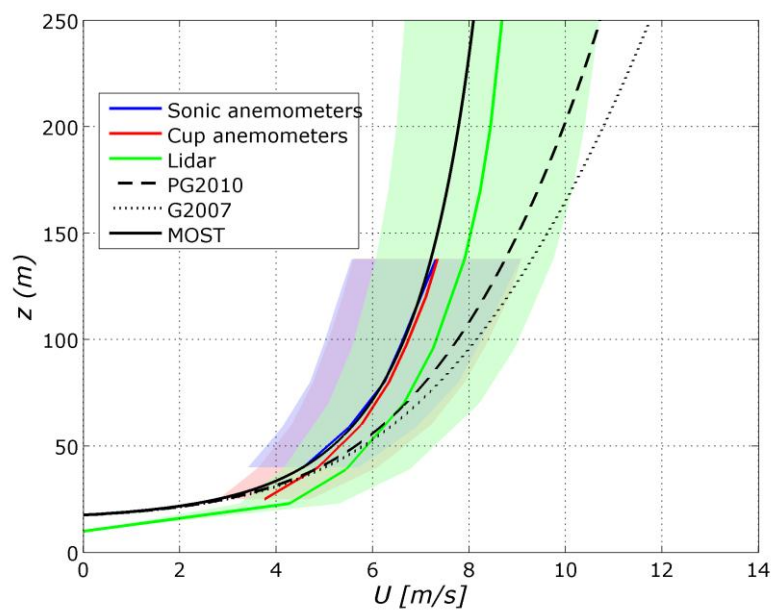


Figure 3-23: The wind profile in unstable, close to neutral conditions. Colored lines are from measurements, with shaded areas that indicate the standard deviation. Black solid line from MOST, dashed line from Pena et al and dotted line from Gryning et al.

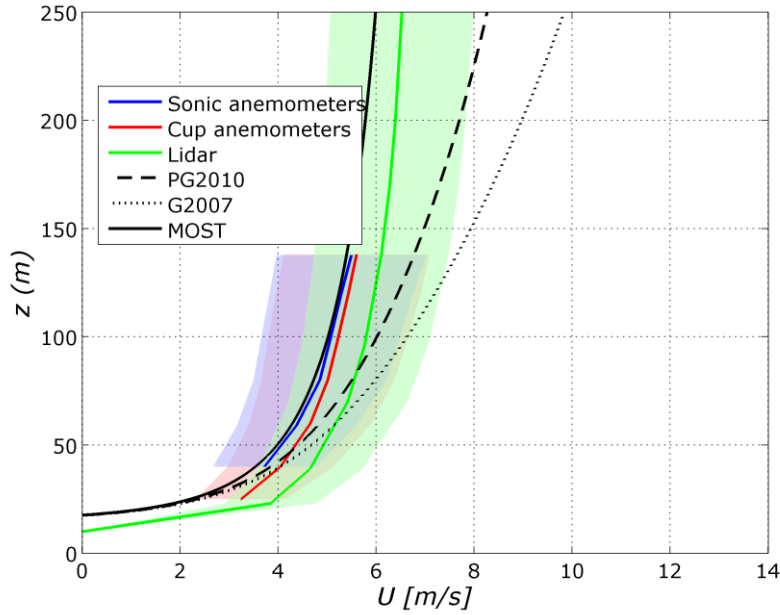


Figure 3-24: The wind profile in unstable conditions Colored lines are from measurements, with shaded areas that indicate the standard deviation. Black solid line from MOST, dashed line from Peña et al and dotted line from Gryning et al.

For unstable conditions the wind profile of Peña et al 2010 reduces to the expression

$$\frac{U(z)}{u_*} = \frac{1}{\kappa} \left[\ln \left(\frac{z-d}{z_0} \right) - \Psi_m \left(\frac{z-d}{L} \right) + \frac{1}{d_p} \left(\frac{\kappa(z-d)}{\eta} \right)^{d_p} - \frac{1}{1+d_p} \frac{z-d}{\delta} \left(\frac{\kappa(z-d)}{\eta} \right)^{d_p} - \frac{z-d}{\delta} \right] \quad (3-14)$$

and for stable conditions it becomes

$$\frac{U(z)}{u_*} = \frac{1}{\kappa} \left[\ln \left(\frac{z-d}{z_0} \right) + 5 \frac{z-d}{L} \left(1 - \frac{z-d}{2\delta} \right) + \frac{1}{d_p} \left(\frac{\kappa(z-d)}{\eta} \right)^{d_p} - \frac{1}{1+d_p} \frac{z-d}{\delta} \left(\frac{\kappa(z-d)}{\eta} \right)^{d_p} - \frac{z-d}{\delta} \right] \quad (3-15)$$

The formulation of l_{MBL} contains the stability function of δ/L , it has been suggested that the limit of applicability for the stability function in stable conditions is $z/L < 1$ which could lead to underestimation of the length scale in stable conditions since that limit is frequently exceeded there. In order to avoid this problem the stability function was limited to its value for $z/L=1$. Modelling of the wind with both the above formulations have been undertaken, but no set of the model constants we tried could produce a series of wind profiles that was an improvement from the MOST as a whole. Individual profiles in certain diabatic conditions did however accurately describe the wind, and although the approach seems promising it is also sensitive to an incorrect set of model constants and an inaccurate description of the boundary layer height. The uncertainty of estimating the boundary

layer height in unstable conditions could partly be responsible for the positive bias in Figure 3-23 and Figure 3-24.

As can be seen in Figure 3-22 the MOST profile is underestimating the wind slightly for neutral conditions. This is a result of slightly too high value of the roughness length. As noted in Figure 3-5 the roughness is slightly lower in the clearing and the clearing direction is included in the data selected for Figure 3-15 to Figure 3-24. In stable conditions the wind speed is also underestimated by the MOST-model. We found a stability dependence of the roughness length for stable stratification that could be modelled by the expression from Zilitinkevich et al. (2009)

$$z_{0m} = z_{0m_n} (1 + 8.13h_c/L)^{-1}, \quad L \geq 0 \quad (3.16)$$

where z_{0m} is the roughness length in neutral conditions. Note that in Figures 3-19 to 3-24 the roughness length is constant.

Spectra

Spectra was evaluated for stationary data from the forest sector with $U_{40} > 3$ m/s. The data was sorted according to stability and average accordingly. The resulting spectra are shown in Figure 3-25. All the heights are included in the figure, and the stability ranges from stable to unstable. Apart from a small contribution from boom vibrations and some high frequency noise, the spectra is falling on a -2/3 line of decay. The stable data is peaking earlier at a higher frequency than, as it should according to theory. In order to reduce the scatter of the spectra another scaling approach was undertaken. The frequency was now scaled with the integral time scale, defined as

$$\Gamma = \int_0^{\infty} r(t') dt' \quad (3.16)$$

Where r is the autocorrelation function

$$r(t') = \frac{\overline{u(t)u(t+t')}}{\overline{u^2}} \quad (3.17)$$

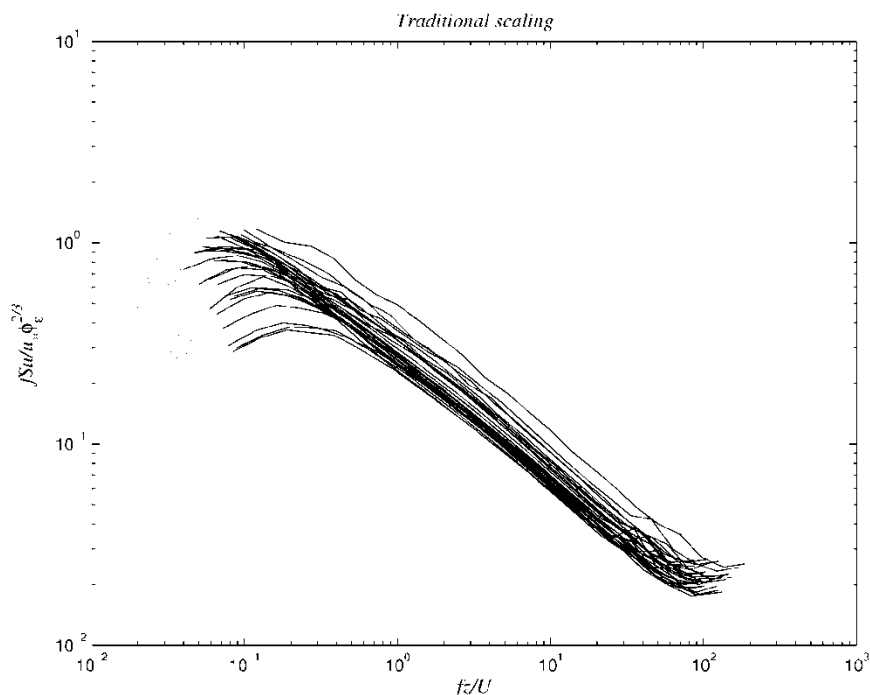


Figure 3-25: The power spectrum for u. The figure includes spectra from all six measurement heights and for the stability range stable to unstable. Spectra have been scaled in a traditional way with the stability function for dissipation and the height over the mean wind speed.

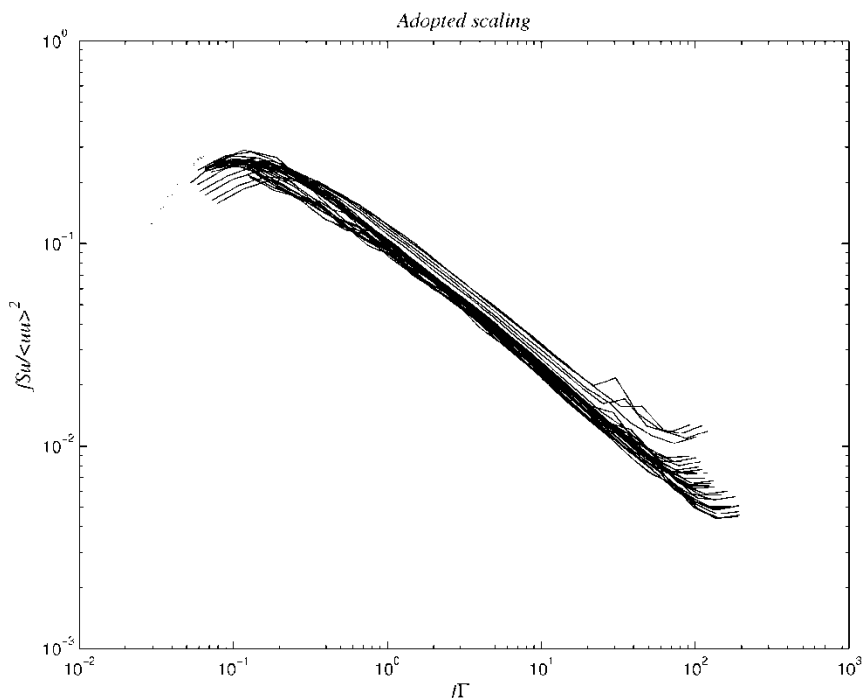


Figure 3-26: Power spectrum for u. Each line is the mean spectrum for a measurement height averaged over a stability class. Scaling by the variance and the integral time scale gather the spectra around a universal shape with quite low scatter.

This makes the spectra collapse in the frequency space. The energy density was then scaled by the variance so that the frequencies dominating the variance end up at the same vertical coordinate. The resulting spectra are shown in Figure 3-26.

Compared to the traditional scaling the approach with the variance and the integral time scale gather the spectra with less scatter. Note that the axis in Figure 3-25 and Figure 3-26 span equally many decades. This is hopeful because if there is a universal shape for the spectra scaled in this way, information on the spectral densities for all frequencies is known if the variance and the integral time scale are known.

A universal spectral shape can be found by assuming that

$$nS_x = \frac{(Af)^a}{(B + (Cf)^b)^c} \quad (3-18)$$

By taking the logarithm of the right hand side a system of the exponentials can be derived that must equal -2/3. Derivative of the expression at the crest should be equal to zero and the place of the crest in dimensionless y and x coordinates should be the same. This reduces the number of unknowns and a spectral shape can be expressed as

$$nS_x = \frac{y_c(1 + 1.5a)^c \left(\frac{f}{x_c}\right)^a}{\left(1 + 1.5a\frac{f}{x_c}^b\right)^c} \quad (3-19)$$

where y_c and x_c is the dimensionless y and x coordinates. The values of a, b and c was determined by forcing their system to -2/3 and fitting the curve to the measured spectra.

Table 3-3: The constants in the universal spectral function.

| | U | V | W |
|-------|--------|--------|--------|
| a | 4/3 | 5/2 | 3/2 |
| b | 2 | 2/3 | 13/15 |
| c | 1 | 19/4 | 5/2 |
| x_c | 0.3758 | 0.5309 | 0.5957 |
| y_c | 0.2559 | 0.2127 | 0.2270 |

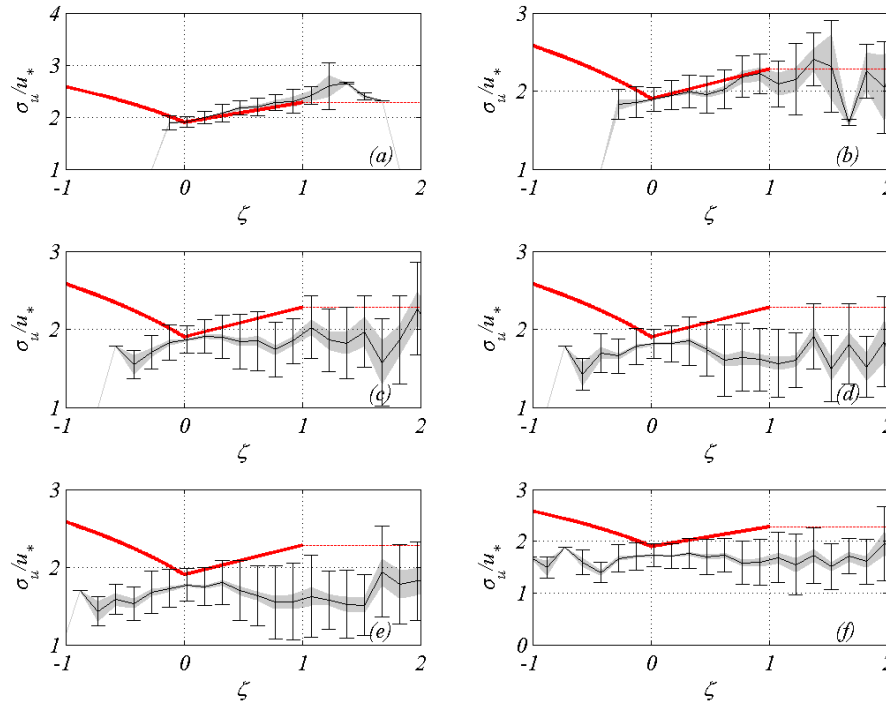


Figure 3-27: Standard deviation of u scaled with the friction velocity as a function of z/L . (a)-40 m, (b)-59 m, (c)-80 m, (d)-98 m, (e)-120 m and (f) 138 m. The black solid line is the mean for small stability interval, the bars indicate the standard deviation of the measurements within that interval and the grey shaded area is the standard deviation of the mean, how well the mean value is determined. The red line is the stability function for σ_u .

In order for the alternative scaling to be useful, the variance and the integral time scale will need to be determined from some other basic variables such as z , L or U . It is well known that the horizontal velocity variance does not follow MOST-scaling (Wilson 2010). Figure 3-27 shows the standard deviation of u , σ_u (square root of the variance), and the stability dependence of σ_u as suggested by MOST.

$$\phi_{\sigma_u} = \begin{cases} 1.9(1 - 1.5z/L)^{1/3} & z/L < 0 \\ 1.9(1 + 0.2z/L) & z/L \geq 0 \end{cases} \quad (3-20)$$

Compared to theory σ_u varies only weakly with both height and stratification. On the unstable side σ_u scaled with the friction velocity is actually decreasing with increasingly unstable conditions as opposed to the theory which says that it should increase. Another way of plotting σ_u is as a function of U/u_* . This will still take into account the stability effects of σ_u , since U/u_* is a unique function of z/L . This is done in Figure 3-28, where the line $\sigma_u=1.9u_*$ is also included.

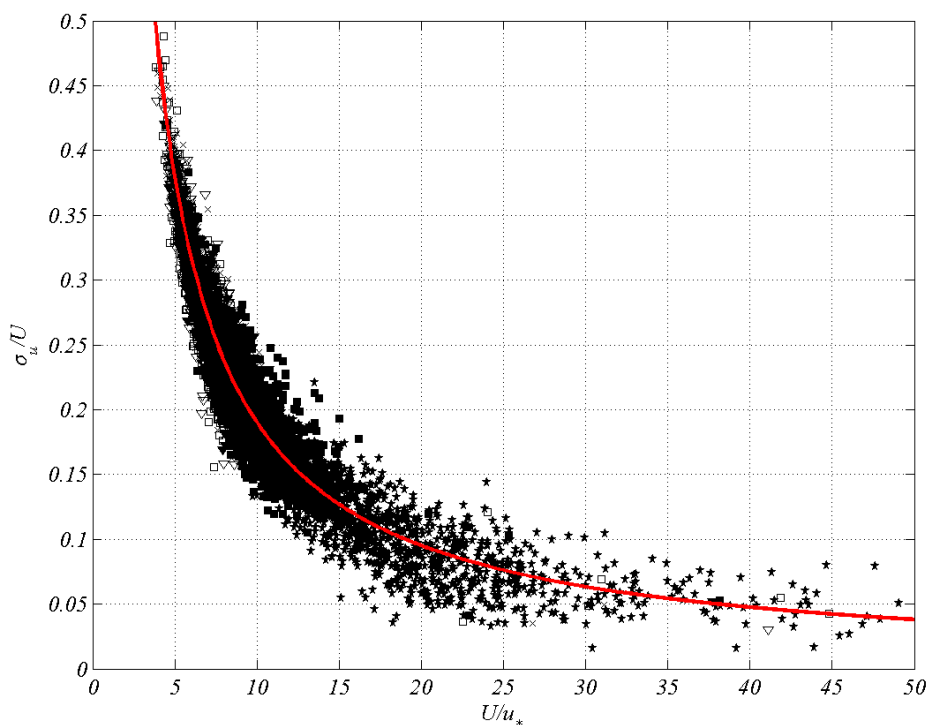


Figure 3-28: σ_u/U plotted against U/u_* . The figure contains data from all heights and all stability classes. Stability symbols according to Table 3-2. The red line is from $\sigma_u=1.9u_*$.

Figure 3-29 shows the standard deviation of w as a function of z/L . The vertical component is believed to carry less mesoscale variations than σ_u and thus more prone to MOST-scaling. However there is not a very good agreement between the stability function for σ_w/u_*

$$\phi_{\sigma_w} = \begin{cases} 1.25(1 - 3z/L)^{1/3} & z/L < 0 \\ 1.25(1 + 0.2z/L) & z/L \geq 0 \end{cases} \quad (3-21)$$

and the measurements. In Figure 3-30 σ_w/U is plotted against U/u_* . The curve $\sigma_w=1.3u_*$ is also included in the figure. Although there seem to be some stability dependence of σ_w the bulk of the data is captured by the simple relation $\sigma_w=1.3u_*$.

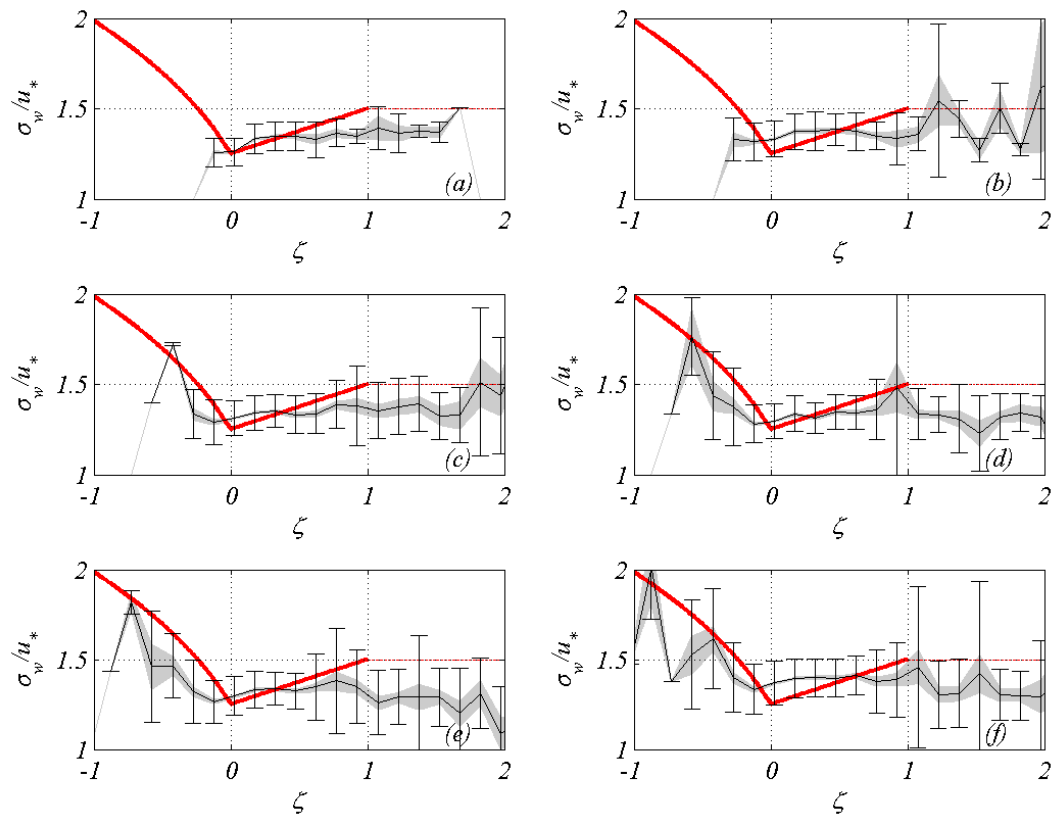


Figure 3-29: Standard deviation of w scaled with the friction velocity as a function of z/L . (a)-40 m, (b)-59 m, (c)-80 m, (d)-98 m, (e)-120 m and (f) 138 m. The black solid line is the mean for small stability interval, the bars indicate the standard deviation of the measurements within that interval and the grey shaded area is the standard deviation of the mean, how well the mean value is determined. The red line is the stability function for σ_w .

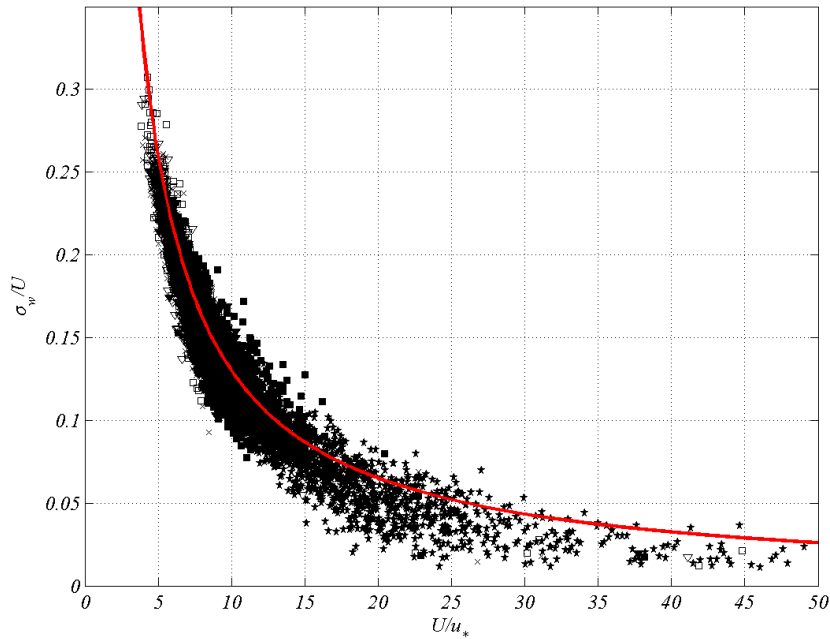


Figure 3-30: σ_w/U plotted against U/u_* . The figure contains data from all heights and all stability classes. Stability symbols according to Table 3-2. The red line is from $\sigma_w=1.3u_*$.

To be able to get a simple relationship also for the integral time scale, non-dimensionalization was done by l_m/u_* , where l_m is defined by

$$l_m = \frac{1}{\frac{1}{z} + \frac{1}{\delta}} \quad (3-22)$$

The result is shown in Figure 3-31 with σ from the Rossby-Montgomery formulation together with the curve

$$\frac{\Gamma_w u_*}{l_m} = a + b(U/u_*)^{-4} \quad (3-23)$$

With $a=0.0075$ and $b=150$.

Using the very simple relationships between U/u_* and Γ and σ the Power spectrum can be determined using the universal spectrum shape. The result is shown in Figure 3-32. Although the scatter is now as large as with the original scaling, the alternative scaling technique has the advantage that a universal spectral shape is known, so a spectrum with dimensions is easy to determine for a given U/u_* .

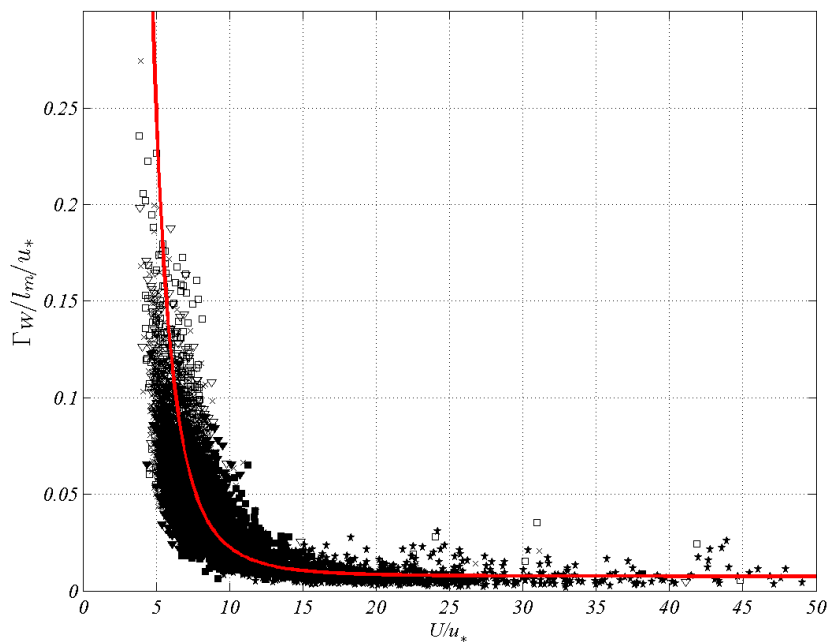


Figure 3-31: Integral time scale Γ made dimensionless by I_m/u_* and plotted against U/u_* . The figure contains data from all heights and all stability classes. Stability symbols according to Table 3-2. The red line is from Eq. 22.

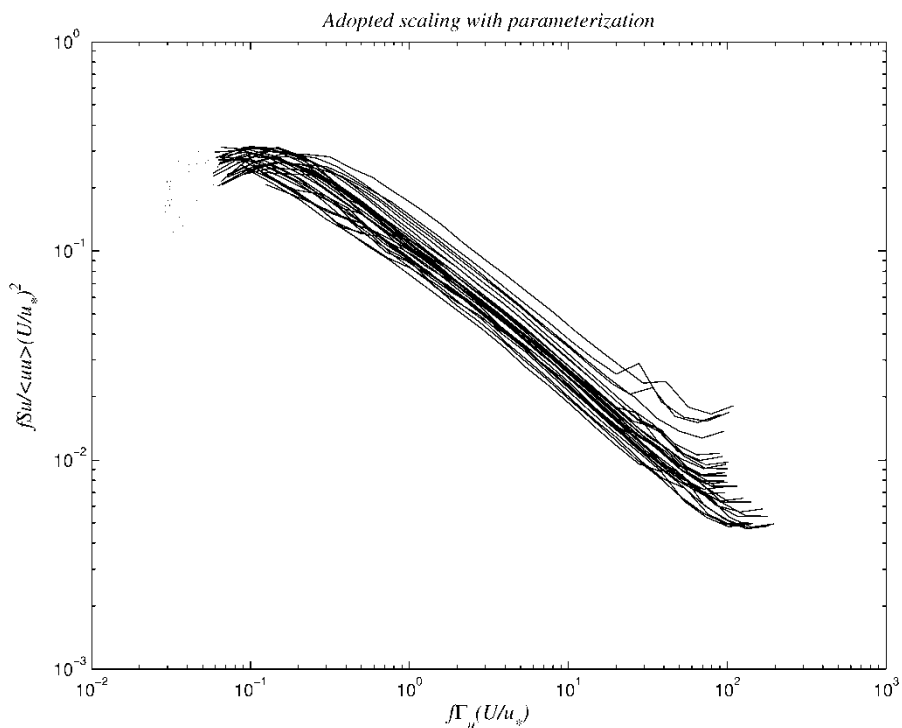


Figure 3-32: Power spectrum for u , both the variance and the integral time scale have been parameterized as a function of U/u_* .

3.2 Skogaryd

3.2.1 Data description

The Skogaryd site is located approximately 50km from the west coast Of Sweden and 10-40 km from the large lake Vänern (Figure 3-33a). The area between the coast and the lake is generally forested but has significant areas of lower-crop agriculture, the closest being to the west of the mast at a distance of 2 km. The forest is very homogeneous only within a radius of 100m in the eastern direction to 280 m in south-west (Figure 3-33b).

The experiment utilized a 38 m tall mast located at 58°21'50.5"N, 12°8'59.4"E. The forest immediately surrounding the mast is an approximately 50 year's old Scots Pine forest (*Picea Abies*), (Figure 3-33c). Near the mast, the forest height was estimated to 24-28 m, where the upper range was reached by a tall deciduous tree to the west of the mast.

The mast is a square lattice construction, where each side is 0.6 m long. Three meters to the east of the mast, a small hut (2.4x6x2.4 m) is located. A few meters further to the east a small clearing starts with the dimensions 25 x 15 m in the approximate directions of 105° and 195° respectively. On the mast, six sonic anemometers (Metek USA-1 Basic) were mounted at 1.2, 6.5, 12.5, 18.5, 31.0 and 38.4 m above local ground level Figure 3-33, d. The boom lengths were 3 m, extending 2.4 m from the mast in the direction of 2°. To minimize local influence from the clearing as well as the measurement hut on the flow, the lowest boom was mounted in the 272° direction. For the levels below the canopy top, the instruments were not closer than approximately 1m from the nearest branch. The North arrows of the sonic anemometers were pointed towards the mast (182°). In addition to the sonic anemometers, temperature was measured at 0.9 and 18.2 with Pt-100 (Risø-DTU) and small unventilated Anderaa screens and a rain sensor at (18 m).

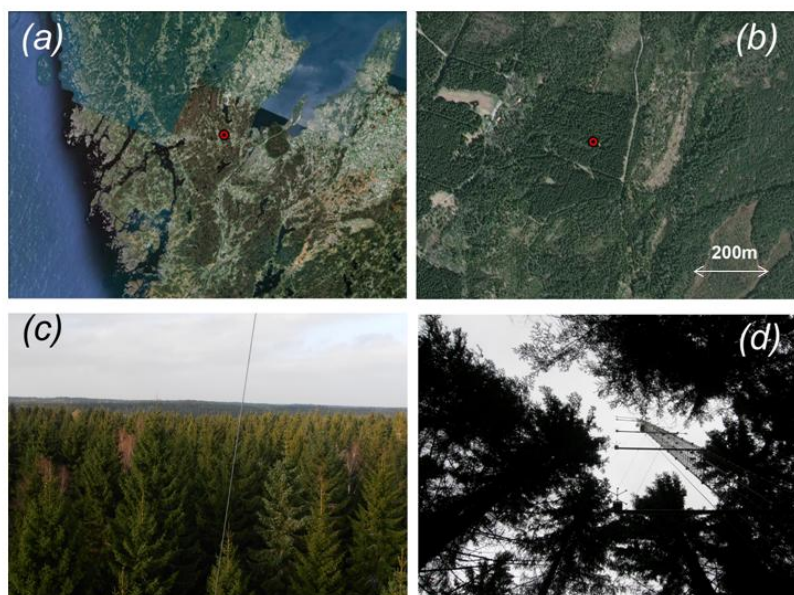


Figure 3-33: The Skogaryd site.

The instrumentation on the mast was operational between 2010-08-19 and 2011-10-25, except the rain sensor that was mounted 2010-10-14. Instrumental failure occurred for the rain sensor and the lowest sonic anemometer, which stopped functioning December 1st 2010. In addition to the in-situ instruments, a remote-sensing wind lidar and a ceilometer (CL31) were deployed. The ceilometer was located in the small clearing next to the mast. The wind lidar was a prototype of the ZephIR lidar. The prototype differs from the commercial version of the instrument in that the optical head is separable from the laser source and sensor. Whereas measurements in forested terrain with wind lidars normally are limited to the location of substantial clearings in the forest to ensure that the laser beams do not interfere with the trees, the utilization of the prototype enables mounting in a mast and measurement of more undisturbed forest flow. In Skogaryd, the optical head was mounted in the mast at 28.4 m on a boom pointing in 315° and with a length of 1.8 m extending 1.2 m from the mast. The prototype lidar worked well for approximately a month between mid-September and mid-October. After this period, the optical fibre was damaged and the attempted repair in the early winter was unsuccessful. During most of the period when the lidar worked well, a power loss in combination with a network problem closed down the mast instrumentation, which unfortunately limited the overlap of a complete functioning setup to approximately a week. A technical drawing of the instrumentation of the Skogaryd tower is provided in Dellwik et al., 2013.

The mast owners at Gothenburg University intended to have the mast instrumented with standard meteorological measurements, such as radiation, temperature, relative humidity and soil property measurements as well as eddy covariance fluxes of water vapour and carbon dioxide, from June 1st 2010. However, this instrumentation was not mounted during the whole of the Vindforsk experiment. At a nearby walk-up tower located 630 m from the mast in the direction of 340°, meteorological and flux measurements were performed continuously during the experiment. The forest at this location is approximately similar to the forest around the mast.

The sonic anemometers were checked and calibrated for zero wind speed before and after the experiment.

3.2.2 Results from Skogaryd

Given the experimental difficulties at the site, the possibilities for analyses are more limited than for the Ryningsnäs data. However, both the sonic anemometers dataset and the lidar data show interesting results. Such information is crucial for the correct parameterization of flow models. The temperature measurements within the canopy showed that the stratification within the canopy is often dramatic and opposite to that measured above the canopy. This result has implications.

The forest height was estimated to be 24-28 meters when the tower was equipped with the sonic anemometers. However, the precise forest height is not known. To determine the height of the forest as felt by the flow, the height to the maximum wind shear was determined. Over the forest the wind

profile is approximately logarithmic and within the forest simple arguments (as well as measurements) show the wind profile to be exponential. Because of this, there must be a height of maximum shear in the wind, an *inflection point* in the wind profile. With certain combinations of stress profile, temperature profile and wind profile, this inflection point will give rise to wave disturbances. It is thought that for most atmospheric conditions these waves have a relatively fast amplitude growth and are also modulated by a second order instability which causes them to quickly break and interact with the surrounding turbulence (Finnigan et al., 2009). The height to the inflection point is therefore central when it comes to processes that have a deep impact on the characteristics of canopy flows. In the following section we will evaluate the forest height h as the height to the inflection point. The inflection point was found by finding the maximum derivative of a piecewise cubic Hermite polynomial interpolation of the wind profile. This type of interpolation is shape preserving as it also take into account the first derivative of the data points (McQuarrie and Murdzek, 2003). Using a fit in logarithmic height would not be good since the wind profile within the forest is exponential rather than logarithmic. Thomas and Foken (2007) used a third order polynomial least square fit to the data to find the inflection point, but the cubic Hermite interpolation was deemed more successful in finding the inflection point by visual inspection. Figure 3-1 shows the inflection point calculated in this way. The average in the sector 210-340° was 25.9 m and is indicated in the figure by a dashed line. This value will hereafter be used as the forest height.

The detailed measurements within the forest make it possible to do estimate the displacement height in several ways. The centre of drag hypothesis says that the displacement height is the same as the height to the mean of the momentum absorption. This was postulated in a paper regarding drag coefficients in canopies (Thom, 1971). Assuming that the momentum can be expressed with a drag coefficient the resulting displacement height becomes

$$d = \frac{\int_0^h zU(z)^2}{\int_0^h U(z)^2} \quad (3-24)$$

But the Skogaryd site was equipped with sonic anemometers so the stress can be determined directly by

$$\tau = \rho \sqrt{u'w'^2 + v'w'^2} \quad (3-25)$$

The mean height of the stress absorption then becomes

$$d = \frac{1}{\tau_{sl}} \int (\tau_{sl} - \tau) dz \quad (3-26)$$

where the *sl* notation means the constant value of the surface layer stress. Figure 3-35 shows the mean stress profile from Skogaryd, with shading to indicate the mean level of momentum absorption. Most of the stress is absorbed near the tree tops, which leads to the maximum of wind shear there. Further above the trees, from the measurement point at 30.5 m and above, there is a region of approximately constant momentum flux.

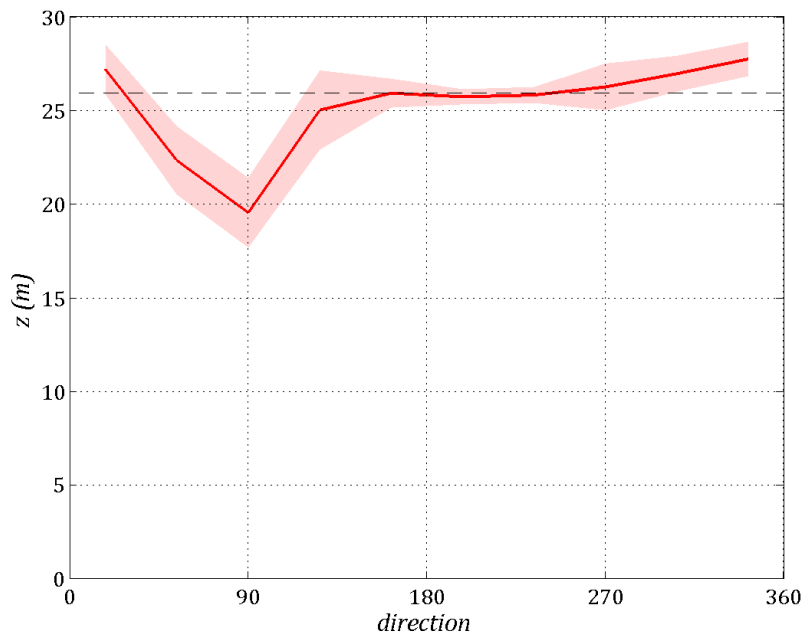


Figure 3-34: Height to the inflection point in the wind profile. Mean value for the directions 210-340° is indicated by a dashed line. The red solid line is a 36° wide bin average and the shaded area is the bin average \pm one standard deviation.

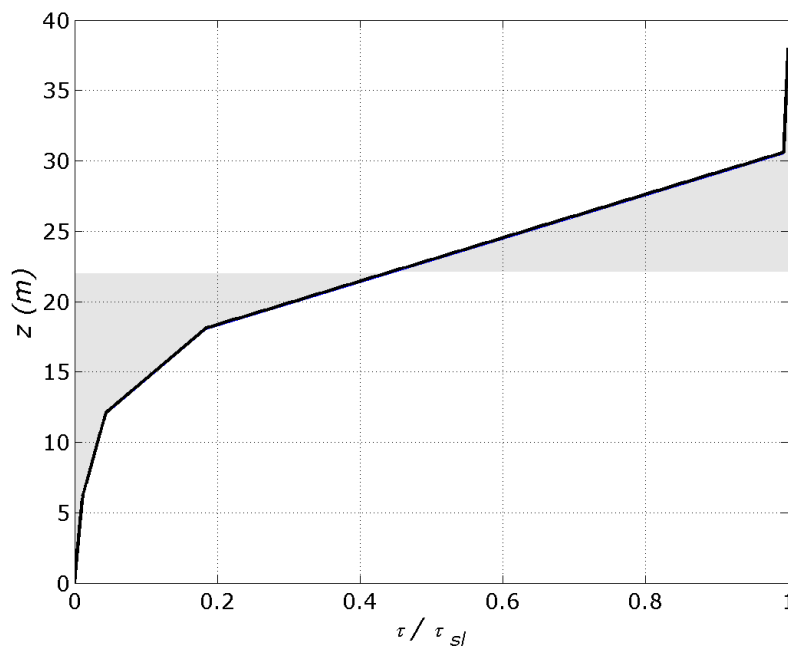


Figure 3-35: The mean scaled shear stress profile from Skogaryd. The shaded area indicates how much momentum has been absorbed above and below the displacement height.

Another, more indirect, way of determining the displacement height is by measuring the wind speed gradient at the top of the trees and then make assumptions on the mean flow. In a paper on mean wind speed in and above the forest, Harman and Finnigan (Harman and Finnigan, 2007) argued that the appropriate length scale for canopy flows is the vorticity thickness, $U/\partial U/\partial z$, at the tree height and that the displacement height could be determined in the following way

$$h - d = \frac{1}{2} \frac{U}{\partial U/\partial z} \quad (3-27)$$

where h is the tree height and U is evaluated at h . This is a somewhat simplified form of the expression proposed by Jackson (1981), which after some reformulation is

$$h - d = \frac{1}{2} \frac{U_h}{(\partial U/\partial z)_h} \left(1 - e^{-2h(\partial U/\partial z)_h/U_h} \right) \quad (3-28)$$

The two expressions are very similar for dense forests and only start to differ when d is less than $0.7h$. In the case of Skogaryd, which is a very dense forest with $d/h \sim 0.9$ the only real difference between the expressions is found for flow directions around 90° when the flow is passing over the small hut and the clearing and so the full equation from Jackson will be omitted for the simpler one by Harman and Finnigan. Figure 3-36 shows the three different methods plotted against the wind direction. The displacement height calculated directly from stress profiles has the largest uncertainty, which is not surprising considering the greater measurement sensitivity inherent with a second order moment. d from stress profiles also shows the most directional variability which is coupled to the influence of the vertical velocity variation which has more of its energy from smaller scales and thus react more strongly to a change in forest density. In the region of undisturbed flow, the three methods agree quite well and give mean value of d from the centre of drag by U -profiles 23.1 m, centre of drag from stress profiles 22.1 m and both the vorticity thickness methods $d=21.7$ m.

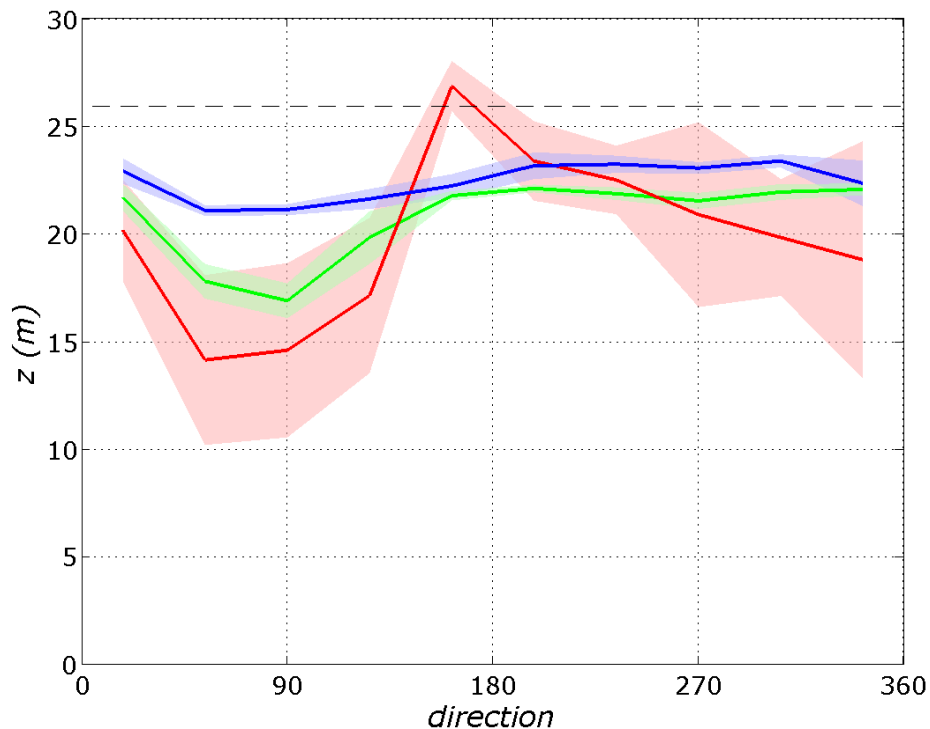


Figure 3-36: The displacement height determined in three different ways. Red: The centre of drag method from stress measurements, blue: centre of drag method from the mean wind profile, green: vorticity thickness approach. The shaded area represents the mean value ± 1 standard deviation.

The estimation of d by the centre of drag method is done without assuming any universal behaviour of the wind profile. Typically d is estimated from the wind profile in neutral conditions using the logarithmic expression

$$\frac{\partial U}{\partial z} = u_* \frac{1}{\kappa(z-d)} \quad (3-29)$$

where $\kappa=0.4$ is the von Kármán constant. One backside to that is the assumption that the wind profile is logarithmic. This requires strictly neutral conditions, and the estimation of the friction velocity needs to be done in stationary conditions which limit the number of neutral cases significantly. Even so, over forests the logarithmic expression only starts to be valid at $z=2-3h$ due to roughness sublayer effects. Since the wind gradient scales as one over z that mean that at the heights where this method becomes applicable the gradients are small and thus the relative error in gradient estimation is large. Using the logarithmic wind profile to determine d is also subject to uncertainties if the friction velocity is not estimated by a 3D-high frequency anemometer, but is instead derived from slow response 2D measurements such as a cup-anemometer.

The atmospheric stability is particularly tricky variable in forests. The stomata control of the leaves and the shading by the tree trunks often cause the stability to be of opposite signs within and above the forest. In Skogaryd this happens in more than 50% of the time. The model tool best developed to include effects of stratification is meso scale models, but they are all run without the inclusion of a forest layer so afterwards the result is lifted to above the displacement height. To include the effects of canopy processes in a meso scale model has therefore been of interest. As a step in that process an analytical wind profile has been developed. The analytical profile could be used to initialize meso scale models and provide closure assumptions such a turbulent length scale. The wind profile expression was derived by coupling one expression from within the forest to one for the flow aloft. The wind within the forest is given by the exponential profile expression from Inoe (1963)

$$U(z) = U(h)e^{-\alpha \frac{z'}{h}} \quad (3-30)$$

where α is a constant and z' is $h-z$.

The wind above the forest was determined using a correction ϕ to the wind gradient expression from Monin Obukhov similarity theory that is dependent on the height of the roughness sublayer z_*

$$\frac{\partial U}{\partial z} = \frac{u_*}{\kappa(z-d)} \phi(z-d, L) \varphi(z, z_*) \quad (3-31)$$

The form of the stability function was taken in it standard form (Högström, 1996)

$$\phi = \begin{cases} (1 - 16z/L)^{-1/4} & z/L < 0 \\ 1 + 5z/L & z/L \geq 0 \end{cases} \quad (3-32)$$

and the form of the correction function was proposed to be

$$\varphi = 1 - \frac{z}{\eta} e^{-z/(h-d)} \quad (3-33)$$

where η is a constant that relates to how much influence the roughness sublayer has on the gradient. This particular form of the correction function ensured that the integral of the gradient expression over the forest was analytically integratable. The profile of φ is shown in Figure 3-37 together with some other recent formulations of φ . The relatively small difference between z and h at the Skogaryd site means that the roughness sublayer will be shallow but have a large effect on the flow close to the forest. This is because the sharp gradient at the tree tops will produce a lot of turbulence, but at the same time, keeps the vertical extent of the vortices at a relatively moderate level according to the scaling that a typical vortex size is in the order of $U/dU/dz$.

The integrated form of the velocity expression above forest now becomes

$$U(z)\kappa/u_* = \ln(z/z_0) - (\Psi(z/L) + \Psi(z_0/L)) + \hat{\Psi} \quad (3-34)$$

Where Ψ is the integrated stability function and the integrated correction function is given by

$$\hat{\Psi} = \begin{cases} \eta^{-1} \frac{Le^{-\frac{z}{d_t}} (1-16z/L)^{3/4} \Gamma(3/4, \frac{16z-L}{16d_t})}{2(\frac{16z-L}{d_t})^{3/4}} & z/L < 0 \\ -\eta^{-1} \frac{d_t e^{-\frac{z}{d_t}} (5d_t+L+5z)}{L} & z/L \geq 0 \end{cases} \quad (3-35)$$

and Γ is the incomplete upper gamma-function and $d_t=h-d$.

Joining the two profile expressions at the tree tops in terms of wind and wind gradient require using the vorticity thickness approach to get d . The roughness length z_0 can then be determined from the relation between d , h and η .

The resulting wind profile is shown together with measurements and the wind profile from Monin-Obukhov similarity theory in Figure 3-38. The new wind profile expression cannot quite capture the dramatic decrease of the flow in the tree trunks and the local maximum the ground, but it is a significant improvement compared to the Monin-Obukhov theory near the tree tops.

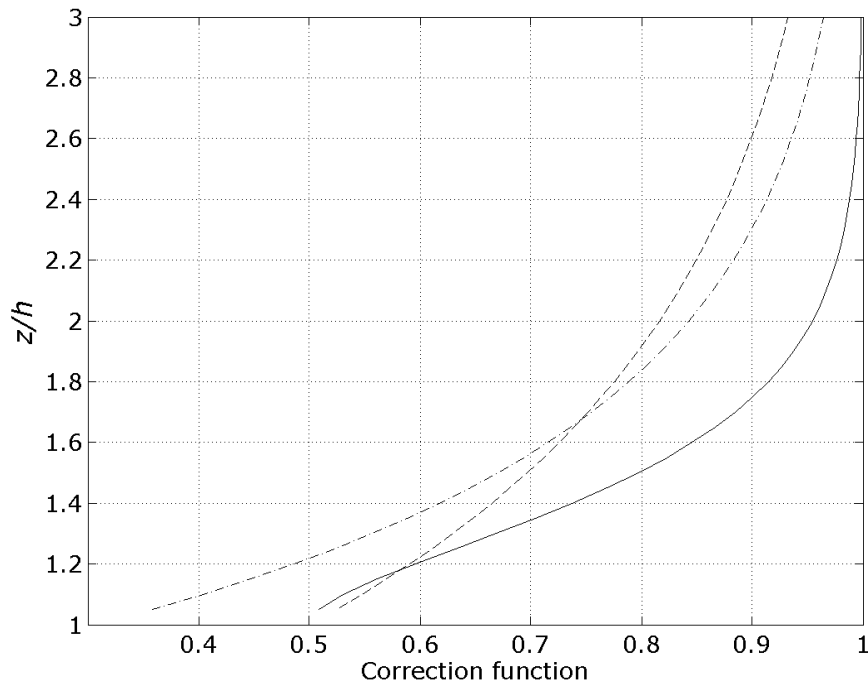


Figure 3-37: The profile of the roughness sublayer correction ϕ . The solid curve is the new expression, the dashed curve is from Harman and Finnigan (2007) and the dash-dotted curve is from Ridder (2009).

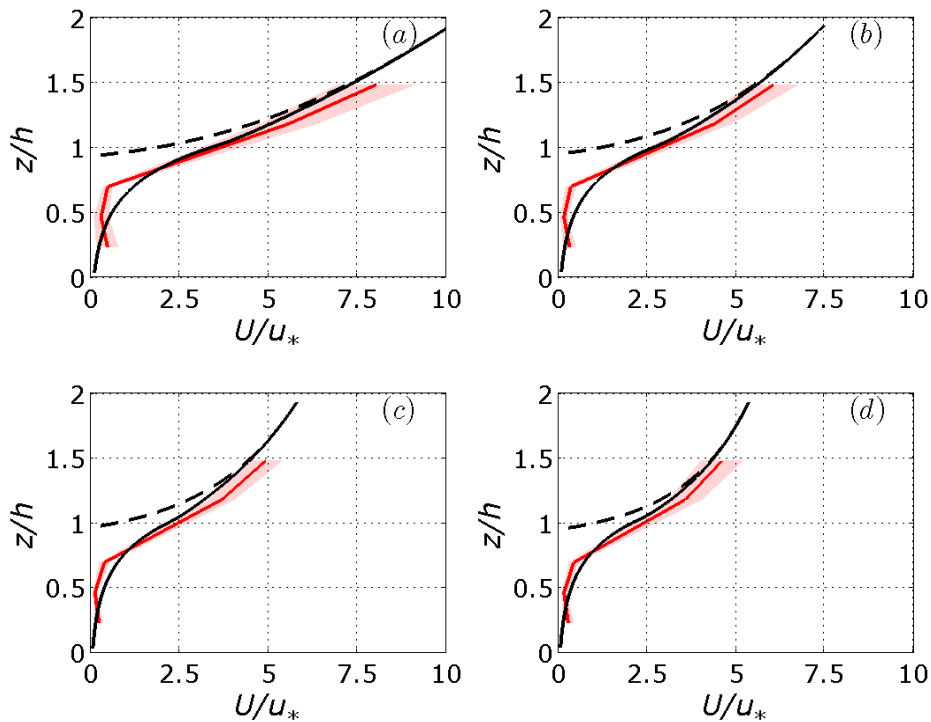


Figure 3-38: A new wind profile expression (black solid line), wind profile from Monin-Obukhov theory (dashed line) and measurements (red line, with one standard deviation marked by red shaded area) for four different stability classes, (a)-very stable, (b)- stable, (c)-neutral and (d)-slightly unstable.

The lidar data from the Skogaryd tower often showed an unexpected wind profile, with large shear in the near the surface, followed by a strong increase in the wind and a relatively flat high-wind speed and low-shear profile above. An example of such layering is shown in Figure 3-39. The explanation for such a layered wind profile could be effects of different surface temperature between land and water, which in the autumn would dampen the growth of the forest internal boundary layer and thereby create more favourable conditions for wind turbines in the area. However, measurement errors are not completely possible to exclude, and we consider the result as interesting but uncertain. Further research is needed to investigate possible beneficial effects of the coast on the wind climate.

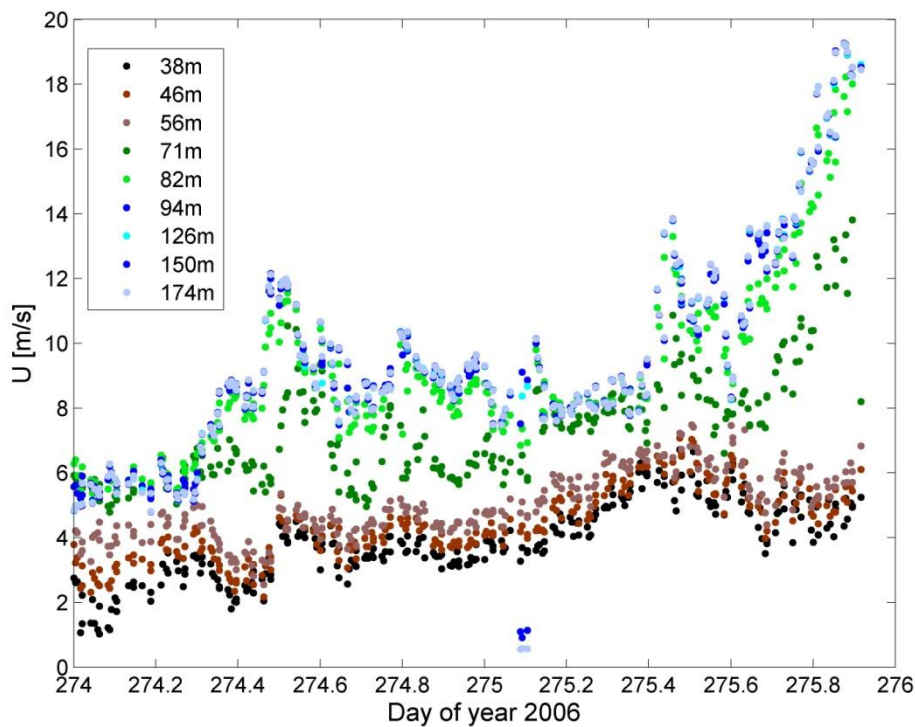


Figure 3-39: Early October lidar measurements of mean wind speed at the Skogaryd site.

3.3 Comparisons with results from other sites

In this Section the detailed results on winds above forests presented above, especially from the Ryningsnäs site, will be compared with wind measurements taken at a large number of other forest sites. These data have been made available for analyses within the Vindforsk project through kind contributions by wind project owners who have made wind measurements at their own sites. The purpose of the comparison is to get more knowledge about to which degree the Ryningsnäs data could be taken to be generally representative for forest sites in Sweden.

3.3.1 The data

The data used in this Section are from 42 forest sites located all over Sweden. Due to restrictions on the use of these data, their exact locations will not be given. At all sites used wind measurements have been taken at a minimum three heights typically ranging between 40-50 m and 80-100 m. Mostly the wind speed have been measured using cup anemometers of different types like NRG, Thies, Vaisala, and Vector, supplemented with wind vanes to measure wind direction. Also propeller anemometers, combined instruments measuring both wind speed and direction, have been used at a few sites. Temperatures have been measured mostly at two heights, which enable an estimate of the thermal stability of the atmosphere to be made. Data have

been sampled typically with 1 Hz and stored as 10 min averages including extreme values and standard deviations. This makes it possible to analyse both average wind profiles and turbulence intensity profiles, i.e. how they vary with height.

To get a general idea of the sites and their surroundings they have been characterized with respects to their topography and vegetation. All sites are located in areas which could generally be characterized as forested areas. But as for the Ryningsnäs site they are located in what could be characterised as "typical Swedish forests", i.e. the forests that are to a smaller or larger extent heterogeneous both as regards the type of forest as such, but also as regards the occurrence of for example marshes, bogs, agricultural fields, meadows, and lakes. Also differences in topography are expected to affect the wind characteristics at a site.

Properties of land cover and topography within 5 km around a site are expected to dominate the boundary-layer wind statistics at the heights investigated here. Statistics regarding topographical variations and land cover within the closest 5 km from each site have consequently been estimated. Land cover data have been taken from Lantmäteriet and have a horizontal resolution of 25 m x 25 m. Also the topography data used for the analyses is from Lantmäteriet and their terrain height data with the horizontal resolution 50 m x 50 m.

Statistics about terrain height variability within the closest 5 km around each site are shown in Figure 3-40. The standard deviation of terrain height, shown in the upper subplot, has the median value 4 m, but some sites have numbers above 10 m indicating that although forest may dominate the sites we might expect topographical effects on the boundary layer winds as well. This is also true looking at the lower subplot which shows the maximum difference in terrain height found within 5 km from the sites. Here the median is 118 m but at some sites reached above 300 m.

Land cover statistics are within the closest 5 km around each site are shown in Figure 3-41. The classification has been simplified summing up into 5 different land cover properties. The urban class indicate mainly villages and towns, but also other humanly influenced areas. The field class includes mainly agricultural fields, but also naturally open areas such as pastures. The forest class is summed up by coniferous forests, mixed forests and deciduous forests, but include also young forests and cutting areas. All sites are in forest areas where forestry is an ordinary activity. The marsh class includes wetlands of different types, often with sparse trees. The water class includes lakes and sea.

It is obvious that forest dominates all sites with the median value 77 %, but a few sites only has 40-50 % forests within the closest 5 km. This is mainly due to the proximity to either fields or open water areas as can be seen from Figure 3-41. The median value for the field class is 11 %, while the median for water is 4 %. The occurrence of marshland amounts as most to about 20 % but has a median value as low as 3 %. The urban areas typically cover very small areas around the sites, but at a few reaches 6-7 %.

The analyses of land cover and topographical variability around each of the sites reveal that, as expected, there is some variability. Although forests

dominate the sites the land cover statistics show that also fields and open water occur to some not negligible percentage at some sites, as do marshlands. Also at least about ten of the sites show variability in topography within the closest 5 km such that we might expect an influence from this on the boundary layer wind structure. Also we may expect differences between the truly forest dominated and reasonably flat sites simply due to differences in details about the forests as such, such as density and heights, and heterogeneity in general. In spite of this only sites identified as having a larger topographical variability will be separated from the rest showing the statistics below.

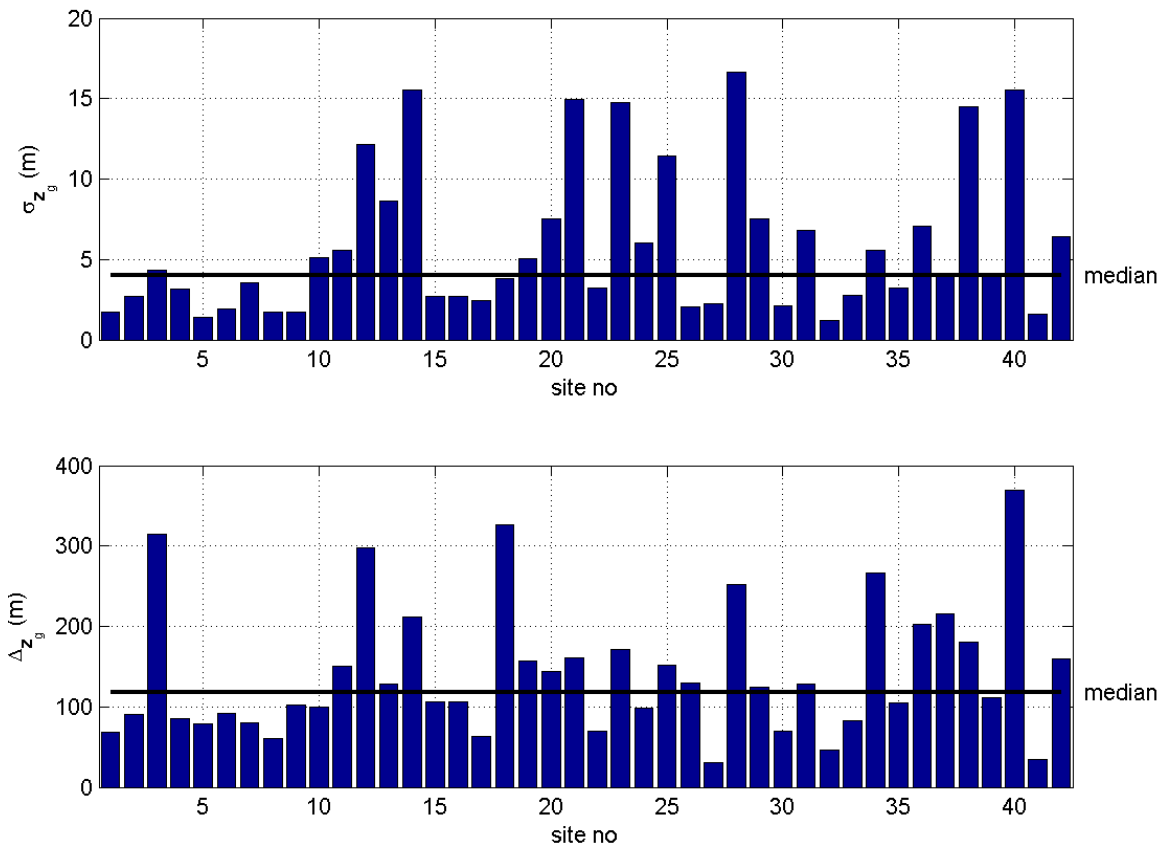


Figure 3-40: Terrain height variations within 5 km around each site. Upper subplot: Standard deviation of terrain height. Lower subplot: Largest difference in terrain height. The median values are shown by the full lines.

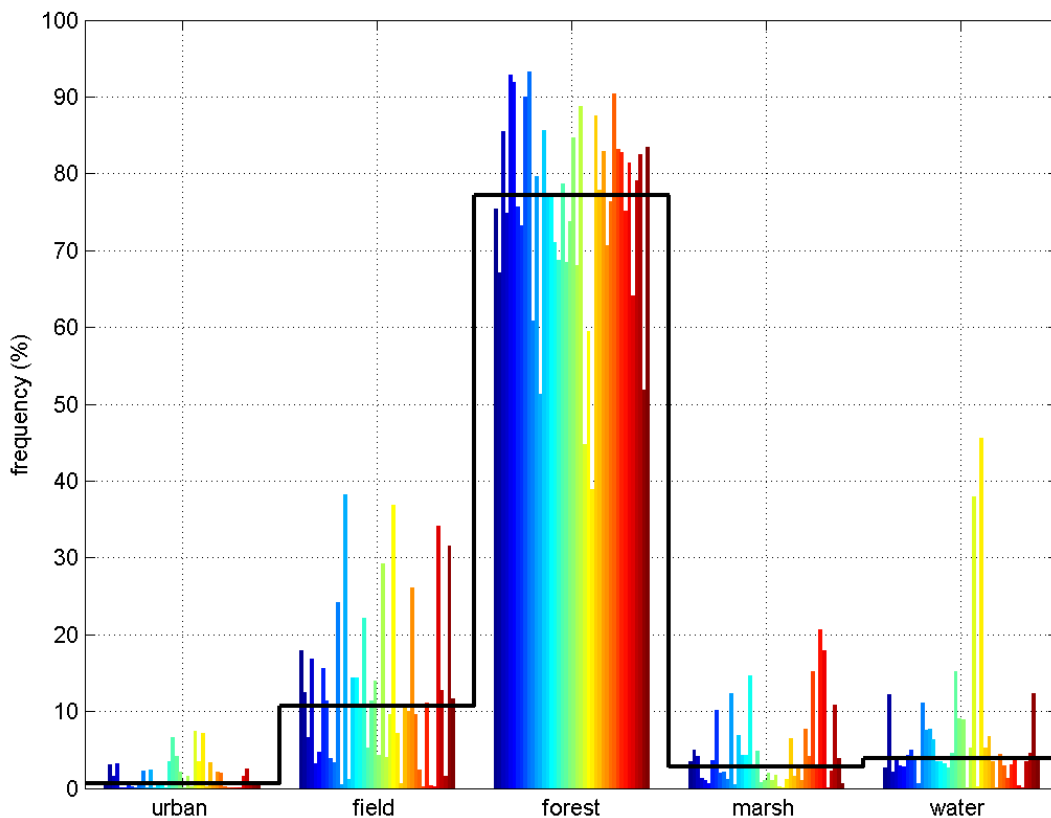


Figure 3-41: Bar chart giving statistics about land cover within 5 km around each site. The narrow coloured bars give the percentages for each site, while the full line gives the median values.

3.3.2 Results

It is well known that the atmospheric boundary layer above a rough surface such as a forest will typically be characterised by a high level of turbulence and a large wind shear. Before making comparisons with the results from Ryningsnäs given in Section 3.1.3 we will present some general statistics regarding wind profile and turbulence intensity, illustrating the variety in these above forests.

The measured wind profiles have been compared using the exponential wind profile commonly used to describe the vertical wind shear in wind energy applications. The exponential wind profile relates the wind speed at two heights using the equation

$$\frac{U(z_2)}{U(z_1)} = \left(\frac{z_2 - d}{z_1 - d} \right)^\alpha \quad (3-36)$$

Here U =wind speed, z =height, d =zero-plane displacement, and α is an exponent giving the magnitude of the wind shear. The numbers 1 and 2 refer

to height level. The exponent is a function of surface roughness and thermal stability of the atmosphere.

Above high vegetation like a forest, the frictional momentum loss for wind will not be dominated by the friction at the surface, but will be highly affected by friction within the canopy, mainly by the trees. The frictional loss is thus an integrated effect throughout the canopy. One may define the zero-plane displacement as the average height for momentum transfer from the flow to the roughness elements. Usually this height is taken to be 2/3 or 3/4 of the tree height, but will depend on the roughness element geometry such as spacing between trees and density of the tree crowns. As a consequence it is in reality a difficult task to estimate d .

Another parameter needed to be estimated is the roughness length z_0 . For thermally neutral atmospheric conditions one may assume the wind profile to be described by the logarithmic profile expression

$$U(z-d) = \frac{u_*}{k} \ln\left(\frac{z-d}{z_0}\right) \quad (3-37)$$

Here u_* =the friction velocity= $\sqrt{-\overline{u'w'}}$, where $\overline{u'w'}$ =vertical kinematic turbulent momentum flux, and k =von Kármán's constant=0.4.

Using the logarithmic wind law at two heights within the surface layer (constant flux layer) where u_* may be assumed constant with height, it is possible to determine both d and z_0 from measurements of average wind speed and standard deviation of wind speed. From surface layer theory we know that there is a relation between the standard deviation of the longitudinal wind component (in the mean wind direction) σ_u and u_* saying that σ_u/u_* is about 2.0-2.5 depending on source and filtering of the data. But according to results of the turbulence measurements at Ryningsnäs presented in Section 3.1.3, this ratio was there found to be 1.9 at the lower height. This may be an effect of the fact that above high canopies like a forest, a so called roughness sublayer exists from the canopy top to about 2-3 times the canopy height h . Thus the value 1.9 has been used here in the calculations used to estimate d and z_0 .

Measurements using the cup anemometer data of average wind speed U and standard deviation of the wind speed σ_u have thus been used to determine d and z_0 at all of the sites using data only for close to neutral thermal conditions. The bulk Richardson number

$$Ri = \frac{g}{T_0} \frac{\Delta\theta/\Delta z}{(\Delta U/\Delta z)^2} \quad (3-38)$$

was then used. Here θ is the potential temperature, g =acceleration of gravity, T_0 =average temperature in K, and Δ means difference between two heights. Data for which $|Ri| < 0.02$ in combination with the condition that the wind speed at the lowest level should be larger than 6 m/s were assumed to be close to neutral and used for estimating d and z_0 .

An additional assumption was then needed; that the standard deviation of wind speed may be used to approximate the standard deviation of the longitudinal components, i.e. that $\sigma_U \approx \sigma_u$. This has earlier been shown to be valid in e.g. Smedman et al. (1991).

Applying the logarithmic equations at two heights z_1 and z_2 , having the average wind speed U_1 and U_2 respectively, and solving this equation system for zero-plane displacement d and roughness length z_0 the results is

$$d = \frac{z_2 - z_1 \cdot \exp\left(\frac{k}{u_*}(U_2 - U_1)\right)}{1 - \exp\left(\frac{k}{u_*}(U_2 - U_1)\right)} \quad (3-39)$$

$$z_0 = \frac{U_1 - d}{\exp\left(\frac{k}{u_*} \cdot U_1\right)} \quad (3-40)$$

Estimates of z_0 and d were made using level one together with data from level two. To avoid the use of σ_u to estimate u_* an iterative technique was also used to determine z_0 and d . The logarithmic equation was used together with data from all three measurement levels. As most of the sites have their lowest level of measurement at 50-60 m, some even as high as 80 m, they are often above the surface layer and it should be remembered that they are thus not ideal for calculating z_0 and d .

The median results using the different methods to determine z_0 and d are presented in Table 3-4. Method 1 means using wind speed at the two lowest measurement level at each site together with the standard deviation of wind speed at the lowest height to estimate the friction velocity. In method two only wind speed at all three measurement levels was used. Results are presented for some different restrictions on topographical variability and forest dominance in the area surrounding the sites, cf. above.

Table 3-4: Median values of roughness length (z_0) and zero-plane displacement (d) using all sites, sites for which topographical variations are smaller than 150 m or for which the standard deviation of terrain height is smaller than 5 m. Results combining these two requirements are also shown, also in combination that the land use shows at least 75 % forests in the surroundings of the sites.

| | Z_0 (m) | | d (m) | |
|---|-----------|----------|----------|----------|
| | Method 1 | Method 2 | Method 1 | Method 2 |
| All sites | 1.3 | 1.4 | 17 | 18 |
| $\Delta_{zg} < 150$ m | 1.4 | 1.3 | 16 | 18 |
| $\sigma_{zg} < 5$ m | 1.4 | 1.4 | 16 | 18 |
| $\Delta_{zg} < 150$ m & $\sigma_{zg} < 5$ m | 1.4 | 1.3 | 16 | 18 |
| $\Delta_{zg} < 150$ m & $\sigma_{zg} < 5$ m & forest > 75 % | 1.4 | 1.4 | 14 | 17 |

The median value for the roughness length is about 1.4 m and for the zero-plane displacement about 16 m. No large differences were found between the results using data from all sites and results limited to sites with no major topographical variations and dominated by forests according to the land use data.

This results is however true only if the median values are studied. Bar charts showing the resulting zero-plane displacements and roughness lengths distributions at all sites are displayed in Figure 3-42. The upper part shows results where data from all sites have been included. This gives a median value for the zero-plane displacement of 17 m and the corresponding median roughness length 1.3 m. Thus also data from sites where effects of topographical variability will affect the results are included in these subplots and the distribution show values between 4 and 24 m as regards zero-plane, and between 0.2 and 2.2 m for roughness length.

Excluding sites for which $\sigma_{z_g} > 5$ m and $\Delta(z_g) > 150$ m we get at the distributions shown in the bottom two subplots of Figure 3-42. The distributions still show extreme values of about the same magnitude as above, using all sites. But there is, especially as regards the roughness length, a tendency towards a somewhat more localized distribution. One site has a value below 0.5 m and this site has smaller urban area within the closest 1-2 km in the dominant wind direction which might affect the result. Including only sites with more than 75 % forests within the closest 5 km did not significantly change the results as can be seen in Table 3-4.

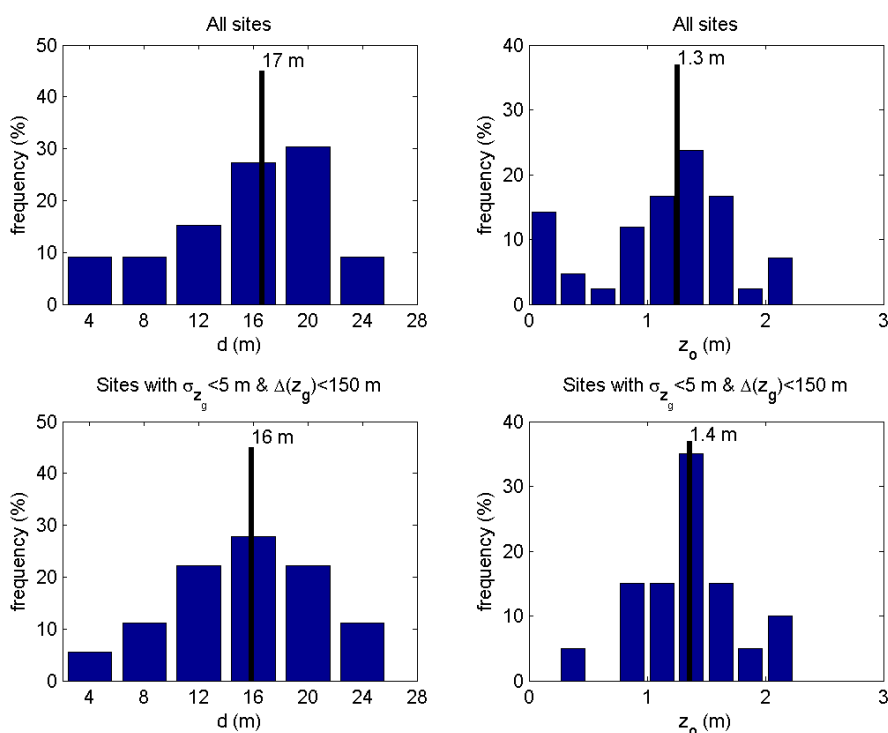


Figure 3-42: Histograms showing the distribution of zero-plane displacement d and roughness length z_0 for the sites. Top row using results for all sites. Bottom row using results only for sites with limited topographical variations. The numbers give the median values indicated by the vertical line.

Of course differences in forest properties, such as height and density, which could not be taken account of here, are reasonable explanations to some of the variability observed in the distributions. But the result show that a zero-plane displacement of the order 15 m is a reasonable value and that the roughness length for forests typically is about 1.5 m. This is in reasonable agreement with values which have been reported in the literature earlier.

The z_0 -value reported in Section 3.1.3, based upon the turbulence measurements at Ryningsnäs, is for the forest sector 2.5 m with the zero-plane displacement 18 m. The corresponding numbers arrived at here for Ryningsnäs using only cup anemometer data are 1.9 m and 13 m. But this result includes data from all wind directions (except wake affected sectors) and a systematic variation in roughness length with wind direction was notes in Figure 3-5. A more detailed analysis also shows this result here. Using only data with winds from the forest sector we here get the roughness length 2.1 m, while for southeasterly winds the roughness length is 1.3 m.

One possible reason for the still remaining small difference in roughness length may be that the cup anemometers do not catch all of the turbulence in the wind. This is definitely so at height below 10 m where the scales of the turbulence is smaller and thus more of the turbulent energy is expected to be found at high frequencies not caught by the cups. But at higher levels the turbulence scales increase and the cups should be expected to catch must of the turbulence. Comparisons made between sonics and cup anemometers at Ryningsnäs show this. However, the results also show that at Ryningsnäs also as high up as 40 m the cup anemometer measured a standard deviation being about 10 % below what was measured with the sonic anemometers. This difference decreased with height to below 5 % at 100 m height. But another cause for the difference may anyhow lie in that turbulent properties adapt much more slowly to horizontal heterogeneities than average wind properties. Using sonic anemometer data for u_* instead of data on the average wind profile may mean a difference. We have also notes that only using the wind speed from the cup anemometers at three heights gave almost the same results. The results show that measurements from Ryningsnäs gave a larger roughness length than what was typical for most of the sites used in this Section.

Comparisons of the average wind profiles normalized with the wind speed at 100 m are shown in Figure 3-43 for the different sites. Comparing all sites the extreme differences are within the range $\pm 4-5$ % at 40 m above and below 100 m. Including only sites with minor topographical variability, defined using the limits $\sigma_{zg} < 5$ m and $\Delta_{zg} < 150$ m, the extreme differences are even more reduced as can be seen from Figure 3-43, the deviation of individual profiles from the median profile being mostly within 1-2 % looking at the height interval ± 40 m around 100 m.

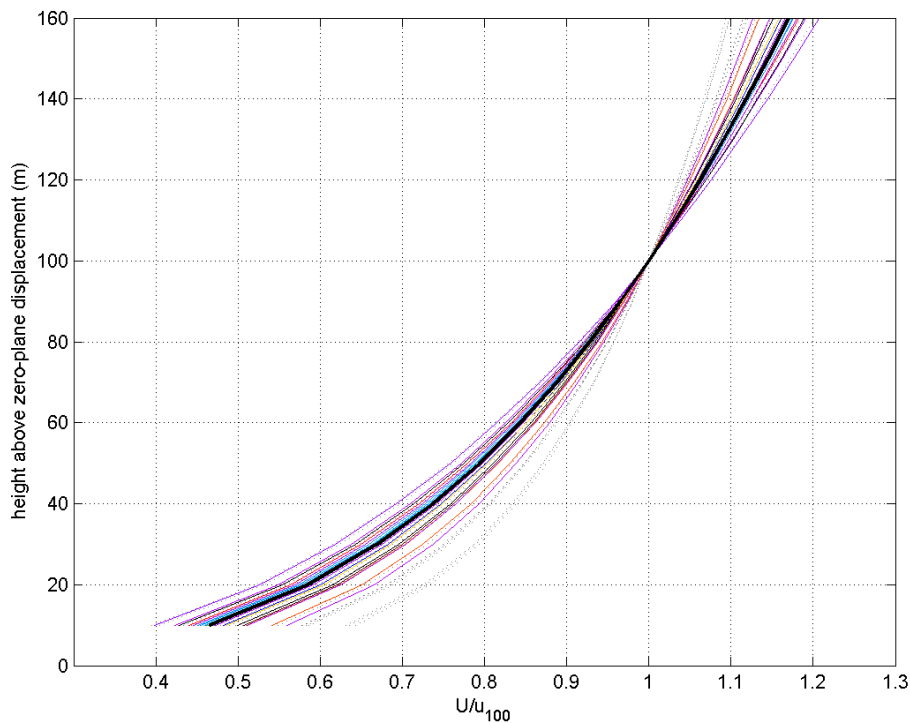


Figure 3-43: Wind speed profiles normalized with wind speed at 100 m above zero-plane displacement. Dotted profiles from all sites. Coloured full line profiles data for sites with small topographical variability. Thick black line profile gives the median profile.

Comparing the wind profiles from the different sites using the exponential wind profile we of course see differences which are significant. The exponent α determined using height above zero-plane displacement when estimating it varies between 0.19 and 0.40 regarding data from all the sites. Data from all three heights were then used. No systematic differences were found regarding measurement heights. Including again only sites with smaller topographical variability the exponent α is limited to the interval 0.25 to 0.40, see Figure 3-44. The median value of α was estimated to 0.33, being a typical value for forest sites.

The relation between α and topography statistics within the closest 5 km from the sites are shown in Figure 3-45. Although there is a clear tendency for α to decrease somewhat with increasing topography, which could be expected as a consequence of flow over hill effects causing a speed up which can be assumed to be larger at low heights thus decreasing the wind shear. But the correlation coefficients, R , giving in Figure 3-45 is rather small showing that also other factors are important for the magnitude of α , such as heterogeneity, density and height of the forest. No significant influence on α from the observed land cover distributions was found.

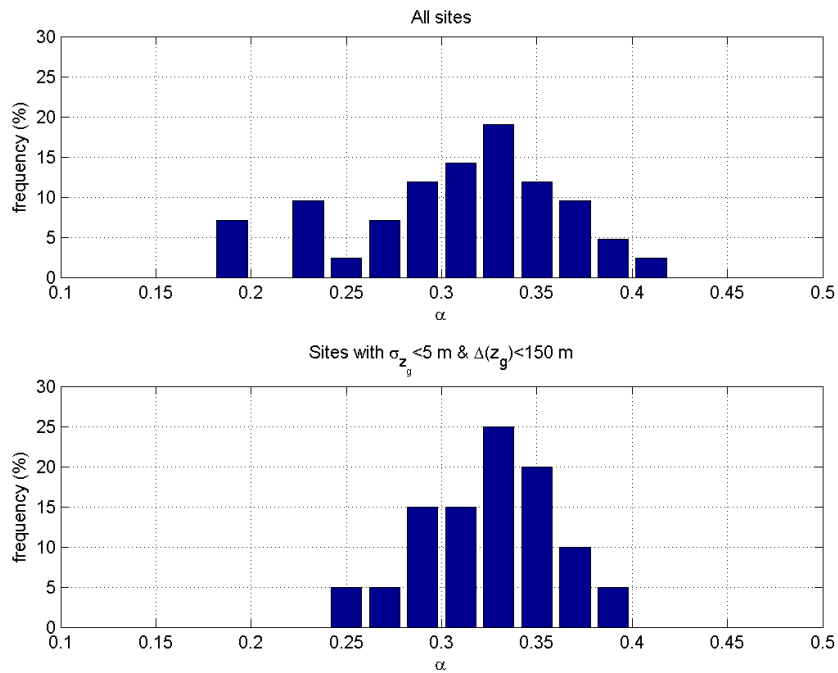


Figure 3-44: Distribution of exponent α in the exponential wind profile. Top subplot shows results using all sites, while in the bottom subplot the sites are limited to the ones with only minor topographical variability.

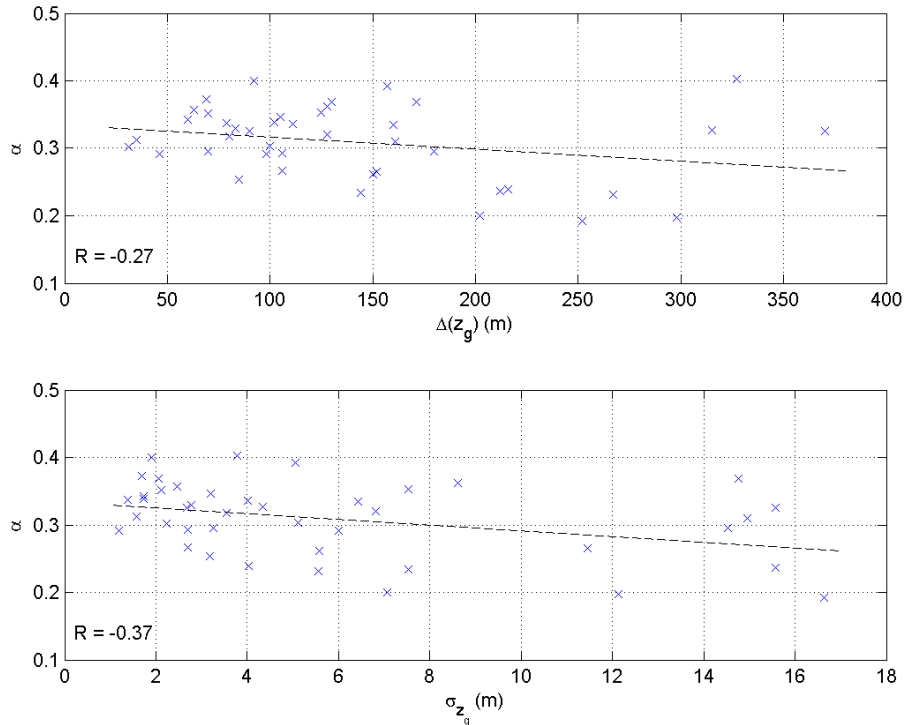


Figure 3-45: Relation between the exponent α in the exponential wind profile and in the top subplot Δz_g , in the bottom subplot σ_{zg} . R is the corresponding correlation coefficient.

The level of turbulence is also an important factor which is important to know planning a wind energy project. The average turbulence intensity TI at 100 m height above ground for the different sites is shown in the upper subplot of Figure 3-46. TI is defined as σ_U/U where σ_U is the standard deviation of wind speed and U is the average wind speed. The median turbulence intensity for all sites is estimated to 0.13 for wind speed above 4 m/s. But the turbulence intensity above forests has been found to vary quite a lot with wind speed, as can be seen in the bottom subplot of Figure 3-46. The dotted lines show data from all sites, the thin full lines data from sites with minor topographical variability, and the thick line shows the median of the turbulence intensity and its dependence on wind speed.

At low wind speed higher turbulence intensity is observed. There is a minimum for a wind speed of moderate strength, and then the turbulence intensity increase again to some higher level, being approximately constant for a wind speed above 13-14 m/s. As the wind load on a turbine could be expected to be higher at higher wind speed, the turbulence intensity at an average wind speed of 15 m/s is commonly used choosing wind turbine type. The median value at 15 m/s is estimated to 0.18.

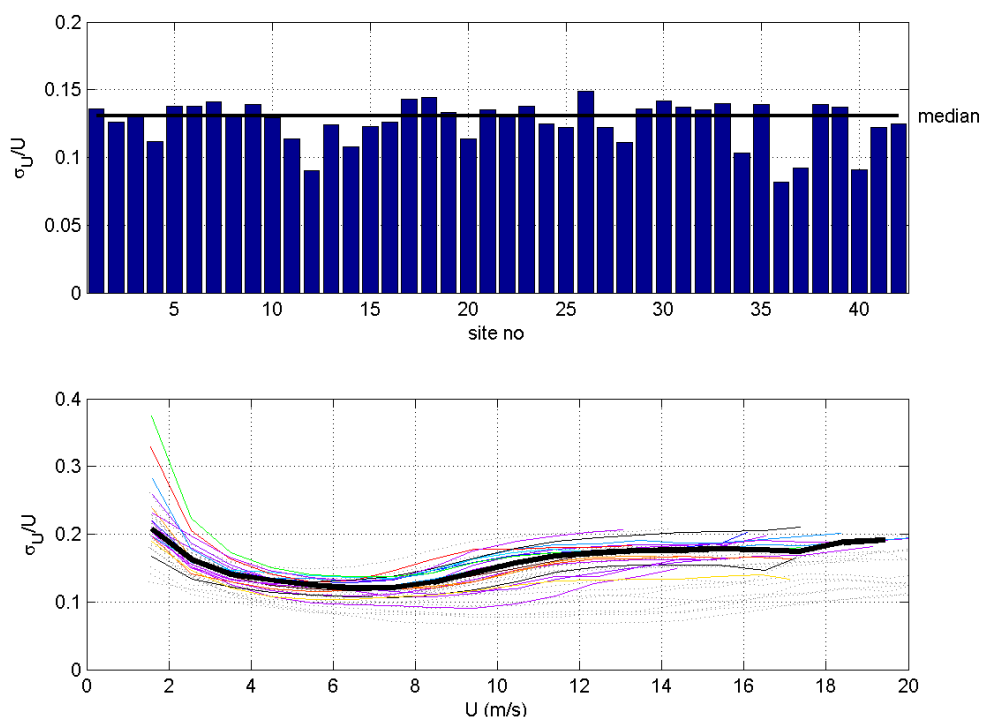


Figure 3-46: The upper subplot shows average turbulence intensity at 100 m height at all sites, and the full line indicates the median of all sites. The bottom subplot shows how turbulence intensity varies with average wind speed. The dotted lines show data from all sites, the thin full lines data from sites with minor topographical variability, and the thick line shows the median of the turbulence intensity.

It should be pointed out that turbulence intensity also to a high degree varies with thermal stability of the atmosphere, so that even if the average level is high over forests the distribution of turbulence intensity shows large variations from very low values around 0.02 to very high values around 0.3-0.4. As an example of this Figure 3-47 shows histograms of turbulence intensity at Ryningsnäs for five stability classes. Only data with wind speed at 25 m higher than 4 m/s were used. The stability was estimated using a bulk Ri-number using wind speed and potential temperature at 25 m and 58 m height. The neutral class was defined as $|Ri| < 0.02$. The border between slightly stable and stable was put at $Ri = 0.1$, while the border between slightly unstable and unstable was put at -0.1 . For the

For unstable stratification the modal value is located at about 0.18-0.19 and decrease to 0.17-0.18 for neutral conditions. For slightly stable situations the peak of the distribution is at 0.12-0.13 and decrease for the stable data to a turbulence intensity of about 0.04 at the same time as the distribution becomes narrower. The distribution for all data shows as a results a double peak; one corresponding to stable stratification and the other to unstable and neutral data.

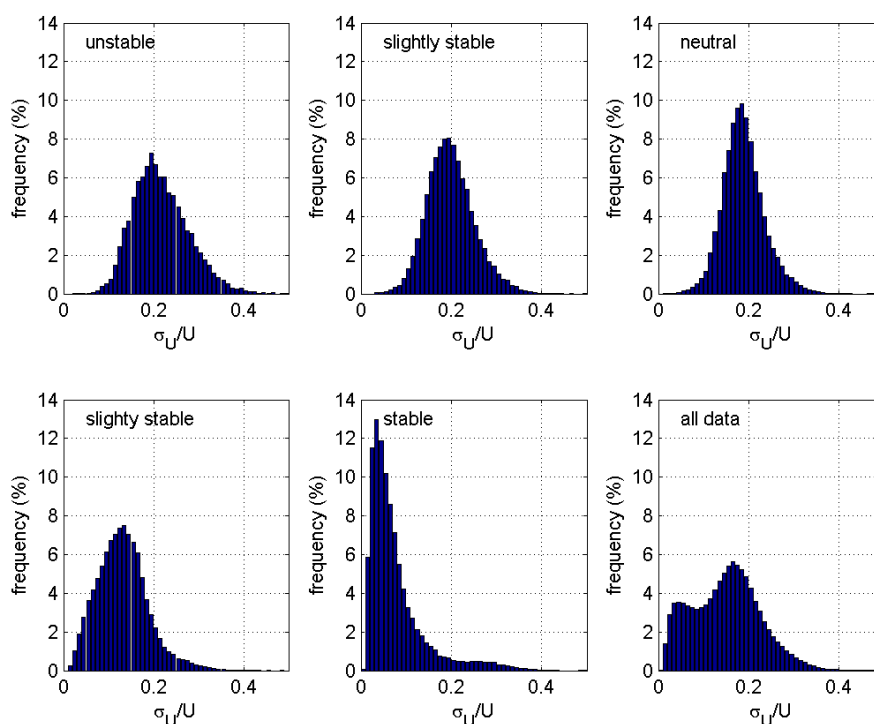


Figure 3-47: Distributions of turbulence intensity at 100 m height at Ryningsnäs for different stability classes and using all data.

A comparison of wind speed profiles normalized with u_* from all sites with the results presented in Section 3.1.3 is shown in Figure 3-48. The thin full line profiles are from sites with small topographical variability, defined using the

limits $\sigma_{zg} < 5$ m and $\Delta_{zg} < 150$ m. There is considerable scatter between the profiles, but the median profile, given by the thick black line, is similar to the results from Ryningsnäs which is shown by the red dashed line, showing wind slightly below the median value. The red, green, and blue thick full lines shows the results presented in Section 3.1.3 for unstable, neutral and stable stratification. The median profile agrees well with these results showing as expected that in the mean the atmosphere is slightly stably stratified. The dotted profiles show sites with appreciable topographic variability. The scatter between the different normalized profiles is very much larger including also these profiles. One site with small topographical variability also shows a somewhat larger deviation from results the majority of sites – the rightmost thin full line profile. This site was above found to have a roughness length value below 0.6 m, and this was identified as possibly caused by effects of a smaller urban area within the closest 1-2 km in the dominant wind direction. As the wind speed is expected to adapt faster to new surface conditions than the turbulence, this means that U/u_* would be expected to be larger as observed at this site.

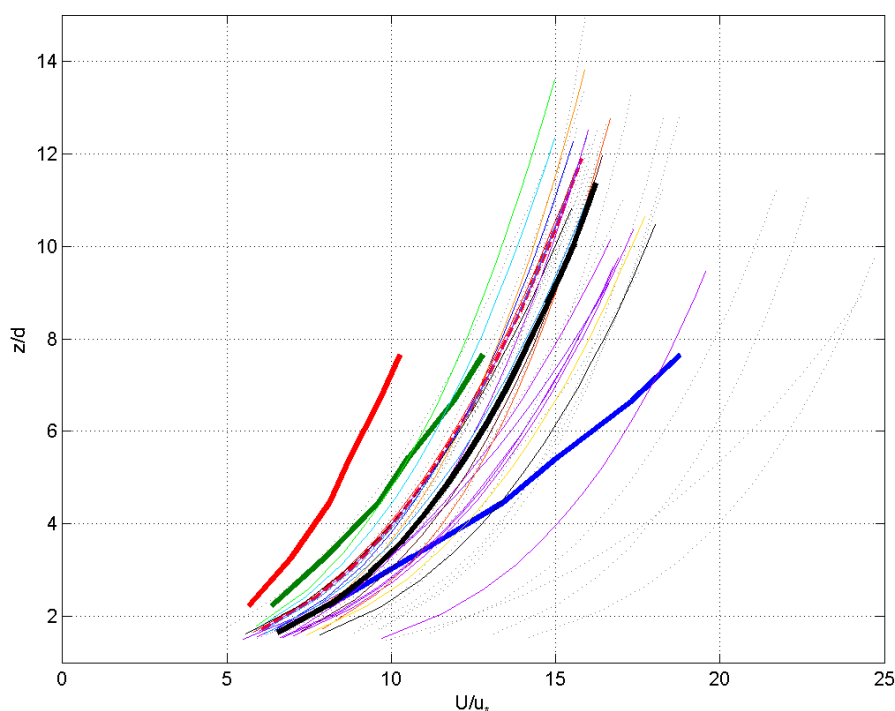


Figure 3-48: Profiles of wind speed normalized with friction velocity u_* . Dotted profiles from all sites. Thin coloured full line profiles data for sites with small topographical variability. Thick black line profile gives the median profile. The red, green, and blue thick full line profiles are the results presented in Section 3.1.3.

The profiles of turbulence intensity from all sites are in Figure 3-49 compared to the results from Ryningsnäs presented in Section 3.1.3. Again the thin full

line profiles show results for sites having smaller topographical variability defined as $\sigma_{zg} < 5$ m and $\Delta_{zg} < 150$ m. Except for the site earlier identified as having an urban area 1-2 km upstream the measurement mast in the dominant wind direction, they all agree reasonably well with each other. The black thick full line shows the median turbulence intensity profile. The dotted lines show profiles with more pronounced topographical variability which typically decrease turbulence intensity. A comparison with the profiles arrived at in Section 3.1.3 for unstable, neutral, and stable stratification are shown by the red, green, and blue thick lines. As for the wind speed profiles the results show the expected in the average slightly stable thermal stratification. The average for Ryningsnäs, shown by the red dashed line, indicates a somewhat more turbulent site than the median of the other sites.

As a whole the comparisons with the sites presented in this Section shows that the results presented in Section 3.1.3 reasonably well could be taken to be representative of forest site conditions, both as regards the normalized wind speed profile and the turbulence intensity profile when plotted against height normalized with the zero-plane displacement. Of course there are differences caused by for example differences in forest height and density which could not be accounted for here, but the dominant deviations from the Ryningsnäs conditions were identified to be caused by topographical effects, which affect both wind speed profile and turbulent intensity profiles. On a forested hill, near a coast or downwind smoother areas the wind conditions may be different, perhaps showing smaller shear and turbulence intensities.

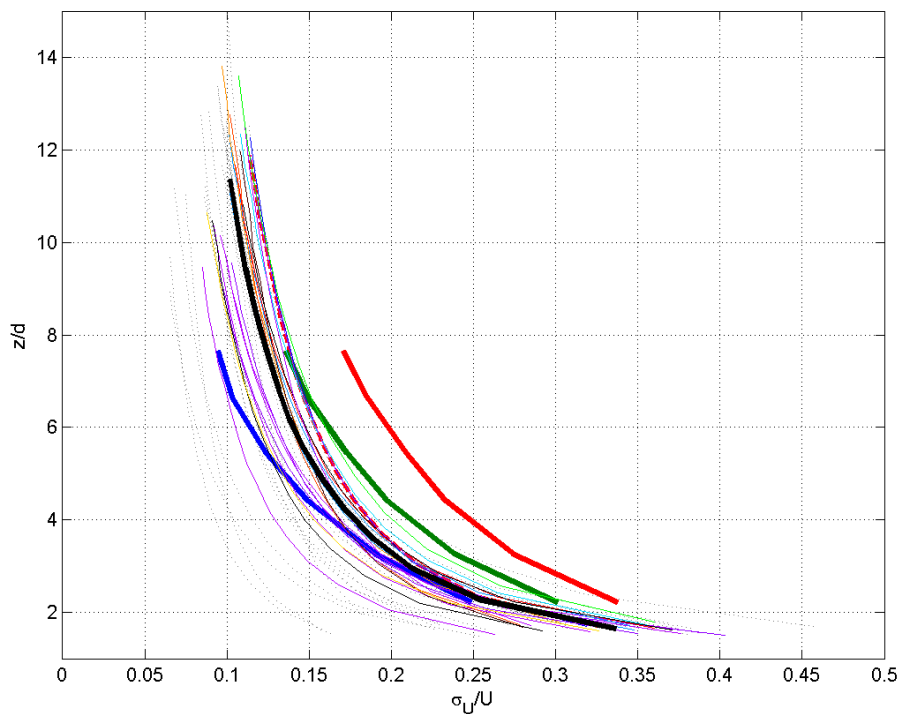


Figure 3-49: Profiles of turbulence intensity. Dotted profiles from all sites. Thin coloured full line profiles data for sites with small topographical variability. Thick black line profile gives the median profile. The red, green, and blue thick full line profiles are the results presented in Section 3.1.3.

Using the variance of wind speed measured with cup anemometers to estimate u_* , with which the wind profile is normalized, may also explain some of the differences. Cup anemometers with different kind of cups will cause different types of measurement errors. Generally cups are also expected to lose some of the wind speed variance due to limitations in instrumental response time. The U/u_* -profiles estimated using sonic anemometers may thus deviate from profiles using cup anemometer data simply due differences in u_* . Profiles of wind speed from cups and sonics actually compare very well when plotted with dimensions. Profiles of turbulence intensity should also be affected by these instrumental differences.

3.4 Summary

Within the project, DTU Wind Energy was responsible for the instrumentation of two sites. When choosing the sites, the criteria were: location in forested areas as well as access to 220 V networks. We chose the 138 m tall mast in Ryningsnäs, run and operated by Vattenfall AB, and the Skogaryd site operated by Gothenburg University.

In this section, the experimental setups at the two sites are described in 3.1.1 and 3.2.1, respectively. Section 3.1.2 describes the data processing and quality assessment. Section 3.1.3 describes some of the experimental results from Ryningsnäs including effects of the atmospheric temperature gradient (stratification).

By choosing data, where the temperature effects are minimized, the roughness length and the displacement height are estimated to between 2 and 3m and 15m, respectively.

At the height span of the measurements, 25-140 meters, we have found clear influence from three major flow regimes, the roughness sublayer, the surface layer and the Ekman layer. For wind power purposes, it seems that effects of the roughness sublayer can be disregarded, apart from its effect on structures in the wind, which is still very much an open question. How much of the flow at typical turbine rotor heights that are controlled by surface layer dynamics have been found to vary strongly with the wind speed and effects of stratification. In neutral stratification we found it to be approximately valid to 100 meters, and less than that in stable stratification.

The results are also analysed in terms of the IEC standardized criteria for the strongest turbines and it is found that the wind conditions at Ryningsnäs are always in conflict with at least one of the IEC parameters. For more neutral conditions when the wind shear is not dramatic the turbulence levels are in the mean above 20%. When stable atmospheric stratification dampens the turbulence, the wind shear becomes very large. The effects of the trees, which slows the wind down, is in stable stratification being restricted to much lower heights because of the resistance of the atmosphere to move vertically. This has the effect of a large wind shear, and also a large wind veer. The

increased wind veer in stable conditions is found to be an effect of the rapid decrease in turbulence and rapid increase of wind speed with height.

An intercomparison using a subset of the data from the Vattenfall setup, the DTU setup and a ZephIR wind lidar is presented. Whereas the mean wind speed measurements by the mast instrumentation agree well, the lidar tends to overestimate the wind, and the mismatch between lidar and in-situ instrumentation increases with increasing turbulence levels.

The wind veer from the different setups has also been compared. Because of uncertainties when aligning the instruments, the veer profile from the Vattenfall setup could only give the difference in veer from one time to another, not the total magnitude. The best estimate was from the DTU instrumentation which showed a mean difference between 40 and 140 meters of more than ten degrees and as large as 23 degrees for stable conditions. After carefully examining the measurement tower uncertainties has remained over the possible turning of the tower itself by some 6 degrees, which would lower the values of wind veer accordingly. Ideally the wind veer is measured by a lidar or sodar instrument, as it has the same base of all measurements. The ZephIR lidar which was used in the experiment did however have large troubles determining the correct direction of the wind $\pm 180^\circ$ which led to large uncertainties in the veer profile.

There is a great scientific interest in detecting and understanding the genesis and evolution of turbulent structures over vegetation. Section 3.1.3 shows some of the work done in this area for Ryningsnäs. The main conclusions so far are that there is clear evidence of evanescent waves in very stable conditions which could be the cause of the organized structures in general forest flows. The period of the structures was found to be around 30 seconds using several different techniques, which is the same as the period for the evanescent waves. Work has also been done on the spatial correlation of the structures and has been published in Segalini et al 2011. The relative contribution to turbulence statistics vary significantly in time and a better understanding of the phenomenon, possibly leading to useful modelling tools, must await further study.

Section 3.1.3 also includes a subsection where spectra have been studied. Velocity spectra from all three velocity components have been scaled in a way that renders a shape applicable to most atmospheric conditions. Parameterisations of quantities used in the scaling are also presented here. The work lead to a model for the velocity spectra that was used together with wind speed and wind veer profile models presented in section 3.1.3 as an input to load modelling of wind conditions over forests. The results from the load modelling can be found in Section 6

For Skogaryd, the analysis in section 3.2.2 is concentrated at estimation of the displacement height and parameterization of the wind profile in the roughness sublayer, which is the layer closest to and above the forest canopy, where the extended height of the forest makes standard parameterizations for surface processes invalid. A new way to correct the wind in the roughness sublayer is presented and work is on-going to incorporate the results of section 3.2.2 to an atmospheric mesoscale model. The initial part of this work is presented in section 5. A result of two days of measurements from the lidar is also presented.

In the comparisons presented in Section 3.3 with observations made at a number of other sites, using routine wind profile measurements, the median value of the roughness length was found to be 1.3 m, that is a lower values than found for Ryningsnäs above. Using only the cup anemometer data also for Ryningsnäs and the same technique to estimate z_0 and d as for all the other sites we got the roughness length 2.1 m. Still somewhat lower than using sonic turbulence data but not so much. This could be due to differences between how cup and sonic anemometers measure wind, and to loss of turbulent energy using cups. But the results point at that the Ryningsnäs site has a more severe wind climate than was typical for the other sites included in the analysis.

The results in Section 3.3 also show that topography, as expected, may have a large influence on average wind and turbulence conditions. For sites with a larger dominance as regards topographical variability both the roughness length and the shear exponent tends to be smaller. The large importance of thermal stability of the atmosphere is also demonstrated. The distribution of turbulence intensity is for example shown to be composed of quite different contributing parts from different stability conditions. Comparisons with profiles of normalized wind speed and turbulence intensity at Ryningsnäs show that the median profiles from all other sites fall somewhere between the neutral and stable stability profiles, which is expected as an annual average.

4 Wind tunnel measurements of a forest boundary layer

4.1 Introduction

The analysis of atmospheric flows over forest is complex due to the increased number of parameters compared to ordinary boundary layers and the high level of uncertainties on both parameters and quantities. Some characteristic parameters of the forest are usually unknown or time dependent, and the flow features of the incoming wind are often hard to measure without specific instrumentation (for instance, the geostrophic wind speed). The analysis is further challenged by the unsteadiness of the incoming wind that requires long sampling time and specific selection criteria to discern thermal instability effects from topography effects.

Wind tunnel experiments do not have these complications and allow the analysis of the flow over forested areas to be performed under well-controlled conditions where the relevant parameters are accessible. Although wind tunnel experiments are performed with downscaled simplified models with lower Reynolds numbers than in a real forest, they offer the possibility to perform detailed measurements which can lead to enhanced physical understanding of different flow processes over forests and to provide simple scaling relationships that can be subsequently tested with other experimental data.

This chapter will provide details about the experimental campaign performed between 2010 and 2012 at KTH in the Minimum-Turbulence-Level (MTL) wind tunnel with a forest model designed to replicate typical flow features over forests. Different experiments have been performed by the KTH group to investigate the turbulence features over homogeneous forests, statistical properties of turbulent structures and effects of the presence of clearings, as discussed in the following sections.

4.2 Experimental setup

The experimental realization of the atmospheric boundary layer and of the canopy model is schematically shown in Figure 4-1a. The atmospheric boundary layer was simulated using four triangular spires placed at the inlet of the test section followed by a 3 m long aluminium mesh placed on the test-section floor (following Irwin, 1981).

The canopy model consists of four 10 mm thick flat plates (each approximately 0.5 m long) and in each plate 3500 holes were drilled in a staggered arrangement. Cylindrical pins with diameter 5 mm and height 60 mm were clamped in these holes to simulate the forest. The height of the canopy is therefore $h_c=50$ mm. The large number of holes easily allows the density and the canopy geometry to be changed, giving the opportunity to investigate, for instance, the effects of clearings (as discussed in Section

4.2.1). Two different pin densities (schematically shown in Figure 4-1b) have been adopted: One has pins in staggered arrangement (from now on denoted the *high density canopy*) with void fraction² 0.866, while the other has a reduced pin density in an in-line arrangement (*low density canopy*) with void fraction 0.933.

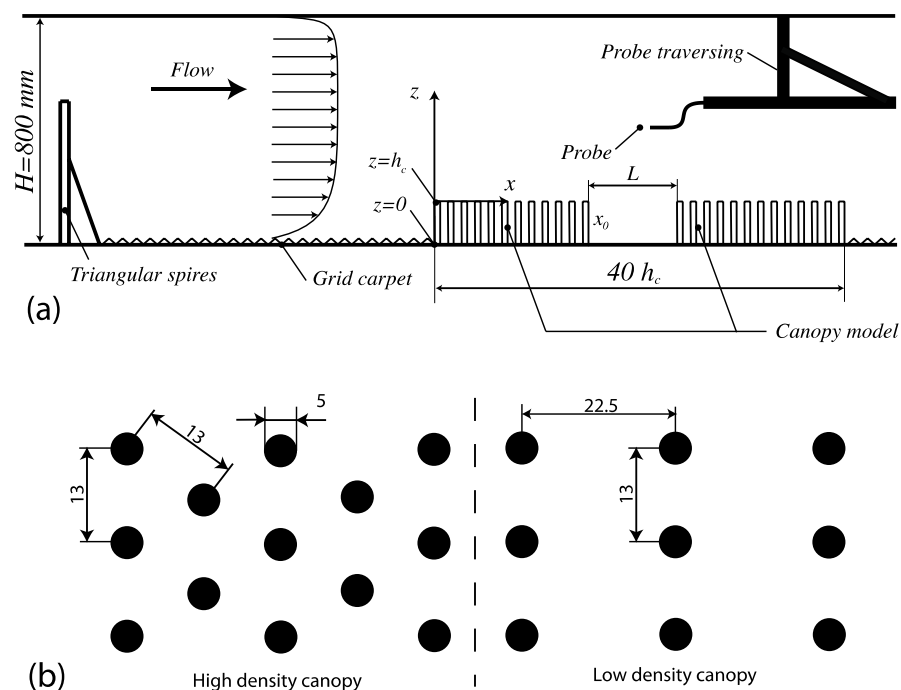


Figure 4-1: Schematic representation of (a) the canopy model and (b) of the pin arrangement for both canopy densities.

Most of the measurements were performed with an in-house manufactured crossed-hot-wire probe with 1.5 mm long wires of 5 μm in diameter, with a measurement volume of 1 mm^3 . The probe measures the stream wise velocity component, u , and either the vertical, w , or span wise, v , velocity statistics depending on its orientation.

The free-stream velocity U_∞ was continuously monitored with a Prandtl tube located outside the boundary layer at the same x -position as the hot-wire probe measurements. During the experimental campaign, the velocity statistics have been measured for both investigated canopy densities (with and without clearings) along the entire canopy model for two free-stream velocities ($U_\infty \approx 11 \text{ ms}^{-1}$ and 22 ms^{-1}). At the last stream wise station ($x/h_c = 30$) and for the configuration without the clearings, five free-stream velocities, ranging from 5.3 to 27.5 ms^{-1} , have been investigated in more detail. The corresponding friction velocity (related to the momentum transferred towards the wall) was not measured directly; instead it was

² The void fraction is here defined as the ratio between the canopy volume occupied by the air and the total canopy volume.

estimated from the maximum of the shear stress close to the canopy top using the relation

$$u_*^2 = \max(-u'w') \quad (4-1)$$

As a notation the time average operator will be indicated with an over bar, while averaged quantities will be indicated with capital letters. Fluctuations $f - \bar{f}$ will be indicated with a prime superscript, as ϕ' . The standard deviation of ϕ , will be abbreviated S_ϕ .

4.2.1 Clearing configurations

Four clearing configurations were tested with different clearing lengths, L , and windward edge positions, x_0 , as reported in Table 4-1. As visible from the table, the first three cases have fixed clearing ending position, while the last one is located upstream of the clearing labelled (a) (which has the same length of (d)), to evaluate the evolution of the disturbances after the clearing and the effect of a different incoming boundary layer thickness. All clearing configurations have been measured with the two different canopy densities used in the full forest configuration in order to evaluate pin density effects on the flow field.

Table 4-1: List of the different cases analysed in the present work.

| Case | (a) | (b) | (c) | (d) |
|-----------|------|------|------|------|
| x_0/h_c | 24.5 | 19.5 | 14.5 | 14.5 |
| L/h_c | 5 | 10 | 15 | 5 |

4.2.2 PIV Details

The hot-wire anemometer is one of the best measurement techniques to study turbulent flows but it has some drawbacks, like its inability to characterize recirculation regions and to provide multi-point statistics in an easy way. Both these points can be solved by means of optical measurement techniques, like Particle Image Velocimetry (PIV), that, on the other hand, do not provide high accuracy and time-resolved statistics. For the PIV measurements one high-speed C-MOS camera (Fastcam APX RS, 3000 fps at full resolution, 1024×1024 pixels, Photron) was positioned in backward-forward scattering mode at an angle of approximately 90° to the acquisition plane. The raw images from the measurements had a resolution of 1024×1024 pixels and a 10-bit dynamic range. The images were taken at a sampling frequency of 500 Hz. A vertical laser light sheet of 1 mm thickness (aligned with the stream wise direction) was produced by a Nd-YLF laser (Pegasus PIV-Laser). Measurements were made at $U_\infty \approx 5 \text{ ms}^{-1}$ and $U_\infty \approx 10 \text{ ms}^{-1}$. The lower velocity provided better PIV images and hence the data is more reliable at this lower velocity.

The PIV measurements provided data that validated the hot-wire measurements over the canopy for both the full forest and forest with clearing configuration (only the case (b) of Section 4.2.1 was analysed). Since only the high density canopy case was investigated with the PIV, pin density effects could not be analysed.

4.3 Results

4.3.1 Full forest configuration

Figure 4-2 reports the mean velocity profiles and the measured variances for all five free-stream velocities available at $x/h_c=30$. The figure shows that the velocity data above the canopy collapse for all U_∞ values, confirming that the flow over the canopy model is approximately Reynolds number independent, at least for the range of Reynolds numbers studied here. The mean velocity profile is weakly affected by the pin density below and above the canopy top, showing a smaller velocity magnitude with the highest pin density. Close to the canopy the velocity variances are enhanced by increasing the pin density, a trend hidden in the present figure by the different friction velocities, u_* , used to normalize the data. Such an enhancement is particularly intense for the vertical velocity variance.

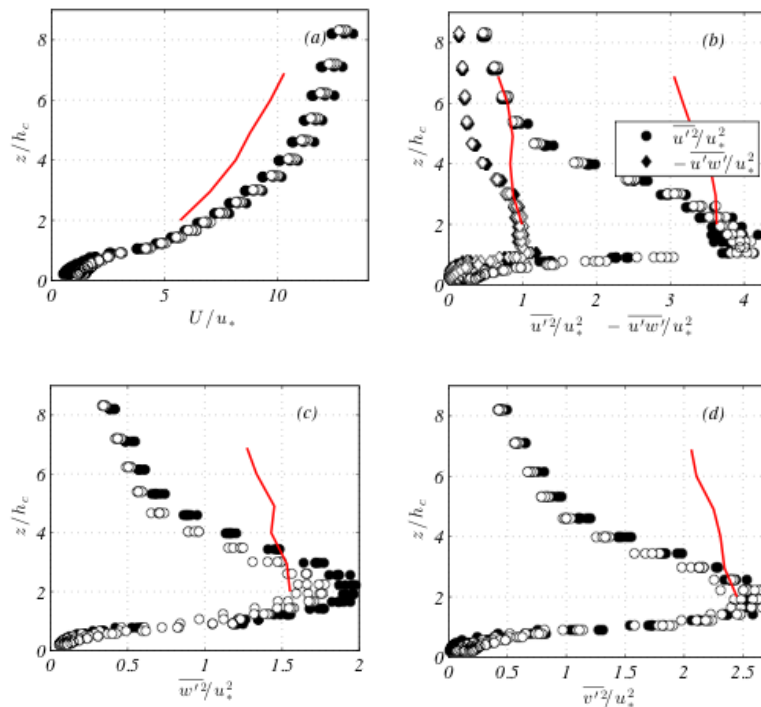


Figure 4-2: Statistics of the high (filled symbols) and low (empty symbols) density canopy boundary layers for all five free-stream velocities available at $x/h_c=30$. (a) U , (b) $\overline{u'^2}$, $-\overline{u'w'}$, (c) $\overline{w'^2}$, (d) $\overline{v'^2}$ profiles normalized accordingly with u_* . The red solid lines indicate the corresponding quantities over the Ryningsnäs forest.

The comparison of the wind tunnel measurements with the Ryningsnäs measurements show poor agreement in the vertical profiles, due to the absence of free-stream turbulence and to the small thickness of the canopy boundary layer in the wind tunnel experiment. Therefore, the wind tunnel data can be considered as representative of the forest turbulence behaviour observed in Ryningsnäs only within the first 2 canopy heights from the ground but, nevertheless, the diffusion of turbulent momentum remains the same and discussed later.

The boundary layer data for both canopy densities at $x/h_c=30$ are reported in tables 2 and 3, where U_h is the measured velocity at the canopy interface. The tables show that, by increasing the canopy density, U_h decreases (less flow within the canopy) and u^* increases (more momentum is absorbed by the pins). Furthermore, by looking at the parameters of the logarithmic velocity profile

$$U = u_* \ln \left(\frac{z-h_c+\epsilon}{z_0} \right) \quad (4-2)$$

it is possible to note that ϵ is reduced by increasing the canopy density, while z_0 remains almost constant, regardless of the canopy density.

Table 4-2: High density canopy boundary layer parameters at $x/h_c = 30$.

| U_∞ [ms^{-1}] | U_∞/U_h | U_∞/u^* | $h_c u^*/\nu$ | ϵ/h_c | z_0/h_c |
|---------------------------------|----------------|----------------|---------------|----------------|-----------|
| 5.3 | 4.01 | 14.2 | 1240 | 0.18 | 0.054 |
| 10.7 | 3.88 | 13.7 | 2620 | 0.21 | 0.061 |
| 16.3 | 3.89 | 13.1 | 4160 | 0.22 | 0.070 |
| 21.9 | 3.86 | 13.1 | 5560 | 0.22 | 0.070 |
| 27.5 | 3.86 | 13.1 | 7000 | 0.23 | 0.070 |

Table 4-3: Low density canopy boundary layer parameters at $x/h_c = 30$.

| U_∞ [ms^{-1}] | U_∞/U_h | U_∞/u^* | $h_c u^*/\nu$ | ϵ/h_c | z_0/h_c |
|---------------------------------|----------------|----------------|---------------|----------------|-----------|
| 5.3 | 3.63 | 14.1 | 1250 | 0.30 | 0.066 |
| 10.7 | 3.71 | 13.8 | 2590 | 0.27 | 0.068 |
| 16.3 | 3.74 | 14.1 | 3860 | 0.27 | 0.066 |
| 21.9 | 3.73 | 13.9 | 5240 | 0.27 | 0.069 |
| 27.5 | 3.73 | 13.8 | 6640 | 0.27 | 0.071 |

A new way to plot boundary layer data (the so called "diagnostic plot") was recently introduced by Alfredsson and Örlü (2010) where the velocity covariances are plotted as function of U normalized with a characteristic velocity (like U_∞ or u^*) that has been shown to scale the data accurately for a large part of the boundary layer. Since the canopy boundary layer is an internal layer, ruled by the amount of momentum transferred downward, the friction velocity appears more suited to the scaling purpose. Here we use this scaling in Figure 4-3 to appreciate Reynolds number and canopy density effects on the measured statistics above and along the canopy. The collapse of the scaled data is good in the region outside the canopy (namely for $U/u^*>4$), at least for the range of Reynolds numbers investigated here. The evident collapse of the data in figure 3 underlines the potential advantage of

using this kind of analysis to determine the turbulence intensities once the mean velocity is known. With the diagnostic plots shown here the data collapse well independently of the canopy density and the x/h_c for all the statistics except for $\overline{w^2}$, which still retains some density dependence.

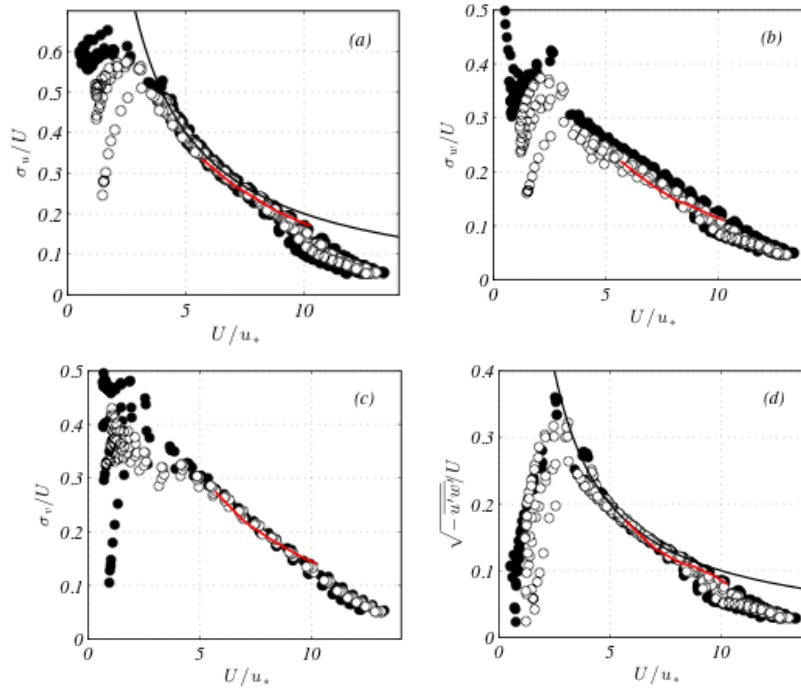


Figure 4-3: Normalized second order velocity moments along the canopy model for all free-stream velocities available at $x/h_c=10, 15, 20, 25, 30$. (a) σ_u (b) σ_w (c) σ_v (d) $-\overline{u'w'}$. (filled symbols) high density canopy, (empty symbols) low density canopy. In (a) the solid line is $\sigma_u = 2u_{*y}$, while in (d) it is $-\overline{u'w'} = u_{*z}^2$. The red solid lines indicate the corresponding quantities over the Ryningsnäs forest.

In Figure 4-3a the rule of thumb of $\sigma_u \approx 2u_*$ is reported and it agrees nicely with the data up to $U/u_* \approx 7$. The same can be observed in figure 3d, where the constant stress relationship is also reported. Above the constant stress layer, the diagnostic scaling continues to show agreement between the data up to $U/u_* \approx 10$ (approximately $z/h_c=3$), where the edge of the internal layer is approached.

The comparison of the present data with the atmospheric measurements performed over the Ryningsnäs site shows this time a much better agreement than the one shown in figure 2, demonstrating that, despite the reduced turbulence intensity in the outer region, the momentum transfer processes are the same, leading to the same diagnostic function. It can therefore be expected that with a longer wind tunnel the vertical statistical profiles will converge towards the Ryningsnäs ones, underlining the quality of the present measurements.

A further step in the comprehension of the dynamics of turbulence is provided by spectral analysis which gives some insight in the analysis of this flow case. The power density spectra of the stream wise velocity at all the available free-stream velocities, stream wise positions ($10 \leq x/h_c \leq 30$), and for $z > h_c$ (but still within the canopy internal boundary layer), are plotted in figure 4. It can be shown that the spectra generally scale in terms of velocity variance and integral time scale, here defined as

$$\Lambda = \frac{1}{\sigma_u^2} \int_0^{+\infty} \overline{u'(t)u'(t + \tau)} d\tau \quad (4-3)$$

For the present set of experiments, the integral time scale is around $\Lambda \approx 0.3h_c/u_*$ from the canopy top up to $z/h_c \approx 5$, in agreement with the measurements of Shaw et al (1995). The proposed scaling normalizes the value of the spectra for small frequencies and simultaneously the integral of the spectra. With such a scaling all the spectra collapse on top of each other up to $f\Lambda \approx 10$. All the shown spectra exhibit three spectral regions, namely

1. the energy containing range ($f\Lambda \leq 0.1$);
2. the inertial subrange ($0.1 \leq f\Lambda \leq 10$);
3. the dissipative range ($f\Lambda \geq 10$) where the viscous action converts turbulent kinetic energy into heat.

Due to the large Reynolds number of the present experiment, the Kolmogorov $f^{-5/3}$ law is observed in region (2) for approximately two orders of magnitude in frequency, ensuring scale separation between region (1) and (3), which is also manifested through the Reynolds number independence observed from the turbulence statistics in Figure 4-2

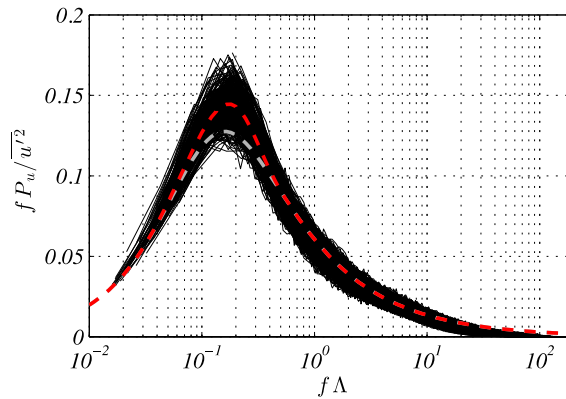


Figure 4-4: Premultiplied stream wise velocity power density spectra, for the same points used in Figure 4-3 with $z > h_c$ and $\sigma_u^2 > 1.5u_*^2$, scaled with Λ and $\overline{u'^2}$. 333 independent spectra are shown in the figure. The grey dashed line is equation (4) with no correction ($G=0$), while the red dashed line is Equation (4-4) with the peak correction reported in Equation (4-5).

The spectra agree reasonably well, giving the possibility to define a universal spectral curve capturing more than 90% of the fluctuating spectral energy including the $f^{-5/3}$ region of the form

$$P_u = \frac{2}{1+32(f\Lambda)^{5/3}G(f\Lambda)} \quad (4-4)$$

with the peak correction given by

$$G(x) = 1 - 2x \exp(-20x^2) \quad (4-5)$$

Figure 4-4 reports the fit with $G=0$ (no correction) and with the G function stated in Equation (4-5) demonstrating a good fit in the inertial region together with a significant improvement in the fit in the energy containing range.

4.3.2 Clearing configurations

After the measurement campaign with the full canopy conditions, some clearings have been added to the forest model in order to provide experimental data of their effect on the turbulence. The measured mean stream wise, U , and vertical velocity, W , in the model middle plane are reported in Figure 4-5 and Figure 4-6, respectively, for all the clearing configurations available for the high canopy density case. The picture that emerges is that the sudden absence of pins forces the fluid to move downward to fill the velocity defect imparted by them. By continuity it could have been expected that all streamlines would deflect downward, providing more wind above the clearing than with full forest conditions. However this is true only close to the forest model, while above two canopy heights the effect is small or even detrimental, namely there is less wind at a given height.

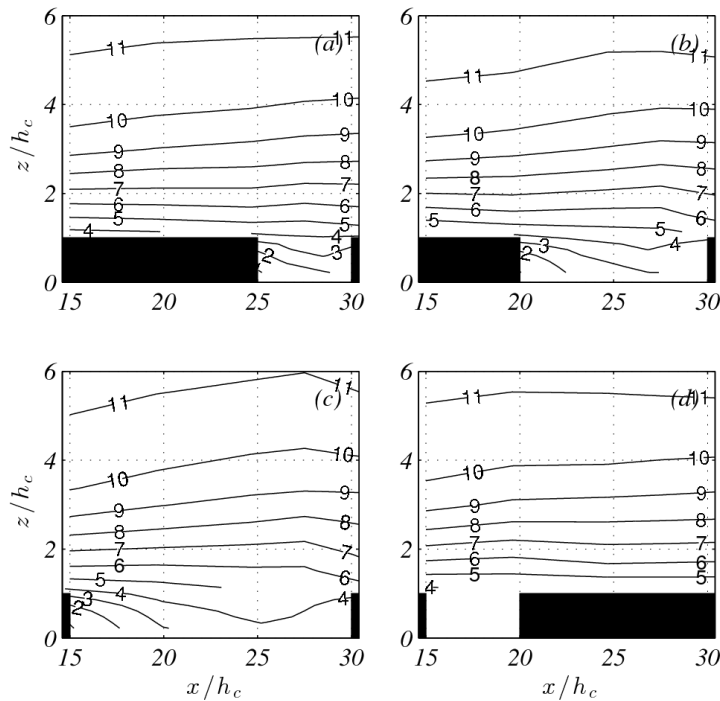


Figure 4-5: Horizontal mean velocity U/u_* along the forest model for the high density canopy for the four different clearing configurations.

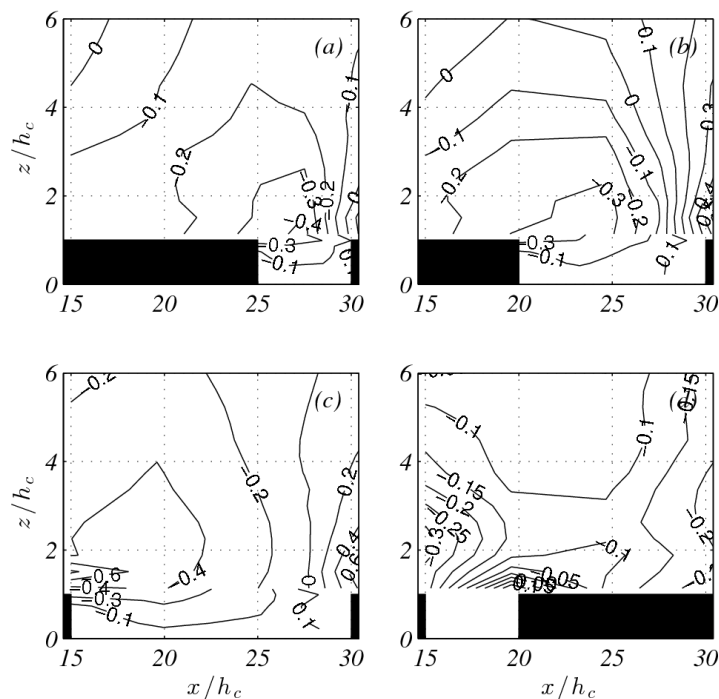


Figure 4-6: Vertical mean velocity W/u_* along the forest model for the high density canopy case for four different clearing configurations.

The vertical velocity W can be considered as an indicator of the clearing effect: If $W < 0$, fast parcels should move downward, increasing the local wind speed, and vice versa when $W > 0$. The different clearing configurations always lead to an increase of the wind speed in the neighbourhood of the clearing windward edge, and to a negative contribution close to the downwind edge. The vertical height affected by this velocity augmentation increases with the clearing length L , as visible from the iso-contour $W = -0.2u_*$, a threshold value that is beyond the measurement uncertainty that affects the measurement of W .

The penetration of flow within the cleared region increases with the clearing length, as evident in Figure 4-5 and Figure 4-6. The iso-contour lines are visibly modified close to the windward edge where the air flowing out from the canopy suddenly starts to accelerate and to move downward, generating a bubble (sometimes called *quiet region*): There is no reason to expect the presence of a recirculating bubble (as suggested by the backward facing step analogy), but the experimental evidence in the literature show generally an enhanced turbulence level behind the windward edge and, sometimes, recirculating patterns as well.

The velocity standard deviations iso-contours (reported in figures 7 and 8), that for the full forest configuration are $\sigma_u \approx 2u_*$ and $\sigma_w \approx 1.4u_*$ for $z \approx h_c$, indicate that the turbulence is convected above the clearing for $z/h_c > 3$. σ_u appears to be reduced by the clearing presence, while there is no clear increase of σ_w above the forest, which may have been expected

The reduction of the forest model density attenuates the jump between the forest model and the clearing, making the transition milder. On the other hand, the smooth-to-rough transition region at the clearing downwind edge seems to be almost unaffected by the forest density. This difference suggests

that the transition rough-to-smooth and smooth-to-rough follow two different physical mechanisms, the former more related to convection and turbulent diffusion, the latter more forced by the high pressure strain present at the clearing trailing edge.

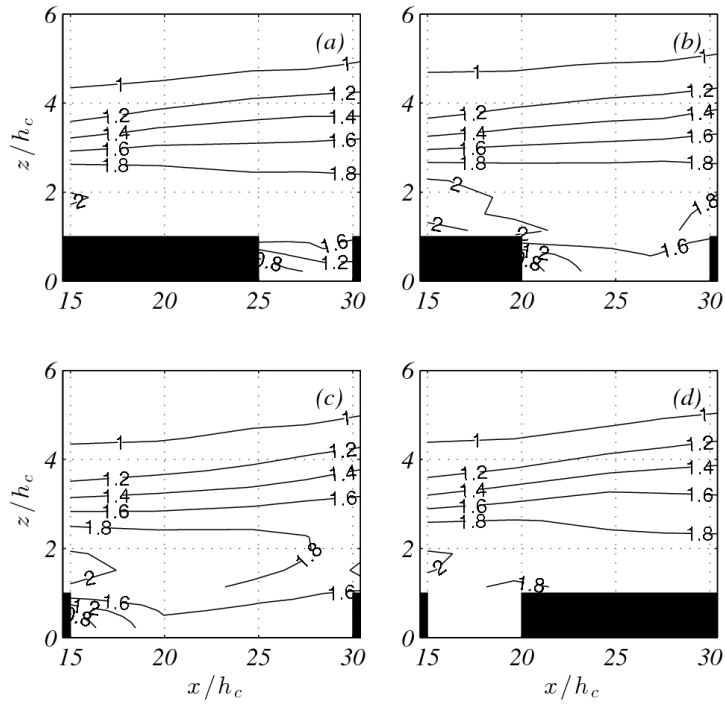


Figure 4-7: Horizontal velocity standard deviation σ_u/u_* along the forest model for the high density canopy case for four different clearing configurations.

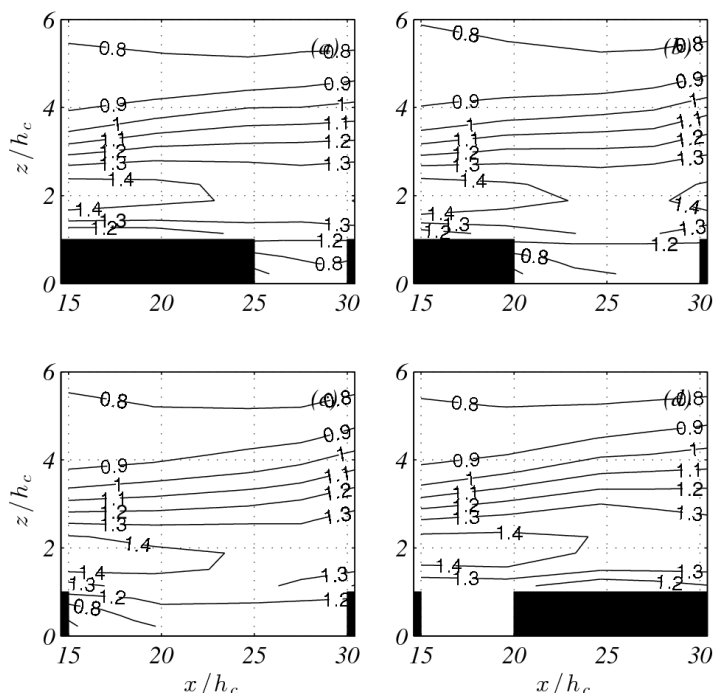


Figure 4-8: Vertical velocity standard deviation σ_w/u_* along the forest model for the high density canopy for four different clearing configurations.

4.3.3 Experiments with Particle Image Velocimetry (PIV)

Different PIV experiments have been performed within the project and the analysis of the results is still going on. The advantage of this measurement technique is the possibility to access multi-point measurements more easily than with hot-wires, leading to an improved description of the correlations and of the coherent structures. An example of the two-point correlation maps can be seen in Figure 4-9 for the full forest configuration. A clear single peak is present in the neighbourhood of the reference point, with a monotonic decay in the radial direction. The correlation map does not appear to be symmetric but it is inclined, as often observed in wall-bounded flows.

An interesting outcome of the two-point correlation analysis is the scaling of the co-variances between two different points. A traditional way to plot them is reported in Figure 4-10a, namely as a function of the separation distance. It has been observed that the present PIV data and the Ryningsnäs data obey to a different scaling relationship of the form

$$\overline{u'(z_1)u'(z_2)} = \sigma_u(z_1)\sigma_u(z_2)f\left(\frac{|z_2-z_1|}{h_c} \frac{2u_*}{U(z_1)+U(z_2)}\right) \quad (4-6)$$

Although Equation (4-6) can appear complex, it simply states that the covariance scales with the local standard deviation and mean velocity of the two points. This scaling improves the collapse of the correlations as visible in Figure 4-10b for the PIV data.

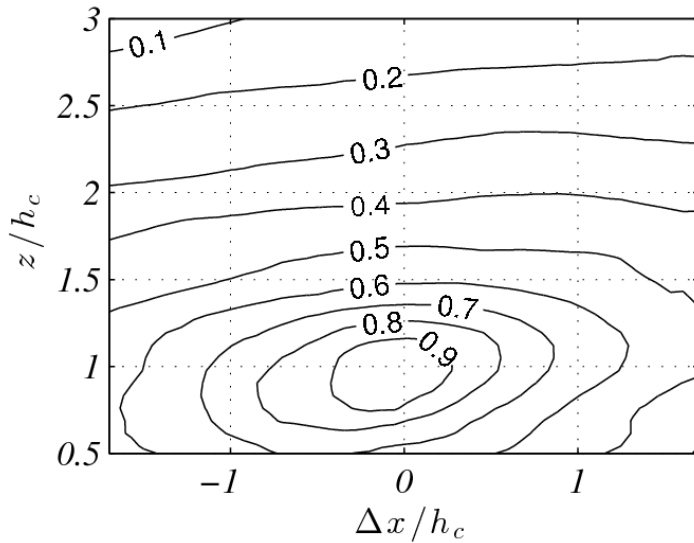


Figure 4-9: Two-point correlation map $R_{uu} = \overline{u'(P)u'(P_R)} / \overline{u'^2(P_R)}$ with the reference point P_R located at $z/h_c=1$.

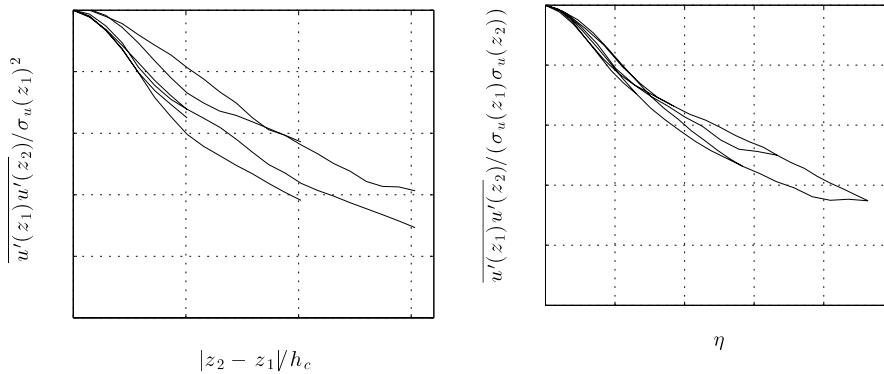


Figure 4-10: Two-point correlation at the same stream wise station for different z_1 and z_2 . (a) Traditional scaling, (b) proposed scaling.

4.4 Concluding remarks

An experimental analysis of canopy flows has been performed and discussed in order to understand typical features of the turbulent boundary layer above forests and clearings. Despite the fact that the canopy has been modelled with cylindrical pins of constant height, most of the present experimental results are in agreement with the ones observed at the Ryningsnäs site at the lowest heights, and at the Skogaryd site, underlining the fact that the present simplified canopy model is able to realistically model the flow above a forest, with the advantage that wind-tunnel measurements ensure a good knowledge of the boundary conditions, like the free-stream velocity and boundary-layer

height, usually not easy to access in field measurements.

A detailed analysis of the statistics measured in the full forest configuration at a stream wise distance of $30h_c$ from the canopy model leading edge was made, showing that mean velocity profiles follow a logarithmic law within the internal canopy boundary layer. Velocity covariances profiles have been reported for different free-stream velocities, vertical positions and for two different canopy densities. The increase of canopy density leads to a higher momentum transfer towards the canopy, consequently increasing the velocity gradient of the wind profile near the canopy top. Furthermore, it has been noted that the vertical velocity variance is significantly affected by the canopy density, while the other statistics do not show this effect if normalized with the friction velocity.

The evolution along the canopy of the mean velocity profile and of the velocity covariances demonstrated the growth of the internal boundary layer above the forest model. This variation has been circumvented by means of diagnostic plots, where the measured velocity covariances are reported as a function of the mean stream wise velocity rather than the vertical distance. The data reported in diagnostic form show a remarkable collapse of the measurement points located above the canopy top regardless of the free-stream velocity, stream wise station and canopy density, with the exception of the vertical velocity standard deviation, which showed a spurious canopy density effect not removed by the diagnostic plot. Nevertheless, the diagnostic approach represents a powerful tool to analyse statistics provided by wind tunnel and atmospheric experiments and to determine Reynolds stress profiles, of utmost importance for wind energy and micrometeorology.

This approach further demonstrated that the present measurements, which do not agree with the Ryningsnäs measurements in terms of vertical profiles, follow the same momentum transfer processes of the atmospheric data and therefore the same diagnostic curves. The observed discrepancy in the vertical profiles can be therefore be attributed to an insufficient developing length of the canopy model.

The scaling of the velocity spectra with the integral time scale has shown a remarkable collapse of the spectra at different stream wise stations, heights, free- stream velocities and canopy densities, demonstrating scale separation for two decades in frequency and suggesting a new possible way to parameterize spectra in canopy flows up to the boundary layer edge. By means of this normalization a new expression for the stream wise velocity spectra has been proposed which accounts for more than 90% of the total turbulent kinetic energy.

The analysis of PIV measurements provided some insight in multi-point statistics and their scaling, suggesting new ways to plot the data that improve their collapse, a property demonstrated for the two-point velocity covariance that scales with the local mean velocities and variances at the two interested points.

An analysis of different forest-clearing configurations has been discussed by comparing velocity statistics measured in wind tunnel with hot-wire anemometry (although new PIV measurements are also available and currently under analysis). During the measurement campaign the clearing

length and position was changed, as well as the forest density, to investigate the sensitivity of these parameters on the velocity statistics. The clearing effects seem to be limited to the flow region close to the canopy top and well within the internal boundary layer due to the canopy. The physical description that can be proposed is that the flow experiences a region of enhanced mixing in the rough-to-smooth transition. The turbulence does not increase because the high turbulence level cannot be sustained anymore with the tree absence, and also it can now penetrate towards the ground since there is no longer the drag force of the trees. One of the consequences of this mixing region is that the stream wise velocity increases within the canopy but it does not increase as expected above it, being the increase limited to the mixing-layer region.

When the flow is approaching the clearing downwind edge there is no mixing layer region anymore, and the flow is deflected upwards by the high pressure strain region present at the forest entrance due to the tree drag. However a significant part of the flow stream enters the canopy region and is subsequently ejected upwards in the Enhanced Gust Zone. This effect increases with the clearing length since more air is entrained in the cleared area with long clearing, and it seems to be absent for the two analysed cases with $L/h_c=5$.

5 Meso-scale modelling of forests

5.1 Results from several models and comparisons with observations at Ryningsnäs

State-of-the-art mesoscale models that are commonly used for wind mapping have been used to simulate the wind climate around Ryningsnäs. Two mesoscale models COAMPS and WRF were run for the winter of 2011/2012 by Weathertech and Risø. This made it possible to directly compare model results with observations during this time period. A third mesoscale model, the MIUU-model, was run by Uppsala University to produce the long-term wind climate at the site using different model configurations.

a) Model description

COAMPS®

COAMPS® (Coupled Ocean/Atmosphere Mesoscale Prediction System) is a numerical mesoscale model developed at the US Naval Research Lab, Monterey, California. Here, version 3.1.1 of the system has been used. It is a non-hydrostatic compressible model with a terrain-following sigma-z vertical coordinate. Turbulence is parameterised with a level-2.5 turbulence closure (Mellor and Yamada, 1982); hence, TKE (turbulent kinetic energy) is a prognostic variable. Ground surface temperature is computed using a surface energy balance scheme. High resolution for a given area of interest can be achieved by using nested grids in idealised and real-case simulations. A more complete model description is found in Hodur (1997).

COAMPS® is used operationally by the US Navy to produce forecasts. Examples of areas in which COAMPS® is used on a daily basis are along the US West Coast and in the Mediterranean Sea. In Sweden, COAMPS® is used as a research tool at Uppsala University and Stockholm University, and operationally by WeatherTech Scandinavia AB to produce wind forecasts. The model has also been used in numerous research studies, e.g. on coastal jets (Burk and Thompson 1996, Burk et al. 1999) and katabatic flow (Söderberg and Parmhed 2005).

In order to cover the measurement site with a high model-grid resolution, nested grids were used. A one-way nesting technique was used here. The outer mesh and nest levels 1 to 3 are illustrated in Figure 5-1. The model grid resolution in the outer mesh is 27x27 km² and increases with a factor 3 to 9x9 km², 3x3 km², and 1x1 km² in nest level 1 to 3. The model was set up with 40 vertical levels ranging from 5 m to 34330 m above ground; 10 of the levels are in the lowest 300 m above ground (Table 5-1).

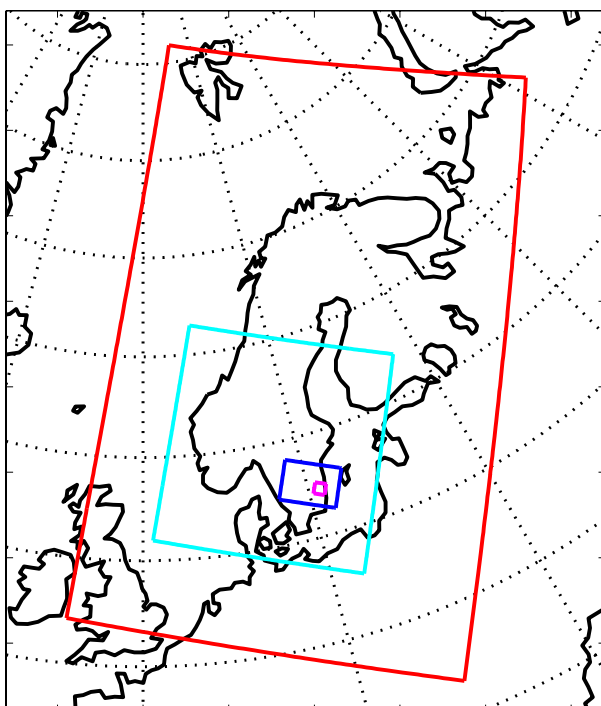


Figure 5-1: COAMPS® model domains. Outer domain, 27x27 km² (red), nest level 1, 9x9 km² (light blue), nest level 2, 3x3 km² (dark blue), and nest level 3, 1x1 km² (magenta).

Table 5-1: The lowest 10 levels in WRF, COAMPS® and MIUU-model runs. Heights are given in meters above zero plane displacement.

| Model level | 1 | 2 | 3 | 4 | 5 | 6 | 7 | 8 | 9 | 10 |
|-----------------|----|----|----|----|-----|-----|-----|-----|-----|-----|
| COAMPS | 5 | 15 | 25 | 35 | 45 | 60 | 85 | 120 | 165 | 220 |
| WRF-Weathertech | 15 | 37 | 53 | 75 | 100 | 127 | 156 | 188 | 222 | 259 |
| WRF-Risø | 14 | 41 | 69 | 83 | 96 | 124 | 182 | ... | ... | ... |
| MIUU-model | 2 | 6 | 12 | 21 | 33 | 49 | 72 | 103 | 147 | 207 |

The model was run from September 2011 to April 2012. Initial and lateral boundary conditions were provided using NCEP FNL (Final) Operational Global Analysis data (U.S. National Centers for Environmental Prediction). NCEP FNL is prepared operationally every six hours on a 1 x 1 degree global grid. Observational data from the Global Telecommunications System (GTS) and other sources are continuously collected in the Global Data Assimilation System (GDAS). The FNLs are made with the same model NCEP uses in the Global Forecast System (GFS). The analyses are available on the surface, at pressure levels from 1000mb to 10mb, and in the surface boundary layer.

The model is run in 18 h cycles and cold-stared at 00 and 12 UTC. The first 6 h of the simulation are not used allowing for model spin-up, necessary for

e.g., turbulence kinetic energy and cloud physics. Outer mesh boundary conditions are updated every 6 h (00, 06, 12 and 18 UTC).

Surface characteristics applied to the lower boundary are given by a database included in the model system. Roughness and ground wetness over land is determined by a land-use classification from a 1 km global land-use dataset (USGS). Terrain height is given by a 1 km global terrain database.

WRF - Weathertech

The Weather Research and Forecasting (WRF) model is a mesoscale numerical weather prediction system that is suitable for modelling the atmosphere with high-resolution. The system supports two dynamical solvers: the Advanced Research WRF (ARW) and the nonhydrostatic Mesoscale Model (NMM). In the present study WRF ARW v3.2 has been used. It is a community model for which development is supervised primarily by National Centers for Environmental Prediction (NCEP) and National Center for Atmospheric Research (NCAR) in the US. The solver in WRF consists of a set of Eulerian equations that is fully compressible, non-hydrostatic and conservative for scalar variables.

The WRF model consists of many different physics schemes that are available to use with the ARW solver. These include different descriptions for microphysics, cumulus parameterizations, surface physics, surface layer physics, planetary boundary layer physics and atmospheric radiation physics. For a full list and description of the schemes available see Skamarock et al. (2008).

WRF surface layer schemes are responsible for calculating friction velocities and exchange coefficients that are needed by the planetary boundary layer and land surface schemes. Over water the surface layer scheme also calculates the surface fluxes. The scheme used herein is called the Eta surface layer scheme (Janjic, 1996, 2002 cited by Skamarock et al., 2008). It is based on the similarity theory by Monin and Obukhov (1954) including parameterizations of a viscous sub-layer following Janjic (1994, cited by Skamarock et al., 2008).

The land-surface models (LSMs) in WRF use input data from many of the other schemes to calculate heat and moisture fluxes. The Noah LSM, which was used in this work, was developed by NCAR and NCEP and is similar to the code used in the NCEP North American Mesoscale Model (NAM).

The planetary boundary layer (PBL) schemes compute tendencies of temperature, moist and horizontal momentum by determining the vertical flux profiles in the well-mixed boundary layer and the stable layer (Skamarock et al., 2008). The surface fluxes needed in the PBL schemes are provided by the surface layer and land-surface schemes. The Yonsei University (YSU) PBL scheme (Hong et al., 2006 cited by Skamarock et al., 2008) was used in this work. It uses counter-gradient terms to represent fluxes and has an explicit term handling the entrainment layer at the PBL top. The PBL top is defined from the buoyancy profile.

To cover all the measurement sites, separate computational model domains in which the sites were grouped in different geographical areas were set up. The

outer mesh and nest levels 1 to 3 are illustrated in Fig. 2. The model grid resolution in the outer mesh is $27 \times 27 \text{ km}^2$ and increases with a factor 3 to $9 \times 9 \text{ km}^2$, $3 \times 3 \text{ km}^2$, and $1 \times 1 \text{ km}^2$ in nest level 1 to 3. The model was set up with 45 vertical levels with 11 levels in the lowest 300 m, see Table 5-1.

The model was run from September 2011 to April 2012. The meteorological initial and lateral boundary conditions are taken from FNL data. Outer mesh boundary conditions are updated every 6 h (00, 06, 12 and 18 UTC). The model is run in 18 h cycles and cold-started at 00 and 12 UTC. The first 6 h of the simulation are not used allowing for model spin-up. A one-way nesting technique is used.

The data describing the lower surface is extracted from several databases including e.g. topography and land-use data. These databases are included in the standard WRF source package.

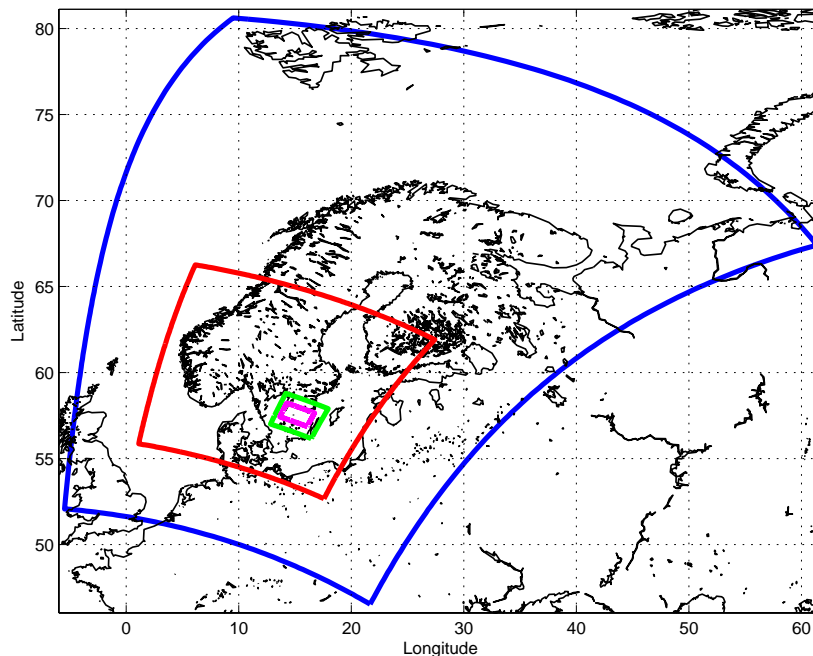


Figure 5-2: WRF[®] model domains. Outer domain, $27 \times 27 \text{ km}^2$ (blue), nest level 1, $9 \times 9 \text{ km}^2$ (red), nest level 2, $3 \times 3 \text{ km}^2$ (green), and nest level 3, $1 \times 1 \text{ km}^2$ (magenta).

WRF - Risø

Risø also used WRF-ARW 3.2.1 to simulate the wind climate around Ryningsnäs. A horizontal resolution of 5 km was used. Vertically, 10 levels were used below approximately 1000 m. Also tests with higher vertical resolution were carried out.

For turbulence, the MYJ scheme (Janic, 2001) and the YSU2 scheme (e.g. Hong et al. (2006)) were used. YSU2 is the updated Yonsei University PBL turbulence scheme (Hong and Kim, 2008), which - especially during stable conditions - should yield better results in the atmospheric boundary layer (e.g., Hu et al. 2010).

For topography Shuttle Radar Topography Mission (SRTM) data was used. For land use Modis data was used. Both belong to the WRF standard setup.

For forest, $z_0 = 0.5$ m was used in the WRF MYJ and WRF YSU2 runs, whereas $z_0 = 2.0$ m was used in the WRF MYJ rough run. For SST, a 1/12 degree database from NOAA was used.

The model was run for 11 days. The first 24h are regarded as model spin-up and not used in the analysis. In the largest domain all parameters above level 10 were nudged towards ERA interim data. A nudging coefficient of 0.0003 s^{-1} was used for wind, temperature and specific humidity. In the nested domains, however, no nudging was applied (Peña et al., 2011).

MIUU-model

The MIUU-model is a three-dimensional hydrostatic mesoscale model, which has been developed at the Department of Meteorology, Uppsala University, Sweden, (Enger, 1990). The model has prognostic equations for wind, temperature, humidity and turbulent kinetic energy. Turbulence is parameterised using a level 2.5 scheme following Mellor and Yamada, (1974). The closure is described in detail in Andrén (1990). The MIUU model has a terrain-influenced coordinate system (Pielke, 1984), roughly following the terrain close to the surface and gradually transforming to horizontal at the model top. To reduce influences from the boundaries, the modelled area is chosen to be much larger than the area of interest. This also makes it possible to account for effects of, for instance, mountains and water areas which are outside the investigated area, but which may anyhow be of importance to the wind field within the area of interest. To limit the number of horizontal grid points, a telescopic grid is often used, with the highest resolution only in the area of interest. In the vertical, the lower levels are log spaced while the higher levels are linearly spaced. The lowest grid point is at height z_0 , where z_0 is the roughness length, and the model top is typically at 10000 m. Commonly 8 levels are used in the model up to 100 m height.

At the lower boundary, roughness length and altitude (of land) have to be specified at each grid point. Topography is taken from Lantmäteriet's digitised maps with a horizontal resolution of 50 m. The roughness over land has been divided into classes according to land cover. Land cover data, with the horizontal resolution of 25 m, was taken from Lantmäteriet. Also temperature has to be given or estimated at the lower boundary for each grid point. The land surface temperature, and its daily and monthly variation, is estimated with a surface energy balance routine using as input solar radiation and land use. Over sea the observed monthly average sea-surface temperatures have been used.

To include effects on the wind climate from areas outside the area of interest, model runs with 5 km resolution were first made covering a large part of the Baltic Sea area, including also Scandinavia, Finland, and the Baltic States. The 1 km model runs were then 'nested' into the 5 km model domains. The results from the 5 km runs were used to give values at the lateral boundaries of the smaller model domains with 1 km resolution. In doing this, account could be taken of topography and land-sea differences on a larger scale which may still affect the local wind climate in smaller areas of specific interest. To minimise

effects of the lateral model boundaries upon the results a region with expanding grid spacing was used along the model borders in a strip around the area with higher resolution.

In the vertical there were 29 grid points. The first one is at the height z_0 , where z_0 is the roughness length. Close to the ground the vertical grid points are logarithmically separated in order to get high resolution close to the surface, giving 8 computational levels up to 100 m height, while higher up the grid points become more and more linearly spaced, and the model top is at the height 10000 m, where the vertical resolution is 760 m.

b) Model results

All mesoscale models use a bulk surface roughness parameterisation, i.e. the forest canopy is only included in the model through the surface roughness length z_0 . Consequently, winds at the lowest level of the mesoscale model (situated at $z = z_0 + d$) are simply set to zero. The displacement height is only included in the post-processing of the model results and not in the model runs itself.

The same displacement height was used for the post-processing of all model results, namely $d = 15$ m. The following values were used for surface roughness at the forest grid points surrounding Ryningsnäs: $z_0 = 0.5$ m in WRF MYJ and WRF YSU2, as well as in WRF 1km, WRF 3km and WRF 9km, $z_0 = 0.9$ m in COAMPS 1km, COAMPS 3km and COAMPS 9km during summer and 0.75 m during winter. In WRF MYJ a rough version with $z_0 = 2$ m was used as well. In the MIUU-model runs surface roughness for forests was put to 0.8 m, but also tests with $z_0 = 2$ m were made.

Figure 5-3 shows average mean wind speeds around Ryningsnäs for the period from Sep. 2011 through Apr. 2012 based upon WRF 1km runs. Even though topographic variations are not that pronounced, there are substantial variations in model-simulated mean wind speeds at 1 km horizontal resolution and 100 m height above ground.

Figure 5-4 shows the average measured and model-simulated wind profile for the whole period from September 2011 to December 2012. Only hours were chosen where measured wind direction was from 0 – 20°, 100 – 125° as well as 205 – 360°. These sectors were chosen, in order to minimise wake effects from the two wind turbines in close vicinity to the meteorological mast at Ryningsnäs. (Wake effects were clearly visible in the measurements.)

All models, except WRF-MYJ rough, give too high wind speeds at all heights above ground. In general, wind profiles from WRF MYJ, WRF YSU2, COAMPS 1km, COAMPS 3 km and COAMPS 9 km seem to agree best with the measured wind profile (Figure 5-4). WRF 1 km, WRF 3 km and WRF 9 km seem to perform worst.

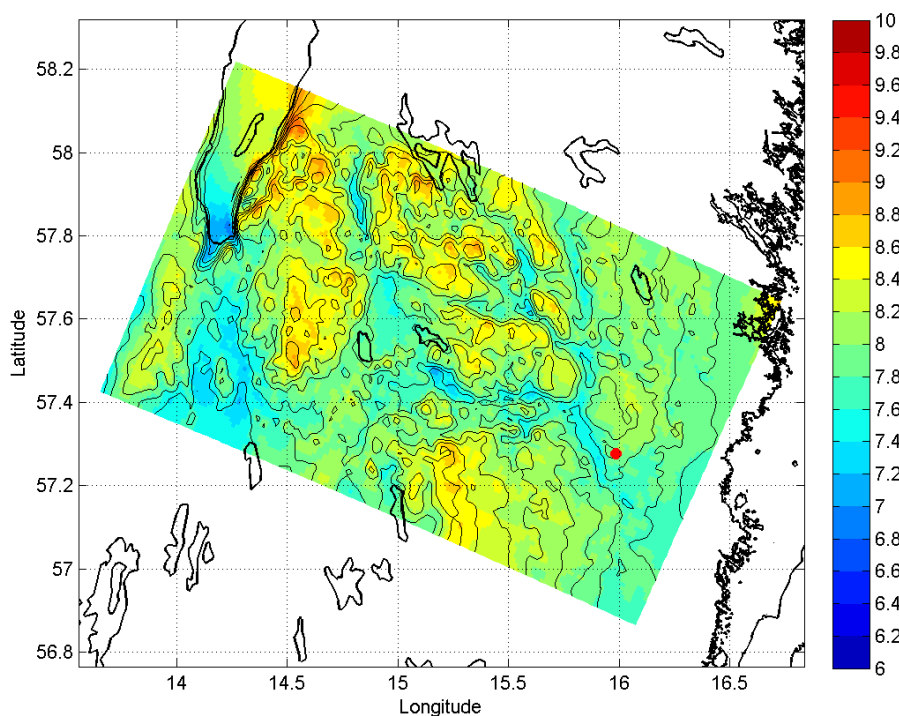


Figure 5-3: Average wind speed estimates for an area around Ryningsnäs (red point) from WRF 1 km runs at 100 m height above zero plane displacement level using standard model settings for Sep. 2011 – Apr. 2012. Comparison with mast data indicates that the wind speed is overestimated by 20-25%.

The wind profile that subjectively agrees best with measurements is from the COAMPS 9 km run. This is somewhat surprising since it could be expected that the COAMPS 1km run should agree better with measurements than COAMPS 9 km and COAMPS 3 km. Also WRF-MYJ rough agrees pretty well with the measurements.

For a real comparison, however, one would have to carry out wind flow model runs for Ryningsnäs with preferably 50 m horizontal resolution, using models such as WASP, MS-Micro or CFD models. This would allow us to estimate the influence of microscale effects on the average wind profile at the site (Mohr, 2012, personal communication).

Figure 5-5 shows the measured and model-predicted wind speed distributions from Ryningsnäs. It is clearly evident that all models, except for WRF-MYJ rough, give wind speeds that are too high. Indeed, WRF-MYJ rough seems to agree best with the measured wind speed distribution.

Analysing model temperature profiles, it became evident that all models, except for WRF 1 km, WRF 3 km and WRF 9 km, had a negative temperature bias of roughly 1.5°C on average at all levels (not shown). This is also evident in the comparison of the temperature distributions (Figure 5-6). The reason for this is not known.

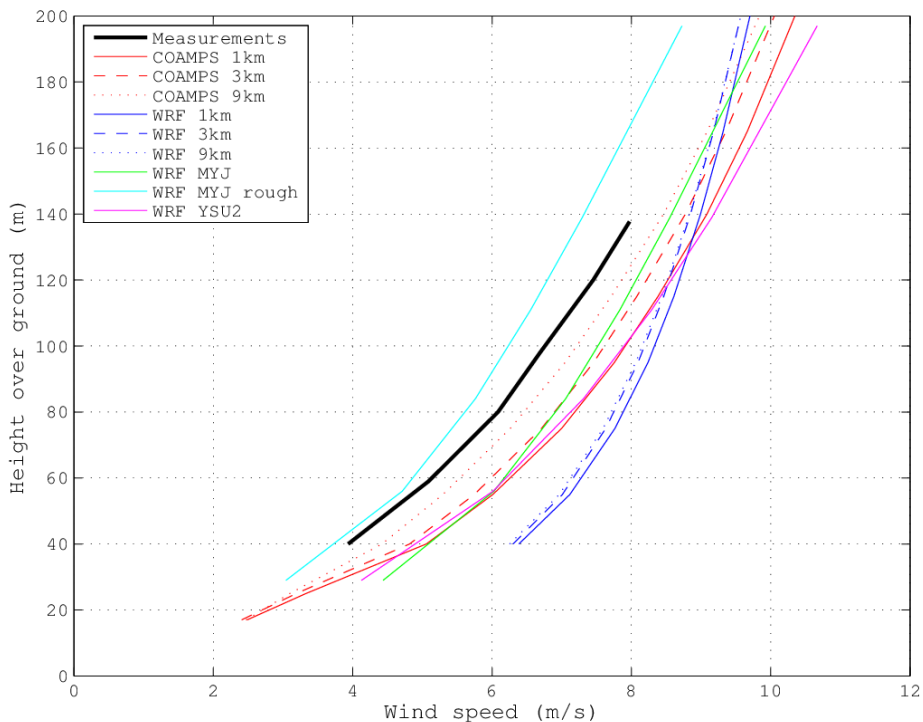


Figure 5-4: Measured and model-predicted wind profiles for Ryningsnäs, averaged from Sep. 2011 through April 2012. Only includes hours with measured wind direction from 0 – 20°, 100 – 125° as well as 205 – 360°.

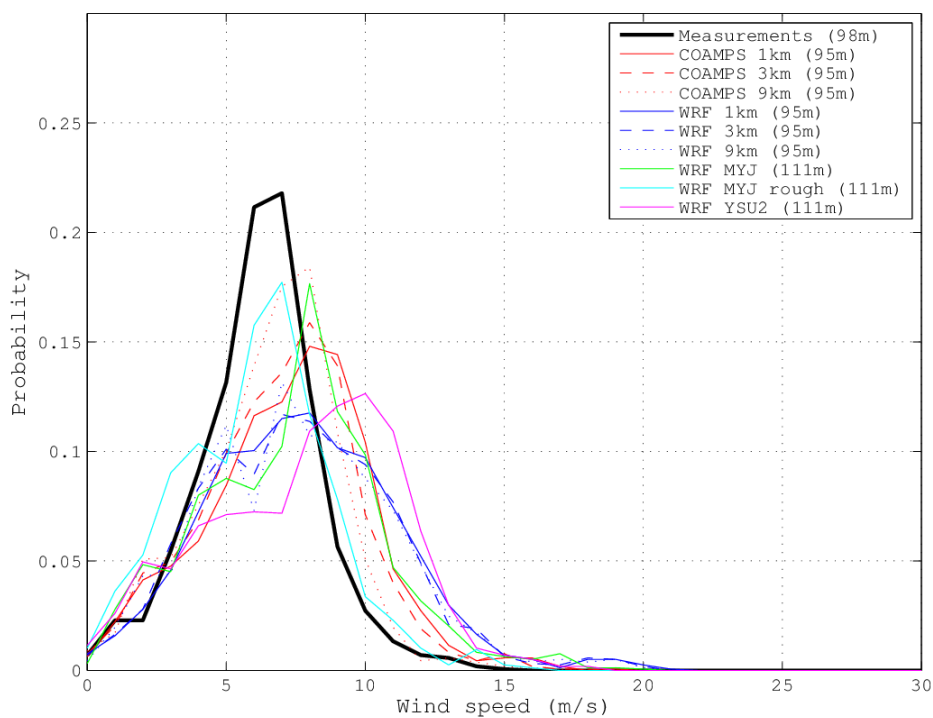


Figure 5-5: Same as Figure 5-4, but comparison of wind speed distributions. Height above ground is given in legend.

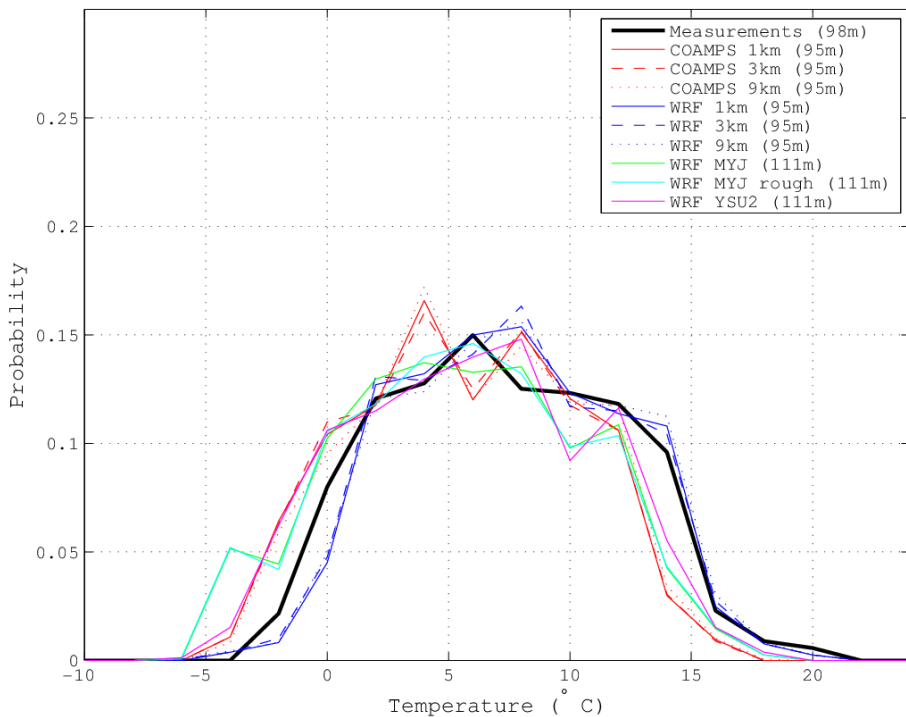


Figure 5-6: Same as Figure 5-5, but comparison of temperature distribution.

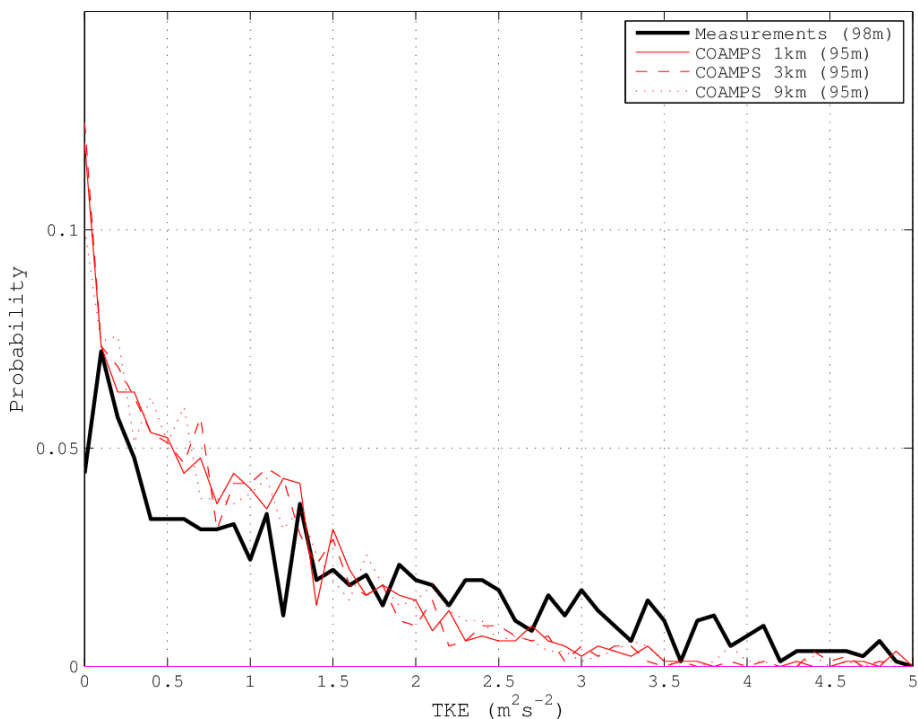


Figure 5-7: Same as Figure 5-5, but comparison of turbulent kinetic energy distribution.

For the COAMPS runs turbulent kinetic energy (TKE) could be compared with measurements (Figure 5-7). From model-predicted and measured TKE profiles it becomes evident that the COAMPS runs underestimate TKE roughly by a factor of two (not shown).

For the WRF MYJ and WRF MYJ rough runs, TKE is predicted by the model, but unfortunately TKE was not stored in the model output. In all other runs, TKE is not calculated by the model.

Wind shear exponents were calculated from the measurements and the model results using a displaced wind profile as

$$\alpha = \frac{\ln\left(\frac{u_2}{u_1}\right)}{\ln\left(\frac{z_2 - d}{z_1 - d}\right)}$$

where u_1 and u_2 are the mean wind speeds at the two levels z_1 and z_2 , and d is the displacement height. The displacement height was chosen to be $d = 15$ m.

Table 5-2 shows the wind shear exponents from the mesoscale model results. All of them are lower than the measured wind shear exponent of 0.44. Not surprisingly, COAMPS 9 km that had the best agreement with measurements (Figure 5-4) shows the closest wind shear exponent (0.42 in COAMPS 9 km compared to 0.44 in measurements). WRF YSU2 came equally close to the measurements. WRF 1 km, WRF 3 km and WRF 9 km show all wind shear exponents that are completely unrealistic for forests with values around 0.20.

Table 5-2: Wind shear exponents from measurements and mesoscale model results for roughly 120 m height above ground. A displacement height of $d = 15$ m was used. Averages for Sep. 2011 to April 2012 except the MIUU-model results which are climatological annual averages. Only includes hours with measured wind direction from 0 – 20°, 100 – 125° as well as 205 – 360°.

| Model run | Heights used | Calculated Wind shear exponent from measurements and used in models | Roughness length Z_0 (m) |
|---------------------|--------------|---|----------------------------|
| Ryningsnäs measured | 98 & 140 m | 0.44 | 2.5 |
| COAMPS 1 km | 95 & 140 m | 0.36 | 0.9 |
| COAMPS 3 km | 95 & 140 m | 0.37 | 0.9 |
| COAMPS 9 km | 95 & 140 m | 0.42 | 0.9 |
| WRF 1 km | 95 & 140 m | 0.20 | 0.5 |
| WRF 3 km | 95 & 140 m | 0.20 | 0.5 |
| WRF 9 km | 95 & 140 m | 0.20 | 0.5 |
| WRF MYJ | 98 & 139 m | 0.34 | 0.5 |
| WRF MYJ rough | 98 & 139 m | 0.42 | 2.0 |
| WRF YSU2 | 98 & 139 m | 0.40 | 0.5 |
| MIUU 1 km | 72 & 147 m | 0.27 | 0.8 |
| MIUU 500 m | 72 & 147 m | 0.30 | 0.8 |
| MIUU 100 m | 72 & 147 m | 0.30 | 0.8 |
| MIUU 500 m rough | 72 & 147 m | 0.33 | 2.0 |

Sensitivity of results to model parameterizations and boundary condition

A modern numerical weather prediction model is a complex system built up by a considerable number of different parts and pieces, all developed to take care of a specific task. For example, in a model system one will find routines that handle model terrain setup, interpolate forcing data (boundary conditions) to the model grid, integrate the equations in time and let the atmospheric state in neighbouring grid points interact through advection of the state variables. In fact, a model should not be viewed as "a model". It is more correct to view it as "a model system" which results depend on the model setup.

In order to assess the impact of different planetary boundary layer and microphysical schemes a number of sensitivity experiments have been carried out. The setup of each sensitivity experiment deviates from the base setup in only one of the following; the planetary boundary layer scheme (and consequentially the surface layer scheme) or the microphysics (phase transitions of water) scheme used.

These sensitivity tests were primarily made within the fellow Vindforsk project "Wind power in cold climates" (V-313, for more details see the final report from this project). Here we give a couple of examples to illustrate the differences between choosing one or the other of the different planetary boundary layer (PBL) or microphysics schemes. The results shown are from a site in the central part of Sweden and are averages for the period September 2010 to April 2011.

In Figure 5-8 the average temperature and wind speed profiles using four different PBL schemes are shown. Large differences in stability are seen. For a couple of PBL schemes the temperature profile shows a huge surface inversion. Also as regards the wind profile large differences are seen due to which PBL scheme is used. At 100 m height above ground the maximum difference in mean wind speed is about 1 m/s.

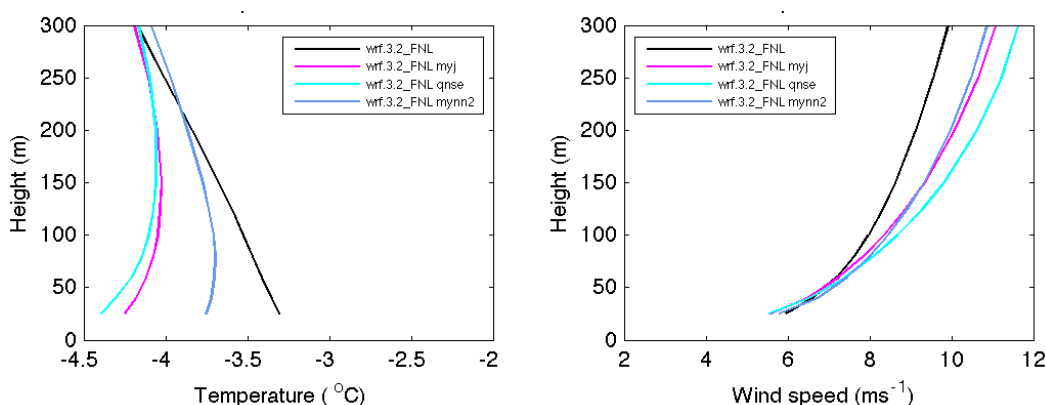


Figure 5-8: Profiles of temperature and wind speed as an average for the period Sep 2010-Apr 2011 using four different PBL schemes in the WRF model.

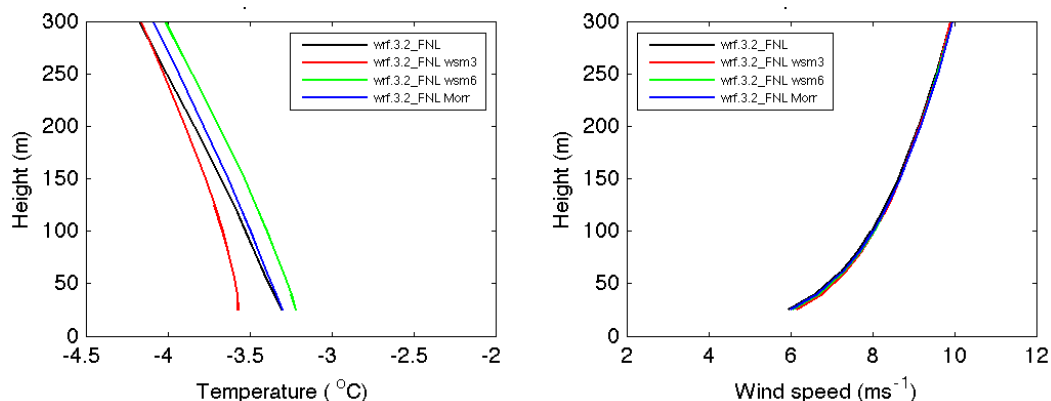


Figure 5-9: Profiles of temperature and wind speed as an average for the period Sep 2010-Apr 2011 using four different microphysics schemes in the WRF model.

In Figure 5-9 a similar comparison is made using four different microphysics schemes. Although the microphysics primarily only involves the different phase transitions of water in the atmosphere, the temperature profile is affected quite a lot. The wind profile is however, at least in the average, not affected very much, but differences may also be seen here.

5.1.1 Wind climatology tests using the MIUU-method

A method to simulate the climatological wind field using the MIUU model has been developed at Uppsala University, the "MIUU-method", reducing the total number of simulations needed (Bergström, 1996; Begrström, 2002). With this method a limited number of climatologically relevant simulations are performed, with different wind and temperature conditions. A weighting based on climatological data for the geostrophic wind (horizontal pressure gradient) is made in order to finally estimate the wind climate. The method is applicable for mapping the wind resources with a resolution of 0.1-10 km. To use this method geostrophic wind (strength and direction), sea and land temperatures, topography, roughness, and land use are needed. No observed boundary-layer winds are needed other than for verification. Earlier comparisons between model results and measurements show good agreement (Bergström and Söderberg, 2009).

A summation over all model runs made (192 runs representing 4 seasons, 3 strengths and 16 directions of the geostrophic wind) and hours (each model runs gives an output of 24 hours – a diurnal cycle), gives the climatological mean value for each grid point and each height. Statistics of the horizontal air pressure gradient (the geostrophic wind) are used to weight the results into a long-term climatological average.

A comparison has been made using three horizontal model resolutions: 1 km, 500 m and 100 m. The resulting climatological annual average wind speed at the height 72 m above zero-plane displacement is shown in Figure 5-10.

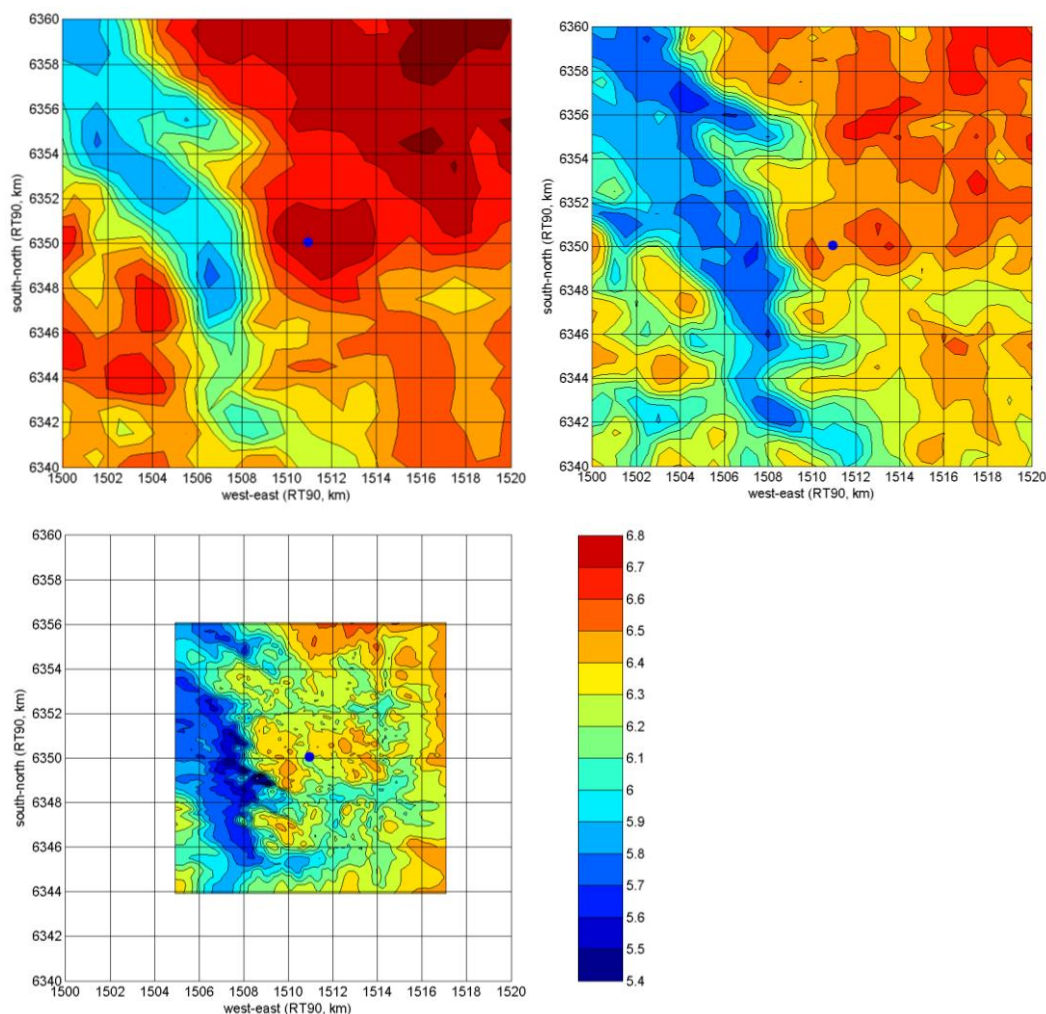


Figure 5-10: Annual average wind speed at 72 m height above zero-plane from the MIUU-model together with the MIUU-method using different horizontal resolutions. Top left: 1 km. Top right: 500 m. Bottom: 100 m. The dots show the location of Ryningsnäs.

The 1 km resolution results are taken from the Swedish wind mapping (Bergström and Söderberg, 2009), in which the average wind speed at Ryningsnäs was estimated to 6.8 m/s at 72 m height. This value was soon recognized as being too high compared to wind measurements at the site. Although this finding was not a general result the question was raised whether it could have to do with model resolution and/or how the forest canopy is accounted for by mesoscale models.

The model resolution was thus increased in two steps. First four times to 500 m. Then an additional 25 times to 100 m, which might be the highest resolution that can be used with this type of mesoscale models. Previous tests using both the MIUU-model and COAMPS (Bergström and Söderberg, 2009) have however shown that at least regarding climatological averages, the use of 100 m model resolution may in general be expected to give reasonable results.

The model results for 500 m resolution show the climatological average wind speed decrease (from 6.8 m/s to 6.4 m/s at 72 m height above zero-plane displacement) at the location of the Ryningsnäs tower. Increasing the model resolution further to 100 m the resulting average wind speed decreases further to 6.2 m/s. The average wind speed profiles are shown in Figure 5-11.

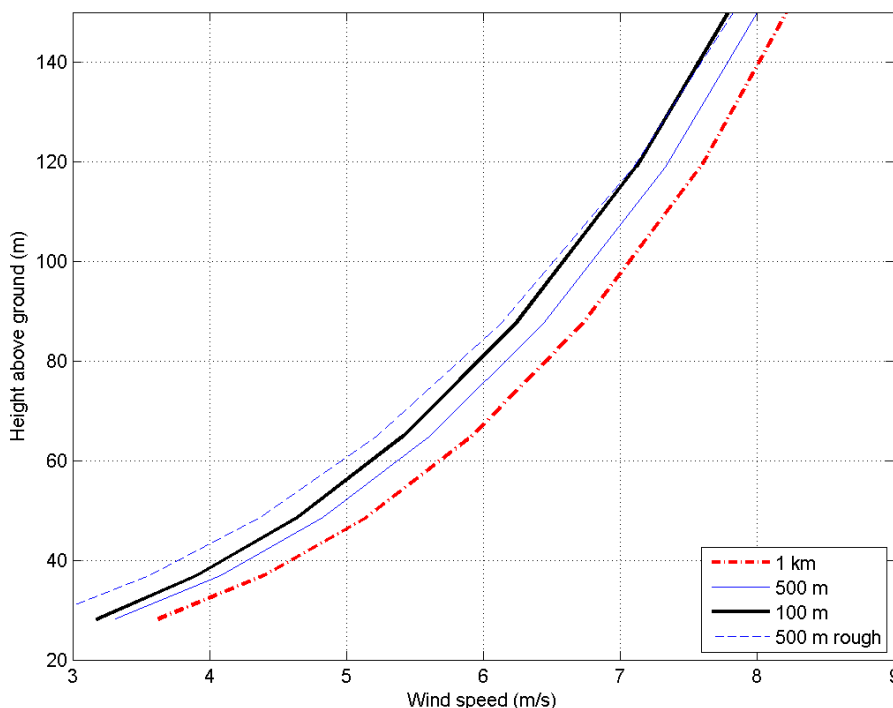


Figure 5-11: Climatological average wind speed profiles at Ryningsnäs estimated with the MIUU-model using the MIUU-method. Results presented using model resolutions 1 km, 500 m, and 100 m. Also included is the profile estimated using 500 m resolution together with a larger roughness.

The roughness length representative for forests is generally assumed to be 0.5 to 1 m (Wieringa, 1992). In the standard configuration files used for WRF $z_0 = 0.5$ m. For COAMPS the standard values are 0.9 m during summer and 0.75 m during winter with snow cover. In the standard MIUU-model setting $z_0 = 0.8$ m was used. These values might be a bit too low as in Section 3.1.3 the roughness length estimated for the forest sector at Ryningsnäs was as high as 2.5 m. Also the average roughness length for 42 typical Swedish forest sites is higher. The median value was here estimated to 1.3 m (see Section 3.3.2).

There is thus reason to investigate how the modelled wind speed changes when using a larger z_0 -value. Included in Figure 5-11 is the wind profile estimated using 500 m model resolution and where for forest a roughness length of 2.0 m was used (rough case). Compared to the wind profile using the standard z_0 -value for forests ($=0.8$ m) we see that the increased roughness length resulted in a lower average wind speed, but not more than about 0.2 m/s at 100 m height above ground. This is quite a bit less than reported using the WRF model, where the decrease found in wind speed was more than 1 m/s at about 100 m height (Figure 5-4).

The reason for this difference is not clear, but may have to do with differences in the turbulence parameterizations between the two models. Also the MIUU-model responds to the increased roughness length as could be expected at low heights, see Figure 5-12. The figure shows the average wind speed profiles estimated at Ryningsnäs using the MIUU-model with forest roughness lengths of 0.8 m and 2.0 m. Assuming a close to logarithmic wind profile below 10 m height and extrapolating to wind speed zero, we can see from the figure that the two wind profiles correspond to z_0 -values of about 2 m and 1 m in magnitude. This is close to the expected values corresponding to the different values used to represent forests in the two model setups. The difference in wind speed at low heights is of the order of 1 m/s, but decreases to about 0.2 m/s at 100 m height. The curvature of the wind profiles indicates a stable stratification. During such conditions the effects of the increased surface roughness may be smaller higher up in the boundary layer as turbulence is reduced due to buoyancy effects.

It should also be pointed out that although the roughness length representing forests was increased from 0.8 m to 2.0 m, the land cover data show that there are not forests everywhere around the site. Thus the difference between the two runs could be expected to be smaller than the difference expected from an increase of surface roughness from $z_0=0.8$ m to 2.0 m. The z_0 -values used for the MIUU-model runs are thus weighted together for each grid point (over a 500 m x 500 m area) using the land cover information given at 25 m x 25 m resolution. In Figure 5-13 the resulting z_0 -fields with 500 m resolution are shown for the same area as in Figure 5-10. Note the difference in resulting z_0 -values when using a roughness length of 0.8 m and 2.0 m for forest pixels (Figure 5-13, left and right). Typical values within some kilometres from the Ryningsnäs site (X in Figure 5-13) are about 0.5-0.8 m for the standard setup, and increase to between 0.5 and 2 m for the rough case.

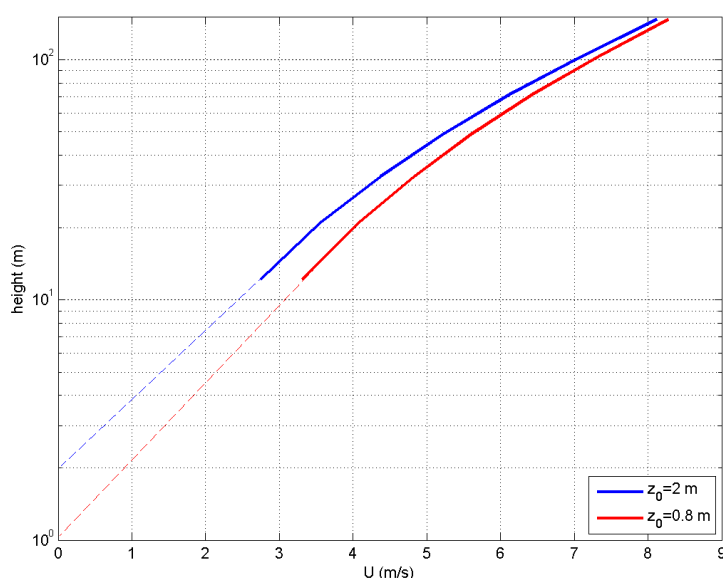


Figure 5-12: Average wind profiles estimated using the MIUU-model at Ryningsnäs using $z_0=0.8$ m and 2.0 m for forests.

In the much coarser land cover data used for the standard WRF setup almost no variations in the roughness length will result in a forested region, resulting in 0.5 m in the whole area around Ryningsnäs. Changing the roughness length for forests to 2 m in the look-up table WRF uses to translate from land cover to roughness, will thus result in 2 m almost everywhere, contrary to what is used in the MIUU-model. This difference will also add to the somewhat unexpected large differences found between how the two models respond to a roughness change with respect to the resulting wind profiles.

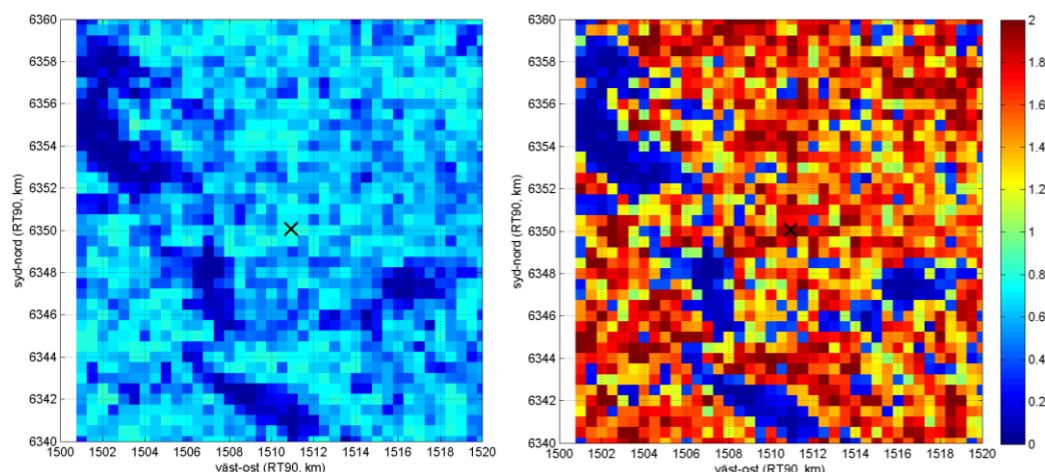


Figure 5-13: The gridded roughness lengths used for the MIUU-model runs using $z_0=0.8$ m (left) and 2.0 m (right). The cross marks the location of the Ryningsnäs site.

The shear exponents estimated using the average wind profiles obtained from the MIUU-model calculations are included in Table 5-2. For 1 km resolution the resulting exponent is 0.27. The standard forest roughness results for 500 m and 100 m resolutions yield both an exponent of 0.30, whereas for the 500 m resolution rough case the exponent is 0.33.

The above results comparing 100 m, 500 m, and 1 km resolutions with the MIUU-model show a decrease in wind speed with increasing resolution. This is not in agreement with what was found comparing 9 km, 3 km, and 1 km resolution results using the WRF and the COAMPS models, see e.g. Figure 5-4. Here an increased resolution resulted in an increase in wind speed at high elevation and a decrease in wind speed in valleys. This might be expected as with low resolution smaller scale topography may be smoothed out such that the highest elevation terrain will not be included in the model results. At low resolution terrain is kind of smoothed and mountains will be lower than at higher resolution. Also valleys are expected to appear more realistically at higher resolution and lower elevation may be found at valley bottoms.

In Figure 5-14 the average wind speed over the Ryningsnäs area estimated using the COAMPS model is shown for a horizontal resolution of 3 km and 1 km. It is obvious that with higher resolution differences in wind speed between high and low elevation increase, with higher wind speeds over mountains and lower wind speeds in valleys.

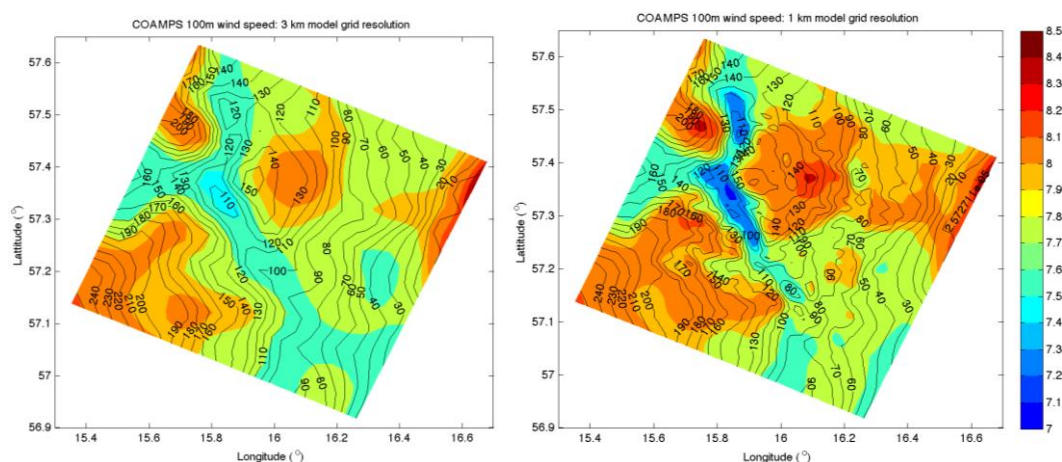


Figure 5-14: Average wind speed over the Ryningsnäs area as estimated using the COAMPS model with 3 km resolution (left) and 1 km resolution (right). Contour lines with labels show topography.

The argument given above that a low resolution will smooth the terrain and level off high peaks is however not obvious in this example. Only small differences were present. Instead another reason for the model results giving higher winds over high elevation terrain and lower winds in valleys may be the model resolution as such, not the actual maximum and minimum in terrain height. A numerical model needs a number of computational points to resolve the influence of e.g. a mountain and how the mountain will affect the wind speed. With only one model grid point in a valley or one at a mountain top and nothing in between, the effects of the topographical differences on the wind will not be resolved by the model. As a minimum at least of the order of 5-6 model grid points should cover the mountain or valley for the model to resolve the major flow effects of topographical variations.

This may be an additional reason to why increased resolution also increases the wind speed over higher elevation terrain. At 3 km resolution the model doesn't accurately resolve the terrain effects upon the winds. But at 1 km resolution a sufficient number of grid points are covering the dominant terrain features making the model capable of resolving the effects on the winds. Figure 5-15 shows differences in wind speed versus differences in terrain height using 1 km and 3 km resolution in the COAMPS model. There is a clear tendency to get a higher wind speed when the terrain height is increased by the higher resolution (correlation coefficient 0.68). But the scatter is quite large and even with no height difference the wind speed may either increase or decrease by 0.2 m/s. This may indicate the need for a sufficient number of grid points covering a terrain feature in order for the model to fully include its effects upon the wind.

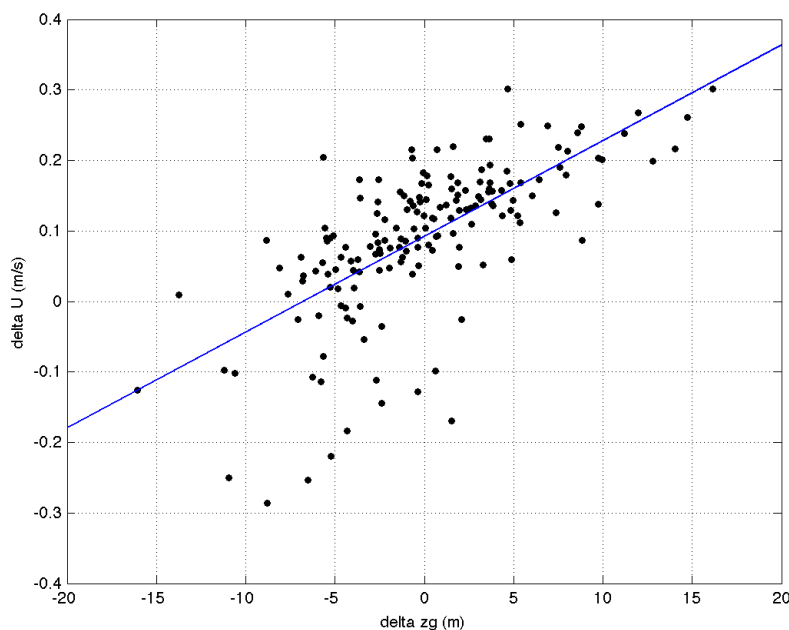


Figure 5-15: Difference in wind speed versus difference in terrain height between 1 km and 3 km resolution as modeled using the COAMPS model.

A further increased model resolution will for the Ryningsnäs area not give rise to a further increase of the maximum terrain height, or a further decrease of valley bottom elevation. To increase resolution from 500 m to 100 m will mainly result in that the model will include smaller scale terrain variations. No dominant deeper valleys or higher mountain peaks will be resolved, just more variability of terrain height. The effect may be that the modelled winds will slow down due to terrain induced roughness, explaining the observed relation between modelled average wind speed and model resolution. In areas with a more pronounced topography than that at Ryningsäs, an increased resolution is expected to increase wind speed differences between low and high elevation areas.

5.2 Results from modelling idealized forests

5.2.1 Methodology and model set-up

a) MIUU mesoscale model set-up

Idealised numerical model simulations for different forest configurations were carried out using the MIUU mesoscale model with 100 m horizontal resolution. Such resolutions are usually only achieved by Computational Fluid Dynamics Reynolds-averaged Navier-Stokes (CFD-RaNS) or Large-Eddy Simulation (LES) models (e.g. Giebel et al., 2002). According to Lopes da Costa (2007), RaNS and LES modelling are two complementary approaches to the modelling of flow over vegetation. Detailed turbulent structures of the flow over trees can only be modelled by LES models. Mean atmospheric velocity and

turbulence fields, on the other hand, can be predicted by RANS models. The MIUU mesoscale model belongs to the category of RaNS models.

The model was run with very high vertical resolution, with the first model levels situated at 0, 2, 6, 11, 17, 23, 31, 40, 50, 62, 76, 93 and 112 m height above zero plane displacement. The lowest vertical model level is situated at a height of $z_0 + d$ above ground. Horizontal resolution was constant up to 13.5 km distance from the centre. Further away from the centre, horizontal resolution was increased by 10% from one grid point to another up to 93 km distance from the centre.

b) Set-up of idealised forest runs

A surface roughness of $z_0 = 1$ m was used for all simulated forest areas whereas $z_0 = 0.05$ m is used for the remaining areas. This is in agreement with the value found in Section 3.3.2. for 42 Swedish forest sites, even though Section 3.1.3 and the experience of Risø DTU (Crockford and Hui, 2007) points to a forest surface roughness of 2 – 2.5 m rather than 1 m.

Idealised forests have been simulated in two dimensions. The model was run to study the forest edge as well as isolated forests and clearings of different lengths. As the model simulations are two-dimensional, the results are only valid for a forest that extends infinitely in y-direction. Three dimensional simulations should probably be more realistic for forests that occur in nature. Also, the results are strictly only valid for a completely flat surface. The effects of complex terrain should be studied separately.

The model was run with westerly geostrophic winds of magnitudes 5, 6, 7, 8, 9, 10, 11, 12, 13, 14, 15, 16, 17, 18, 19, 20, 25 and 30 m/s. This should cover all hub height wind speeds relevant to wind power. Furthermore, the model was run for different atmospheric stabilities (neutral, stable and unstable conditions).

The model was run in a steady-state mode, meaning that all input data was kept constant in time. After 1 – 2 hours, depending on the magnitude of the geostrophic wind, the model fields should have adjusted completely to the underlying surface. In some cases gravity waves developed during initialisation and disappeared only gradually. In very rare cases for mostly very low wind speeds, gravity waves could be present even after 6 hours of integration time, disturbing the picture.

Moreover for non-neutral runs after some time, the lowest 200 m above ground gradually became more and more neutral due to the enhanced turbulent mixing over the forest. In the neutral runs, however, the stratification of the lowest 200 m above ground did not change with time as on-going turbulent mixing does not change a stratification that is already neutral.

The latitude was set to 59° North. The temperature profile was specified in such a way that neutral, slightly stable, stable, very stable, unstable and very unstable stratification was achieved in the model runs. The model was run for 20 hours to a steady state, with boundary conditions kept constant over time. Surface temperature was set constant at the lowest model level.

c) Analysis of model results

Different hours were chosen for the analysis:

- 1) For the neutral runs, hour 3 seemed to yield acceptable results.
- 2) For stable cases, it turned out that model stratification becomes more and more neutral after some hours of simulation time owing to turbulent mixing at the lowest model levels. Hence for stable cases, hour 1 was used for geostrophic wind speeds larger than 9 m/s. Otherwise hour 2 was used.
- 3) In the unstable case, gravity waves were present in some runs after initialisation. The gravity waves, however, gradually became weaker and weaker. Therefore, hour 11 was used in the unstable case, in order to reduce disturbing effects of gravity waves triggered by model initialisation.

Two parameters are looked at in particular:

1. Horizontal mean wind speed at a certain height above ground
2. Turbulence intensity at a certain height above ground

Both parameters are calculated from model simulations at a certain height above ground. Over forested areas, flow displacement is taken into account as

$$d_{forest} = 15 \cdot z_{0,forest} \quad (5-1)$$

where d is the displacement height and z_0 is the surface roughness length. This translates to a flow displacement height of $d_{forest} = 15$ m for a surface roughness of $z_{0,forest} = 1$ m and corresponds well to the value found in Section 3.3.2 for 42 Swedish forest sites.

d) Discussion

Due to the sudden increase (or drop) of the displacement height at forest edges from 1 to 15 m (or from 15 m to 1 m), there is a discontinuity directly at the forest edge. This is clearly not realistic.

Another possibility would have been to use a rule of thumb for the change of the displacement height at forest edges (see Brady et al. (2010), p. 15). Brady et al. proposed a linear transition of the displacement height at the forest edges rather than a discontinuity. They suggested that the displacement height would increase (decrease) linearly from 0 to 15 m (from 15 to 0 m) over a distance of 50 times canopy height before and after the forest.

A forest canopy version of the MIUU model, however, once completely implemented, should not produce such a discontinuity. This eliminates the problem of determining the displacement height as a function of place and canopy height. Some results from the forest canopy version of the MIUU model are presented in Section 5.3.

5.2.2 Influence of forest on wind and turbulence fields

A transition from grass ($z_0 = 0.05$ m) to forest ($z_0 = 1$ m) is studied using 2-dimensional MIUU model runs. The forested area starts in the middle of the model domain at $x = 0$ km and extends eastwards.

An internal boundary layer develops over the forest. Lower wind speeds and higher turbulence can be found over the forest as compared to the area upstream of the forest. The development of such an internal boundary layer has been studied by many authors, for instance, Bergström et al. (1988) and Dellwik and N. O. Jensen (2000). A summary of some of the numerous different equations used to describe the vertical growth of the internal boundary layer can be found in, for instance, Kaimal and Finnigan (1994).

The internal boundary layer growth is most commonly approximated by a power law equation (e.g. Dellwik and Jensen, 2000). A summary of some IBL formulas can be found in Table 5-3. An equation similar to the power law was used for percentage wind and turbulence intensity change over forest for the smooth-rough transition studied herein.

Table 5-3: Various formulas for internal boundary layer (IBL) height growth for a smooth-rough transition. Some formulas give the height of the internal equilibrium layer (IEL) rather than IBL height.

| Formula for IBL height | Reference | Comments |
|---|--|---|
| $\frac{\delta}{z_{0,forest}} = M \left(\frac{x}{z_{0,forest}} \right)^{0.8}$ $M = 0.75 + 0.03 \ln \left(\frac{z_0}{z_{0,forest}} \right)$ | Elliott (1958) – as cited in Kaimal and Finnigan (1994) | Rough to smooth transition has exponent of 0.43 |
| $\frac{\delta}{z_{0,mean}} = 10.56 \left(\frac{x}{z_{0,mean}} \right)^{0.33}$ | Cheng and Castro (2002) | $z_{0,forest} = 10z_{0,smooth}$ $z_{0,mean} =$ $(z_{0,smooth} + z_{0,rough})/2$ |
| $\frac{\delta}{z_{0,forest}} = 0.28 \left(\frac{x}{z_{0,forest}} \right)^{0.8}$ | Wood (1982) | |
| $\delta = 0.2x^{(0.78-0.33z/L)}$ | Bergström et al. (1988) | Coast to land transition, Näsudden, Gotland |
| $\delta \sim x^{0.77 \dots 1.39}$ | Rao (1975) | Exponent increases from neutral to unstable |
| $\frac{\delta}{z_{0,forest}} = 0.09 \left(\frac{x}{z_{0,forest}} \right)^{0.77}$ | Dellwik and Jensen (2000) | IEL height |

a) Change of Wind Speed

Percentage wind speed reduction over a forest downwind from the forest edge is studied. Such an approach was suggested and used by Bergström et al. (1988). Percentage wind speed reduction is calculated at a certain height above ground as

$$\Delta U = \frac{U_0 - U(x)}{U_0} \cdot 100\% \quad (5-2)$$

where U_0 is the upwind wind speed ahead of the forest and $U(x)$ is the wind speed over the forest at a certain distance (x) from the forest edge (forest edge located at $x = 0$). The reference upstream wind profile U_0 is taken at $x = -8$ km (i.e. 8 km upwind from the forest edge). All wind speeds used in Equation (5-2) are model-simulated horizontal mean wind speeds.

Hence, $\Delta U = 0\%$ applies to regions where no wind speed reduction occurs, whereas $\Delta U > 0\%$ applies to regions where forest-induced changes in surface roughness and displacement height become important and cause a reduction in horizontal mean wind speed.

For 10 m/s geostrophic wind and neutral stability (Figure 5-16), one can see that wind speeds are reduced by up to $\approx 14\%$ at 100 m height above ground due to the combined effects of surface roughness and vertical flow displacement. At larger heights above ground, wind speed reductions become less pronounced (Figure 5-16).

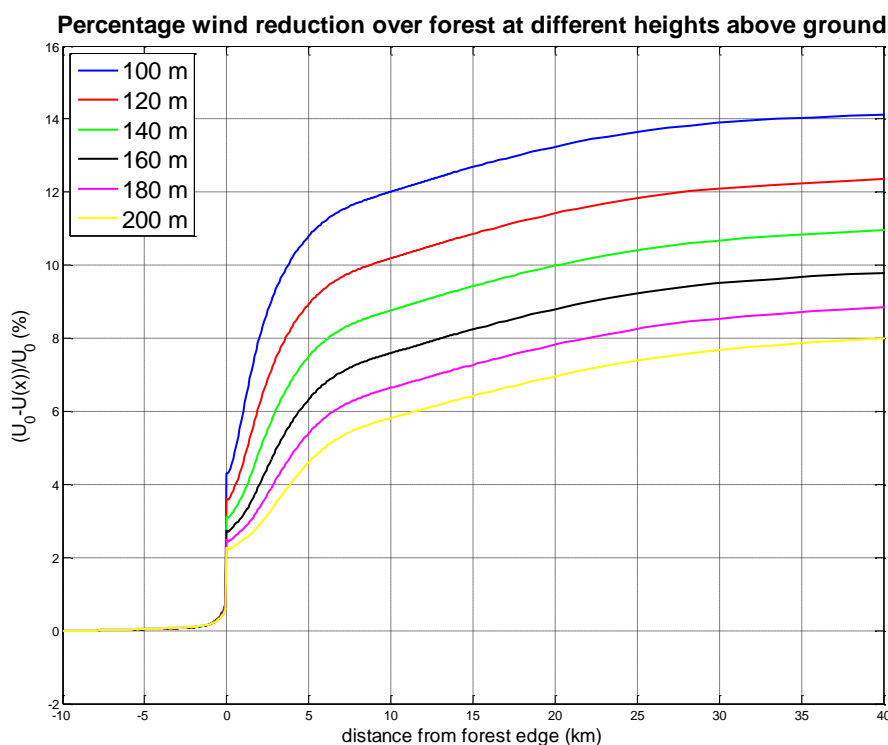


Figure 5-16: Percentage wind reduction over idealised flat forest at different heights above ground. Forest edge is located at $x = 0$ km. Calculated using eqn. (5-2), with the reference upstream wind profile taken at $x = -8$ km. Valid for 10 m/s geostrophic wind and neutral stability.

A very good fit of the wind speed reduction can be achieved by a power law in conjunction with a linear term, i.e. an equation of the form

$$\Delta U = a \cdot x^b + c \cdot x \quad (5-3)$$

where x is the distance from the forest edge and a , b and c fitting coefficients. The coefficients were obtained using the MATLAB curve fitting toolbox. Note that x has to be given in meters in the equation above.

For neutral conditions, the equation seems to describe modelled wind speed reductions reasonably well, even without the additional linear term. It seems to apply to all wind speeds relevant for wind energy (i.e. from roughly 5 to 25 m/s) at distances from 0 to 20 km from the forest edge (Figure 5-17). Furthermore, the equation seems to be valid universally for all geostrophic wind speeds between 5 and 25 m/s.

The fitting constants for the different heights are summarised in Table 5-4. The coefficients don't seem to be dependent on wind speed. However, they are strongly dependent on height above ground. The linear term in Equation (5-3) seems to be unimportant for neutral conditions.

Table 5-4: Fitting coefficients and correlation for percentage wind speed reduction over forest (forest edge at $x = 0$ m). Percentage wind speed reduction can be calculated for distances $0 \leq x \leq 20$ km. Valid for neutral stratification only and for a smooth-rough transition at $x = 0$ km with $z_0(\text{smooth}) = 0.05$ m and $z_0(\text{rough}) = 1$ m. Displacement height is assumed as $d = 15 \cdot z_0$.

| Height above ground (m) | Coefficient a | Coefficient b | Coefficient c | Correlation coefficient R^2 |
|-------------------------|-----------------|-----------------|-----------------|-------------------------------|
| 100 | 1.20 | 0.25 | - | 0.88 |
| 120 | 0.68 | 0.29 | - | 0.87 |
| 140 | 0.41 | 0.33 | - | 0.86 |
| 160 | 0.26 | 0.36 | - | 0.83 |
| 180 | 0.17 | 0.39 | - | 0.80 |
| 200 | 0.12 | 0.42 | - | 0.76 |

The exponent b in Equation (5-3) seems to become larger, the higher the height above ground. On the other hand the multiplication factor a seems to become smaller for higher heights (Table 5-4). The exponent, however, is nowhere near the most quoted value of 0.8 for the growth of the internal boundary layer for a smooth-rough transition (Table 5-4).

The fitted expressions for all heights above ground are summarised in Figure 5-18. In most cases, the expressions seem to give a conservative estimate of the wind speed reduction, i.e. a percentage wind speed reduction that is slightly higher than the model-predicted one.

Finally Figure 5-19 describes the influence of atmospheric stability on the wind speed reduction over a forest. A height of 100 m above ground was chosen. In general, when atmospheric stability is included the scatter seems to be much larger and correlation much weaker. Also, stronger winds tend to produce less stable (= "more neutral") stratification after a couple of hours of

simulation time in the lowest 200 m above ground or so. This is especially important for stable stratification.

Percentage wind reduction over forest for different geostrophic wind speeds

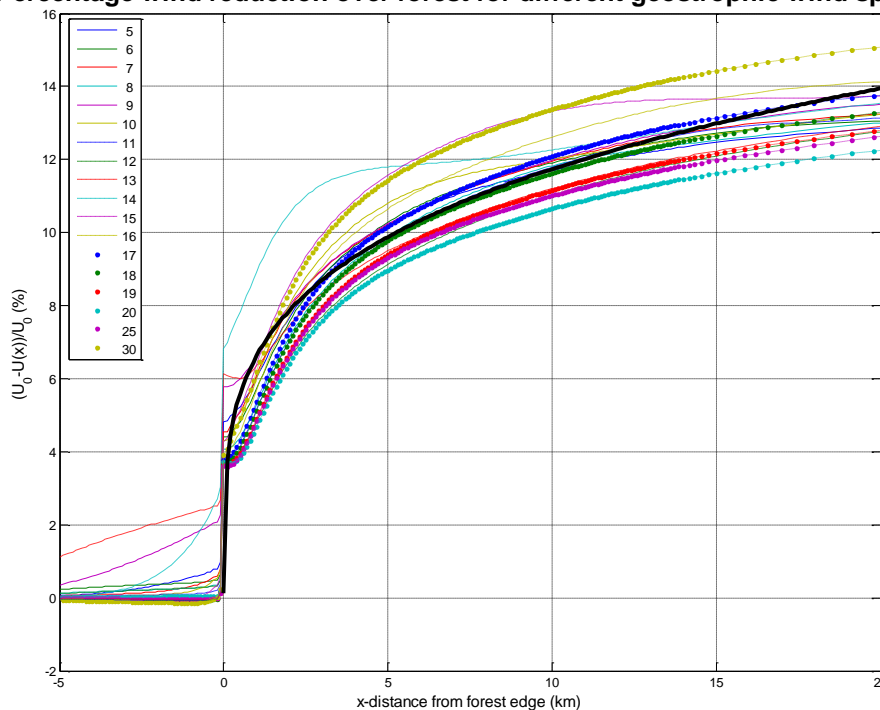


Figure 5-17: Same as Figure 5-16, but for different geostrophic wind speeds and 100 m height above ground. Geostrophic wind speed is given in legend in figure. Run for 14 m/s geostrophic wind speed seems to be an outlier and was removed before further analysis. Fitted equation for percentage wind speed reduction (thick black line) seems to agree remarkably well with model results.

For non-neutral stratification, the wind speed decrease over the forest seems to depend more on the magnitude of the geostrophic wind than in the neutral case. Therefore, correlation is weaker than in the neutral case (Table 5-5).

There seems to be slightly less wind speed reduction over the forest for unstable stratification as compared to neutral stratification (Figure 5-19). The reason for this is that there is already quite some thermally produced turbulence in the atmospheric boundary layer over both the smooth (grass) and the rough surface (forest). Therefore the addition of a small degree of mechanically produced turbulence over the forest doesn't seem to make that much of a difference.

Surprisingly for stable stratification at low wind speeds and higher heights than 100 m above ground, the wind speed seems to be roughly the same over the forest as compared to upstream of the forest (not shown). For 140 m height this seems to occur below around 7 m/s geostrophic wind. However, this conclusion should not be generalised as it is only based upon a few idealised model simulations.

Percentage wind reduction over forest at different heights above ground

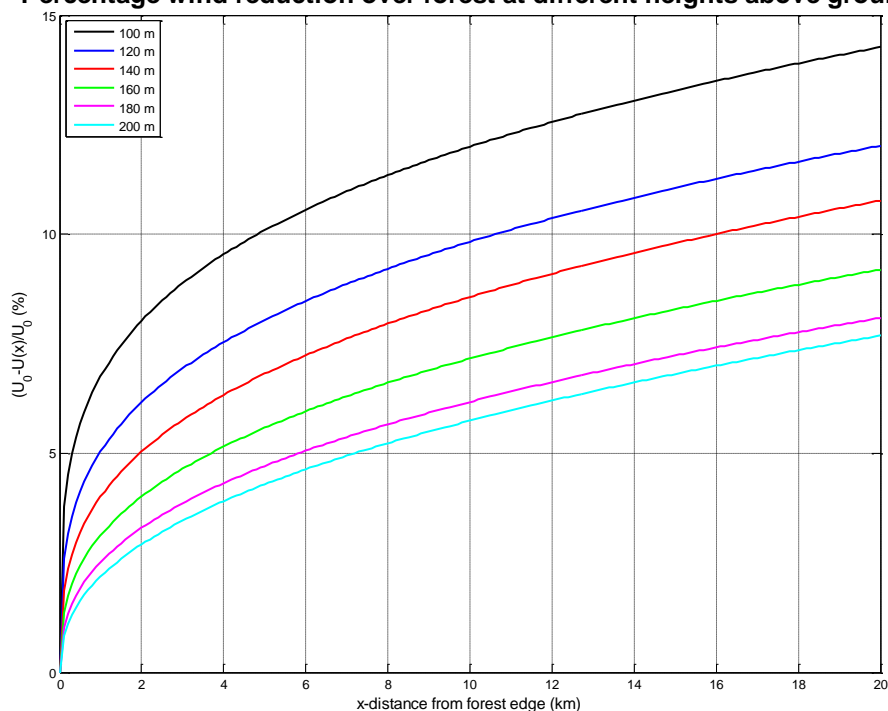


Figure 5-18: Percentage wind speed reduction over idealised flat forest at different heights above ground. Forest edge is located at $x = 0$ km. Calculated using eqn. (5-3) together with coefficients from Table 5-4. Valid for geostrophic wind speeds between roughly 5 and 25 m/s and neutral stability.

Table 5-5: Same as in Table 5-4, but for neutral, stable and unstable atmospheric stability. The coefficients are valid for 100 m height above ground.

| Atmospheric stability | Coefficient a | Coefficient b | Coefficient c | Correlation coefficient R^2 |
|-----------------------|-----------------|-----------------|-----------------|-------------------------------|
| Neutral | 0.68 | 0.328 | -0.00021 | 0.89 |
| Stable | 11.03 | 0.003 | 0.00018 | 0.55 |
| Unstable | 0.31 | 0.414 | -0.00043 | 0.72 |

Percentage wind reduction over forest for different atmospheric stabilities

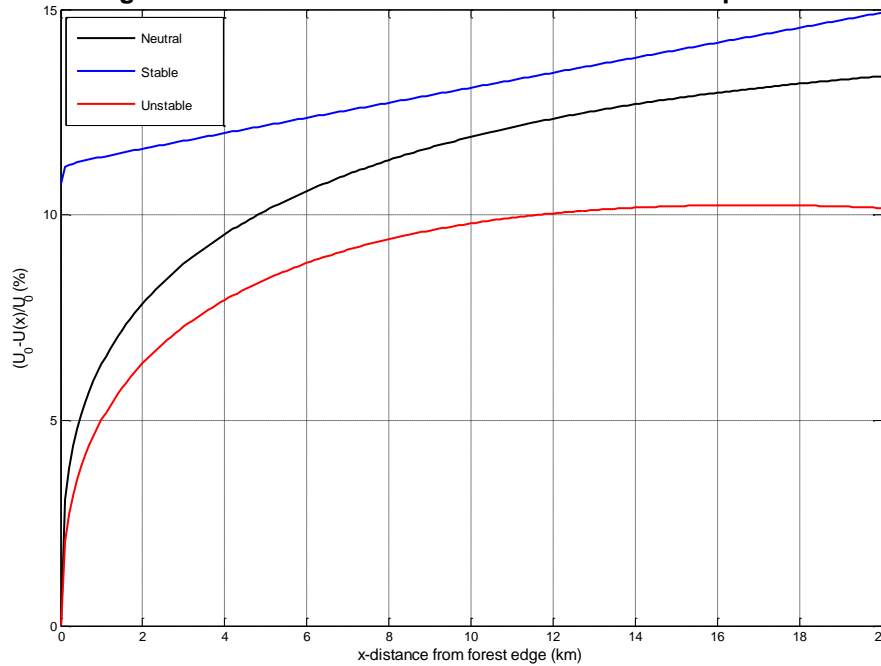


Figure 5-19: Same as in Figure 5-18, but for neutral, stable and unstable atmospheric stability. Calculated using Eq. (5-3) together with coefficients from Table 5-5. Valid for 100 m height above ground.

b) Change of Turbulence Intensity

Turbulence intensity (TI) is calculated from model-predicted turbulent kinetic energy (TKE) as

$$TI = \frac{\sqrt{\frac{2}{3}TKE}}{U} \quad (5-4)$$

where U is the model-predicted horizontal mean wind speed. As the MIUU model is a higher order closure model, turbulence intensity could also be calculated from the variance of the along-wind component of the wind speed as specified in the IEC standard (e.g. Burton et al., 2011). However, for simplicity reasons this was not done here.

The same calculations as above were carried out. Hence, turbulence intensity was compared to the upstream value at a distance of 8 km before the forest edge. Turbulence intensity enhancement (ΔTI) was calculated as

$$\Delta TI = \frac{TI(x) - TI_0}{TI_0} \cdot 100 \% \quad (5-5)$$

where TI_0 is the upstream turbulence intensity and $TI(x)$ is the turbulence intensity over the forest at a certain distance x from the forest edge.

An example of the percentage turbulence intensity enhancement over an idealised flat forest at different heights is shown in Figure 5-20. For 100 m height above ground, the turbulence intensity enhancement reaches its maximum over the forest at about 10 km from the forest edge. For higher heights, the maximum seems to be situated further away from the forest edge (Figure 5-20).

A very good fit of the turbulence intensity enhancement can be achieved by a power law in conjunction with a linear term, i.e. an equation of the form

$$\Delta TI = a \cdot x^b + c \cdot x \quad (5-6)$$

where x is the distance from the forest edge and a , b and c fitting coefficients.

Turbulence intensity enhancement over forest at different heights above ground

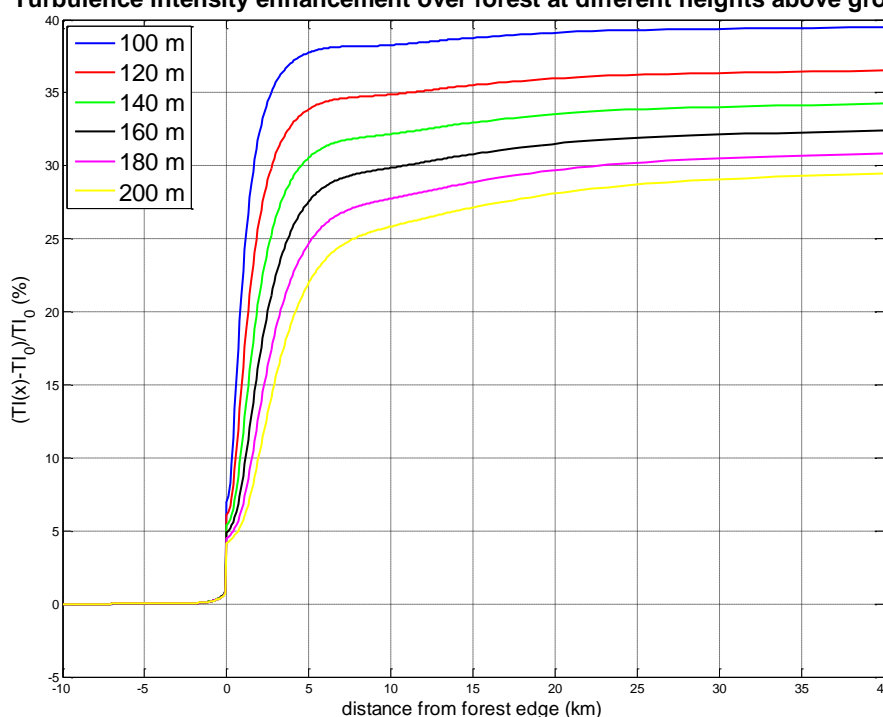


Figure 5-20: Percentage turbulence intensity enhancement over idealised flat forest at different heights above ground. Forest edge is located at $x = 0$ km. Calculated using eqn. (5-5), with the reference upstream turbulence intensity profile taken at $x = -8$ km. Valid for 10 m/s geostrophic wind and neutral stability.

The equation seems to describe modelled turbulence intensity enhancement reasonably well for wind speeds between roughly 5 and 30 m/s at distances from 0 to 10 km from the forest edge (see Figure 5-21). The equation seems to be valid universally for all geostrophic wind speeds. Further away than 10 km from the forest edge the equation gives worse results, as turbulence intensity enhancement seems to stay relatively constant with increasing distance from the forest edge. Turbulence intensity enhancement values calculated from the fitted expressions (Table 5-6), however, decline

moderately after $x = 10$ km (not shown). This appears to be unrealistic and a constant value seems to agree better with the model predictions.

The values from our model experiments can be compared with turbulence intensity values calculated by the CFD-model Ventos in Brady et al. (2010). The authors found turbulence intensity over the forest to increase with up to 100% for a 3 km wide forest at 80 m height above ground. Figure 5-21, however, yields a maximum increase of turbulence intensity of roughly 40% at 100 m height above ground. The reason for the difference is unclear.

Table 5-6: Same as in Table 5-4, but for turbulence intensity enhancement above forest up to roughly 10 km from forest edge.

| Height above ground (m) | Coefficient a | Coefficient b | Coefficient c | Correlation coefficient R^2 |
|-------------------------|-----------------|-----------------|-----------------|-------------------------------|
| 100 | 2.72 | 0.33 | -0.0019 | 0.92 |
| 120 | 1.10 | 0.44 | -0.0025 | 0.93 |
| 140 | 0.45 | 0.54 | -0.0033 | 0.94 |
| 160 | 0.19 | 0.65 | -0.0044 | 0.95 |
| 180 | 0.08 | 0.77 | -0.0075 | 0.95 |
| 200 | 0.05 | 0.91 | -0.0187 | 0.95 |

Percentage turbulence intensity enhancement over forest for different geostrophic wind speeds

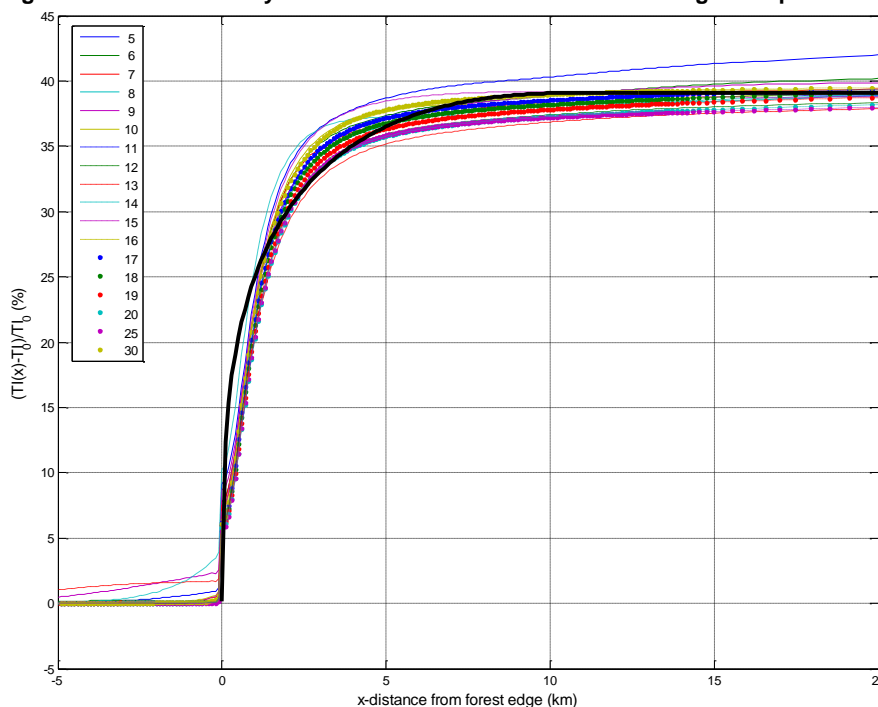


Figure 5-21: Same as Figure 5-20, but for different geostrophic wind speeds and 100 m height above ground. Geostrophic wind speed is given in legend in figure. Fitted equation for percentage turbulence intensity enhancement (thick black line) seems to agree remarkably well with model results. However, the decrease in turbulence intensity enhancement for $x > 10$ km appears to be unrealistic.

The fitted expressions for all heights above ground are summarised in Figure 5-22. In most cases, the expressions seem to give a good estimate of the turbulence intensity enhancement over the forest. However, since the decrease in turbulence intensity enhancement for $x > x_{max}$ is not realistic, a constant value was chosen for $x > x_{max}$. The following values were chosen for x_{max} : 10 km at 100 m height above ground, 13 km at 200 m height above ground, and a linear interpolation with height in between.

Also here, there seems to be an influence of atmospheric stability (Figure 5-23 and Table 5-7). Again correlation coefficients are much lower in the non-neutral case as compared to the results for neutral stratification. In general, turbulence intensity enhancement appears to be slightly higher during stable stratification compared to neutral stratification (Figure 5-23). In the unstable case turbulence intensity enhancement appears to be slightly lower than in the neutral case.

Percentage turbulence intensity enhancement over forest for different geostrophic wind speeds

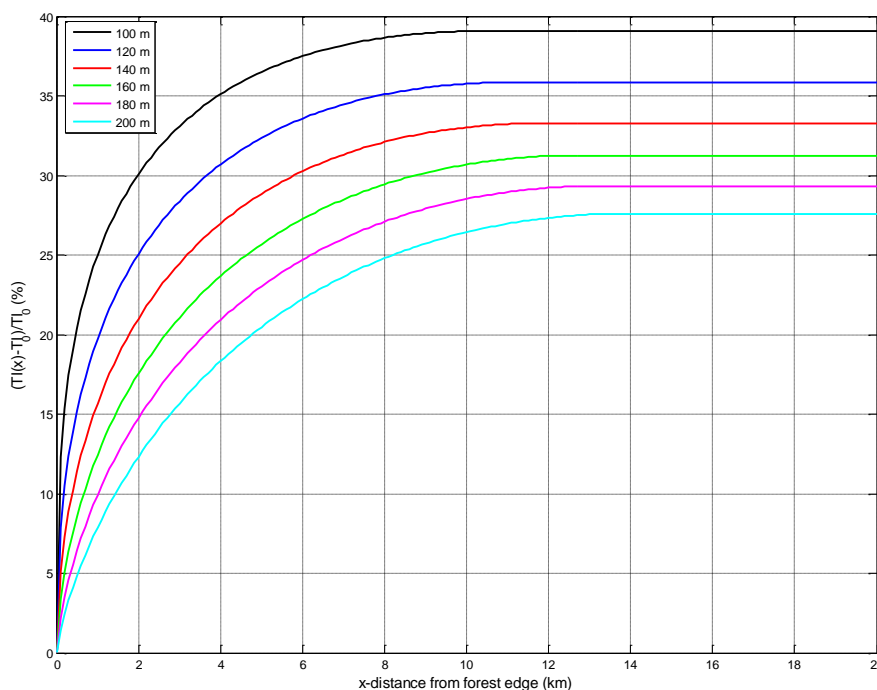


Figure 5-22: Percentage turbulence intensity enhancement over idealised flat forest at different heights above ground. Calculated using Eq. (5-6) together with coefficients from Table 5-6. Valid for geostrophic wind speeds between roughly 4 and 30 m/s and neutral stability.

Table 5-7: Same as in Table 5-6, but for neutral, stable and unstable atmospheric stability. Valid for 100 m height above ground.

| Atmospheric stability | Coefficient a | Coefficient b | Coefficient c | Correlation coefficient R^2 |
|-----------------------|-----------------|-----------------|-----------------|-------------------------------|
| Neutral | 2.72 | 0.33 | -0.0019 | 0.92 |
| Stable | 7.39 | 0.20 | -0.0005 | 0.55 |
| Unstable | 1.75 | 0.38 | -0.0021 | 0.63 |

Percentage turbulence intensity enhancement over forest for different atmospheric stabilities

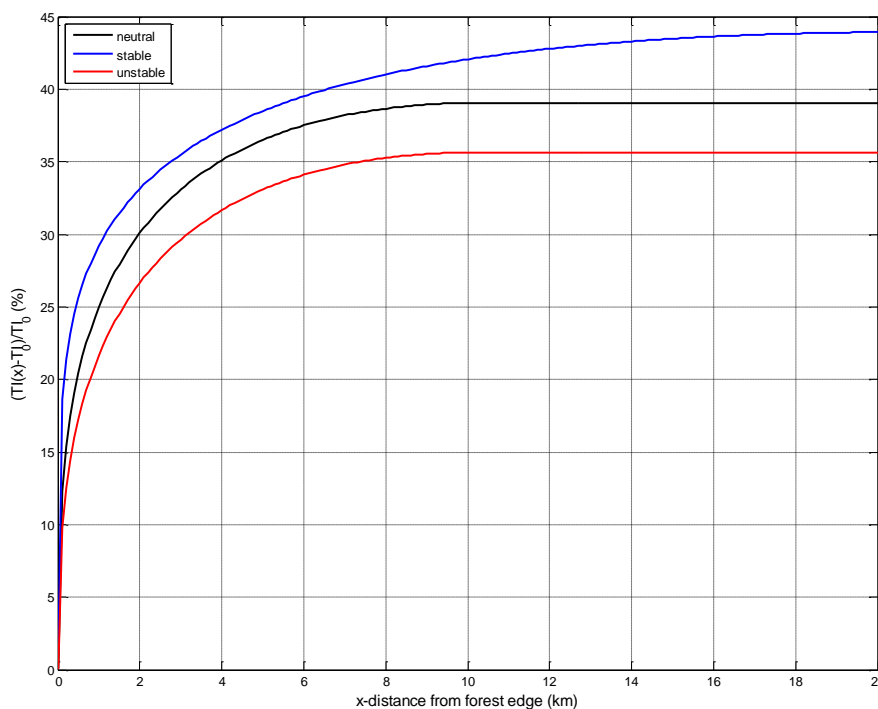


Figure 5-23: Same as in Figure 5-22, but for neutral, stable and unstable atmospheric stability. Calculated using Eq. (5-6) together with coefficients from Table 5-7. Valid for 100 m height above ground.

5.2.3 Wind reduction downstream of forests as function of distance to forest edge

Idealised two-dimensional model simulations with a forest edge were carried out for geostrophic wind speeds between 5 and 30 m/s as well as neutral, stable and unstable atmospheric stratification. The same model set-up as above was used except that there was forest over the western parts of the model domain, i.e. at $x < 0$ km. The forest edge is located at $x = 0$ km.

a) Change of Wind Speed

In contrast to the section above, the reference wind profile was taken at a grid point downwind from the forest edge. Somewhat arbitrarily, the reference wind profile was taken at $x = 55$ km, i.e. 55 km downwind from the forest edge. At such a large distance downwind from the forest edge, it is believed that the wind speed reduction owing to the forest assumes zero and the wind profile should completely resemble a grass surface.

Eq. (5-2) is used to calculate percentage wind reduction downwind from the forest edge. Wind speed reduction seems to decrease exponentially with increasing distance from the forest (Figure 5-24). Hence, wind speeds can be expected to increase exponentially downwind of the forest edge.

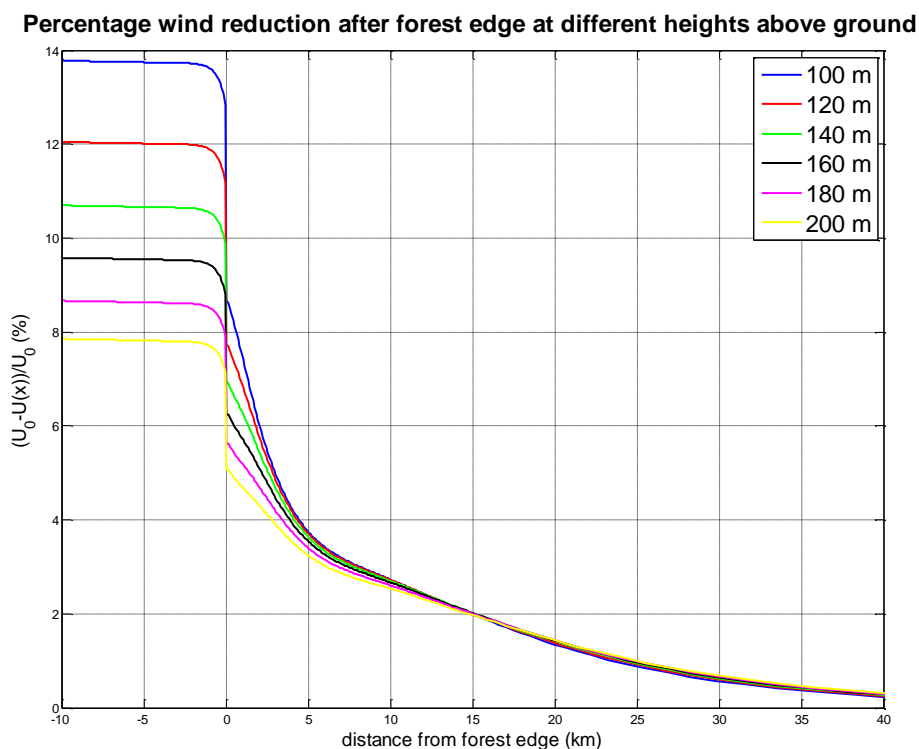


Figure 5-24: Percentage wind reduction downwind of idealised flat forest at different heights above ground. Forest edge is located at $x = 0$ km. Calculated using Eq. (5-2), with the reference downwind wind profile taken at $x = 55$ km. Valid for 10 m/s geostrophic wind and neutral stability.

Exponential functions were fitted to the wind speed reduction values downwind of the forest edge. Hence, ΔU values were approximated as

$$\Delta U = a \cdot e^{-bx} \quad (5-7)$$

where x is the distance from the forest edge and a and b fitting constants. The inverse of coefficient b corresponds to the distance where percentage

wind speed reduction has decreased to 36.7% of the value directly behind the forest at, say $x \approx 50 - 100$ m distance from the forest edge.

Correlation seems to be relatively good and there was no clear dependency of the fitting coefficients on geostrophic wind speed (Figure 5-25 and Table 5-8). Results from the runs with 10, 14 and 25 m/s geostrophic wind were removed from the analysis as they seem to be outliers. The reason for this is currently not known.

The fitted expressions for all heights above ground are summarised in Figure 5-26. There is a higher reduction in wind speed at lower heights above ground. However, the decay in wind speed reduction after the forest is faster at lower heights as compared to higher heights above ground.

Percentage wind reduction after forest edge for different geostrophic wind speeds

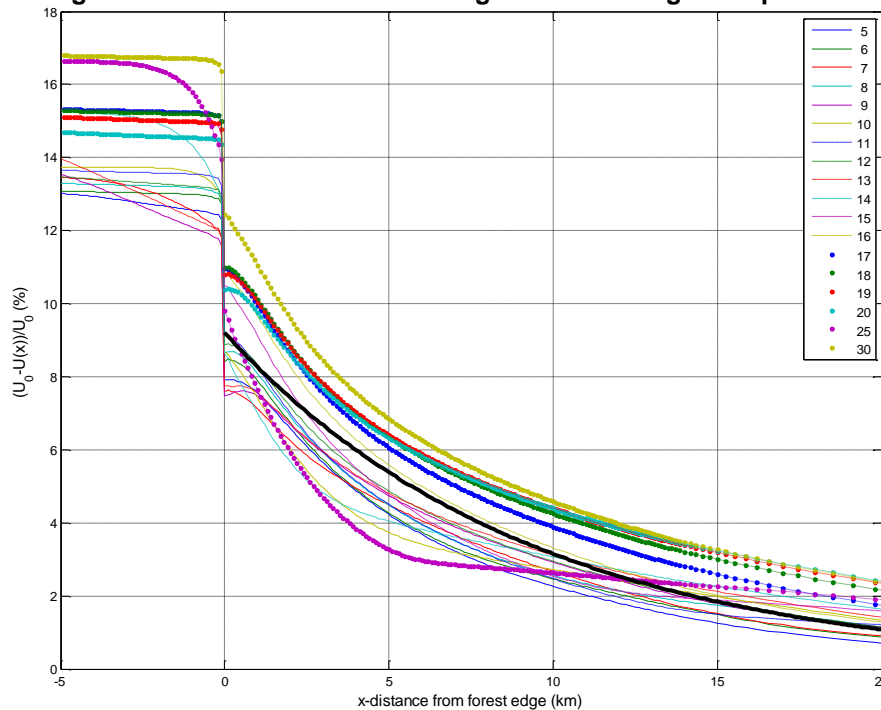


Figure 5-25: Same as Fig. 9, but for different geostrophic wind speeds. Geostrophic wind speed is given in legend in figure. Fitted equation for percentage wind speed reduction (thick black line) seems to agree remarkably well with model results. Valid for 100 m height above ground.

Table 5-8: Fitting coefficients and correlation for percentage wind speed reduction downwind from forest edge (forest edge at $x = 0$ m). Percentage wind speed reduction can be calculated for distances $0 \leq x \leq 20$ km. The coefficients are valid for neutral stratification only and for a rough-smooth roughness transition from $z_0(\text{rough}) = 1$ m to $z_0(\text{smooth}) = 0.05$ m at $x = 0$ km. Displacement height is assumed as $d = 16 \cdot z_0$.

| Height above ground (m) | Coefficient a | Coefficient b^{-1} | Correlation coefficient R^2 |
|-------------------------|-----------------|----------------------|-------------------------------|
| 100 | 9.20 % | 9.3 km | 0.85 |
| 120 | 8.53 % | 10.2 km | 0.83 |
| 140 | 7.89 % | 11.1 km | 0.81 |
| 160 | 7.29 % | 12.1 km | 0.78 |
| 180 | 6.69 % | 13.2 km | 0.73 |
| 200 | 6.14 % | 14.4 km | 0.68 |

Percentage wind reduction after forest edge for different heights above ground

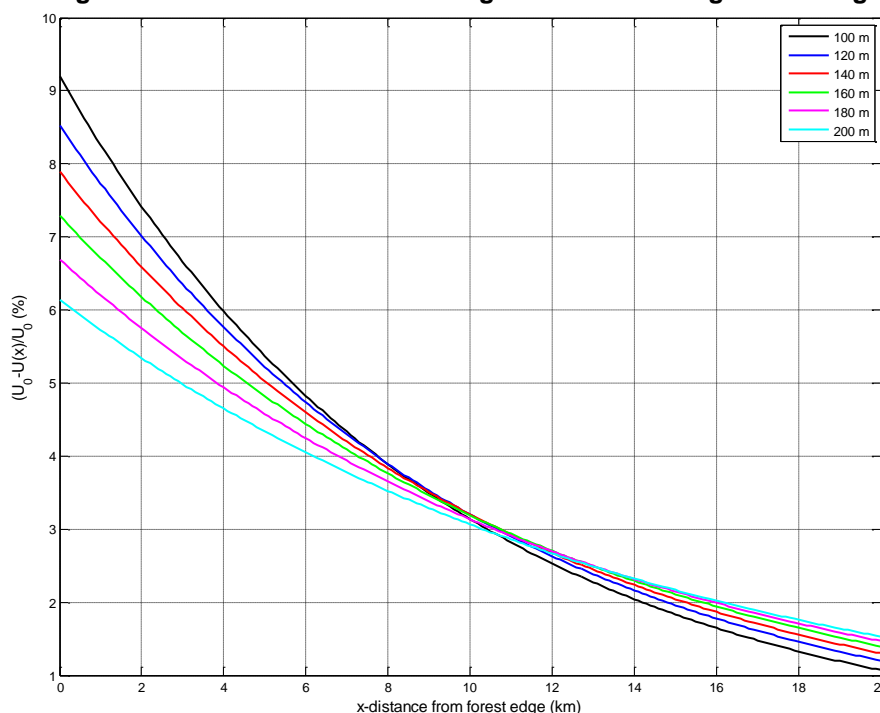


Figure 5-26: Percentage wind reduction downwind of idealised flat forest at different heights above ground. Forest edge is located at $x = 0$ km. Calculated using Eq. (5-7) together with coefficients from Table 5-8. Valid for geostrophic wind speeds between roughly 5 and 25 m/s and neutral stability.

Table 5-9: Same as in Table 5-8, but for neutral, stable and unstable atmospheric stability. Valid for 100 m height above ground.

| Atmospheric stability | Coefficient a | Coefficient b^{-1} | Correlation coefficient R^2 |
|-----------------------|-----------------|----------------------|-------------------------------|
| Neutral | 9.20 % | 9.3 km | 0.85 |
| Stable | 3.80 % | 13.5 km | 0.62 |
| Unstable | 8.84 % | 10.4 km | 0.62 |

As shown in Figure 5-27, there seems to be slightly less wind speed reduction after the forest for unstable stratification as well as stable stratification (Figure 5-27). Immediately after the forest, the model gives percentage wind speed reductions of 8.7% in the neutral case as compared to only 6% in the stable and unstable case (cf. coefficient a in Table 5-9). The reason for this is not quite obvious. However, in the unstable case, there is a lot of thermally produced turbulence and the additional mechanically produced turbulence from the forest canopy has a smaller effect on the wind field than in the neutral and stable case. In the stable case, however, it is not quite clear what is happening.

Percentage wind reduction after forest for different atmospheric stabilities

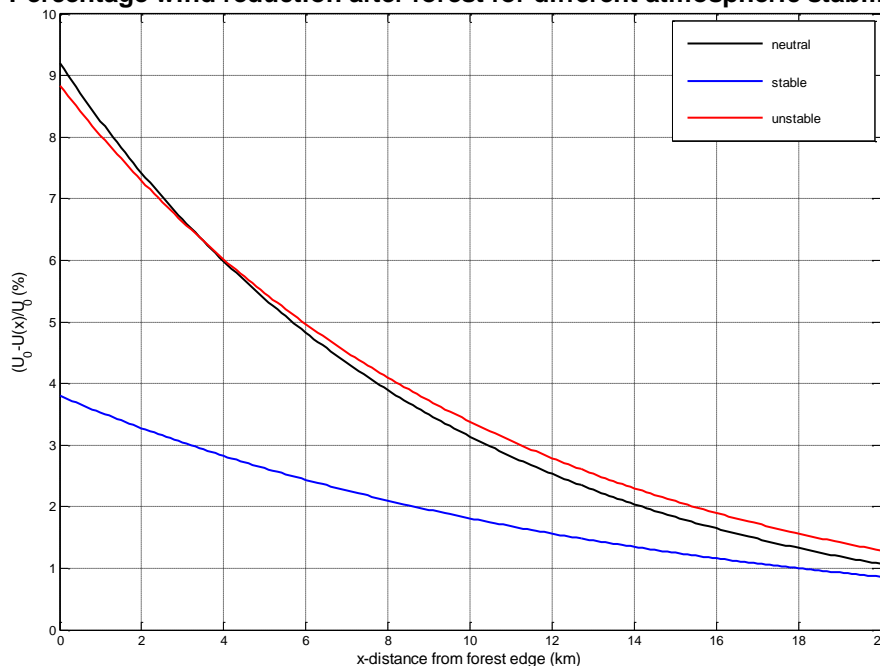


Figure 5-27: Same as in Figure 5-26, but for neutral, stable and unstable atmospheric stability. Calculated using Eq. (5-7) together with coefficients from Table 5-9. Valid for 100 m height above ground.

Surprisingly for stable stratification at low wind speeds (< 9 m/s or so) and higher heights above ground (> 100 m), the wind speed seems to be roughly the same after the forest as compared to upstream over the forest (not shown). For 140 m height this seems to occur below around 9 m/s geostrophic wind. However, this conclusion should not be generalised as it is only based upon a few idealised model simulations.

b) Change of Turbulence Intensity

Turbulence intensity seems to approach the equilibrium turbulence intensity for downwind conditions at an exponential rate (Figure 5-28). As discussed above, also turbulence intensity shows a discontinuity directly at the forest edge which clearly is not realistic and should be avoided in the forest-canopy version of the mesoscale model.

The findings can also be compared to the results from Pedersen and Langreder (2007) based upon measurements, who found that turbulence intensity created by a forest is visible within 5 times the forest height vertically as well as 500 meters downstream from the forest edge horizontally. Outside of these boundaries turbulence intensity should rapidly approach normal values again.

Turbulence intensity enhancement after forest edge at different heights above ground

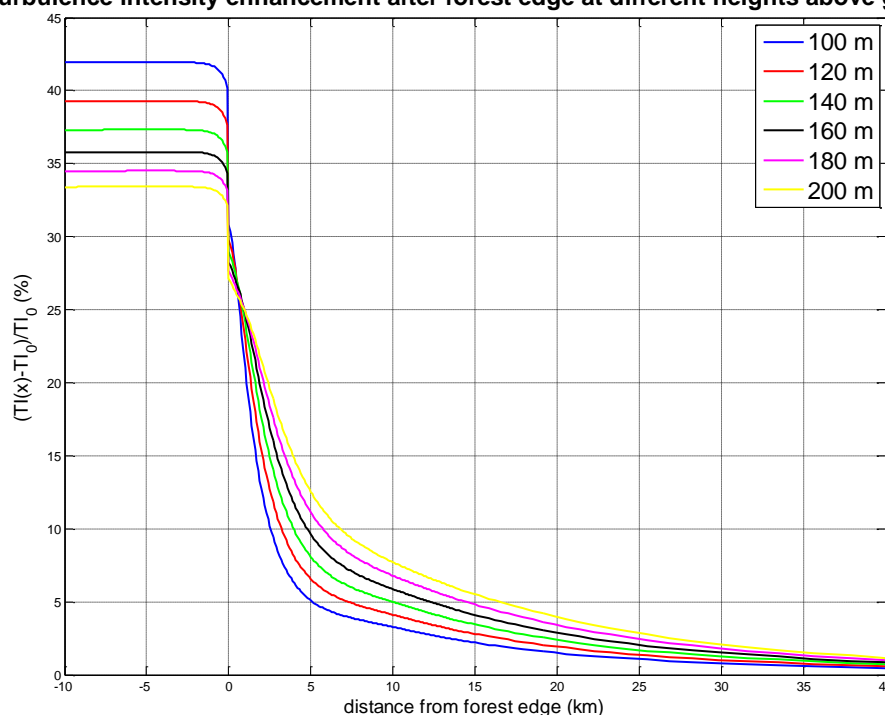


Figure 5-28: Percentage turbulence intensity enhancement after forest edge at different heights above ground. Forest edge is located at $x = 0$ km. Calculated using Eq. (5-5), with the reference downstream turbulence intensity profile taken at $x = 55$ km. Valid for 10 m/s geostrophic wind and neutral stability.

A very good fit of the turbulence intensity decay after the forest edge can be achieved by an exponential function, i.e. an equation of the form

$$\Delta TI = a \cdot e^{-bx} \quad (5-8)$$

where x is the distance from the forest edge and a and b fitting constants. The equation is valid for distances from 0 km up to 20 km from the forest edge.

The equation seems to describe the decay of modelled turbulence enhancement very well for wind speeds between 5 and 30 m/s (see Figure 5-29). The equation seems to be valid universally for all geostrophic wind speeds. Turbulence intensity enhancement values can be estimated from Eq. (5-8) using coefficients from Table 5-10.

Percentage turbulence intensity enhancement after forest edge for different geostrophic wind speeds

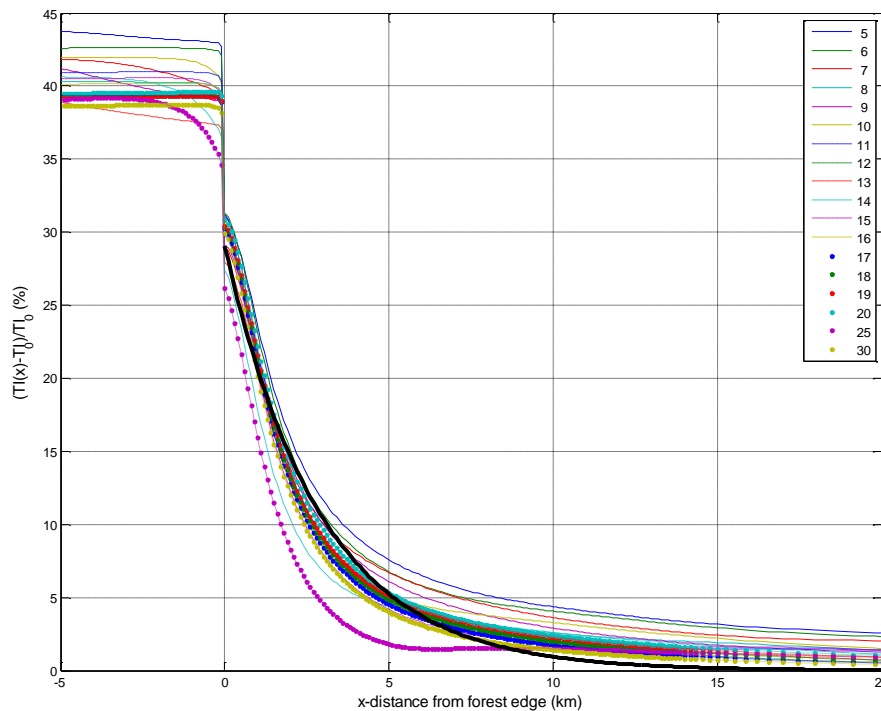


Figure 5-29: Same as Figure 5-28, but for different geostrophic wind speeds. Geostrophic wind speed is given in legend in figure. Fitted equation for percentage turbulence intensity enhancement (thick black line) seems to agree very well with model results. Valid for 100 m height above ground.

Table 5-10: Same as in Table 5-8, but for turbulence intensity enhancement after forest edge. Valid from 0.5 up to 20 km from the forest edge.

| Height above ground (m) | Coefficient a | Coefficient b^{-1} | Correlation coefficient R^2 |
|-------------------------|-----------------|----------------------|-------------------------------|
| 100 | 29.05 % | 2.92 km | 0.94 |
| 120 | 28.09 % | 3.76 km | 0.93 |
| 140 | 27.48 % | 4.63 km | 0.93 |
| 160 | 27.07 % | 5.49 km | 0.92 |
| 180 | 26.62 % | 6.41 km | 0.90 |
| 200 | 26.25 % | 7.36 km | 0.89 |

The values obtained herein can be compared with turbulence intensity values compiled from measurements by Sundgaard and Langreder (2007). The authors also found an exponential decay of turbulence intensity downwind of forests (Fig. 4 in Sundgaard and Langreder, 2007). In agreement with our results the decay starts directly at the forest edge. Their study, however, shows a faster decay than the one found herein. Unfortunately, the authors have only included measurements up to 60 m above ground level compared to the lowest level of 100 m above ground level in our study.

Also here, there seems to be an influence of atmospheric stability (Figure 5-31 and Table 5-11). Again correlation coefficients are lower in the non-neutral case as compared to neutral stratification. In general, turbulence intensity enhancement appears to decrease faster during unstable stratification compared to neutral stratification. In the stable case, however, turbulence intensity enhancement after the forest appears to decrease slower than in the neutral case. For all cases, absolute values of turbulence intensity enhancement are not that different to the neutral case.

Percentage turbulence intensity enhancement after forest edge for different heights above ground

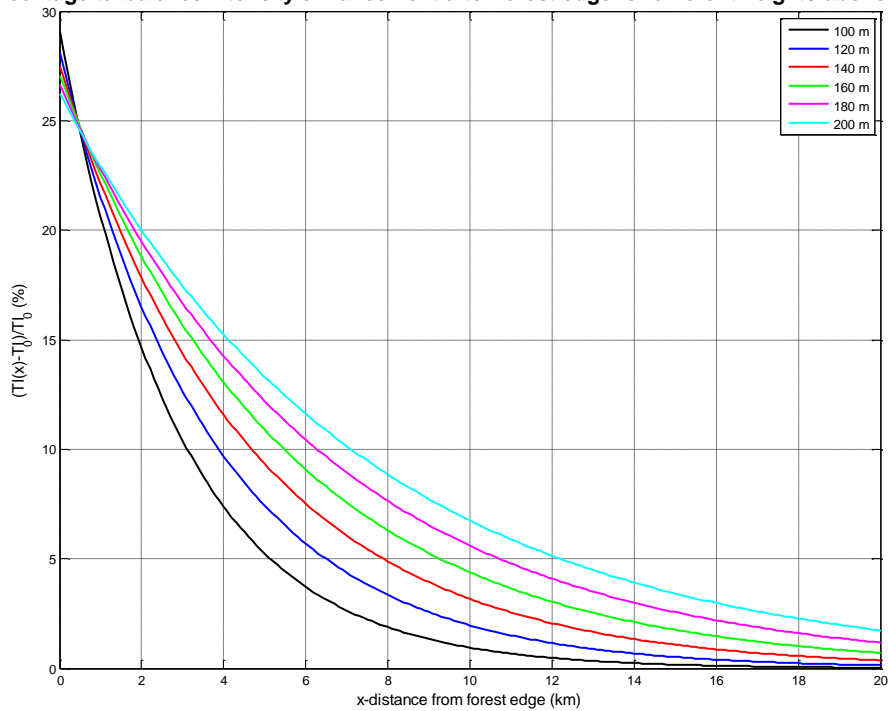


Figure 5-30: Percentage turbulence intensity enhancement after forest edge at different heights above ground. Calculated using Eq. (5-7) together with coefficients from Table 5-10. Valid for geostrophic wind speeds between roughly 4 and 30 m/s and neutral stability.

Table 5-11: Same as in Table 5-10 but for neutral, stable and unstable atmospheric stability. Valid for 100 m height above ground.

| Atmospheric stability | Coefficient <i>a</i> | Coefficient <i>b</i> | Correlation coefficient R^2 |
|-----------------------|----------------------|----------------------|-------------------------------|
| Neutral | 29.1 % | 2.9 km | 0.94 |
| Stable | 19.1 % | 5.2 km | 0.88 |
| Unstable | 29.5 % | 2.0 km | 0.71 |

Percentage turbulence intensity enhancement after forest edge for different atmospheric stabilities

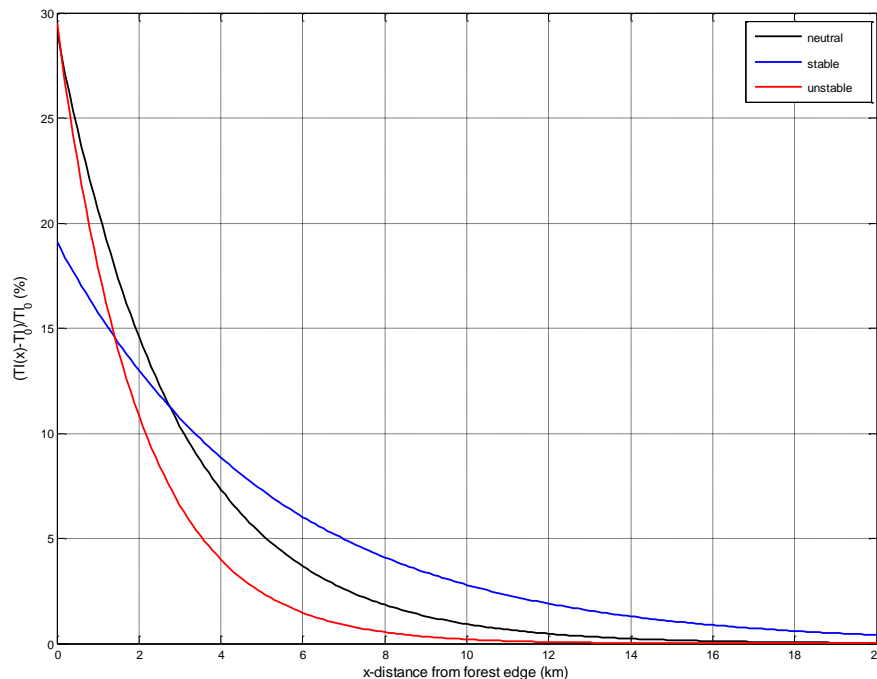


Figure 5-31: Same as in Figure 5-30, but for neutral, stable and unstable atmospheric stratification. Calculated using Eq. (5.8) together with coefficients from Table 5-11. Valid for 100 m height above ground.

5.2.4 Influence of isolated forests on wind and turbulence fields

Here, isolated forests of different sizes are studied in order to find out how the wind and turbulence field is modified. Three cases with isolated forests of 1, 2 and 4 km horizontal extension were simulated in two dimensions. Percentage wind speed reduction and percentage turbulence intensity enhancement were calculated with eqn. (5-2) and (5-5), respectively. As in Section 5.2.2, the reference upstream wind profile U_0 and the reference upstream turbulence intensity profile TI_0 were taken at $x = -8$ km.

a) Change of Wind Speed

Wind speed seems to decrease with roughly 1.5 to 4.5% directly above the forest at different heights above ground (Figure 5-32). Directly after the forest, wind speed reduction values “jump” to 0% from 1.5 to 4.5% (Figure 5-32). This is due to the effects of the displacement height dropping to zero meters directly after the forest (from 16 meters directly above the forest). Both effects seem to be unrealistic and a forest canopy model should give much better results in this case.

Downwind of that discontinuity, wind speed reduction values rise again to a distance between 2 and 5 km from the forest edge. After that, wind speed reduction values seem to decrease exponentially with distance up to roughly 15 km from the downwind forest edge. In this run, a slight wind speed reduction can still be seen up to more than 40 km distance from the forest. However, this might not be realistic and such a reduction is indeed not present in other runs with different geostrophic wind speeds.

At higher heights above ground, percentage wind speed reduction is generally smaller. Indeed, at 140 m height above ground percentage wind speed reduction seems to be roughly half the value from 100 m height above ground.

Percentage wind reduction over isolated forest at different heights above ground

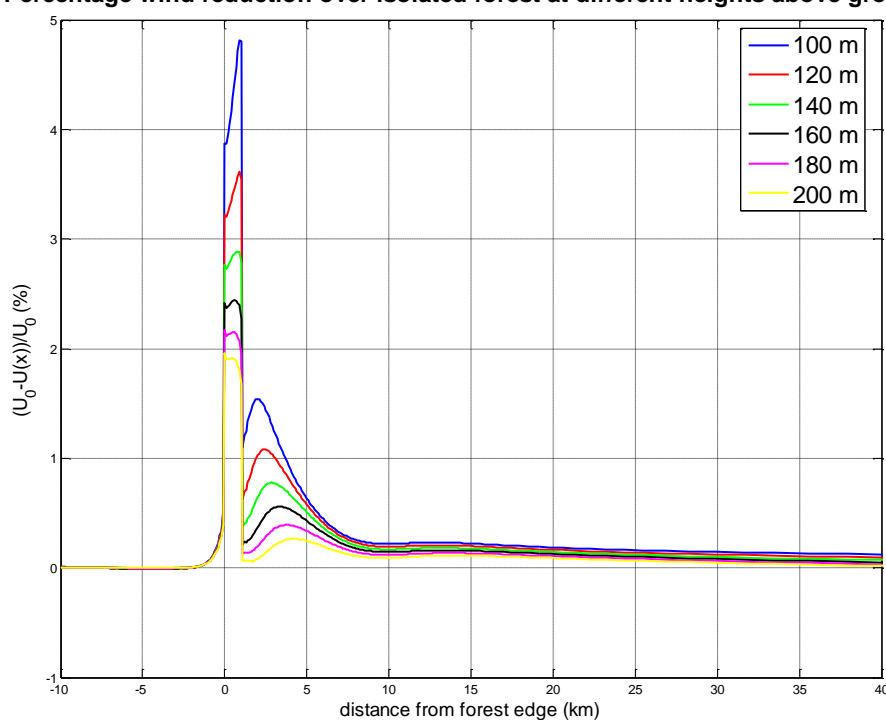


Figure 5-32: Percentage wind reduction downwind of idealised flat isolated forest at different heights above ground. Forest extends from 0 to 1 km. Calculated using Eq. (5-2), with reference upwind wind profile taken at $x = -8$ km. Valid for 10 m/s geostrophic wind and neutral stability.

Table 5-12: Fitting coefficients and correlation for percentage wind speed reduction downwind from isolated forest (x = distance from downwind forest edge). For distances $0 \leq x \leq 20$ km. Valid for neutral stratification only and for an isolated forest with $z_0(\text{forest}) = 1$ m and $z_0(\text{surroundings}) = 0.05$ m. Displacement height is assumed as $d = 16 \cdot z_0$. All coefficients are for 100 m height above ground.

| Size of isolated forest | Coefficient a | Coefficient b^{-1} | Correlation coefficient R^2 |
|-------------------------|-----------------|----------------------|-------------------------------|
| 1 km | 2.3% | 3.52 km | 0.72 |
| 2 km | 3.3% | 4.30 km | 0.78 |
| 4 km | 4.7% | 5.32 km | 0.85 |

Percentage wind reduction over isolated forest for different geostrophic wind speeds

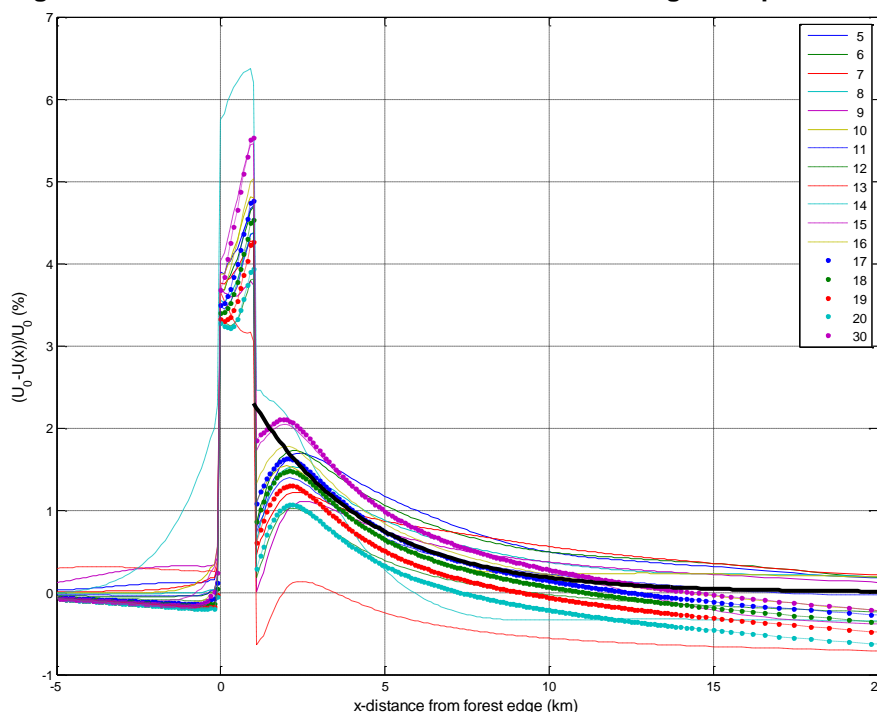


Figure 5-33: Same as Figure 5-32, but for different geostrophic wind speeds and 100 m height above ground. Geostrophic wind speed is given in legend in figure. Run for 13 m/s geostrophic wind speed seems to be an outlier and was removed before further analysis. Fitted equation for percentage wind speed reduction (thick black line) seems to agree relatively well with model results.

Exponential functions (Eq. (5-7)) were fitted to the wind speed reduction values downwind of the isolated forest. Here, x is the distance from the downwind forest edge and a and b are fitting constants. The inverse of b corresponds to the distance where percentage wind speed reduction has decreased to 36.7% of the value directly behind the forest at the downwind forest edge. Because of the somewhat unrealistic wind speed reduction values

directly after the forest up to roughly 2.4 km from the downwind forest edge, these values were discarded during curve fitting.

The correlation seems to be relatively good (Figure 5-33 and Table 5-12). As above, there was no clear dependency of the fitting coefficients on geostrophic wind speed. There are a couple of interesting findings, some of them quite obvious:

- The longer the isolated forest, the larger the percentage wind speed reduction directly after the downwind forest edge (2.2, 3.3 and 4.5%, respectively, for the 1, 2 and 4 km wide forest).
- The longer the forest, the longer distance it takes for wind speeds to recover to their upstream values (3.8, 4.3 and 5.1 km distance for the 1, 2 and 4 km wide forests to recover by 63% to their upstream speeds).
- Percentage wind speed reductions are smaller at higher heights (Table 5-13).
- Wind speeds seem to need a longer distance to recover to their upstream values at higher heights (Table 5-13).

Table 5-13 shows how wind speeds recover downwind of an isolated forest of 4 km length at different heights above ground. The results from Table 5-13 are summarised in Figure 3-34.

Also here, effects of atmospheric stability can be expected. Downwind of the forest, stability effects are probably similar to those for the rough-smooth transition, with a longer decay distance in the stable case as compared to the unstable case. However, this was not investigated in the present study.

Table 5-13: Same as Table 5-12, but for isolated forest of 4 km length and for different heights above ground.

| Height above ground | Coefficient a | Coefficient b^{-1} | Correlation coefficient R^2 |
|---------------------|-----------------|----------------------|-------------------------------|
| 100 | 4.7% | 5.32 km | 0.85 |
| 120 | 4.0% | 5.87 km | 0.81 |
| 140 | 3.4% | 6.60 km | 0.75 |
| 160 | 2.8% | 7.57 km | 0.66 |
| 180 | 2.1% | 9.57 km | 0.55 |
| 200 | 1.7% | 10.4 km | 0.43 |

Percentage wind reduction after isolated forest at different heights above ground

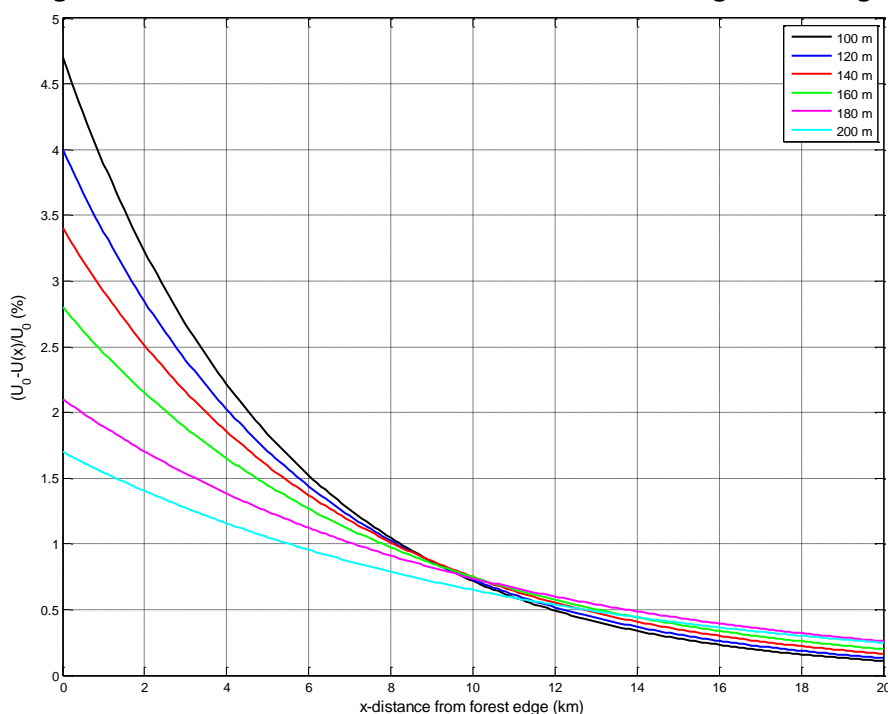


Figure 5-34: Percentage wind reduction downwind of idealised flat isolated forest at different heights above ground. Downwind forest edge located at $x = 0$ km. Calculated using Eq. (5.7) together with coefficients from Table 5-13. Valid for geostrophic wind speeds between roughly 7 and 25 m/s and neutral stability.

b) Change of Turbulence Intensity

Turbulence intensity seems to increase linearly directly above the forest (Figure 5-35). Again, there are discontinuities owing to the sudden increase and drop of the displacement height from 0 to 15 m and from 15 to 0 m at both forest edges. After some 1 – 3 km downwind from the forest, however, turbulence intensity is again approaching the equilibrium turbulence intensity for upwind conditions at an exponential rate (Figure 5-35). The discontinuity in turbulence intensity at the downwind forest edge is clearly not realistic and should be avoided in the forest-canopy version of the mesoscale model.

A very good fit of the turbulence intensity decay after the isolated forest can be achieved by eqn. (5-8), with x being equal to the distance from the downwind forest edge. Again, a and b are fitting constants (Table 5-14). The equation seems to be valid for distances from 0 km up to 20 km from the downwind forest edge (Figure 5-36) and for all geostrophic wind speeds between roughly 5 and 30 m/s.

Table 5-15 and Figure 3-37 show how turbulence intensity enhancement develops downwind of an isolated forest of 4 km length at different heights above ground.

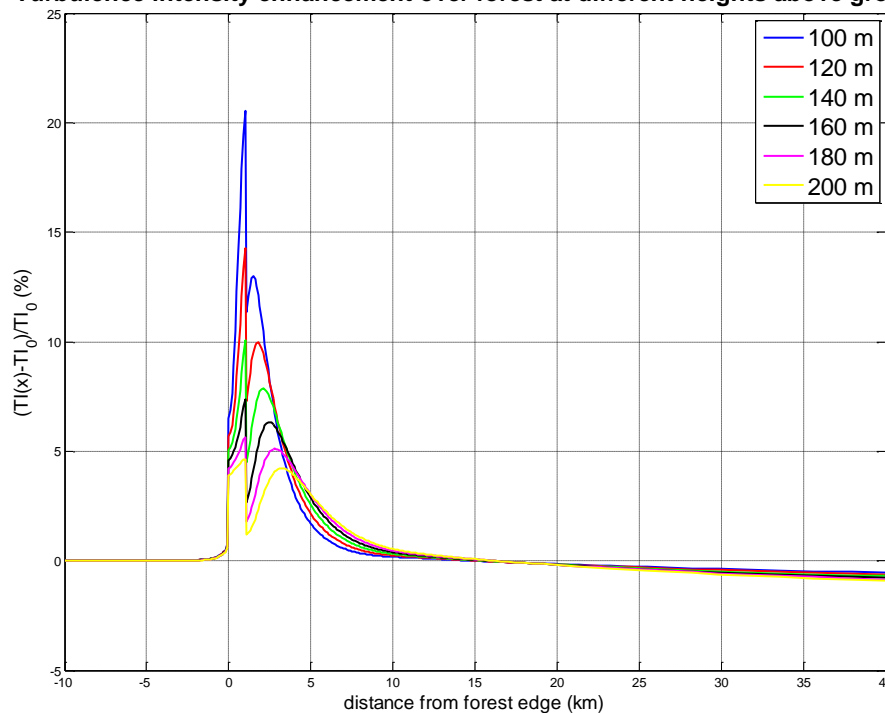
Turbulence intensity enhancement over forest at different heights above ground

Figure 5-35: Percentage turbulence intensity enhancement downwind of isolated forest at different heights above ground. Forest extends from 0 to 1 km. Calculated using eqn. (5-5), with reference upwind turbulence intensity profile taken at $x = -8$ km. Valid for 10 m/s geostrophic wind and neutral stability.

The values obtained herein can be compared with turbulence intensity values from Brady et al. (2010, page 9) who studied the increase in turbulence intensity over an isolated forest using the Ventos CFD model. Their study, however, shows a much more pronounced increase of turbulence intensity over a forest of 1 km length. For 80 m height above ground level and 20 m high trees, the authors found a maximum turbulence intensity enhancement of 50% compared to 30% in our study.

Furthermore, owing to the very high turbulence, they found an increase of the wind shear exponent to 0.37 at 80 m height above ground from an upstream value of 0.14. They also found from their CFD model that a 3 km long forest with 15 m high trees can increase turbulence intensity by 100% from the upstream value at 80m height above ground (Brady et al., 2010, page 12). Our results, however, give a maximum turbulence intensity enhancement of 41% at 80 m height above ground for 20 m high trees and a 4 km long forest.

Percentage turbulence intensity enhancement over isolated forest for different geostrophic wind speeds

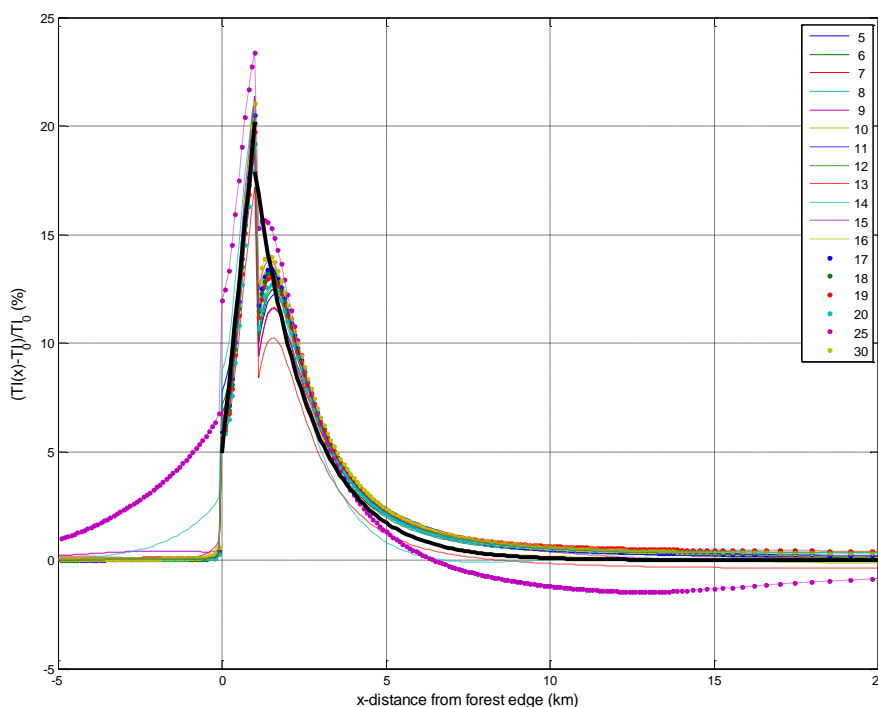


Figure 5-36: Same as Figure 5-35, but for different geostrophic wind speeds and 100 m height above ground. Geostrophic wind speed is given in legend in figure. Fitted equation for percentage turbulence intensity enhancement (thick black line) seems to agree very well with model results.

Table 5-14: Fitting coefficients and correlation for percentage turbulence intensity enhancement after isolated forest (x = distance from downwind forest edge). Valid for $0 \leq x \leq 20$ km. Valid for neutral stratification only and for isolated forest with $z_0(\text{forest}) = 1$ m and $z_0(\text{surroundings}) = 0.05$ m. Displacement height is assumed as $d = 16 \cdot z_0$. All coefficients are for 100 m height above ground.

| Size of isolated forest | Coefficient a | Coefficient b^{-1} | Correlation coefficient R^2 |
|-------------------------|-----------------|----------------------|-------------------------------|
| 1 km | 18.5% | 1.82 km | 0.97 |
| 2 km | 26.6% | 1.76 km | 0.98 |
| 4 km | 31.1% | 1.89 km | 0.97 |

Table 5-15: Same as Table 5-14, but for isolated forest of 4 km length and for different heights above ground.

| Height above ground | Coefficient a | Coefficient b^{-1} | Correlation coefficient R^2 |
|---------------------|-----------------|----------------------|-------------------------------|
| 100 | 31.1% | 1.89 km | 0.97 |
| 120 | 27.4% | 2.40 km | 0.97 |
| 140 | 24.3% | 2.96 km | 0.96 |
| 160 | 21.5% | 3.59 km | 0.95 |
| 180 | 18.7% | 4.33 km | 0.92 |
| 200 | 16.2% | 5.24 km | 0.88 |

Percentage turbulence intensity enhancement downwind of isolated forest at different heights

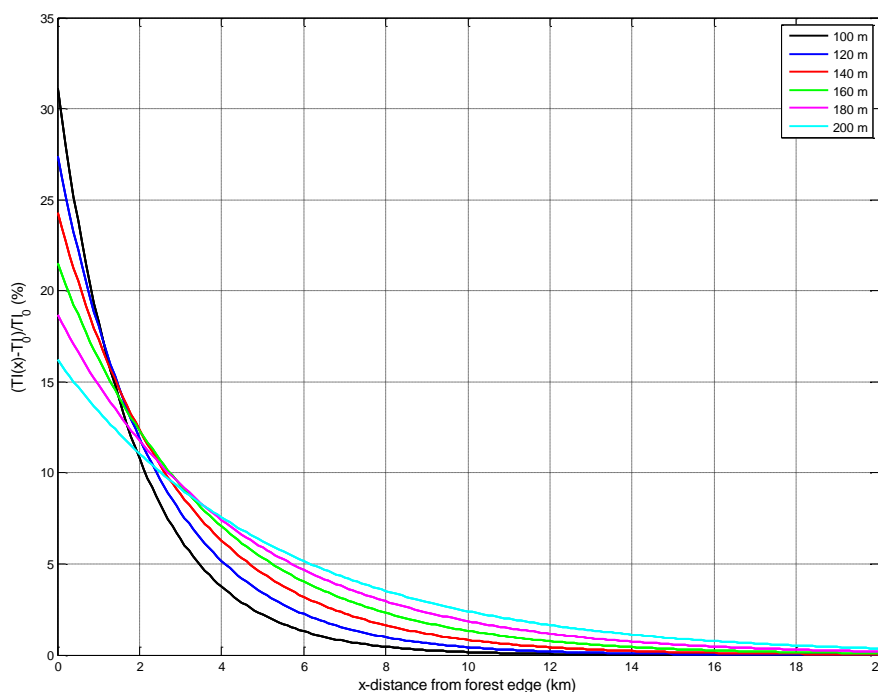


Figure 5-37: Percentage turbulence intensity enhancement after isolated forest at different heights above ground. Calculated using Eq. (5-7) together with coefficients from . Valid for geostrophic wind speeds between roughly 4 and 30 m/s and neutral stability.

Table 5-16, finally, shows fitting coefficients and correlation for percentage turbulence intensity enhancement above the isolated forest. Here x is distance from upwind forest edge. A linear increase in turbulence intensity enhancement (i.e. $\Delta TI = a \cdot x + b$) worked pretty well.

Table 5-16: Same as Table 5-14, but fitting coefficients and correlation for percentage turbulence intensity enhancement above isolated forest (x = distance from upwind forest edge). A linear increase in turbulence intensity enhancement was assumed (i.e. $\Delta TI = a \cdot x + b$)

| Size of isolated forest | Coefficient a | Coefficient b | Correlation coefficient R^2 |
|-------------------------|------------------------|-----------------|-------------------------------|
| 1 km | 15.2% km ⁻¹ | 4.9% | 0.94 |
| 2 km | 13.0% km ⁻¹ | 6.5% | 0.94 |
| 4 km | 7.0% km ⁻¹ | 12.4% | 0.81 |

5.2.5 Influence of clearings on wind and turbulence field

Here, isolated clearings of different sizes are studied in order to find out how the wind and turbulence field is modified. Three cases with clearings of 1, 2 and 4 km horizontal extension were simulated.

Percentage wind speed increase and percentage turbulence intensity reduction over the clearing were calculated with eqn. (5-2) and (5-5), respectively. As in Section 5.2.2, the reference upstream wind and turbulence intensity profile U_0 and TI_0 were taken at $x = -8$ km.

a) Change of Wind Speed

Wind speeds increase with roughly 3 to 6% directly above a clearing of 1 km length at different heights above ground (Figure 5-38). Directly after the clearing, values "jump" to 1 – 2% from 3 to 6%, revealing a discontinuity at the clearing edge. Both discontinuities at the clearing edges are due to the displacement height dropping from 15 m to 0 m directly over the clearing and increasing back to 15 m again after the clearing. These effects seem to be unrealistic and a forest canopy model should give much better results in this case.

Downwind of the clearing, wind speeds rise again up to a distance between 1.5 and 3 km from the downwind clearing edge. Further out, however, wind speeds seem to decrease exponentially with distance to the forest clearing. A slight wind speed reduction can be seen from 10 km distance downwind of the clearing in this run. However, this might not be realistic and such a reduction is also not present in other runs with different geostrophic wind speeds.

At higher heights above ground, percentage wind increase is generally smaller. Indeed, at 180 m height above ground percentage wind increase seems to be roughly half the value at 100 m height above ground.

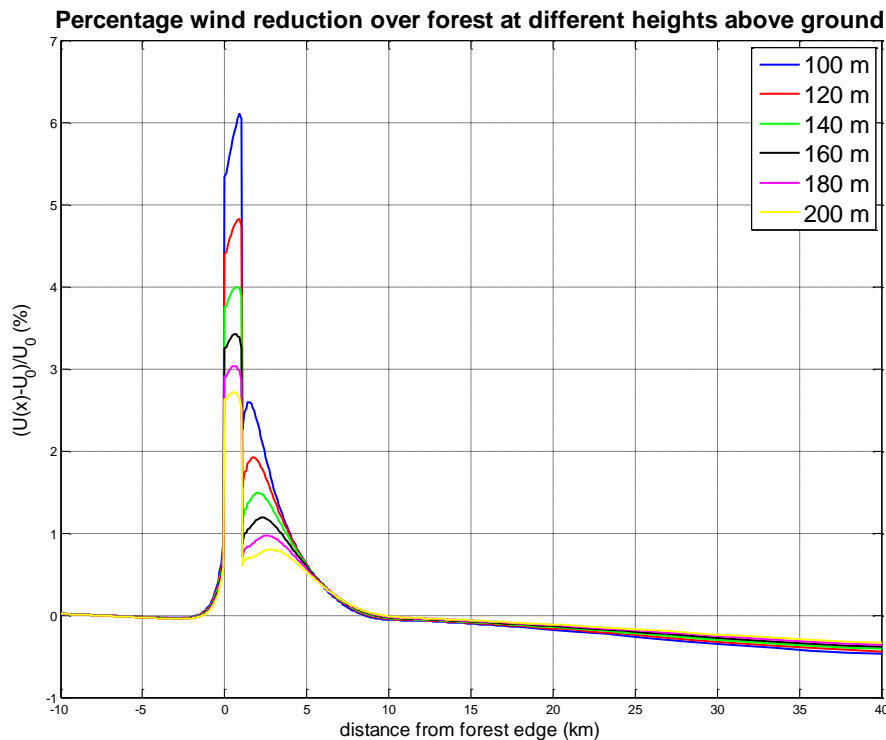


Figure 5-38: Percentage wind increase over isolated forest clearing at different heights above ground. Clearing extends from $x = 0$ to 1 km. Calculated using Eq. (5-2), with reference upwind wind profile taken at $x = -8$ km. Valid for 10 m/s geostrophic wind and neutral stability.

Exponential functions (Eq. (5-7)) were fitted to the percentage wind speed increase downwind of the isolated clearing. Note that, in this case, x is the distance from the downwind clearing edge. Again, a and b are fitting constants. The inverse of b corresponds to the distance where percentage wind increase has decreased to 36.7% of the value directly behind the clearing. Because of the somewhat unrealistic wind speed increase directly after the clearing up to roughly 1.5 – 3 km from the downwind clearing edge, these values were discarded during the curve fitting.

Correlation seems to be relatively good (Figure 5-39 and Table 5-17). Also in this case, there was no clear dependency of the fitting coefficients on geostrophic wind speed. Nevertheless, there are a couple of interesting findings, some of them quite obvious:

- The longer the clearing, the larger the percentage wind increase directly after the downwind clearing edge (2.2, 3.8 and 5.5%, respectively, for the 1, 2 and 4 km long clearings).
- It takes approximately the same distance for wind speeds to adjust back to their upstream values after the clearing irrespective of the size of the clearing (around 4 km distance for the 1, 2 and 4 km long clearings (Table 5-17)).

- Percentage wind speed increases are smaller at higher heights (Table 5-18)
- At higher heights wind speeds seem to need a longer distance to adjust back to their upstream values (Table 5-18)

Percentage wind increase over forest clearing for different geostrophic wind speeds

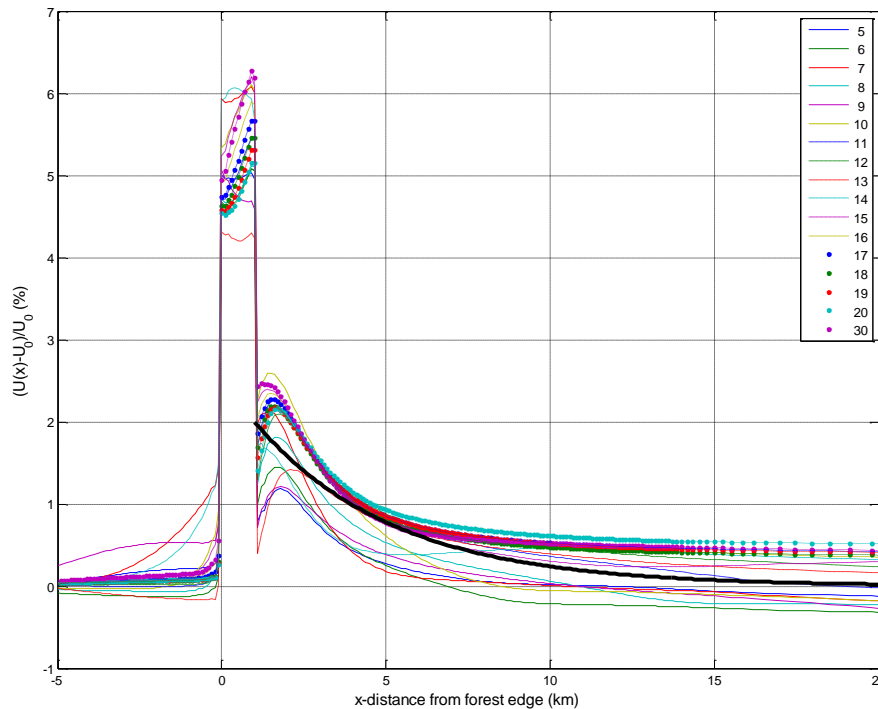


Figure 5-39: Same as Figure 5-38, but for different geostrophic wind speeds and 100 m height above ground. Geostrophic wind speed is given in legend. Fitted equation for percentage wind speed reduction (thick black line) seems to agree relatively well with model results.

Table 5-18 shows how wind speeds adjust back to their upstream values downwind of an isolated clearing of 4 km length at different heights above ground. The results from Table 5-18 are summarised in Figure 5-40. Also here, effects of atmospheric stability can be expected. Downwind of the clearing, stability effects are probably similar to those for the smooth-rough transition (see above). However, this was not included in the present study.

Table 5-17: Fitting coefficients and correlation for percentage wind speed increase downwind from isolated clearing (x = distance from downwind clearing edge). Valid for $0 \leq x \leq 20$ km. Valid for neutral stratification only and for an isolated clearing with $z_0(\text{forest}) = 1$ m and $z_0(\text{clearing}) = 0.05$ m. Displacement height is assumed as $d = 16 \cdot z_0$. All coefficients are for 100 m height above ground.

| Size of isolated clearing | Coefficient a | Coefficient b^{-1} | Correlation coefficient R^2 |
|---------------------------|-----------------|----------------------|-------------------------------|
| 1 km | 2.2% | 3.82 km | 0.74 |
| 2 km | 3.8% | 3.78 km | 0.83 |
| 4 km | 5.6% | 4.05 km | 0.87 |

Percentage wind increase over forest at different heights above ground

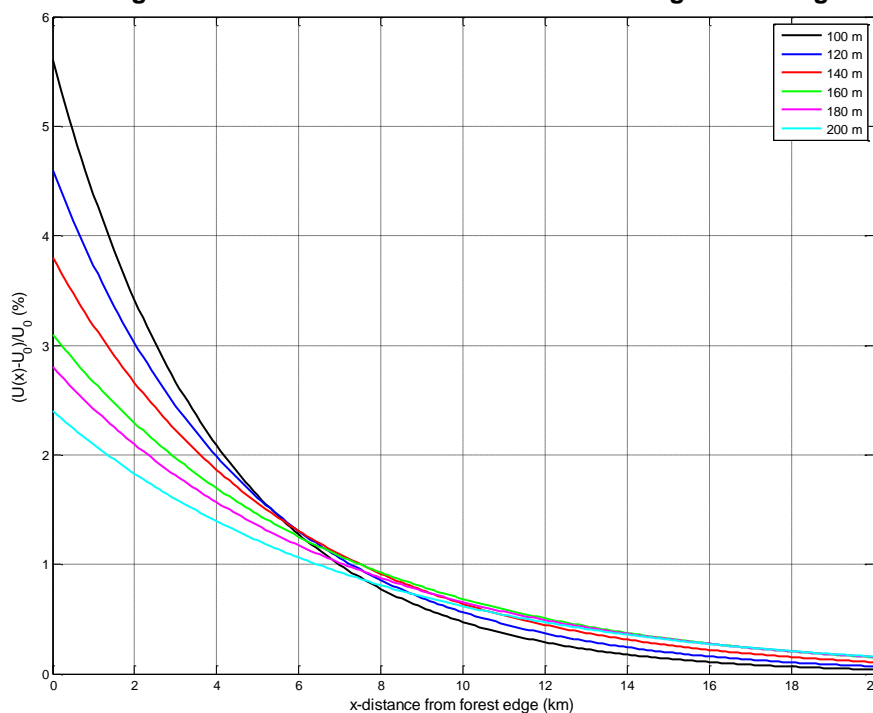


Figure 5-40: Percentage wind increase downwind of isolated forest clearing of 4 km length at different heights above ground. Downwind clearing edge is located at $x = 0$ km. Percentage wind speed reduction is calculated using Eq. (5-7) together with coefficients from Table 5-17 Valid for geostrophic wind speeds between roughly 5 and 25 m/s and neutral stability.

Table 5-18: Same as Table 5-17 but for isolated clearing of 4 km length and for different heights above ground.

| Height above ground | Coefficient a | Coefficient b^{-1} | Correlation coefficient R^2 |
|---------------------|-----------------|----------------------|-------------------------------|
| 100 | 5.6% | 4.05 km | 0.87 |
| 120 | 4.6% | 4.76 km | 0.84 |
| 140 | 3.8% | 5.61 km | 0.78 |
| 160 | 3.1% | 6.62 km | 0.70 |
| 180 | 2.8% | 6.89 km | 0.64 |
| 200 | 2.4% | 7.36 km | 0.52 |

b) Change of Turbulence Intensity

Over the isolated clearing, turbulence intensity seems to decrease steeply directly above the clearing (Figure 5-41). Again, there are discontinuities at the edges of the clearing owing to the sudden change of the displacement height from 16 m to 0 m and back to 16 m. After some kilometre or so, however, turbulence intensity is again approaching the equilibrium turbulence intensity for upwind conditions at an exponential rate (Figure 5-41). The discontinuity in turbulence intensity reduction at both clearing edges is clearly not realistic and should be avoided in the forest-canopy version of the mesoscale model.

Turbulence intensity reduction over forest clearing at different heights above ground

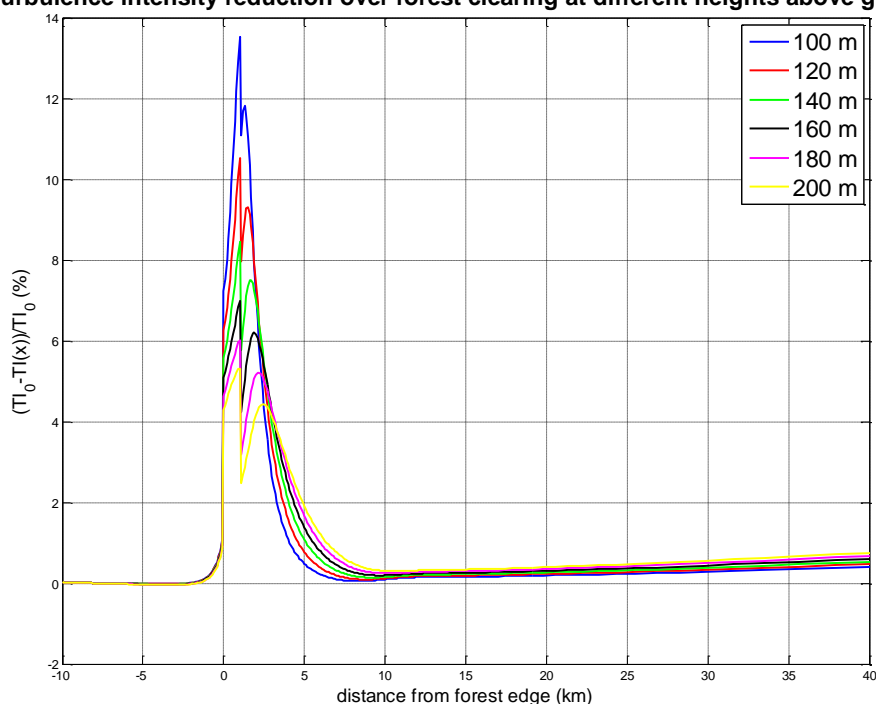


Figure 5-41: Percentage turbulence intensity reduction downwind of isolated clearing at different heights above ground. Clearing extends from 0 km to 1 km. Calculated using Eq. (5-5), with reference upwind turbulence intensity profile taken at $x = -8$ km. Valid for 10 m/s geostrophic wind and neutral stability.

A very good fit of the turbulence intensity reduction after the isolated clearing can be achieved by Eq. (5-8) using x equal to the distance from the downwind clearing edge. Again, a and b are fitting constants (Table 5-19 and Figure 5-42) The equation seems to be valid for distances from 0 km up to 20 km from the downwind clearing edge. It describes the increase of modelled turbulence extremely well for geostrophic wind speeds between roughly 5 and 30 m/s. Also it seems to be valid for all geostrophic wind speeds (Figure 5-42).

A reasonable fit of the turbulence intensity decrease above an isolated clearing can be achieved by a linear fit (Table 5-20). Here, however, x is distance to upwind clearing edge.

Percentage turbulence intensity reduction over forest clearing for different geostrophic wind speeds

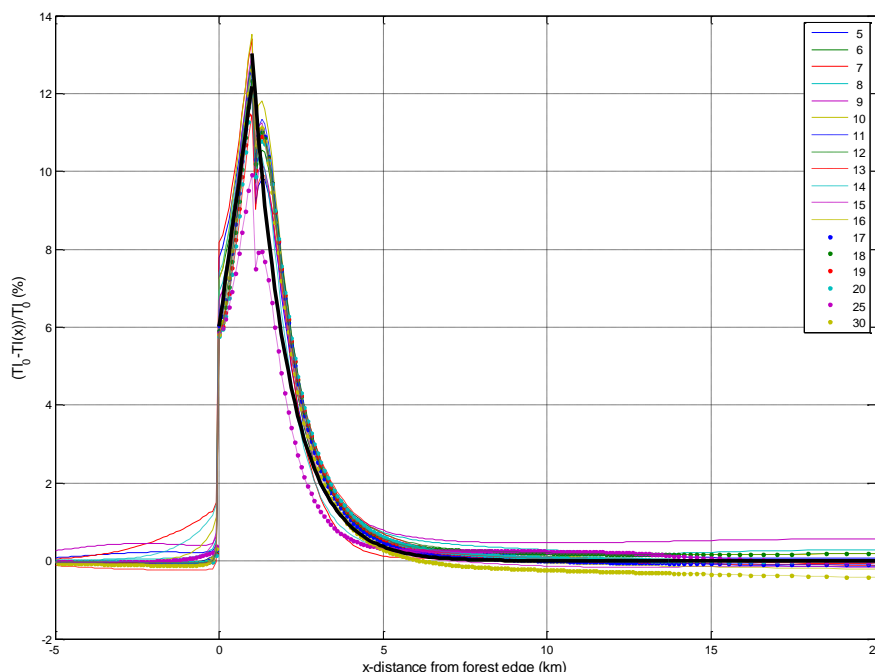


Figure 5-42: Same as Figure 5-41, but for different geostrophic wind speeds and 100 m height above ground. Geostrophic wind speed is given in legend in figure. Fitted equations for percentage turbulence intensity reduction (thick black line) seem to agree very well with model results.

Table 5-19: Fitting coefficients and correlation for percentage turbulence intensity reduction after isolated clearing (x = distance to downwind clearing edge). Valid for $0 \leq x \leq 20$ km. Valid for neutral stratification only and for an isolated clearing with $z_0(\text{forest}) = 1$ m and $z_0(\text{clearing}) = 0.05$ m. Displacement height is assumed as $d = 16 \cdot z_0$. All coefficients are for 100 m height above ground.

| Size of isolated clearing | Coefficient a | Coefficient b^{-1} | Correlation coefficient R^2 |
|---------------------------|-----------------|----------------------|-------------------------------|
| 1 km | 13.0% | 1.11 km | 0.98 |
| 2 km | 20.1% | 1.12 km | 0.98 |
| 4 km | 24.3 % | 1.25 km | 0.98 |

Table 5-20 same as Table 5-19 but fitting coefficients and correlation for percentage turbulence intensity reduction above isolated clearing (x = distance to upwind clearing edge). A linear increase in turbulence intensity reduction was assumed (i.e. $\Delta TI = a \cdot x + b$).

| Size of isolated clearing | Coefficient a | Coefficient b | Correlation coefficient R^2 |
|---------------------------|-----------------------|-----------------|-------------------------------|
| 1 km | 6.2% km ⁻¹ | 6.0% | 0.89 |
| 2 km | 6.4% km ⁻¹ | 6.2% | 0.95 |
| 4 km | 4.3% km ⁻¹ | 8.4% | 0.90 |

Table 5-19 shows how turbulence intensity adjusts back to upstream values downwind of an isolated clearing of 4 km length at different heights above ground. The results from Table 5-19 are summarised in Figure 5-43. Also here, effects of atmospheric stability can be expected. Downwind of the clearing, stability effects are probably similar to those for the smooth-rough transition (see above). However, this was not included in the present study.

Percentage turbulence intensity reduction after forest clearing for different heights above ground

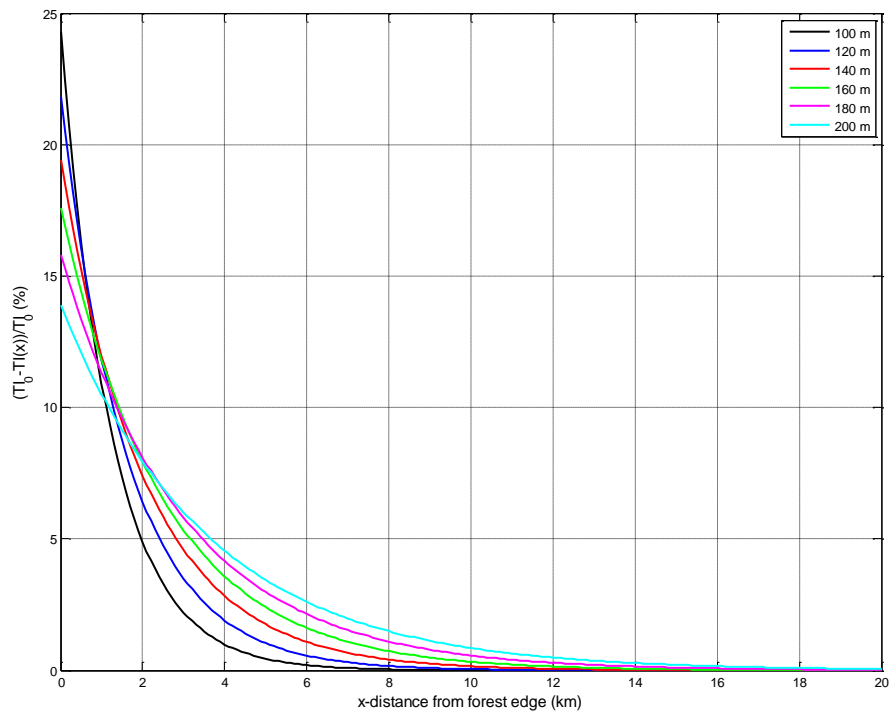


Figure 5-43: Percentage turbulence intensity reduction after isolated clearing at different heights above ground. Calculated from equation (5) together with coefficients from Error! Reference source not found.. Valid for geostrophic wind speeds between roughly 5 and 30 m/s and neutral stability.

Table 5-21 same as Table 5-19 but for isolated clearing of 4 km length and for different heights above ground.

| Height above ground | Coefficient a | Coefficient b^{-1} | Correlation coefficient R^2 |
|---------------------|-----------------|----------------------|-------------------------------|
| 100 | 24.3 % | 1.25 km | 0.98 |
| 120 | 21.8% | 1.64 km | 0.97 |
| 140 | 19.4% | 2.08 km | 0.97 |
| 160 | 17.6% | 2.51 km | 0.95 |
| 180 | 15.8% | 3.00 km | 0.94 |
| 200 | 13.9% | 3.58 km | 0.92 |

5.3 Implementing forest canopy parameterisations in the MIUU mesoscale model

Detailed forest modelling for wind energy purposes is commonly done using CFD models (e.g. Stuart et al. (2008), Lopes da Costa (2007), Frank and Ruck (2008), Teneler (2011), Silva Lopes et al. (2012)) or other simplified models such as WASP (e.g. Dellwik et al., 2005). There is no reason that the parameterisations from CFD models cannot be used in mesoscale models.

Within the scope of this project, we have started to implement forest parameterisations in the MIUU mesoscale model (Mohr et al., 2012). However, it turned out that the task is more complicated than originally thought (especially implementing the forest canopy energy balance and modifying lower boundary conditions in the mesoscale model). Also running the forest canopy version of the MIUU mesoscale model at say 100 m horizontal resolution is computationally very expensive.

It is expected that a full forest canopy version of the MIUU mesoscale model will be available during 2013. This version of the MIUU model could, in principle, be used instead of commonly available CFD models. However, it is not clear how many cases (or days) would have to be simulated, in order to get a reliable wind climate.

While CFD models mostly use neutral stratification (i.e. a state of the atmosphere where there is neither buoyant production nor buoyant destruction of turbulent kinetic energy), mesoscale models predict the real vertical temperature structure of the atmosphere. Hence, in mesoscale models the thermal stratification is generally non-neutral.

In a similar way as in CFD-models, forest drag was included in the MIUU mesoscale model through additional drag terms in the equations for the horizontal wind speed components as well as production and dissipation terms in the equation for TKE. The forest drag coefficient depends on the leaf area density that is a function of height, leaf area index (LAI) and tree type. Very high vertical resolution was used in order to resolve the forest canopy with at least a couple of vertical levels.

From section 5.2.3 and 5.2.4 for isolated forests and clearings, respectively, it becomes evident that the approach using surface roughness and displacement height has its limitations. A forest canopy model is expected to give much better results in these cases; especially very close to the upwind forest or clearing edge.

5.3.1 Description of forest-canopy version of MIUU model

A new canopy version of the MIUU model has been developed. Work is still in progress, but some results from the canopy version are nevertheless presented below. The original version of the MIUU mesoscale model with surface roughness and flow displacement (hereinafter called "bulk version")

was compared with the forest canopy version (hereinafter called "canopy version") of the MIUU mesoscale model.

a) Vertical resolution of canopy model

In the forest canopy version of the MIUU model, the lowest vertical model levels were chosen to be at 1, 3, 6, 8, 12, 16, 20, 25, 31, 38, 47, 56, 67, 80, 95, 113, 133, 156 and 183 m height above ground. In total 49 vertical levels were used up to a height of 10000 m above ground. This results in 6 vertical levels within a typical forest canopy of 20 m height.

However, 29 vertical levels in total also seemed to be enough to resolve the forest canopy (Mohr et al., 2012). In the latter case, the lowest vertical model levels were situated at 1, 3, 6, 10, 16, 24, 35, and 52 m height above ground. This results in 5 vertical levels within a typical forest canopy.

Since the lowest level is situated at 1 m as compared to the default value of 2 m in the MIUU model, a much lower time step has to be used in the forest canopy version of the model.

b) Additional terms in momentum equations

In the momentum equations for the two horizontal wind components u and v , an additional forest drag term is added as

$$\frac{\partial u}{\partial t} = \dots - C_d \cdot LAD \cdot |\vec{u}_{horizontal}| \cdot u$$

where C_d is a drag coefficient for the forest (usually taken as $C_d = 0.2$) and LAD is the leaf area density (LAD). The magnitude of the horizontal wind vector ($|\vec{u}_{horizontal}|$) is also included in the term. The same term was added in the prognostic equation for the v -component of the wind, simply replacing the variable u with v in the above equation.

It was decided to use the LAD profile suggested by Lalic and Mihailovic (2004) for pine forests. Table 5-22 summarises all the values that have been used.

Table 5-22: Values used in forest canopy version of MIUU mesoscale model.

| Variable Name | Notation | Value |
|-------------------------------------|--------------------------------|-----------------------------|
| Drag coefficient for forest | C_d | 0.2 |
| Forest canopy height | h_c | 20 m |
| Leaf area index | $LAI = \int_0^{h_c} LAD(z) dz$ | 5 |
| Height of maximum leaf area density | $z_m = 0.6h_c$ (pine forest) | 12 m |
| Leaf area density | $LAD(z)$ (pine forest) | Lalic and Mihailovic (2004) |
| Maximum leaf area density | $L_m = LAI / h_c \cdot 1.70$ | 0.425 |

c) Additional terms in TKE equation

In contrast to CFD models, where the mostly used turbulence model consists of prognostic equations for turbulent kinetic energy and turbulent dissipation ("k-ε-model"), the MIJU model only has a prognostic equation for turbulent kinetic energy (TKE). Therefore, additional forest terms can only be included in the prognostic equation for TKE, whereas the dissipation term in the TKE equation of the MIJU model was not modified. Dissipation in the TKE equation, however, is parameterised using the master length scale, which is modified in the forest canopy.

In the prognostic equation for TKE, production and dissipation terms were added as

$$\frac{\partial q^2}{\partial t} = \dots + C_d \cdot LAD \cdot (\beta_p \cdot |\bar{u}_{horizontal}|^3 - \beta_d \cdot |\bar{u}_{horizontal}| \cdot q^2)$$

where q^2 is the turbulent kinetic energy and β_p and β_d constants accounting for the production and destruction of TKE within the forest canopy. Several values have been proposed for the constants (Table 5-23). It was decided to use the same constants as most of the authors, i.e. $\beta_p = 1$ and $\beta_d = 4$.

Table 5-23: Constants used for forest source and sink terms in prognostic equation for turbulent kinetic energy (TKE) .

| Reference | β_p -value | β_d -value |
|-------------------------------|------------------|------------------|
| Svensson and Häggkvist (1990) | 1.0 | 0.0 |
| Green (1992) | 1.0 | 4.0 |
| Liu et al. (1996) | 1.0 | 4.0 |
| Foudhil (2002) | 1.0 | 4.0 |
| Sanz (2003) | 1.0 | 5.1 |
| Katul et al. (2004) | 1.0 | 5.1 |
| Krzikalla (2005) | 0.0 | 4.0 |
| Foudhil et al. (2005) | 0.8 | 4.0 |

d) Mixing length in canopy

The same mixing length was used for the whole forest. The scale of canopy eddies in the vertical direction was estimated to

$$l_c = 0.47 \cdot (h_c - d)$$

according to Inoue (1963), where l_c is the canopy mixing length and d the displacement height calculated as $d = 15 \cdot z_0$. The master length scale (mixing length) in the mesoscale model was then set to

$$l = \max(l, l_c)$$

within the forest canopy for all model levels below h_c . There might be newer/better estimates of the canopy length scale. However, the canopy mixing length has very little influence on the model results above the forest canopy.

e) Energy balance

The energy balance has to be solved at each level within the forest canopy. Surface temperatures for leaves, branches and stems have to be calculated at each vertical model level.

A very simple formulation for short-wave radiation was chosen in Mohr et al. (2012), following Beer's law, i.e.

$$S_{\downarrow} = S_{\downarrow 0} \cdot \exp(-0.5 \cdot \int_{z_{model}}^{h_c} LAD(z) dz)$$

where $S_{\downarrow 0}$ is the incoming shortwave radiation at the canopy top, S_{\downarrow} the incoming shortwave radiation at each vertical level within the canopy and z_{model} the height above ground of the respective model level.

For longwave radiation, the expressions from Zhao and Qualls (2006) were chosen.

f) Lower boundary conditions

An elevated Monin-Obukhov (MO) similarity theory model has to be used. All lower boundary conditions have to be modified, replacing MO-similarity theory terms below the zero displacement height d with something else. It is still not clear what should be used.

Friction velocity is now computed at the lowest model level above d , instead of using the lowest model level above ground. A roughness sub-layer has also to be implemented in the model.

5.3.2 Comparison of forest-canopy version of MIUU model with bulk-layer roughness version

The model was run one-dimensionally with exactly the same input data. However in the canopy version a leaf area density profile was used instead of a surface roughness length. Input values from Table 5-22 were used for the canopy version, whereas a surface roughness length and displacement height of $z_0 = 1$ m and $d = 15$ m were used in the bulk version. In order to avoid any influences from different temperature profiles, model temperatures at the lowest vertical levels were kept constant in time.

Figure 5-44 shows that both versions agree very well with each other. There is a discontinuity in the canopy version at 20 m height above ground which clearly is unrealistic. Although friction velocity u_* was 0.75 m/s in the canopy version and 0.42 m/s in the bulk version, wind profiles agree remarkably well.

In addition wind tunnel measurements from Section 4 (see also Segalini et al., 2012) are shown in the figure. Wind tunnel measurements were corrected in order to give approximately the same wind speed at the highest level of the

wind tunnel measurements, i.e. at 8.2 times the canopy height ($= 164$ m above ground).

Comparison of wind profiles from bulk and canopy versions with wind tunnel measurements

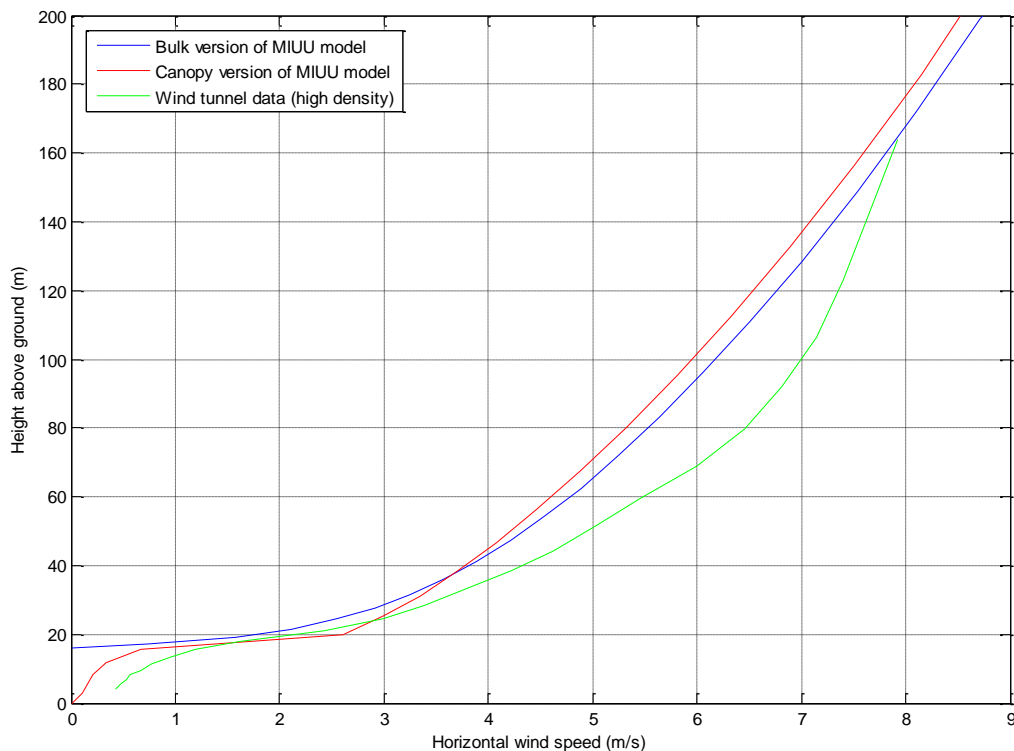


Figure 5-44: Comparison of “bulk version” with “canopy version” of MIUU model (blue and red) as well as wind tunnel measurements (green). Wind tunnel measurements are described in Section 4.

5.3.3 Comparison of 1D MIUU model with wind tunnel measurements

Wind tunnel measurements from Section 4 (see also Segalini et al., 2012) were used for the comparison (Figure 5-44). It has to be pointed out that wind tunnel measurements are valid for neutral stratification only. In the model runs, however, neutral stratification was used only up to 1000m height above ground, whereas a slightly stable atmosphere with a temperature lapse rate of $0.65^{\circ}\text{C}/100$ m height was used above that.

It can be seen that all three curves agree nicely from 0 up to 25 m height above ground ($=$ up to 1.25 times canopy height). Above that both model versions give lower wind speeds than the wind tunnel measurements. In the wind tunnel measurements u_* was approximately 0.8 m/s.

Because of the wind tunnel ceiling being situated at $16 \cdot h_c$ the upper parts of the wind tunnel measurements (say above $2 - 3 \cdot h_c$) could be strongly influenced by wall effects from the ceiling.

5.3.4 Comparison of 2D MIUU model with wind tunnel measurements

Wind tunnel measurements from Section 4 (see also Segalini et al., 2012) were used for the comparison (Figure 5-45). Also shown in these figures is the measured wind profile at Ryningsnäs for neutral stratification.

The MIUU model was run with the same set-up as in Section 5.2.2. In both model simulations and wind tunnel measurements the canopy edge is situated at $x = 0h_c$.

It has to be pointed out that wind tunnel measurements are valid for neutral stratification only. In the model runs, however, neutral stratification was used only up to 1000m height above ground, whereas a slightly stable atmosphere with a temperature lapse rate of $0.65^\circ\text{C}/100 \text{ m}$ height was used above that.

Heights were normalised using the canopy height h_c of 20 m and 50 mm for model simulations/measurements and wind tunnel measurements, respectively.

For the upstream wind profile the bulk version agrees better with the wind tunnel measurements than the canopy version (Figure 5-45). Also up to $2h_c$, the bulk version agrees better with the wind tunnel measurements than the canopy version. Above $2h_c$ or so, wind tunnel profiles probably seem to be influenced by the wind tunnel ceiling. This also explains that wind speeds increase above the wind tunnel canopy with increasing distance x for heights above $3h_c$.

Wind shear above the canopy appears to be better predicted by the canopy version than the bulk version. Also the wind speed reduction above the canopy seems to be better simulated by the canopy version. All in all, the canopy version seems to agree better with the measurements from Ryningsnäs, whereas the bulk version seems to agree better with the wind tunnel data (up to $2h_c$ or so).

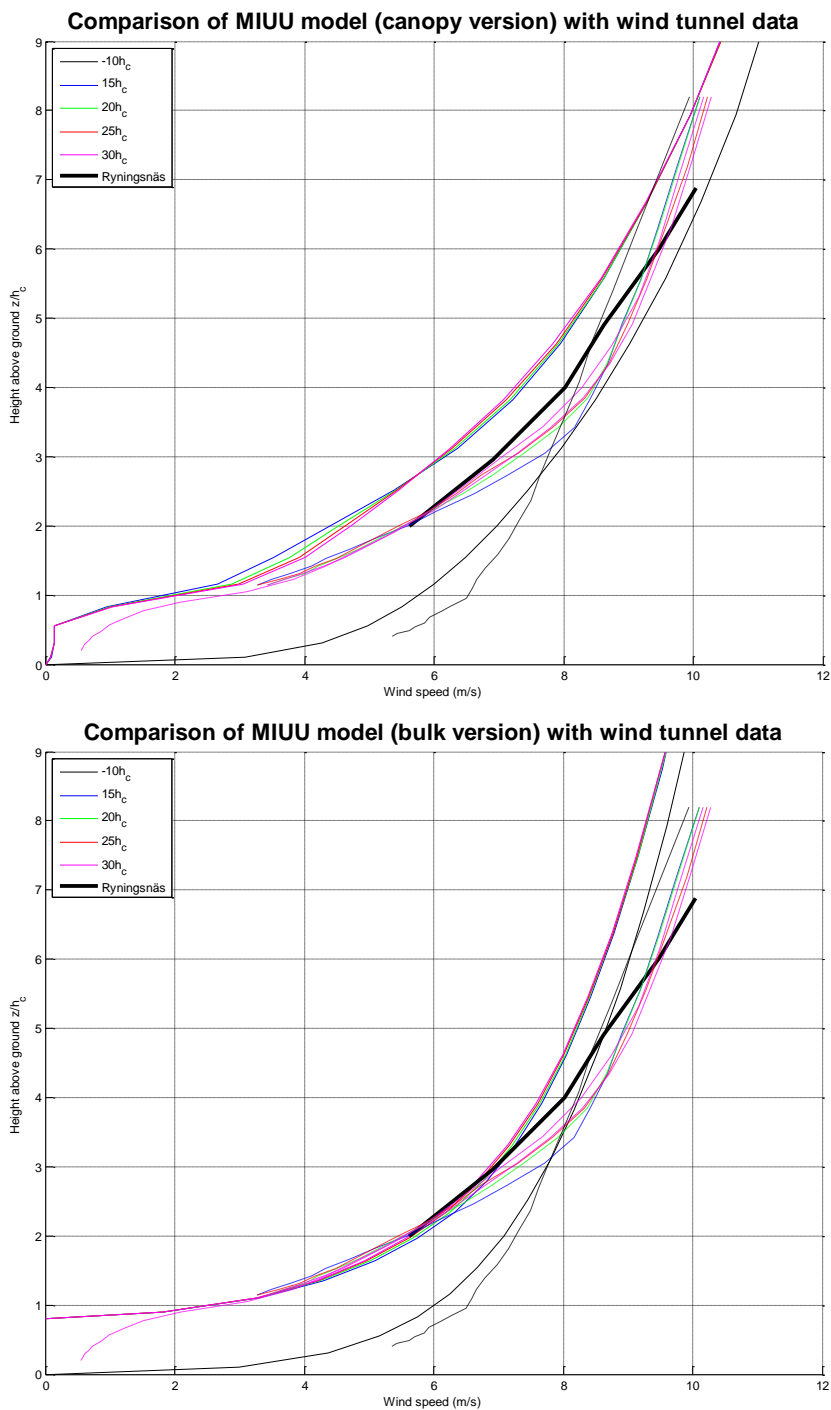


Figure 5-45: Comparison of “canopy version” and “bulk version” of MIUU model (upper and lower figure, full lines) with wind tunnel measurements (dashed lines). Distances and heights were normalised with canopy height ($h_c = 20$ m for MIUU model and $h_c = 50$ mm for wind tunnel). Eastward distance x is given in legend. Forest is present for $x \geq 0$. Also shown are data from Ryningsnäs for neutral conditions.

5.4 Summary & Conclusions

a) Mesoscale model results for forests

Results from three mesoscale models (WRF, COAMPS and MIUU) were analysed and compared to measurements from Ryningsnäs. Even though a real validation over forests has to be based on many different forest sites, some important conclusions can be drawn:

- Mesoscale results do not only depend on horizontal and vertical resolution, but also to a very significant degree on the turbulence or planetary boundary layer scheme chosen (e.g. WRF YSU compared to WRF YSU2). The newest version of the turbulence/PBL scheme should always be used, as essential errors might have been corrected in the meantime (e.g. WRF YSU). This is an advantage of WRF where several PBL schemes can easily be tested, whereas in most other mesoscale models only one turbulence/PBL scheme is available for use.
- Mesoscale model results over forests should be validated not only in terms of mean wind speed, but also in terms of wind shear; i.e. the model has to get the wind shear right.
- Some mesoscale models (e.g. WRF Risø) are very sensitive to surface roughness (e.g. increasing/doubling z_0) with respect to wind speed at 100 – 150 m height above ground, whereas other models (e.g. MIUU) are not. The reason for this is still unclear.
- Wind shear exponents as results of most mesoscale models seem to be at the lower end compared to measurements. Commonly used roughness values for forests in these models are probably too low (e.g. 0.5 m in WRF, 0.8 m in MIUU, in contrast to 2 m in WRF MYJ rough).

There is still some disagreement about what values for the surface roughness for forests, that should be used in mesoscale calculations as pointed out in this report. However, it seems as the use of roughness values in the region of 1 to 2 m give the best results for a typical Swedish forest. The value of the surface roughness that results in the the best match with measurements also depends on the method chosen to compute it from measurements (Sections 3.1.3 and 3.3.2). Moreover, there is a large variation in tree height across Sweden, with latitude and height above sea level probably being the two most important factors, apart from the intense forestry which seldom leaves naturally growing forests in Sweden.

b) Idealised study of forest edges

Idealised 2-dimensional mesoscale model simulations of forests have been carried out with the MIUU model. The effect of forest edges was studied for smooth-rough and rough-smooth transitions. Moreover, 1, 2 and 4 km long isolated forests and clearings were studied. The model was run at 100 m

horizontal resolution, a resolution typical for CFD models commonly used in the industry. Also, effects of atmospheric stability were looked into.

It was planned to use the wind tunnel measurements from Section 4 for validating the mesoscale model. However, this was not possible as wind tunnel data was undisturbed only up to levels of 2-3 times the canopy height. Above those levels, the wind tunnel data presented herein was influenced by the wind tunnel ceiling. Hence, the wind tunnel data could not be used for model validation at heights relevant to wind power.

Mesoscale models use a bulk surface layer scheme. Hence, they have their lowest vertical level at the height of the surface roughness (z_0) plus zero-displacement height (d), where wind speed is simply set to zero. Therefore, model results have to be post-processed accounting for the displaced wind profile. In this study, it was assumed that $d = 15 \cdot z_0$ (with $d = 15$ m and $z_0 = 1$ m for forests).

The bulk approach, however, yields a discontinuity in the wind and turbulence field at the forest edges, where the displacement height suddenly increases from 0 to 15 m or drops from 15 to 0 m. Brady et al. (2010) suggested using a linear interpolation for d between the forest edge and ≈ 1 km away from the forest as a rule of thumb, an approach that could be tested in the future. However, using a mesoscale model with a forest canopy explicitly included (see next pages and Section 5.3) would probably yield better results.

Percentage reduction in wind speed and increase in turbulence intensity downwind of a forest edge was studied. A reference wind and turbulence intensity profile was used, either shortly upstream of the forest or a long distance downstream from the forest. Absolute values, however, should be treated with utter caution as the results have not been validated yet. The suggested expressions and coefficients should not be used for wind turbine siting or energy yield calculations until properly verified against measurements. Other studies using CFD models found larger values for wind speed decrease and TI enhancement over forests and further work is needed to clarify this.

Only heights relevant to wind power (between 100 and 200 m above ground) have been studied.

General findings

General conclusions for a flat and homogeneous surface are:

- Wind speeds adjust much slower to a new surface than turbulence intensity.
- Winds above a forest require some tens of km's distance from the forest edge to be in equilibrium with the forest surface. (This depends on height and atmospheric stability.)
- In the lee of a forest, forest effects on wind speed seem to exist up to some tens of km's downstream from the forest edge.

- At higher heights, wind speed reduction due to forests is smaller and adjustment to the new surface is slower. (In the lee of a forest, however, this reverses to higher percentage wind speed reduction values at higher heights as compared to lower heights at distances more than roughly 10 km from the downwind forest edge.)
- Turbulence intensity (TI) over the forest requires roughly 10 – 13 km distance from the forest edge to be in equilibrium with the forest surface. (This depends on height and atmospheric stability.)
- At higher heights, TI enhancement due to forests is smaller and adjustment to the new surface is slower. (In the lee of a forest, however, this reverses to higher TI enhancement values at higher heights as compared to lower heights at distances more than roughly 0.5 km from the downwind forest edge.)
- For non-neutral conditions, scatter is generally much larger and correlations are much weaker (probably the magnitude of the wind speed is important as another factor).

Grass-forest transition

For the transition from grass ($z_0 = 0.05$ m) to forest ($z_0 = 1$ m), the main findings are:

Percentage wind speed reduction follows a power law with increasing distance from the forest edge (eqn. (5-3) – correlations of ≈ 0.91). This is similar to the growth of the internal boundary layer over the forest. Power law exponents increase with increasing height above ground. Exponents are roughly half (≈ 0.4) the value commonly quoted for internal boundary layer growth at heights from 150 – 200 m above ground and roughly a third (≈ 0.3) of that value at heights from 100 – 150 m above ground. The multiplication factor for the power law of eqn. (5-3) seems to become smaller with increasing height above ground. For stable conditions, a linear expression fits wind speed reduction values much better than a power law.

TI enhancement seems to be described best by a power law in conjunction with a linear term (eqn. (5-6) – correlations of ≈ 0.97). More than 10 – 13 km downstream from the forest edge (depending on height) no further change of TI is found in the model.

Forest-grass transition

For the transition from forest ($z_0 = 1$ m) to grass ($z_0 = 0.05$ m), the main findings are:

In the lee of the forest, percentage wind speed reduction due to the forest decreases exponentially with increasing distance to the forest edge (eqn. (5-7) – correlations of ≈ 0.88). Directly after the forest wind speed reduction at 100 m height is roughly twice that at 200 m height. Distances where wind speed reduction has dropped to e^{-1} ($\approx 37\%$) of the original value are roughly 10 – 14 km, increasing with height. There seems to be slightly less wind

speed reduction in the unstable case as well as much less wind speed reduction in the stable case.

Similarly, TI enhancement from the forest seems to decrease exponentially with increasing distance to the forest edge (eqn. (5-8) – correlations of ≈ 0.96 .) At lower heights (100 – 150 m above ground), TI enhancement decays to e^{-1} ($\approx 37\%$) of its original value over the forest at around 3 – 5 km distance, whereas at higher heights (150 – 200 m above ground) this occurs at around 5 – 7 km distance.

Isolated forests

For isolated forests conclusions are:

The longer the isolated forest, (i) the larger the percentage wind speed reduction directly in the lee of the forest and (ii) the longer distance it takes for wind speeds to recover to their upstream values. An exponential law seems to fit wind speed reductions and TI enhancement values downstream of an isolated forest well.

The longer the isolated forest the larger the TI enhancement directly after the forest. Also, TI enhancement directly after the isolated forest seems to be roughly twice at 100 m height compared to 200 m height. The distance it takes for TI to recover to its reference upstream value, however, seems to be independent of the length of the isolated forest.

Isolated clearings

For isolated clearings main findings are:

The longer the clearing is the larger is the percentage of increase in wind directly after the downwind clearing edge. Irrespective of the size of the clearing, it takes approximately the same distance for wind speeds to adjust back to their upstream values after the clearing.

Over the clearing, TI reduction increases with distance to the upstream forest edge. After the clearing, TI adjusts back to the upstream/equilibrium value over the forest at an exponential rate. The distance for this, however, is almost independent of the size of the clearing.

c) Implementing a forest canopy in mesoscale models

A forest canopy version of the MIUU mesoscale model was developed based upon forest parameterisations commonly used in CFD/RaNS models. Within the forest canopy, additional terms for mechanical friction as well as for production and dissipation of turbulent kinetic energy were added. Also, a minimum value of roughly 2.5 m was used for the turbulent mixing length. The energy balance of the model was modified and the lower boundary conditions were adjusted correspondingly.

The new "canopy version" of the model agrees well with the previous version of the model (the "bulk version") in 1D, as well as with the wind tunnel measurements from Section 4. For a 2D smooth-rough transition both versions of the model seem to agree qualitatively with each other, as well as with the wind tunnel data. Model results also agree well with measured wind speeds from Ryningsnäs for neutral conditions and for the forest sector. Over the canopy, the "canopy version" gives roughly twice the wind speed reduction compared to the "bulk version".

6 Turbine load modelling

With very few exceptions, modern megawatt sized wind turbines today hold a type certificate according to the international standard IEC 61400-1 (2005). This means that the design basis for all components/cross-sections relies on a chosen wind turbine class regarding level of turbulence and wind speed distribution. The basic wind models given in the standard are carefully chosen to represent most possible sites for wind energy developments, and over the years there have been updates with specific wind models for turbines operating in wind farms or areas of complex terrain. However, up to this date there is no such support for wind turbine development in forest areas.

When a certified turbine model is to be installed at a specific site, the local regulations normally require a *site assessment study*, where it has to be proven that the structural loads experienced at the site are lower than those defined in the certificate. A simplified approach to site assessment is to assess just some fundamental site properties, such as standard deviations of turbulence, wind shear, and extreme wind speed etc. It should be noted that this simplified approach fails if the assessment is inconclusive (i.e. if not all the assessed parameters give *conservative* values). In this case site specific wind models have to be used for complementary design calculations in order to demonstrate sufficient margins against fatigue/ultimate failure. Therefore, good understanding of the flow characteristics above forests is essential for wind energy development in such areas. Thus, the novel models of the turbulent flow above a Scandinavian pine forest, provide an important contribution of new knowledge to the wind energy community.

In any design study the nine IEC classes (turbulence classes A, B, C, combined with wind speed classes I, II, III), cf. Figure 6-1, forms an interesting scale when trying to figure out the best strategy for certification. In the analyses presented below, the IEC wind models have served as references (together with other well defined wind descriptions). Both the IEC wind models and the common meteorological theories for the surface part of the atmospheric boundary layer, are extensively treated in the literature and will therefore not be given detailed attention here.

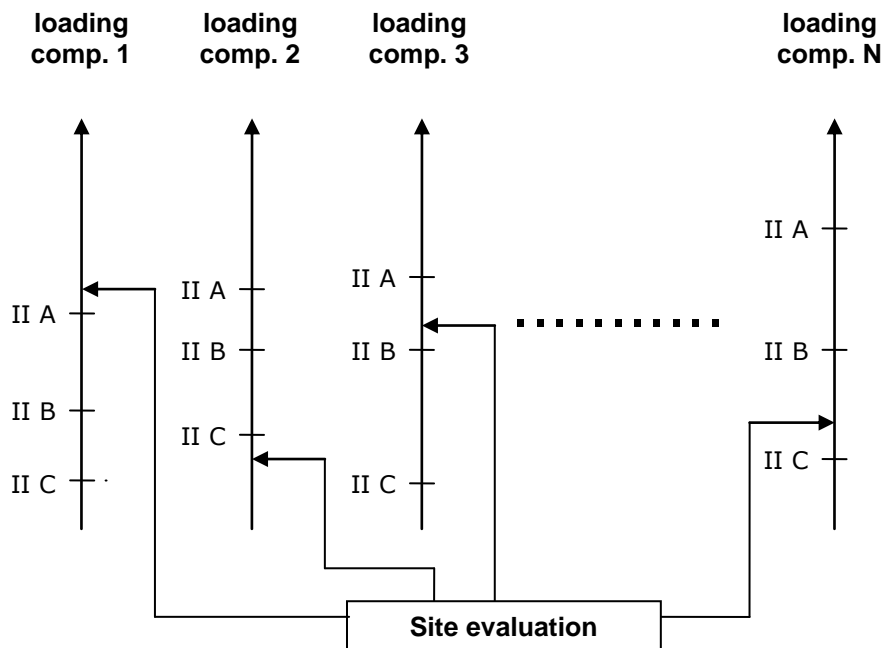


Figure 6-1: Schematic description of a situation when use of IEC wind models as design basis becomes problematic (in this case wind class II was assumed).

6.1 Background meteorological data used

In the present study three different wind models have been used for generating 3D turbulent wind input to time domain aeroelastic simulations. These are the already mentioned IEC wind model, a traditional diabatic surface layer description, and a recently proposed wind model for flow over a Scandinavian pine forest. The three models all consist of mean profiles (shear and veer), together with spectra and cross-spectra of turbulence. This information is then transformed into stochastic time series of wind vector components of a Cartesian grid covering the rotor plane [REF].

6.1.1 IEC wind model

The wind models (mean field and turbulence spectra) prescribed in the IEC standard 61400-1, are normally used when calculating component/section load spectra for *Type Certification*. These models do not represent the *cutting edge of science*, but are instead the result of extensive studies, wind data analyses, and long committee negotiations. The idea has been to find alternatives for the definitions of external conditions that facilitate design of wind turbines suitable for installation on sites of varying type and character. The IEC wind models are often used as reference in various studies where load consequences of various wind conditions are investigated.

6.1.2 Diabatic surface layer model (Panofsky & Dutton)

Since the IEC wind models and wind classes have no direct coupling to a real site description, in terms of roughness, distribution of wind speed and atmospheric stability parameters etc., it was here also chosen to define two reference site descriptions corresponding to expected conditions for *near shore* and *flat* terrain respectively (inspired by previous investigations of the Alsvik and Näsudden sites). It is here assumed that the mean flow and turbulence is well described by standard models for the *diabatic* surface regime of the *Atmospheric Boundary Layer*. The implemented formulas for spectra, spatial correlation, and wind shear can be found in various textbooks on the subject (here Panofsky and Dutton, 1984, was chosen).

6.1.3 Forest wind model

Input to the wind model is wind speed U_1 , height z_1 , Obukhov length L , and wind direction. The roughness length is assumed to be 2.6 m and the displacement height 17 m. First, the friction velocity is determined by the wind profile described in Section 3.2.2, evaluated at the initial height z_1 . The wind speed is then determined at all heights using the profile expression from Section 3.2.2. The boundary layer height is determined by the Rossby-Montgomery formulation with $C=0.1$ (see Section 3.1.3). Wind direction at arbitrary height z is then given by the wind veer from height z_1 based on the wind veer model presented in Section 3.1.3. The constant a in the wind veer model was first set to 4, but later changed to a final 1.5 to account for an estimated turning of the measurement tower by 6° , which would have led to an overestimation of the measured veer. The K_0 -parameter is determined as in Section 3.1.3. Power spectra are given by the method presented in section 3.1.2. The constants used in determining the spectral shape are taken from Table 3-3. Parameterisations for variance and integral time scale are taken from a formulation similar to that in Section 3.1.3, on the form

$$\Gamma = \frac{c_{\Gamma_1} + c_{\Gamma_2} \frac{U}{u_*}}{u_*}$$

and

$$\sigma^2 = \left(c_{\sigma_1} + c_{\sigma_2} \frac{U}{u_*} \right) U^2$$

The constants c_1 and c_2 was determined through a least square fit of the expression to the data at each height. Linear interpolation of the constants is made between measurement heights.

The wind model representing *Forest* is this context characterized by a) high levels of turbulence, b) a dramatic wind shear, and c) a significant wind veer (i.e. direction change with height).

All wind models used throughout this study are presented in Table 6-1.

Table 6-1: Identification/categorisation of wind models.

| | |
|-------------------|---|
| IEC | According to IEC 61400-1 ed.3 (Annex B.2) , turbulence classes A,B,C , wind classes I,II,III |
| Near shore | Profiles and spectra according to Panofsky and Dutton (1984), roughness length $z_0=0.0035$ (Alsvik , Gotland) |
| Flat | Profiles and spectra according to Panofsky and Dutton (1984), roughness length $z_0=0.04$ (Näsudden, Gotland) |
| Forest | Wind profile according to Section 3.2.2. Veer profile according to Section 3.1.3. Spectra according to Section 3.1.3. Roughness length $z_0=2.6$ and displacement height $d=17$ |

In Figure 6-2 three different realisations of turbulence (U component) and mean wind profiles are shown, where the corresponding simulations are based on three of the wind representations described above. It is here clearly seen that the *Near shore* wind seems rather gentle in comparison. The *IEC-A* and *Forest* realisations look similar in terms of turbulence, but the vertical wind shear is dramatically larger in the *Forest* case. From this simple comparison at one representative mean wind speed, it is already obvious that the *IEC-A* model is not perfectly suitable when designing wind turbines targeted for forest installation.

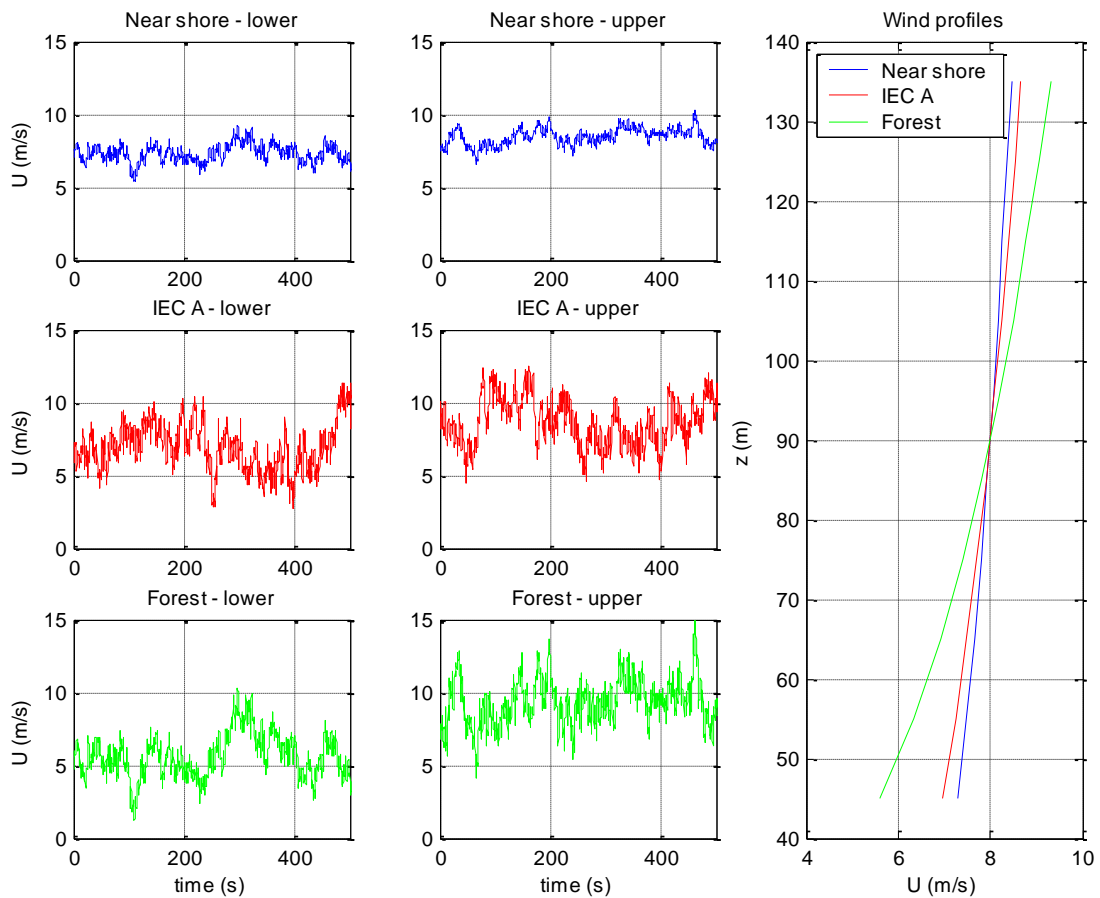


Figure 6-2: Visualisation of three different realisations of turbulent wind input to aeroelastic load calculations, corresponding to models *near shore*, *IEC-A*, and *forest* (as described above).

6.2 Dynamic turbine model

In order to investigate the consequences of forest operation, the previously described wind models were used in a simplified wind turbine design study. A “generic” 2.5 MW wind turbine was modelled using the aeroelastic code VIDYN (Ganander, 2003), where the aerodynamic design is based on the common FFA-W3/NACA-636XX airfoils, and the structural properties have been scaled from blade data presented in the literature. The remaining mechanical properties were chosen as *typical* for similar turbine models on the market. Following standard procedures for wind turbine structural design, the main mechanical properties were then “tuned” in order to avoid resonances that could affect the interpretation of fundamental results. Finally the variable-pitch/variable-speed controller presented in Jonkman et al. 2009 was implemented and adjusted for the chosen rotor characteristics. The developed simulation model will in the following be used for fatigue load assessment.

6.3 Calculations

6.3.1 Wind realisations

The wind models and simulation models described above were initially used for calculating fatigue loads in some chosen cross-sections, where the resulting load spectra were weighted against the wind speed distributions of the IEC wind classes I, II, and III (mean wind speeds of 10, 8.5, and 7.5 m/s respectively). Finally, *Damage Equivalent Loads* were calculated as normalized values, using IEC-A as reference. During this procedure, five 10 min simulations were performed for 21 wind speed bins between 5 and 25 m/s. For the near shore, flat, and forest cases, a distribution of stability (Monin-Obukhov length L) was assumed when defining values for each realisation. The stability *classes* are here formed to be *representative*, and the corresponding values of L are interpreted as *characteristic* values for five probability bins of approximately equal probability of occurrence.

$$\left\{ \begin{array}{l} 1. \quad L = -150U / 5 \\ 2. \quad L = -400U / 5 \\ 3. \quad L = 10^5 \\ 4. \quad L = 200U / 5 \\ 5. \quad L = 500U / 5 \end{array} \right.$$

6.3.2 Fatigue equivalent loads

In the following, the loading in various cross-sections will be evaluated as *load ranges* (deterministic loading), and *fatigue equivalent loads* (stochastic loading). The concept of equivalent loads provides a convenient method to compare different load spectra in a similar way as for static loading.

A fatigue equivalent load, ${}^{eq}L_{ij}$, corresponding to structural cross-section/spot no. i , is here for wind speed bin no. j formulated as the weighted sum over P representative sequences of load histories (each with its defined probability of occurrence p_{jk})

$${}^{eq}L_{ij} = \left(\frac{\sum_{k=1}^P \sum_{l=1}^R p_{jk} (L_{ijkl})^m}{{}^{eq}N_{bin}} \right)^{1/m}$$

where m denotes the Whöler exponent, ${}^{eq}N_{bin}$ denotes the equivalent number of cycles chosen to represent 10 minutes (typically corresponding to 1 Hz, or 1 p), and index l refers to a specific load cycle in the load history. The individual load cycles are extracted from time histories, typically using the fast and popular *Rain Flow Count* algorithm (RFC).

Result of this work is in the following presented as relative change of the fatigue equivalent load, often as normalised with some reference condition. Interpretation in more practical terms as corresponding relative lifetime change can be done according to

$$\frac{T_2}{T_1} = \left(\frac{{}^{eq}L_2}{{}^{eq}L_1} \right)^m$$

6.3.3 Turbine loads

For the following discussion and interpretation of results, load types and cross-sections are described in Table 6-2.

Table 6-2: Load entries and cross-sections

| Load | Description |
|-----------|---|
| Mf1/Mflap | Blade flapwise bending moment 5 m from blade root |
| Me1 | Blade edgewise bending moment 5 m from blade root |
| Fxtc | Longitudinal force in tower top |
| Myaw | Torsional moment in tower top |
| Mytc | Tower top bending moment around lateral axis |

6.4 Results

Results from the calculations described in the previous section are presented in Figure 6-3. It is here clearly seen that the high levels of turbulence in the forest model, in combination with the identified shear and veer, significantly increase the levels of fatigue life consumption in all turbine components (IEC-1A here chosen as reference). The hub height turbulence intensity typically reaches 20 % close to the mean wind speed, while fitted values of the wind shear exponent approach 0.5.

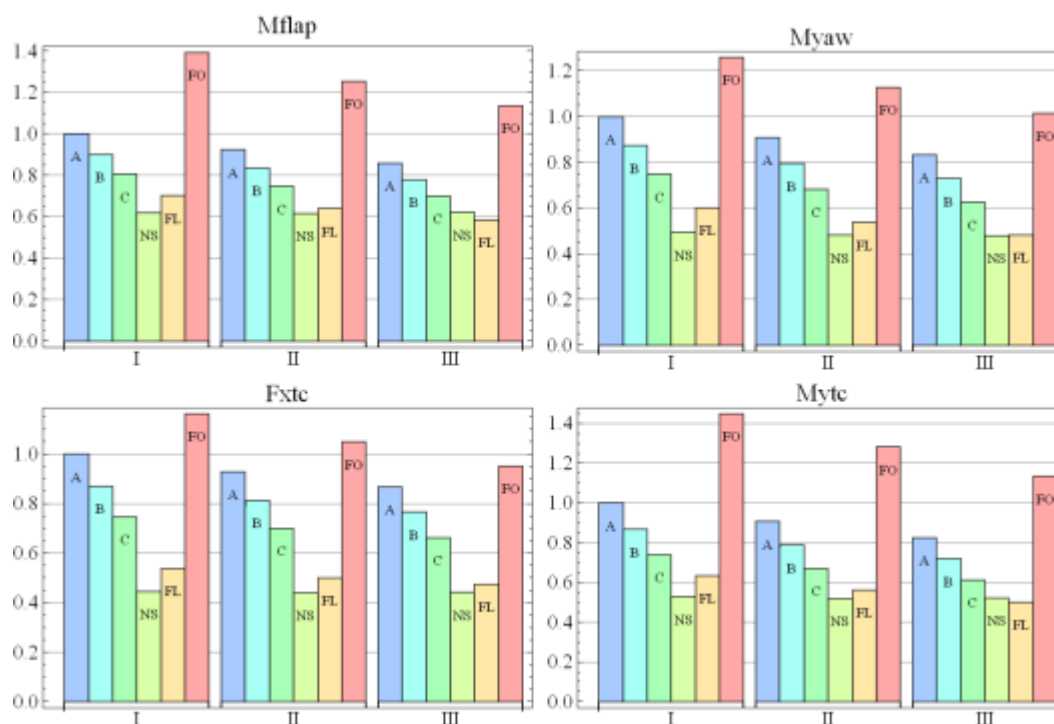


Figure 6-3: Damage Equivalent Loads representing 6 different wind models and 3 wind distributions (IEC wind classes I, II, and III). IEC-1A was here chosen as reference.

In summary the damage equivalent load for forest conditions are 35% larger than the IEC-A condition for all wind classes I, II and III, for blade and as well for the tower loads. In terms of life time change this means that for blade loads ($m=10$) the life time is about 5% for forest conditions compared to comparable IEC-A case. For tower loads ($m=4$) the life time is about 30% for forest conditions compared to comparable IEC-A case. On the other hand to withstand the increased fatigue loads without changing the life time critical dimensions have to be increased by the same factor 1.35 as the increase of the fatigue equivalent loads. For an IA designed turbine at Forest III conditions the relative design life time is reduced to about 25% and 60 % for blades and tower respectively.

6.5 Cyclic pitch analysis

In recent years there have been numerous studies published where *individual pitch control*, or *cyclic pitch control*, have been proposed as a possible approach to load reduction in various situations. Usually the control algorithms are based on some type of wind prediction (look-ahead sensor), or on-line load measurements in blades, main shaft, or yaw system. The drawbacks might here be that the complexity of the system increases and the addition of sensors has a negative impact on reliability. Moreover, the loading and wear on pitch servos and bearings is not fully understood, since modern

large rotor blades are very flexible, and significant contribution from the eigenweight might have influence during rotation.

Both shear and veer represent *asymmetric* loading on the turbine that in some sense also is *deterministic* (variation obviously vertical over the rotor), and it is therefore possible to make assumptions about the asymmetric loading without the need for additional sensor signals. In the following the cyclic pitch approach to load reduction in case of forest operation will be investigated. The basic idea is here to try to identify values of blade pitch amplitude and azimuthal phase for an added pitch action over one revolution. The previously described simulation model is used but the *forest* wind model is here implemented without turbulence.

Short simulations are performed for a large number of amplitude/phase values, and the corresponding periodic load ranges are extracted. In Figure 6-4 those results are presented for yaw moment and blade root flap moment (amplitudes 0°, 1°, 2°, 3°, and 4°). The *optimal* selections are here marked with vertical blue lines, and the numbers are also presented in Table 6-3. Parameter scans were here performed for mean wind speeds 8, 12, and 16 m/s.

Table 6-3: Chosen cyclic pitch parameter values, at no turbulence.

| Wind [m/s] | Mflap | | Myaw | |
|---------------|-------|------|-------|------|
| | phase | ampl | phase | ampl |
| 8 | 80 | 1.77 | 170 | 0.98 |
| 12 | 70 | 2.00 | 210 | 2.15 |
| 16 | 70 | 2.88 | 230 | 4.00 |

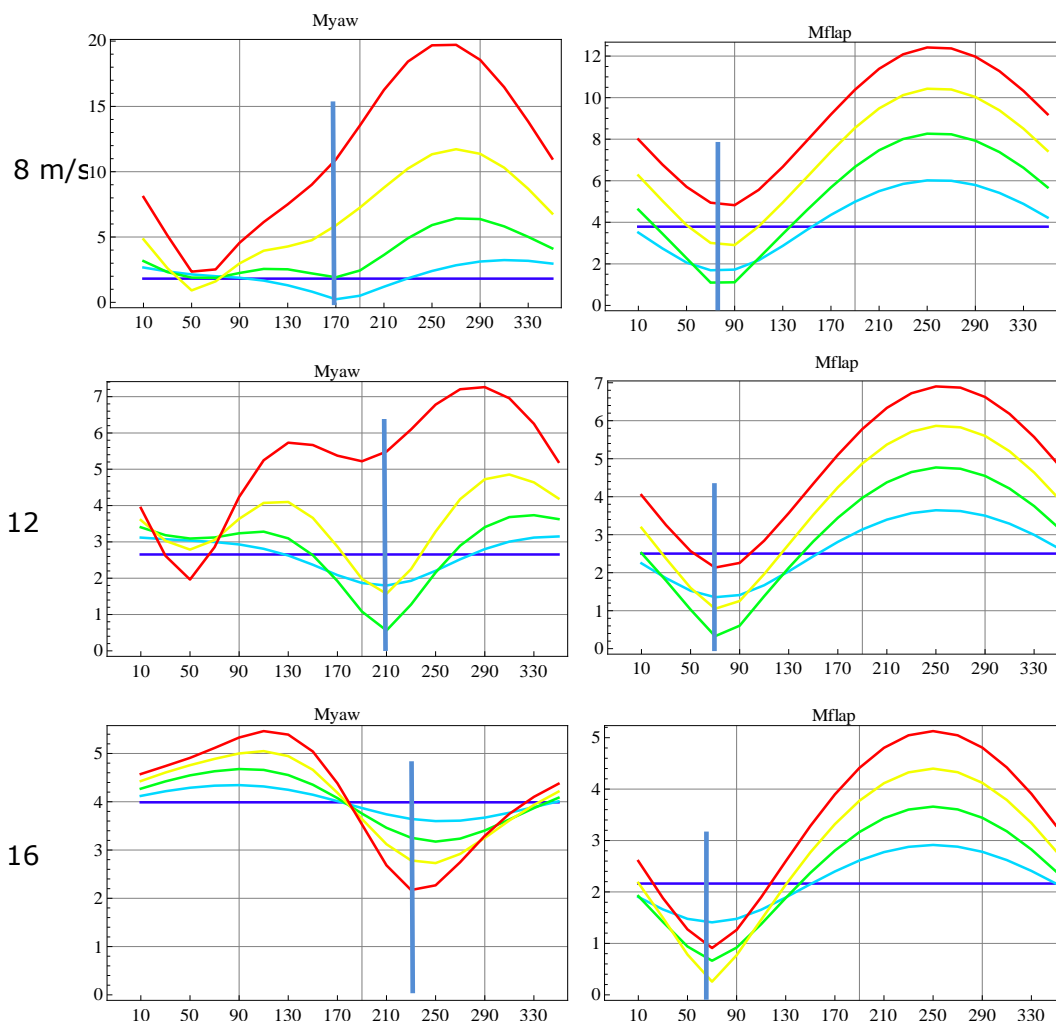


Figure 6-4: Load amplitude scans for selection of *cyclic pitch* parameters (amplitude/phase) for a) minimum yaw load range, and b) minimum flap load range at no turbulence. Amplitudes ranging from 0° (purple) to 4° (red). The selected values are presented in Table 6-3.

Using [0°, neutral] as reference, the relative load range changes due to cyclic pitch action are presented in Figure 6-5 (maximum flap load reduction) and Figure 6-6 (maximum yaw load reduction). Separate calculations were here performed for 8, 12, 16 m/s, and *unstable, neutral, and stable* conditions.

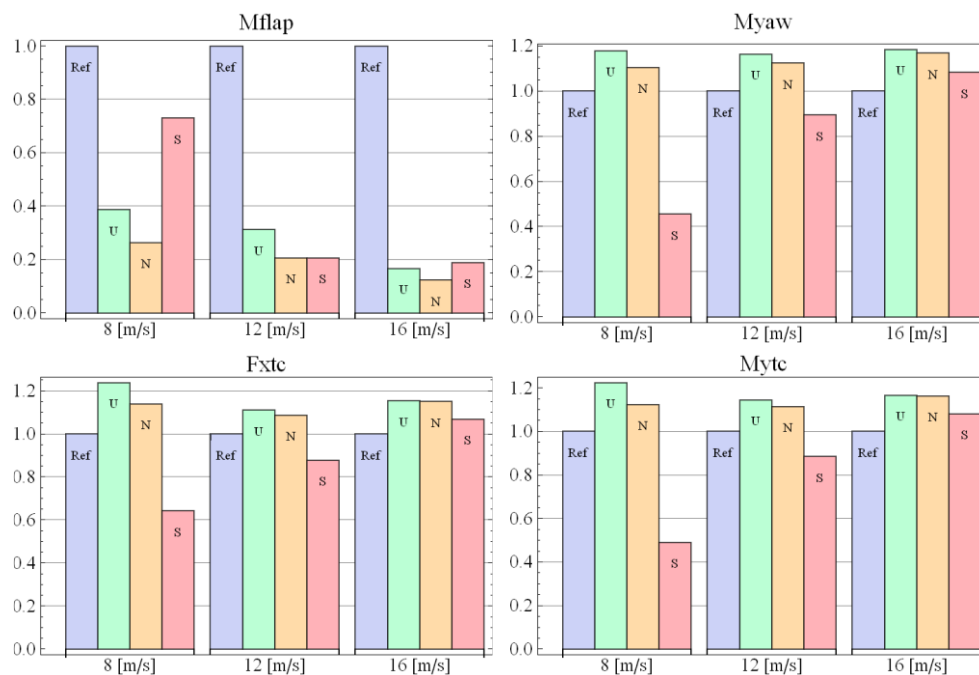


Figure 6-5: Relative changes in load ranges due to cyclic pitch action (flap load reduction is here the target). The corresponding relative changes are also shown for yaw moment, tower top thrust force, and tower top out-of-plane bending moment). No turbulence.

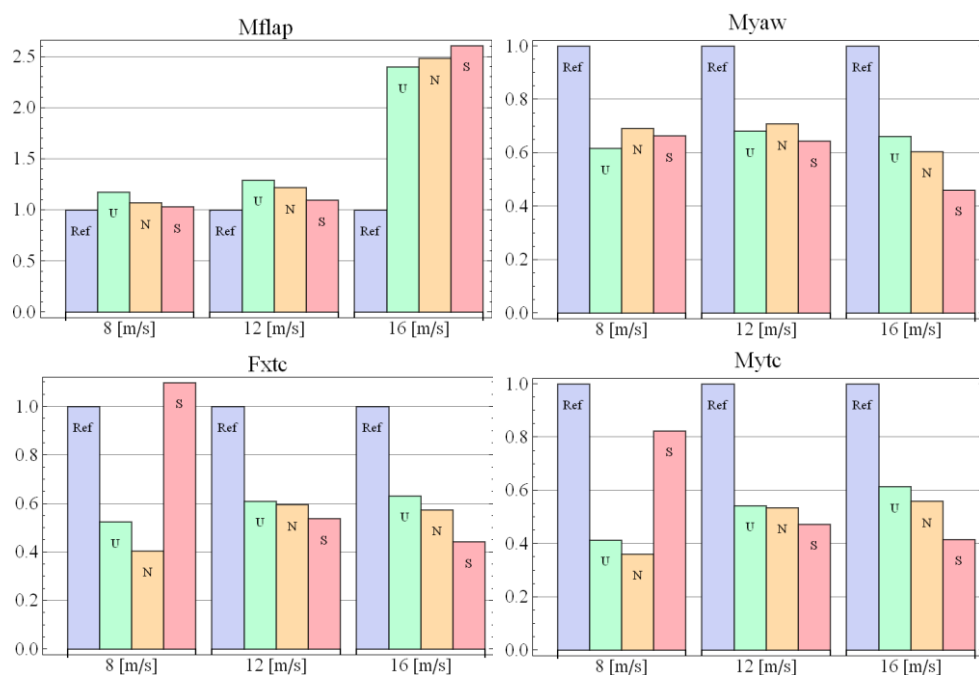


Figure 6-6: Relative changes in load ranges due to cyclic pitch action (yaw load reduction is here the target). The corresponding relative changes are also shown for flap moment, tower top thrust force, and tower top out-of-plane bending moment). No turbulence.

Results from this initial cyclic pitch control study indicate a significant potential for load reduction, especially for the blade loads. To this point, control parameter values presented above were derived without taking turbulence into account, including just the substantial wind gradient and the wind veer. In order to quantify the effects of cyclic in a more realistic situation, forest turbulence was now added and results from 5 stability classes where weighted as before.

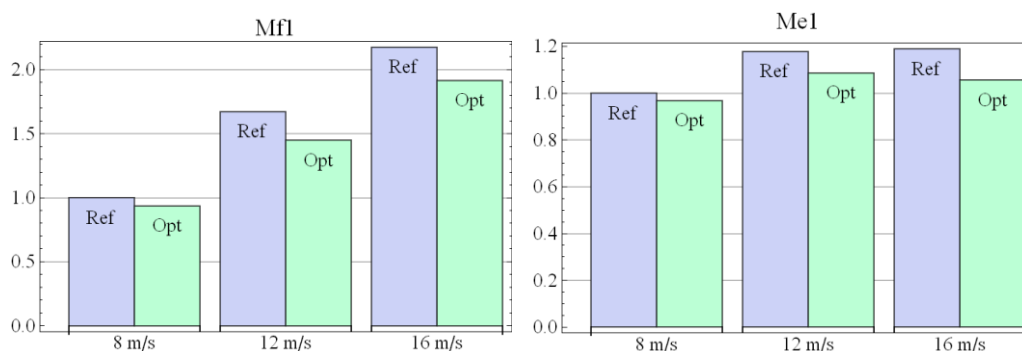


Figure 6-7: Relative changes in fatigue equivalent loads (blade flap and edge) when forest turbulence is added to the comparison (here only wind speeds 8, 12, and 16 m/s).

As seen in Figure 6-7 compared to Figure 6-5, the potential for load reduction now seems considerably less promising than before the turbulence was added, and the difference (with/without cyclic pitch) for other components than the blades, are very small. However, since a rather high value ($m=10$) was assumed for the Wöhler exponent in the blades, the $\sim 5\%$ reduction in fatigue equivalent load for 8 m/s, here correspond to $\sim 60\%$ lifetime increase. The results indicate that the stochastic loading from high levels of turbulence dominate fatigue life consumption in the rotor blades. In order to try to reach further understanding, an additional study was performed. Here the IEC wind model was used with turbulence intensity increasing from 1% to 25%, while keeping the wind shear exponent constant ($\alpha = 0.5$).

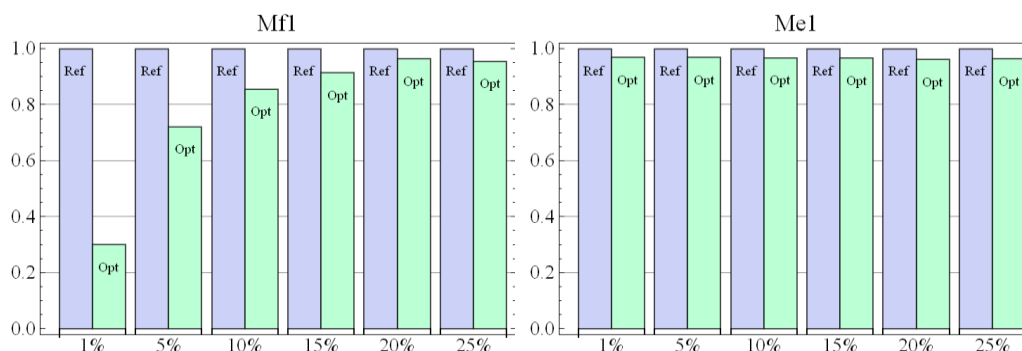


Figure 6-8: Effect of optimal cyclic pitch on blade loads with turbulence intensity increasing from 1% to 25 % (IEC wind model , $\alpha = 0.5$), at 8 [m/s].

The results presented in Figure 6-8 shows how the potential to reduce deterministic load variations due to large wind shear by use of cyclic pitch control, varies with increasing turbulence intensity. A combination of large shear and low turbulence may e.g. occur during very stable atmospheric conditions.

It should be pointed out that with a more sophisticated controller than the one used in the present study, the load reduction effect can of course be further improved. The most obvious next step to try is to let the time history of the pitch motion have some other shape than sinusoidal.

For any control algorithm, the optimal choice of parameter values always has to rely on an *objective function* with high confidence. The definition of such relationships remains one of the most complicated tasks in wind turbine design, and requires detailed knowledge about risks and costs for all components.

6.6 Conclusions

In general the wind models presented in the previous chapters of this report have proven to be very useful when trying to understand the loading conditions for turbines installed in forest terrain. Initial studies indicate that a wind turbine in the Scandinavian pine forest terrain may experience fatigue loading more severe than what is covered by the current IEC61400-1 wind turbine classes. It seems obvious that specific forest classes have to be defined for design purposes.

In more detail turbulence of the actual wind model for loads calculations have an unexpected large impact on fatigue loads, compared to an expected and large vertical wind shear. Wind measurements at Ryningsnäs in Småland have been the basis for the actual wind model. The question is to what extent that model is representative for forest conditions, e.g. in northern parts of Sweden?

Some initial studies using a cyclic pitch control system indicate a potential to reduce the fatigue life consumption due to the large wind shear, but high levels of turbulence are clearly limiting the effects of simple load control.

Finally it has to be emphasized that this limited study indicate strong influence on fatigue of both blades and tower, but also very large variations of load results, depending on assumed wind forest conditions and the turbine. Site assessment to define site specific wind conditions and for verification of the design will be an important part of wind turbine development for forest conditions.

7 Discussions and conclusions

In the project "Wind power in forests" the research has gone along several paths with the main goal to better understand the mean wind and turbulence properties in the boundary layer above high vegetation and how wind turbines located in forests will be affected by the somewhat harsh wind conditions which are expected above a forest.

As regards the wind conditions as such both measurements and modelling has been subject for research. Focus has been on measurements in the atmosphere and in a wind tunnel. The atmospheric measurements, made at two forest sites, have resulted in a large number of high quality data. At one forest site measurements are made up to 140 m above ground, focusing on the heights from just above the tree tops to heights around typical turbine hub heights. At the other site focus has been on the within canopy flow up to heights just reaching slightly above tree tops. A large number of wind statistics have been presented using these atmospheric data. Comparisons with routine wind measurement from a large number of forest sites have been made and with wind models published in the literature.

The advantage of using data taken in the atmospheric boundary layer is that they are taken in an environment where wind turbines actually are supposed to work. A drawback may however be that the land cover and topography in reality both typically are heterogeneous, making idealized process studies more difficult. One method to overcome this is to use wind tunnel data. This has also been made within the project producing a large database with very detailed turbulence measurements within and above a model forest. Comparisons with atmospheric data show good agreement up to about two canopy heights, while higher up the wind tunnel results deviate from the atmospheric data due to the limited physical dimensions of the tunnel. Another drawback with the wind tunnel data is that they are limited to thermally neutral conditions, and the atmospheric measurements show large differences between stable and unstable stratification.

For future research a deeper understanding about winds higher up in the boundary layer is needed. The wind turbines are expected to become taller and taller, why knowledge about wind conditions up to about 250 m can be expected to be of relevance for future wind power development.

Although measurements, which commonly are just available at single sites, may form the main basic knowledge about the wind conditions, models are needed in order to transfer this knowledge to other sites where wind power might be developed. Within the research project mesoscale models have been used and compared to the measured wind profiles. The results indicate that mesoscale models tend to overestimate the wind speed over forests. One possible reason for this was identified to be associated with the default values of the roughness length, taken to represent forests. These default values are typically used in the standard setup of the models. The value obtained from detailed turbulence measurements made in the project resulted in roughness lengths of the order of 2-3 m. The median value from a large number of

measurements in Sweden was 1.3 m. Both estimates are significantly larger than the standard values used in mesoscale models which are 0.5-0.9 m. Depending on which mesoscale model is used the sensitivity to an increased roughness length was found to vary, but this is definitely something about which more research is needed.

A large number of idealized mesoscale model investigations were made as regards forest edges, clearings in the forest and for isolated forests. These results clearly show the non-local nature of the boundary layer wind conditions. The flow needs several kilometres downstream from e.g. a forest edge for the winds to be in balance with the new surface conditions. Although many of these results are just based on model results, they are supported both by earlier findings and by some of the wind tunnel measurements with which comparisons were made.

Most mesoscale models do not include a forest canopy in an explicit way. It is simply accounted for in a bulk manner, giving rise to a zero-plane displacement. An approach in which the canopy is resolved was here introduced in the MIUU-model. In the canopy additional forest drag terms as well as additional terms for production and dissipation of turbulent kinetic energy were introduced. The new canopy version of the model was found to produce realistic winds in agreement with the wind tunnel measurements. At higher elevations the canopy version of the model gave a larger wind speed reduction over a forest compared to the standard version of the model. This could however not be confirmed by the wind tunnel measurements as they could not be used above about two canopy heights due to the limited size of the wind tunnel. Much future research is needed regarding the inclusion of a canopy model in mesoscale models.

One of the advantages of including a canopy model in a mesoscale model is that one gets a better representation of the surface energy balance. This is important as it governs both the stratification and the boundary layer height, which are both important for the winds at hub height. Thus a better representation of and understanding of what is happening at low heights, in the canopy, may be of an even greater importance higher up.

One of the aims of the project was research regarding the effects of the forest boundary-layer wind climate upon wind turbines. Based on the new atmospheric forest boundary-layer wind measurements, a full set of statistics needed for this was developed. Using these statistics, 3D turbulent winds needed to run a dynamic turbine model were produced. Comparisons were made using standard IEC wind conditions. The results indicate that the forest wind climate may cause a wind turbine to experience fatigue load more severely than what is covered by the current IEC61400-1 wind turbine classes. There are indications that some of the more severe load cases may be overcome by optimizing the wind turbine control system to the wind conditions above a forest. These are however initial results and more research are needed to fully understand this.

8 References

- Alfredsson PH, Örlü R (2010) *The diagnostic plot-a litmus test for wall-bounded turbulence data*. *Eur J Mech B/Fluids* **29**:403–406.
- Andrén, A., 1990: Evaluation of a turbulence closure scheme suitable for air pollution applications. *J. Appl. Meteor.*, **29**, 224-239.
- Bergström, H., 2002: Boundary-layer modelling for wind climate estimates. *Wind Engineering*, **vol. 25**, No. 5, 289-299.
- Bergström, H., 1996: A climatological study of boundary layer wind speed using a meso- γ -scale higher-order closure model. *J. Appl. Meteor.*, **35**, 1291-1306.
- Bergström, H. and Söderberg, S., 2009: Wind mapping of Sweden – Summary of results and methods used. *Elforsk rapport 09:04*, 84 pp.
- Bergström, H., P.-E. Johansson and A.-S. Smedman (1988): A study of wind speed modification and internal boundary-layer heights in a coastal region. *Boundary Layer Meteorology* **42**, 313-335.
- Brady, O., P. Bugeat and C. Abiven (2010): *Wind profiles downwind of forest*. Proceedings from European Wind Energy Conference 2010, Warsaw, Poland. [Available at <https://www.naturalpower.com/sites/default/files/images/EWEC-2010-P-Bugeat-et-al---Presentation.pdf>]
- Burk, S. D., T. Haack, and R. M. Samelson, 1999: Mesoscale simulation of supercritical, subcritical and transcritical flow along coastal topography. *J. Atmos. Sci.*, **56**, 2780-2795.
- Burk, S. D., and W. T. Thompson, 1996: The summertime low-level jet and marine boundary-layer structure along the California coast. *Mon. Wea. Rev.*, **124**, 668-686.
- Burton, T., N. Jenkins, D. Sharpe and E. Bossanyi (2011): *Wind Energy Handbook*. 2 edition. Wiley, Hoboken, 780 pp.
- Carlén, I., Ganander, H., "Fatigue loading of wind turbines operating in forest terrain", Teknikgruppen Report , TG-R-12-11 , 2012.
- Collineau, S. & Brunet, Y.:
- Crockford A. and Hui S.Y., 2007: Validation of Wind Resource Assessment Methodologies Including the Effects of Forests, M.Sc. report, DTU, Denmark.
- Dellwik, E., Arnqvist, J., and Segalini, A., 2013: Measurements from "Wind power in forests" – a database description. Report DTU Wind Energy E-0017-
- Dellwik E., Mann J., Bingöl F. (2010): Flow tilt angles near forest edges – Part 1: Sonic anemometry, *BioGeoSciences*, 7(5), 1745-1757.
- Dellwik, E., L. Landberg and N. O. Jensen (2004): *WAsP in the forest*. Scientific Proceedings, European Wind Energy Conference and Exhibition 2004, London, England, 22-25 November.

- Dellwik, E., L. Landberg and N. O. Jensen (2006): WAsP in the forest. *Wind Energy*, Vol. **9**, p. 211-218.
- Dellwik E and Jensen N.O., 2005: Flux-profile relationships over a fetch limited beech forest. *Boundary Layer Meteorology*, 115:2, 179-204.
- Enger L., 1990: Simulation of dispersion in a moderately complex terrain. Part A. The fluid dynamic model. *Atmos Environ.*, **24A**, 2431-2446.
- Finnigan, J. J.; Shaw, R. H. & Patton, E. G.: Turbulence structure above a vegetation canopy. *Journal of Fluid Mechanics*, **2009**, 637, 387-424.
- Foudhil, H. (2002). Développement d'un modèle numérique de dispersion atmosphérique de particules à l'échelle d'un paysage hétérogène. Thèse de doctorat, Université Bordeaux I. spécialité Mécanique.
- Foudhil, H., Y. Brunet and J.-P. Caltagirone (2005): A Fine-Scale k- ϵ Model for Atmospheric Flow over Heterogeneous Landscapes. *Environmental Fluid Mechanics*, Vol. **5**, p. 247-265.
- Frank, C. and B. Ruck (2008): Numerical study of the airflow over forest clearings. *Forestry*, Vol. 81, No. 3, 2008.
- Ganander, H., "The use of a Code-generating System for the Derivation of the Equations for Wind Turbine Dynamics", *Wind Energy*, No 4 , Vol 6 2003, pp 333-345.
- Garratt, J. R: *The Atmospheric Boundary Layer Cambridge University Press, UK*, pp 64, **1992**.
- Giebel, G., J. Badger, P. Louka, G. Kallos, C. Lac, G. Descombes, A-M Palomares and I. Martí Perez (2002): *Development of a Next Generation Wind Resource Forecasting System for the Large-Scale Integration of Onshore and Offshore Wind Farms. Description of NWP, Mesoscale and CFD models.* Project ANEMOS, DELIVERABLE 4.1 a, 51 pp.
- Green, R. S. (1992): Modelling Turbulent Air Flow in a Stand of Widely-Spaced Trees. *Phoenix Journal*, Vol. **5**, p. 294-312.
- Grisogono, B.: The angle of the near-surface wind-turning in weakly stable boundary layers. *Quarterly Journal of the Royal Meteorological Society*, **2011**, 137, 700-708.
- Gryning S-E, Batchvarova E, Brümmner B, Jørgensen H., Larsen S., 2007: On the extension of the wind profile over homogeneous terrain beyond the surface layer. *Boundary-Layer Meteorol.*, 124:251-268.
- Hong, S.-Y. and S.-W. Kim, 2008: Stable boundary layer mixing in a vertical diffusion scheme. Proc. Ninth Annual WRF User's Workshop, Boulder, CO, National Center for Atmospheric Research, 3.3. [Available at <http://www.mmm.ucar.edu/wrf/users/workshops/WS2008/abstracts/3-03.pdf>]
- Hong S.-Y., Y. Noh, and J.Dudhia (2006): A new vertical diffusion package with explicit treatment of entrainment processes. *Mon. Wea. Rev.*, **134**, 2318-2341.

- Hu, X.-M., J. W. Nielsen-Gammon, F. Zhang (2010): Evaluation of Three Planetary Boundary Layer Schemes in the WRF Model, *Journal of Applied Meteorology and Climatology*, Vol. **49**, p. 1831-1844.
- IEC 61400-1 third edition 2005-08 Wind turbines – Part 1: Design requirements, International , Electrotechnical Commission, IEC, 2005.
- Inoue, E. (1963): On the Turbulent Structure of Airflow within Crop Canopies. *Journal Met. Soc. Japan*, Vol. **41**, p. 317 – 326.
- Irwin HPAH (1981) *The design of spires for wind simulation*. *J Wind Eng Ind Aerod* **7**:361–366
- Janjic, Z. I. (1994): The step-mountain eta coordinate model: further developments of the convection, viscous sublayer and turbulence closure schemes. *Mon. Wea. Rev.*, 122, 927-945.
- Janjic, Z. I. (1996): The surface layer in the NCEP Eta Model. Eleventh Conference on Numerical Weather Prediction, Norfolk, VA, 19-23 August 1996; *Amer. Meteor. Soc.*, Boston, MA, 354-355.
- Janjic, Z.I., 2001: Nonsingular implementation of the Mellor-Yamada level 2.5 scheme in the NCEP Meso model. NOAA/NWS/ NCEP Office Note 437, 61 pp. [Available at <http://ploneprod.met.psu.edu/people/fuz4/publication-pdf-files/HuNGZhang2010JAMC.pdf>]
- Janjic, Z. I. (2002): Nonsingular Implementation of the Mellor-Yamada Level 2.5 Scheme in the NCEP Meso model. NCEP Office Note No. 437, 61 pp
- Jonkman, J., Butterfield, S., Musial, W. and Scott, G. ,“Definition of a 5-MW Reference Wind Turbine for Offshore System Development”, National Renewable Energy Laboratory, 2009.
- Kaimal, J. C. and J. J. Finnigan (1994): *Atmospheric Boundary Layer Flows – Their Structure and Measurement*. Oxford University Press, New York, 289 pp.
- Katul, G. G., L. Mahrt, D. Poggi, C. Sanz (2004): One- and Two-Equation Models for Canopy Turbulence. *Boundary-Layer Meteorology*, Vol. **113**, p. 81-109.
- Krzikalla, F. (2005): *Numerical Investigation of the Interaction between Wind and Forest under Heterogeneous Conditions*. Diploma Thesis, Institute for Hydromechanics, University of Karlsruhe, Germany, and INRA-EPHYSE, Villenave d’Ornon, France, 94 pp.
- Lalic, B. and D. T. Mihailovic (2004): An Empirical Relation Describing Leaf-Area Density inside the Forest for Environmental Modeling. *Journal of Applied Meteorology*, Notes and Correspondence, Vol. **43**, p. 641-645.
- Lettau HH (1962) Theoretical wind spirals in the boundary layer of a barotropic atmosphere. *Beitr Phys Atmos* 35:195–212
- Lindahl, A. (2009): *Utvärdering av svensk vindkraft Skillnaden mellan skogs- och traditionella placeringar*. Examensarbete vid Mälardalens Högskola i samarbete med Södra Vindkraft AB, Växjö, Sweden.

- Liu H., Peters G. and Foken T., 2001: New equations for sonic temperature variance and buoyancy heat flux with an omnidirectional sonic anemometer, *Boundary Layer Meteorology*, 100, 459-468.
- Liu, J., J. M. Chen, T. A. Black, and M. D. Novak (1998): E- ϵ Modelling of Turbulent Air Flow Downwind of a Model Forest Edge. *Boundary-Layer Meteorology*, Vol. **72**, 21-44.
- Lopes da Costa, J. C. P. (2007): Atmospheric Flow over Forested and Non-Forested Complex Terrain. PhD-thesis, University of Porto, Portugal, 127 pp.
- Mellor, G. L., and Yamada, T. (1974): A hierarchy of turbulence closure models for planetary boundary layers, *J. Atmos. Sci.*, **31**, 1791-1806.
- Mohr, M., J. Arnqvist, H. Bergström (2012): *Simulating wind and turbulence profiles in and above a forest canopy using the MIUU mesoscale model*. Proceedings, 12th EMS Annual Meeting & 9th European Conference on Applied Climatology (ECAC), Łódź, Poland. [Available from http://presentations.copernicus.org/EMS2012-364_presentation.pptx]
- Monin, A.S. and A.M. Obukhov (1954): Basic laws of turbulent mixing in the surface layer of the atmosphere. *Contrib. Geophys. Inst. Acad. Sci., USSR*, 151(1):163-187.
- Mölder M., Grelle A., Lindroth A., Halldin S., 1999: Flux-profile relationships over a boreal forest – roughness sublayer corrections, 98-99, 645-658.
- Panofsky, H. Dutton, J. New York (US): "Atmospheric turbulence, models and methods for engineering applications. 1984.
- Pedersen, H. S. and W. Langreder (2007): *Forest-added Turbulence: A parametric study on Turbulence intensity in and around forests*. *Journal of Physics: Conference Series* **75** 012062, p. 1-7.
- Peña A., Gryning S.E., Hasager C.B., 2010: Comparing mixing-length models of the diabatic wind profile over homogeneous terrain, *Theor. Appl. Climatol.*, 100, 325-335.
- Peña, A., A. Hahmann, C. B. Hasager, F. Bingöl, I. Karagali, J. Badger, M. Badger and N.-E. Clausen, 2011: South Baltic Wind Atlas - South Baltic Offshore Wind Energy Regions Project. Risø report no. Risø-R-1775(EN). [Available from <http://130.226.56.153/rispubl/reports/ris-r-1775.pdf>]
- Pielke, R. A., 1984: *Mesoscale Meteorological Modelling*. Academic Press, 612 pp.
- Raupach, M. R.; Finnigan, J. J. & Brunet, Y.: Coherent eddies and turbulence in vegetation canopies: the mixing-layer analogy. *Boundary-Layer Meteorology*, **1996**, 78, 351-382
- Sanz, C. (2003): A Note on k- ϵ Modelling on a Vegetation Canopy. *Boundary-Layer Meteorology*, Vol. **108**, p. 191-197.
- Segalini, A., J. H. M. Fransson and P. H. Alfredsson (2012): Scaling laws and coherent structures in canopy flows. Manuscript submitted to *Boundary Layer Meteorology*, 22 pp.

- Shaw RH, Brunet Y, Finnigan JJ, Raupach MR (1995) *A wind tunnel study of air flow in waving wheat: two-point velocity statistics*. *Boundary-Layer Meteorol* **76**:349–376
- Skamarock, W. C.; J. B. Klemp; J. Dudhia; D. M. Gill; M. Duda; X.-Y. Huang; W. Wang; and J. G. Powers (2008): A Description of the Advanced Research WRF Version 3. NCAR Technical Note.
- Smedman A.-S., Lundin K., Brgström H., and Högström U., 1991: A precision kite or balloon-borne mini-sonde for wind and turbulence measurements. *Boundary-Layer Meteorology*, **56**, 295-307.
- Stangroom, P. (2004): *CFD Modelling of Wind Flow over Terrain*. PhD-thesis, University of Nottingham, Nottingham, UK, 298 pp.
- Stuart, P., I. Hunter, J. Lopes da Costa and J. L. Palma, 2008: *Wind Flow Over Forested Hills: Mean Flow and Turbulence Characteristics*. Proceedings of European Wind Energy Conference 2008, Brussels, Belgium. [Available from <http://www.res-group.com/media/473183/ewec%202008,%20wind%20flow%20over%20forested%20hills,%20%20mean%20flow%20and%20turbulence%20characteristics.ppt>]
- Svensson, U. and H. Häggkvist (1990): A Two-Equation Turbulence Model for Canopy Flows. *Journal of Wind Engineering and Industrial Aerodynamics*, Vol. **35**, p. 201-211.
- Söderberg, S., and O. Parmhed, 2006: Numerical modelling of katabatic flow over a melting outflow glacier. *Bound.-Layer Meteor.*, **120**, 509-534.
- Teneler, G. (2011): *Wind Flow Analysis on a Complex Terrain - A reliability study of a CFD tool on forested area including effects of forest module*. Master Thesis, Högskolan på Gotland, 35 pp. [Available at <http://www.hgo.se/wpmaster/3065-hgo/version/default/part/AttachmentData/data/Wind%20Flow%20Analysis%20on%20a%20Complex%20Terrain%20by%20G%C3%B6rkem%20Teneler.pdf>]
- Thomas, C. & Foken, T.: Organised motion in a tall spruce canopy: temporal scales, structure spacing and terrain effects. *Boundary-Layer Meteorology*, **2007**, *122*, 123-147
- Thomas, C. & Foken, T.: Detection of long-term coherent exchange over spruce forest using wavelet analysis. *Theoretical and Applied Climatology*, **2005**, *80*, 91-104
- Torrence, C. & Compo, G. P.: A Practical Guide to Wavelet Analysis *Bulletin of the American Meteorological Society*, **1998**, *79*, 61-78
- Verkaik J.W., Holtslag A. A. M, 2007: Wind profiles, momentum fluxes and roughness lengths at Cabauw revisited, *Boundary-Layer Meteorol*, *122*:701–719.
- Wieringa, J., 1992: Updating the Davenport roughness classification. *Journal of Wind Engineering and Industrial Aerodynamics*, **41-44**, 357-368.
- Wilson, J. D.: Monin-Obukhov Functions for Standard Deviations of Velocity *Boundary-Layer Meteorology*, **2008**, *129*, 353-369.

Zhao, W., and R. J. Qualls (2006): Modeling of long-wave and net radiation energy distribution within a homogeneous plant canopy via multiple scattering processes. *Water Resources*, Vol. **42**, W08436.

Zilitinkevich S, Mammarella I, Baklanov A, Joffre S: The effect of stratification on the aerodynamic roughness length. In: Baklanov A, Sue G, Alexander M, Athanassiadou M: *Meteorological and Air Quality Models for Urban Areas*, Springer Berlin Heidelberg, **2009**, pp 59-66, DOI 10.1007/978-3-642-00298-4_7, URL http://dx.doi.org/10.1007/978-3-642-00298-4_7.

9 Publications and presentations

Journal publications

Arnqvist J. et al, 2013: Flux-profile expressions with roughness sublayer correction. Manuscript submitted to Boundary-Layer meteorology.

Arnqvist J., Segalini A., Dellwik E., Bergström H., 2013: Wind statistics from a forested landscape. Manuscript Boundary-layer Meteorology.

Chougule A., Mann J., Segalini A and Dellwik E (2013): Spectral tensor parameters for wind turbine load modeling from forested and agricultural landscapes, to be submitted to Wind Energy.

Segalini A. and Alfredsson P.H., 2012: Techniques for the eduction of coherent structures from flow measurements in the atmospheric boundary layer. Boundary-Layer Meteorology, DOI: 10.1007/s10546-012-9708-7.

Segalini A. and Odemark Y., 2013: An analytical model to account for the effects of forest turbulence on the outputs of a wind turbine, Wind Energy (submitted).

Segalini A., Fransson J. H. M., and Alfredsson P. H., 2013: Scaling laws and coherent structures in canopy flows, Boundary-Layer Meteorology (under revision).

Conference presentations

Dellwik E., Arnqvist J., Bergström H., and Segalini A., 2012: Flow characteristics at a forested site with wind turbines. Conference contributions, EMS Łódź, Poland, September 2012.

Mohr, M., J. Arnqvist, H. Bergström, 2012: *Simulating wind and turbulence profiles in and above a forest canopy using the MIUU mesoscale model*. Proceedings, 12th EMS Annual Meeting & 9th European Conference on Applied Climatology (ECAC), Łódź, Poland.

Odemark Y. and Segalini A., 2012: *A wind tunnel study on the effects of forest turbulence on wind turbine outputs*, EAWC conference "The science of making torque from wind", 9-11 October 2012, Oldenburg, Germany

Segalini A, Fransson J.H.M., Dahlberg J.-Å., Alfredsson P.H., 2011: Gust structure and generation in canopy flows. Conference proceeding, EWEA, Brussels, Belgium.

Segalini A., Fransson J.H.M. and Alfredsson P.H., 2011: An experimental analysis of canopy flows. Conference proceeding, 13th European Turbulence Conference, Warsaw, Poland.

Segalini A., Alfredsson P. H., Dellwik E., Arnqvist J., and Bergström H., 2012: Velocity statistics and spectra over a forested site measured with a tall mast, 65rd Annual Meeting of the APS Division of Fluid Dynamics Sunday-Tuesday, 18-20 November, San Diego, California.

Other presentations

Arnqvist J., 2012: Vind över skog. Konferenspresentation, Vindkraftforskning i fokus 2012.

Arnqvist J., 2012: Wind power in forests. Conference contribution, STandUP for Energy, KTH 30 May 2012.

Bergström H., 2009: Vindkraft i skog – Vindforsk III projekt V-312. Konferenspresentation, Vindkraftforskning i fokus 2009.

Bergström H., 2010: Vindmodeller för dimensionering av vindkraft i skogsmiljö. Konferenspresentation, Vindkraftforskning i fokus 2010.

Bergström H., 2011: Vind i skog och kallt klimat. Konferenspresentation, Nationella vindkraftskonferensen, Kalmar, 2011.

Bergström H., 2012: Vindkraft i skog – Vindforsk projekt V-312. Konferenspresentation, Vindkraftforskning i fokus 2012.

Bergström H., 2012: Windpower in forests and wind power in cold climates. Conference contribution, STandUP for Energy, KTH 30 May 2012.

Segalini A., Fransson J.H.M. and Alfredsson P.H., 2012: Konferenspresentation, Vindkraftforskning i fokus 2012.

Segalini A., Fransson J.H.M., and Alfredsson P.H., 2012: Turbulent structures in canopy flows, Euromech colloquium "Wind Energy and the impact of turbulence on the conversion process", 22-24 February 2012, Oldenburg, Germany.

Reports

Carlén, I., Ganander, H., "Fatigue loading of wind turbines operating in forest terrain", Teknikgruppen Report , TG-R-12-11 , 2012.

Dellwik, E., Arnqvist, J., and Segalini, A., 2013: Measurements from "Wind power in forests" – a database description. Report DTU Wind Energy E-0017-

Edvinsson L., 2012: Analys av vinddata från lidar. Master thesis at Uppsala University, Department of Geosciences. ISSN 1650-6553 Nr 232, 43 pp.

ELFORSK

SVENSKA ELFÖRETAGENS FORSKNINGS- OCH UTVECKLINGS - ELFORSK - AB

**Elforsk AB, 101 53 Stockholm. Besöksadress: Olof Palmes Gata 31
Telefon: 08-677 25 30, Telefax: 08-677 25 35
www.elforsk.se**